The LiH_2^+ system: interaction forces and quantum dynamics

12th December 2001

Preface

This work is the natural development of what I did in the graduate Thesis work with Prof. M. Raimondi. At that time, thanks to a well established collaboration between the Raimondi's group here in Milan and the Gianturco's group in Rome, I started to be interested in the $LiH + H^+$ system. I was working in the Spin Coupled Valence Bond theory, of which I had just learned the basics. The excitement in viewing chemistry through a pair of quantum mechanical lens was big. Molecules, for the first time, could form and dissociate, starting from isolated atoms, going through "distorted atoms in molecules" and ending possibly with product molecules. I was going toward "chemical reactions", at the heart of Chemistry. The meeting with collision theory was unavoidable and was accelerated by the casual discovery of the Taylor's book. Then, the $LiH + H^+$ system became an occasion to merge the interest in Valence Bond theory with that in Scattering theory. Indeed, the system was an "interesting" excited state and (as we recognized later) was a particular collision system.

Thus, my PhD course started with some ideas (at a very early stage) on how to face the excited state problem and with the study of basic scattering theory. The development of a simple approach to the electronic excited problem and a preliminary meeting with the practice of collision theory were the content of the first stage of my course. I was ready to go as a visitor student in the group of Prof. F. A. Gianturco, where the second stage of the PhD course started.

In Gianturco's group I met a colleague, E. Bodo, which soon became a friend. Our interests (and those of our supervisors!) were quickly attracted by the LiH_2^+ system: we recognized that not only the $LiH + H^+$ collisions could have a relevance for what is called "Early Universe" but the full LiH_2^+ system needed to be considered. Thus, the second stage of my course was devoted to the understanding of the interaction forces and the dynamics in the title system.

The work is organized in two Parts. The *report* of the PhD course is the content of Part II, which the reader is strongly recommended to start with. In Part II the above "story" is placed on a firm, scientific ground. An introductory Chapter gives an overview of the system, showing its relation with the LiH

"problem" in the Early Universe. Here the reader is supplied with a brief review of the relevant astrophysics in order to make him confident with the "Post-Recombination Era". The novel method in the Spin Coupled Valence Bond framework which allowed us to gain sights into the energetics of the title system is presented in Chapter 6. The subsequent Chapter summarizes the results of our extensive *ab-initio* calculations and draws some conclusions on the Li ionic network. Chapters 8 and 9 describe a reduced dimensionality approach to the quantum dynamics of the system. Chapter 10 describes a novel algorithm for solving the Time-Independent Close-Coupling equations at long-range, a method that appears to be promising for the study of the low-energy (non reactive) dynamics in charge-dipole systems like our $LiH + H^+$. Finally, Chapter 11 summarizes the conclusions.

The content of Part I is the "theoretical background" that was needed to carry out this work. In principle, it was designed in such a way to closely parallel the Wigner's suggestions on chemical dynamics (also known as Wigner's three trees): first, one separates nuclear and electronic motions, taking into account the disparity of masses and the similarities of forces between electrons and nuclei; then, he studies the electronic motion, here treated in the Valence Bond framework and in particular in the modern Spin Coupled Valence Bond formulation; and finally, he studies the nuclear motion, here considered in the general framework of collision theory, both in the single- and in the multi-channel cases. However, as the reader will soon recognize, the Born-Oppenheimer approximation doesn't appear. The reason is that this Part I grew enormously and at the end we had no more space available. This approximation is however so well known that its exclusion should be tolerated.

The reason for the existence of this introductory Part is twofold: on the one hand the author's need to reorganize what he laboriously learned during these years and on the other hand the possibility of focusing in Part II on the work in the LiH_2^+ system without continuous "introductory" breaks. It is worth to note at this point that this Part contains *known* results, although the presentation follows the personal tastes of the author.

One more note about this work. We use as much as possible the Dirac notation for the state vectors of a system. Possible misleading with this notation could arise when dealing with "improper" vectors; they are used in the so-called stationary scattering theory and will be always indicated with their "continuous" quantum numbers. No special symbols will be used for operators. Vector quantities (either vector operators or their vector eigenvalues) will be indicated with bold characters, although bold characters will be used also for special operators, like the scattering matrix, which act on "enlarged" spaces. Hilbert spaces and subpaces will be denoted with emphasized capital characters, like $\mathcal{H}$. Unless otherwise stated atomic units are used throughout.

Acknowledgments

Foremost, I would like to thank my supervisors, Prof. Ermanno Gianinetti and Prof. Mario Raimondi, for the continuous support and encouragement that have made this work possible. In particular, I have known Prof. Raimondi since my graduate course, during which he taught me the valence bond theory and, above all, he taught me to grasp physics from complicated formulas and barren numbers which overwhelmingly spread over theoretical chemistry.

Prof. Franco Antonio Gianturco is greatly acknowledged. He was a kind host during my (long) stay in Rome and soon became my third supervisor. He was an alert teacher whose enthusiasm allowed me to overcome the unavoidable difficulties of a PhD work.

The meeting with Enrico Bodo in Rome was a key event for this work and for this Enrico is sincerely acknowledged. We shared passion for science and excitement for satisfactory results, once we surmounted the difficulties of the beginning without resorting to the drastic "agriturismo" solution.

Large part of this work has arisen through discussion and collaboration with the above mentioned persons.

Prof. Gian Franco Tantardini is greatly acknowledged too. He has been continuously interested in my work, allowing me to put in contact with very important books on which my background in chemical dynamics has been largely based. Furthermore, his critical reading of this manuscript has been of invaluable help.

Other people contributed in a less direct (but not less important) way to this Thesis, above all through their friendship. Among these, I have to thank the friends in Rome (Franceschino, Francesco, Chiara, Emanuele, Mauro, Gianni, Alex, Roman, Cono and Simona in the Gianturco's group and Francesca, Mariateresa and Isabella which are "chemically" bound to that group) and those in Milan (Federico, Fausto, Max, Roberto, Giorgio and Gabriele in various groups here in Milan)[1].

One special thank to my parent which have always believed in me without

---

[1]The order of the names inevitably follows as close as possible a "total interaction time". A further person, Giuliana, can be hardly ascribed to Milano or Rome.

6

knowing any actual reason for doing so. Finally, I surely have to thank Lisa whose encouragement (and patience) has been always invaluable.

All the mentioned events really happened and all the mentioned persons really exist. The remaining things are fiction..

Contents

List of Figures

11

Part I

Theoretical background

Chapter 1

Valence Bond Theory

We begin by reviewing in this Chapter the *modern* Valence Bond (VB) theory which provides accurate description of electronic states while still preserving a clear physical picture of the underlying interactions in term of "classical" valence bond concepts. We first review the "classical" theory in Section (1.1) by looking at the Heitler-London wavefunction and then introduce in Section (1.2) the Spin Coupled wavefunction which is central to the modern version of the VB theory, much like the Hartree-Fock wavefunction is for the MO's theories. Its relation to general electronic wavefunctions is discussed in Section (1.4), after collecting some properties of the spin space of an N electron system in Section (1.3). In particular, it will be shown that the Spin-Coupled wavefunction is the most general one-electron approximation to an electronic wavefunction. Then, we close this Chapter describing the modern Valence Bond theory, the so-called Spin-Coupled Valence Bond theory, either in its original formulation (Section (1.6)) and in the more recent improved version (Section (1.7)).

1.1 The Heitler-London wavefunction

In 1927, soon after Schrödinger(1926) founded the "wave mechanics", Heitler and London(1927) (hereafter HL) explained the stability and bonding of the H_2 molecule by writing the first molecular wavefunction of the history of Quantum Chemistry. They recognized that a product of *atomic* hydrogen orbitals is an exact solution of the clumped nuclei Schrödinger equation when the atomic centers are at infinite separation and, thus, used such *ansatz* for a perturbative treatment of the electronic problem, in which the unperturbed hamiltonian was the sum of the *isolated* hydrogen atom hamiltonians (at the *finite* separation in consideration).

Here we follow a somewhat different approach and write directly the HL (normalized) wavefunctions for the singlet and for the triplet states, respectively, as[1]

$$\psi(^1\Sigma_g^+) = \sqrt{\frac{2}{1+|S|^2}} A \left\{ \chi_A \chi_B \frac{\alpha\beta - \beta\alpha}{\sqrt{2}} \right\} \tag{1.1}$$

$$\psi(^3\Sigma_u^+) = \sqrt{\frac{2}{1-|S|^2}} A \left\{ \chi_A \chi_B \frac{\alpha\beta + \beta\alpha}{\sqrt{2}} \right\} \tag{1.2}$$

In these formulas χ_A and χ_B are hydrogenic atomic orbitals centered at the nuclei H_A and H_B (so that $\chi_A \chi_B$ is the unperturbed wavefunction), α and β are the usual spin functions of the electrons, $S = \langle \chi_A | \chi_B \rangle$ is the overlap integral and A is the antisymmetrizer (projection) operator, which for the general N electron system reads as

$$A = \frac{1}{N!} \sum_{P \in S_N} \epsilon_P P$$

where S_N is the "symmetric group" to be discussed later, P is a permutational operator in this group and ϵ_P is the corresponding parity. (We adopt the convention that in a string of orbitals $\phi_a \phi_b .. \phi_\xi$ the electronic labels are in the "natural" order, i.e. $\phi_a(\mathbf{r}_1)\phi_b(\mathbf{r}_2)..\phi_\xi(\mathbf{r}_i)$).

When the wavefunctions of eq.s(1.1,1.2) are used to compute the electronic energy one obtains the following expression for the interaction potentials

$$V(R) = \frac{J \pm K}{1 \pm |S|^2}$$

where the plus sign refers to the singlet state and the minus sign to the triplet. J and K are called "Coulomb" and "Exchange" integrals, respectively, and are given by[2]

$$J = \left\langle \chi_A \chi_B \left| H^{(1)} \right| \chi_A \chi_B \right\rangle$$

$$K = \left\langle \chi_A \chi_B \left| H^{(1)} \right| \chi_B \chi_A \right\rangle$$

where

$$H^{(1)} = H - H^{(0)} = -\frac{1}{r_{1B}} - \frac{1}{r_{2A}} + \frac{1}{r_{12}} + \frac{1}{R}$$

---

[1] In the triplet manifolds we focus attention on the $M_S = 0$ state.

[2] This labeling is similar to that of the HF theory and differs from the usual practice of semiempirical VB theory and of the magnetism theories, where J represents the exchange integral.

is the perturbed hamiltonian in the original HL treatment, with the usual meaning of the symbols ($r_{iZ} = |\mathbf{r}_i - \mathbf{R}_Z|$, $r_{ij} = |\mathbf{r}_i - \mathbf{r}_j|$ and $R = |\mathbf{R}_A - \mathbf{R}_B|$, $\mathbf{r}_i$ being the position vector of the i-th electron and $\mathbf{R}_Z$ the position vector of the Z-th nucleus).

The Coulomb integral is a "classical" interaction term

$$
J = \frac{1}{R} - \int d^3\mathbf{r} \frac{|\chi_A(\mathbf{r})|^2}{|\mathbf{r} - \mathbf{R}_B|} - \int d^3\mathbf{r} \frac{|\chi_B(\mathbf{r})|^2}{|\mathbf{r} - \mathbf{R}_A|} + \int d^3\mathbf{r}_1 d^3\mathbf{r}_2 \frac{|\chi_A(\mathbf{r})|^2 |\chi_B(\mathbf{r})|^2}{r_{12}}
$$

and varies only slightly as the nuclei are brought from infinity to their equilibrium separation. The second, exchange integral is purely quantum mechanical in origin

$$
K = \frac{|S|^2}{R} - \int d^3\mathbf{r} \frac{\chi_A(\mathbf{r})^* \chi_B(\mathbf{r})}{|\mathbf{r} - \mathbf{R}_A|} S^* - \int d^3\mathbf{r} \frac{\chi_B(\mathbf{r})^* \chi_A(\mathbf{r})}{|\mathbf{r} - \mathbf{R}_B|} S +
$$
$$
+ \int d^3\mathbf{r}_1 d^3\mathbf{r}_2 \frac{(\chi_A^* \chi_B)(\mathbf{r}_1)(\chi_B^* \chi_A)(\mathbf{r}_2)}{r_{12}}
$$

and it is its rapid variation around the equilibrium geometry that causes the formation of the bond in the singlet state. In the triplet state it appears with the sign reversed and thus it leads to a repulsive state.

Curiously enough, this first treatment of the chemical bond was a *correlated* one: the molecule correctly dissociates into two asymptotic partners and it appears made by two building blocks with their *atomic* nature.

The work was soon extended by Pauling, Slater and Van Vleck, thereby posing the chemistry on a quantum mechanical ground. They showed that molecules are formed by favorable exchange interactions between *valence* orbitals of the constituent atoms, either with their isolated shapes or with an "hybridized" shape that rationalized the previous Van't Hoff observations on molecular geometries. A chemical theory was established: molecules appeared to be formed by atoms whose wavefunctions enter *directly* (with their properties) into the molecular wavefunction, hence giving a simple explanation of the regularities of the *chemical* properties of the elements. There were founded reasons for which the periodic variations of the *physical* properties of the atoms across the Mendeleev's table are brought into molecules and molecular formation.

Despite these tremendous impact in the chemistry world the quantitative application of this "classical" Valence Bond theory was somewhat unsatisfactory. The dissociation energy of the HL treatment of H_2 is 66% of the experimental value and the equilibrium distance is 117%. The reason was soon recognized to be the lack of terms in the wavefunction representing the electronic rearrangement that occurs during the bond formation. Hence the need

for "ionic" and "excited" configurations. However, it turned out that the contributions of these configurations was so large that, when used, completely obscured the original "reference" configuration.

1.2   The Spin-Coupled wavefunction

In 1949 Coulson and Fisher (CF) (1949) wrote the first *Spin-Coupled* wavefunction, making a substantial improvement on the HL's results for the H_2 molecule. Their (unnormalized) wavefunction for the singlet ground-state was

$$\psi(^1\Sigma_g^+) = A\left\{\phi_A\phi_B\frac{\alpha\beta - \beta\alpha}{\sqrt{2}}\right\} \tag{1.3}$$

where

$$\phi_A = \chi_A + \lambda\chi_B \tag{1.4}$$

(and analogously for ϕ_B) with χ_A and χ_B hydrogenic orbitals as before and λ a variational parameter. The logic behind this wavefunction is clear: the superposition of atomic orbitals in eq.(1.4) allows the polarization of the atomic orbital in the molecular environment, thereby accounting for the above mentioned electronic redistribution. Indeed, the CF wavefunction contains *implicitly* some ionic configurations. The interesting result was that the λ parameter never becomes big: as the atoms are brought together from infinity to their equilibrium geometry, λ varies smoothly from 0 to 0.14. *This means that the orbitals preservs their "atomic" character, being only slightly distorted by the formation of the bond.* Thus, the VB picture was preserved while allowing a substantial improvement of the results (the D_e and R_e turned out to be 85% and 102%, respectively, of the experimental value).

The *ansatz* was generalized in 1971 by Gerratt(1971) who wrote the Spin-Coupled (SC) wavefunction for a generic N electron system in the form

$$\psi_{SM}^N = A\left\{\phi_1\phi_2..\phi_N\Theta_{SM}^N\right\} \tag{1.5}$$

where $\{\phi_1\phi_2..\phi_N\}$ are N (spatial) orbitals, free to overlap, whose shape is variationally determined and Θ_{SM}^N is a spin eigenfunction with quantum numbers (SM) which is variationally determined too. Since the spin eigenfunctions can be expanded in a complete set of eigenfunctions of dimension f_S^N (to be discussed later, in Section (1.3))

$$\Theta_{SM}^N = \sum_{k=1}^{f_S^N} c_k\Theta_{SM;k}^N$$

the SC wavefunction can also be written as

$$\psi_{SM}^N = \sum_k c_k \psi_{SM;k}^N$$

This is not only an obvious relation: each basis element $\Theta_{SM;k}^N$ entails a particular *spin coupling* (e.g. a Lewis structure) and the $\psi_{SM;k}^N$'s are thus conventional *chemical structures*. Their superposition is the quantum mechanical transcription of the chemical "resonance" phenomena and the coefficient c_k are the weights of the classical structures. This interpretation is clearly well within the Valence Bond picture and is possible since the orbitals usually turn out to be *localized* on the atomic centers (Cooper et al., 1987; Cooper et al., 1991).

The Spin-Coupled wave function is a *correlated wavefunction,* in that it incorporates almost the whole $(80 - 90\%)$ *non-dynamical* correlation, which we operationally define as the correlation energy recovered by a 'N electrons in N orbitals' CASSCF calculation. Indeed, the SC function describe correctly the dissociation processes, i.e. it is size consistent: when two fragments AB are brought far apart the system's SC function

$$\psi_{SM}(AB) = A \left\{ \phi_1^A \phi_2^A .. \phi_{N_A}^A \phi_1^B \phi_2^B .. \phi_{N_B}^B \Theta_{SM}^N \right\}$$

(in which we label the orbitals with the relevant fragment superscript in view of their above mentioned *localization*) correctly reduces to

$$\psi_{SM}(AB) \rightarrow \frac{N_A!N_B!}{(N_A + N_B)!} \sum_{M_A M_B} A_A \left\{ \phi_1^A \phi_2^A .. \phi_{N_A}^A \Theta_{S_A M_B}^{N_B} \right\} \cdot$$

$$\cdot A_B \left\{ \phi_1^B \phi_2^B .. \phi_{N_B}^B \Theta_{S_B M_B}^{N_B} \right\} \langle S_A M_A S_B M_B | SM S_A S_B \rangle$$

when one uses the simplification

$$(N_A + N_B)!A = \sum_{P \in S_N} \epsilon_P P \simeq \left\{ \sum_{P \in S_{N_A}} \epsilon_P P \right\} \left\{ \sum_{P \in S_{N_B}} \epsilon_P P \right\}$$

That is, the asymptotic AB wavefunction reduces to a simple product of fragment wavefunctions with the correct total spin properties (the coefficients $\langle S_A M_A S_B M_B | SM S_A S_B \rangle$ are the usual Clebsh-Gordon (CG) coefficients that accomplish the spin decoupling $SM S_A S_B \rightarrow S_A M_A S_B M_B$) and the SC energy is the sum of the energies of the isolated (sub)systems computed at the same, Spin Coupled, level[3].

---

[3]Clearly, the correct asymptotic wavefunction is the *full* antisymmetrized wavefunction

Thus, we have seen that the Spin Coupled wavefunction is physically consistent, sufficiently accurate and still simple enough to allow the realistic description of the chemical bond in terms of classical valence bond concepts: we strongly believe that such wavefunction brings *chemistry* on a firm *quantum mechanical* ground. Let us now go slightly deeper into this theory, reviewing first some properties of the spin space of an N electron system.

1.3   The spin space of an N-electron system

Experimental evidences show that the three spatial coordinates are insufficient to describe the state of an electron. In a given point of space the electron state is entirely characterized only when the projection of its intrinsic angular momentum on a reference z axis is specified. Although the origin of this angular momentum is not due to the existence of an internal structure it is invariably referred to as a *spin* angular momentum.

Since the electron spin projection can take up only two values $\{1/2,\ -1/2\}$ we denote with $|\alpha\rangle$ and $|\beta\rangle$, as usual, the eigenvectors of s_z. They spans the bidimensional vector space which is the spin space of a single electron, $\mathcal{H}_1$. The spin space of an N electron system, $\mathcal{S}^N$, given by the tensor product

$$\mathcal{S}^N = \ = \underbrace{\mathcal{H}_1 \otimes \mathcal{H}_1 .. \otimes \mathcal{H}_1}_{N \ \text{times}}$$

has dimension 2^N and it is spanned by the "primitive" vectors

$$\{|i_1\rangle |i_2\rangle .. |i_N\rangle\} \quad \text{where} \ |i_k\rangle = |\alpha\rangle ,\ |\beta\rangle$$

These vectors are eigenvectors of the total spin component on the reference z axis,

$$S_z \{|i_1\rangle |i_2\rangle .. |i_N\rangle\} = \frac{N_\alpha - N_\beta}{2} \{|i_1\rangle |i_2\rangle .. |i_N\rangle\}$$

but are not in general eigenvectors of S^2. Thus, they must be combined in order to exploit the spin symmetry properties of the usual electrostatic hamiltonian. This can be done in several different ways, leading to a number of widely used spin basis. Here we note only that when this is done the N electron spin

---

that represents that actual limit of the SC wavefunction. The vanishing overlap between orbitals that belong to different fragments makes null the inter-fragment spin couplings (see Section (1.5)) and thus the total spin function tends to be the product of the spin functions of the two isolated fragments. The actual S_A and S_B values depend on the relation between the AB state in consideration and the asymptotic fragments (Wigner-Weitmar correlation rules).

space $\mathcal{S}^N$ is decomposed in a certain number of (SM) subspaces $\mathcal{V}_{SM}^N$ in which $\{S^2, S_z\}$ are diagonal

$$\mathcal{S}^N = \sum_{SM}^{\oplus} \mathcal{V}_{SM}^N$$

(here (SM) run over all values allowed by the usual vector coupling rules, see below). The dimension f_S^N of each subspace is an angular momentum property and it does not depend on the M quantum number

$$f_S^N = \frac{N!}{\left(\frac{N}{2} + S + 1\right)! \left(\frac{N}{2} - S\right)}(2S + 1)$$

since M actually depends on the choice of the reference system[4]. Thus,

$$\sum_{SM}(2S + 1)f_s^N = 2^N$$

The spin spaces corresponding to a different number of electrons are related by the usual vector coupling rules; for example, adding an electron to the spin subspace $\mathcal{V}_{SM}^N$ gives elements to the spaces $\mathcal{V}_{S'M'}^{N+1}$ with

$$M' = M \pm \frac{1}{2}$$

$$S' = \left|S - \frac{1}{2}\right|, S + \frac{1}{2}$$

More precisely, the following formula holds

$$f_{S-1}^{N-1} + f_S^{N-1} = f_{S-1/2}^N \quad\quad S = \frac{N-1}{2}, .. \left|S - \frac{1}{2}\right|$$

where the dimension of the space with maximum spin, $S = N/2$, is always one. The reason for this relation is easily explained with the help of the *branching diagram* (Fig.(1.1)). In this diagram for each value of (N, S) the dimension f_S^N is reported at the corresponding intersection point; for given (N, S) this quantity can be obtained from those of the $N - 1$ case by summing the value(s) of the circle(s) connected by the lines. Thus, starting with one electron $(N = 1, S = 1/2)$ we can add one electron to form a singlet (along the path $(1, 1/2) \to (2, 0)$) or to form a triplet (along the path $(1, 1/2) \to (2, 1)$); with the same token we can add an electron to $(N, S) = (2, 1)$ and go in $(3, 3/2)$ or in $(3, 1/2)$, where $f_{1/2}^3 = 2$ since we could have also followed the

---

[4]The (sub)spaces $\mathcal{V}_{SM}$ which differ only for M are brought in a one-to-one correspondence by the rising and lowering operators $S_{\pm}$.
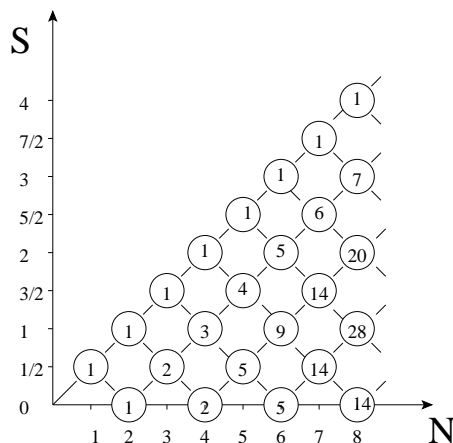
Figure 1.1: The branching diagram which gives the dimensions of the *(SM)* subspaces. It is really a three-dimensional diagram, in that each circle is splitted in *2S+1* equivalent circles, corresponding to the different values of *M*.

path $(2,0) \to (3,2)$. In general, the highest spin states $S = N/2$ can be obtained only from the highest spin states of the corresponding $N-1$ electron system (i.e. $f^N_{N/2} = 1$), the $S = 0$ spin state of an even electron system can be obtained only from the $S = 1/2$ state of the $N-1$ system ($f^{2n}_0 = f^{2n-1}_{1/2}$) and other intermediate spin states can be obtained both from the $S - 1/2$ and the $S + 1/2$ states of the $N-1$ system (e.g. $f^6_1 = f^5_{1/2} + f^5_{3/2}$).

We can uniquely define a "path" in the branching diagram by listing the S quantum numbers of the $1, 2, ..N$ intermediate numbers of electrons[5]

$$(s_1, s_2, .., S)$$

Each path corresponds to a particular spin coupling of the electrons; for example, in $(1/2, 1, 1/2, 0)$ the first two electrons are coupled to form a triplet, the third electron is added to form a doublet and the fourth electron gives the final singlet state, which is one of the two possible (linearly independent) states of a 4 electron system (the other being given by $(1/2, 0, 1/2, 0)$). Since this construction exactly parallels the vector coupling rule each coupling defines actually a basis vector in the $\mathcal{V}^N_{SM}$ space. These basis vectors are orthogonal since they are eigenvectors with different quantum numbers of (at least) one "intermediate" S^2 operator; for example the S^2 operator of the first two electrons actings on $(1/2, 1, 1/2, 0)$ and $(1/2, 0, 1/2, 0)$ gives $s_2 = 1$ and $s_2 = 0$, respectively.

---

[5]We could avoid the use of the first and last quantum number since the first is obvious and the last is the final point in consideration.

These paths identify the basis elements of the so-called Yamanouchi-Kotani basis and in practice they are obtained by making use of the relevant CG coefficients

$$\left|\Theta_{SM;k}^{N}\right\rangle = -\left(\frac{S-M+1}{2S+2}\right)^{1/2}\left|\Theta_{S+\frac{1}{2},M-\frac{1}{2};k}^{N-1}\right\rangle\left|\alpha\right\rangle +$$
$$+\left(\frac{S+M+1}{2S+2}\right)^{1/2}\left|\Theta_{S+\frac{1}{2},M+\frac{1}{2};k}^{N-1}\right\rangle\left|\beta\right\rangle$$

$$\left|\Theta_{SM;k}^{N}\right\rangle = \left(\frac{S+M}{2S}\right)^{1/2}\left|\Theta_{S-\frac{1}{2},M-\frac{1}{2};k}^{N-1}\right\rangle\left|\alpha\right\rangle +$$
$$+\left(\frac{S-M}{2S}\right)^{1/2}\left|\Theta_{S-\frac{1}{2},M+\frac{1}{2};k}^{N-1}\right\rangle\left|\beta\right\rangle$$

where the first equation refers to the $(S+1/2) \rightarrow S$ coupling and the second to the $(S-1/2) \rightarrow S$ coupling.

Several other basis can be considered, even non-orthogonal ones. For example, one very useful from a chemical point of view is that of Rumer(1932) in which for a given S spin state $2S$ electrons are left unpaired and the remaining $N-2S$ electrons are paired to form singlet-two electron spin states (like that used by Heitler and London for the singlet state). Rumer(1932) and then Simonetta et al.(1968) devised a graphical scheme to chose from all the possible "pairs" those that give rise to a linearly independent set of spin functions. It is interesting to note that in their schemes, placing N regularly spaced points on a circle that represent the electrons, one obtains for the case $N = 6$ and $S = 0$ the three Dewar and the two Kekulé structures of benzene.

The spin subspaces $\mathcal{V}_{SM}^{N}$ have important group-theoretical properties. Indeed, since they are defined as eigenspaces of *symmetric* operators (S^2 and S_z), they are invariant under the action of the *symmetric group* S_N, i.e. the group, of dimension $N!$, of the permutations of N objects. In other words, if we fix a basis $\left\{\left|\Theta_{SM;k}^{N}\right\rangle\right\}$ in $\mathcal{V}_{SM}^{N}$, from the commutation relations $[S^2, P] = [S_z, P] = 0$, it follows

$$P\left|\Theta_{SM;k}^{N}\right\rangle = \sum_{l=1}^{f_s^N} U_{lk}^{N}(P)\left|\Theta_{SM;l}^{N}\right\rangle \ \forall P \in S_N$$

where the set of matrices $\left\{\mathbf{U}^{N}(P)\right\}_{P \in S_N}$, independent of M, performs a representation of S_N with dimension f_S^N. The important result is that these representations are *irreducible* (see for example Hammermesh(1989)). Each

(SM) subspace carries a different representation[6], which is more symmetric
the higher is the spin S. For example, the $S = N/2$ state of an N electron
system is always totally symmetric (or invariant) under the action of S_N

$$P \left| \Theta_{N/2,M;k}^{N} \right\rangle = \left| \Theta_{N/2,M;k}^{N} \right\rangle \ \forall P \in S_N$$

It is worth to note at this point that the spin space can contain only a
limited number of representations of S_N, except for the case $N = 2$ where the
only representations are the one-dimensional symmetric and antisymmetric
ones ($S = 1$ and $S = 0$ respectively). For $N > 2$ the spin space cannot contain
the most antisymmetric representations; for example, it is clearly impossible
to antisimmetrize a spin state with more than 2 electrons or, in other words,
three electrons are prevented to be in the same position in space. Let us now
see how to use these properties.

1.4   Wigner's representation theorem

We have discussed in the previous Section the relation between the spin space
and the symmetric group. Since we know that every state of a fermion system
must be a basis of the antisymmetric representation of the symmetric group,
the question arises of how to combine the group properties of the spin space
with those of the "spatial" space in order to get a vector that is antisymmetric
with respect to electron permutations. For the case $N = 2$ we know that such
a state can be written in the form

$$\left| \Psi_{SM} \right\rangle = \left| \Phi \right\rangle \left| \Theta_{SM} \right\rangle$$

where

$$P^\sigma \left| \Theta_{SM} \right\rangle = (-)^{S+1} \left| \Theta_{SM} \right\rangle$$

$$P^r \left| \Phi \right\rangle = (-)^{S} \left| \Phi \right\rangle$$

(the permutation operator has been written as product of a "spatial" P^r oper-
ator and a "spin" P^σ operator, $P = P^r P^\sigma$); how can we generalize this method
being unable in forming antisymmetric spin states with $N > 2$? Furthermore,
from a mathematical point of view, the spin free electronic hamiltonian has,
in general, degenerate ("spatial") eigenvectors because of the permutational
symmetry and it is not clear at all if these vectors are "allowable" and if the
permutational degeneracy is, to some extent, preserved.

The answers to these questions follow from the application of the Wigner's
representation theorem of group's theory; the result can be stated as follows

---

[6]Strictly speaking a "non-equivalent" representation. We are referring to the different
representations that come from varying the N and S numbers.

Wigner's representation theorem. The following statements are equivalent:

1. $|\Psi_{SM}\rangle$, a N electron state vector with quantum numbers (SM), is antisymmetric.

2. $|\Psi_{SM}\rangle = \sum_{k}^{f_s^N} |\Phi_k\rangle |\Theta_{SM;k}\rangle$, where $\{\Theta_{SM;k}\}$ is an orthonormal basis set of $\mathcal{V}_{SM}^N$ which carries the $\Gamma = \{\mathbf{U}^N(P)\}_P$ representation of S_N and $\{\Phi_k\}$ is a basis of the "dual" representation $\Gamma^* = \{\epsilon_P \mathbf{U}^N(P)^*\}_P$.

3. There exists $|\Phi\rangle$ and $|\Theta_{SM}\rangle$ such that $|\Psi_{SM}\rangle = A\{|\Phi\rangle |\Theta_{SM}\rangle\}$ is non null (A is the previously defined antisymmetrizer operator).

Before discussing some consequences of this theorem, it is worth to note that the equivalence $1 \Leftrightarrow 3$ is not so trivial as it may seem. Indeed, on the one hand, it is not clear that a *generic* antisymmetric wavefunction can be obtained by projecting a *product* of spatial and spin vectors and, on the other hand, the outcome of the projection of an arbitrary spatial-spin product is "likely" to be null. Let us now focus on the $1 \Leftrightarrow 2$ and $1 \Leftrightarrow 3$ equivalences.

Point 2 tells us, in practice that an antisymmetric state can be obtained by two sets of f_S^N vectors, one set of spatial vectors and the other of spin vectors: under the action of the symmetric group the two sets behave in a opposite, "dual" way so that their product gives the correct antisymmetric property to the full vector. This generalizes the $N = 2$ case discussed above to the case $f_S^N > 1$. Furthermore, it gives a sense to a statement like '..the more symmetric the spin vector is the more antisymmetric the spatial vector must be..', which implies for example the Hund's rule: the higher is the spin the more antisymmetric is the spatial vector and, then, the less is the Coulomb repulsion between electrons[7]. Finally, point 2 factors out from the full set of spatial vectors of the hamiltonian those vectors that are *incompatible* with the Pauli principle: if Γ is the representation carried by a degenerate set of eigenvectors $\{\Phi_k\}$ it gives rise to a physical state only if Γ^* can be carried by one spin subspace. The case of the lowest energy (bosonic) state is a well known example in which Γ^* is the antisymmetric representation, i.e. it is "forbidden" for $N > 2$.

Point 3 is very important for our purposes: it states that every electronic state can be put in the form of a(n antisymmetrized) product of spatial and spin states. Thus, the Spin Coupled wavefunction can be seen as the simple product orbital approximation to the spatial vector state or, in other words,

---

[7]It is worth to mention in this context that the stability of the electronic structures depends also on the maximum occupancy of the lowest "monoelectronic" states; the Hund's rule refers to the set of states that arise from a given configuration.

the Spin Coupled wavefunction is the most general one electron approximation.
It follows that the singlet RHF wavefunction or, in general, any Configuration
State Function can be written in a Spin Coupled form. Furthermore, since the
SC function is variationally optimized, we have always $E_{SC} \leq E_{HF}$, i.e. the SC
function is a *correlated* function being still a *monoelectronic* wavefunction[8].

1.5   The Spin-Coupled equations

Let us now discuss the Spin Coupled equations which arise from the application
of the variational principle. Although the optimization of the SC function
is actually performed directly by minimizing the energy expression with an
efficient Newton-Raphson algorithm (Goldfed et al., 1996), it is interesting to
briefly sketch the derivation of the SC equations in order to make easier the
comparison with the well known HF equations.

We consider only the variations of the orbitals since the variations of the
spin-coupling coefficients lead to a common secular problem (with fixed orbital
configuration). Furthermore, it is clearly sufficient to consider only the varia-
tion of one orbital, say ϕ_1, the other variations differing only in the labeling of
the orbitals. Thus, we consider in the energy expression an orbital variation
$|\delta\phi_1\rangle$ subject to the orthogonality condition

$$\langle \delta\phi_1 | \phi_1 \rangle = 0, \ \ i.e. \ |\delta\phi_1\rangle \in |\phi_1\rangle^{\perp} \tag{1.6}$$

that arises from the normalization condition

$$\langle \phi_1 | \phi_1 \rangle = 1$$

The variation of the energy functional assumes the form

$$\left\langle \delta\phi_1..\phi_N \middle| (H - E) \sum_P \epsilon_P \langle \Theta_{SM} | P^{\sigma} | \Theta_{SM} \rangle P^r \{\phi_1..\phi_N\} \right\rangle = 0$$

where the energy E reflects the normalization condition of the *full* wavefunction
which is not guaranteed by the orbital normalization. This energy comes from
the secular (spin) problem, which is solved for fixed $\{\phi_1..\phi_N\}$ orbitals. Then,
if one uses the factorization of the symmetric group S_N brought by the S_{N-1}
subgroup of the $\{2,3,..N\}$ electrons, he obtains

$$\langle \delta\phi_1 | \sum_{m=1}^{N} \sum_{P \in S_{N-1}} \epsilon_{PP_m} \langle \Theta_{SM} | P^{\sigma} P_m | \Theta_{SM} \rangle \cdot$$

$$\cdot \langle \phi_2..\phi_m..\phi_N | (H - E) P^r \{\phi_2..\phi_1..\phi_N\} \rangle | \phi_m \rangle = 0$$

---

[8]The correlation brought by the SC function is the non-dynamical correlation discussed
above. Furthermore, some contributions arises from relaxing orthogonality conditions: these
conditions are inessential only when the wavefunction has a determinantal form.

where P_m is the permutation $(1, m) \to (m, 1)$ and

$$\langle \phi_2..\phi_m..\phi_N | (H - E) P^r \{\phi_2.\phi_1.\phi_N\} \rangle$$

is a scalar product in the $N - 1$ electron space of the electrons $\{2, 3, ..N\}$. Now, the above double sum must be orthogonal to $|\delta\phi_1\rangle$ which, in turn, spans the orthogonal complement of $|\phi_1\rangle$, eq.(1.6). Thus, it follows

$$\sum_{m=1}^{N} \sum_{P \in S_{N-1}} \epsilon_{PP_m} \langle \Theta_{SM} | P^\sigma P_m | \Theta_{SM} \rangle \cdot$$

$$\cdot \langle \phi_2..\phi_m..\phi_N | (H - E) P^r \{\phi_1..\phi_2..\phi_N\} \rangle | \phi_m \rangle = \epsilon_1 |\phi_1\rangle$$

or in general

$$\sum_{m=1}^{N} F_{km} |\phi_m\rangle = \epsilon_k |\phi_k\rangle \tag{1.7}$$

where the F_{km} are monoelectronic operators given by the previous equation and by other analogous equations obtained from the variation of the k-th orbital. These operators can be defined as Gerratt(1971) originally did[9], (for brevity $|u\rangle = |\phi_u\rangle$)

$$F_{km} = D(k|m)(h - \gamma_{km}) + \sum_{u,v}^{N} D(ku|mv)[\gamma_{km} \langle u|h|v \rangle + G(uv)] +$$

$$+ \frac{1}{2} \sum_{u_1 u_2 v_1 v_2}^{N} D(ku_1 u_2 | mv_1 v_2) \langle u_1 u_2 | v_1 v_2 \rangle \gamma_{km}$$

In this expression the D's are the spin-free density matrices of the first ($D(u|v)$), of the second ($D(u_1 u_2 | v_1 v_2)$) and of the third ($D(u_1 u_2 u_3 | v_1 v_2 v_3)$) order, $\gamma_{km} = 1 - \delta_{km}$ and $G(uv) = \langle u|g|v \rangle$, with g the usual electronic repulsion operator $g = r_{12}^{-1}$. In general, the n-th derivative of the energy needs the use of the density matrix of the $(n + 2)$-th order. Their computation is the bottleneck of the SC optimization, which at present can handle up to $N = 12$ "active" electrons.

The D's density matrices are actually discrete representations of the Spin Coupled (spin-free) density matrices, that is

$$\gamma^{(p)} = \sum_{u_1 u_2..u_p v_1 v_2..v_p} |u_1 u_2..u_p\rangle \, D^{(p)}(u_1 u_2..u_p | v_1 v_2..v_p) \, \langle v_1 v_2..v_p |$$

---

[9]They are not uniquely defined since we can always add a projector onto $|\phi_m\rangle^\perp$ and leave unchanged eq.(1.7).

where

$$\gamma^{(p)} = \mathrm{Tr} \left| \psi_{SM}^N \right\rangle \left\langle \psi_{SM}^N \right|$$

is the p-th order spin-free density matrix (Tr is the trace in the spin space and in the particle space of $N - p$ electrons). These discrete density matrices can be obtained form the following recurrence relation[10]

$$D^{(p)}(u_1 u_2 .. u_p | v_1 v_2 .. v_p) = \sum_{q=1}^{N} D(u_1 u_2 .. u_p u_{p+1} | v_1 v_2 .. v_{p+q}) \left\langle u_{p+1} \middle| v_{p+q} \right\rangle \quad (1.8)$$

Apart from the spin-coupling dependence, the highest order density matrix is a pure group-theoretical object

$$\gamma^{(N)} = \sum_{u_1 u_2 .. u_N v_1 v_2 .. v_N} \left| u_1 u_2 .. u_N \right\rangle D^{(N)}(u_1 u_2 .. u_N | v_1 v_2 .. v_N) \left\langle v_1 v_2 .. v_N \right|$$

since

$$D^{(N)} = \sum c_k^* c_l D_{kl}^{(N)}$$

and

$$D^{(N)}(u_1 u_2 .. u_N | v_1 v_2 .. v_N) = \epsilon_P \left\langle \Theta_{SM;k}^N \middle| R \middle| \Theta_{SM;l}^N \right\rangle$$

where R is the permutation that brings $\{v_1 v_2 .. v_N\}$ in $\{u_1 u_2 .. u_N\}$. Thus, one may start from the highest order matrix and use the recurrence relations eq.(1.8) to obtain the matrices of any desired order. In practice, the *in situ* generation of the matrices, using the so-called "super-cofactor" approach, have been shown to be more efficient (Sironi, 1989; Cooper et al., 1993) and it has allowed to reach the present capabilities of the SC codes.

The F_{km}'s operators are the Spin-Coupled counterparts of the Hartree-Fock operator. They enter the SC equations much like the HF effective operator enters the HF equations, that is they depend on the orbitals and entail an "effective-field" which the orbitals are subjected to. The difference with the HF equation is that, now, each orbital has its *own set* of operators. This set

---

[10]This amounts to take the following monoelectronic trace

$$\gamma^{(p)} = \frac{1}{N - p} tr \, \gamma^{(p+1)}$$

where the $(N - p)^{-1}$ factor arises from the McWeeny's normalization

$$Tr \, \gamma^{(p)} = \left(\begin{array}{c} N \\ p \end{array} \right) p! = \frac{N!}{(N - p)!}$$

which gives the number of p-uples taken among N elements in any order. With this normalization, the "extensivity" is brought into the density operator; for example, a bielettronic operator $A = \sum_{kl}^{k \neq l} A_{kl}$ has mean value $Tr(\gamma^{(2)} A_{12})$.

couples the motion of the electron described by the orbital in consideration with those of the other $N - 1$ electrons. The on-diagonal operator

$$F_{kk} = D(k|k)h + \sum_{u,v}^{N} D(ku|kv)G(uv)$$

resembles the *Hartree* operator of the Hartree method (the selection rule $D(kk|uv) = 0$ eliminates the self-interaction term) and it is expected to give the main contribution to the "effective field" for the k-th orbital. In this way all the orbitals are allowed to fit in the molecular environment, looking for the greatest nuclear attraction while keeping low the electronic repulsion.

In order to highlight the differences with the HF method it is worth to introduce an *"external* direct sum" much like we will do in the different context of the multichannel scattering theory (see Chapter 3 and in particular Section (3.2); there are remarkable similarities between this problem and the multichannel scattering problem). We define an enlarged orbital space as the direct sum of each orbital space, $\mathcal{H}_k$,

$$\mathcal{H}_N = \sum_{k}^{\oplus} \mathcal{H}_k$$

in such a way our orbitals $\{\phi_1..\phi_N\}$ are the components of a vector in this space

$$|\Phi\rangle = \{|\phi_1\rangle, .. |\phi_N\rangle\}$$

Then, the F_{km} operators become the matrix elements of an effective operator F (a "super operator") which acts in this space. The SC equations, eq.(1.7) can be written as

$$\mathbf{F}|\Phi\rangle = \boldsymbol{\epsilon}|\Phi\rangle$$

where $\boldsymbol{\epsilon}$ is a *diagonal* operator in $\mathcal{H}_N$, the diagonal elements being simple scalar multiplications (note that this problem differs from eigenvalue or pseudo-eigenvalue problems). The difference with the HF method is soon evident: if we realize the same construction for an HF wavefunction we are lead to a similar equation in which the superoperator $\mathbf{F}$ is *already* diagonal, with the usual Hartree-Fock operator on each diagonal element[11].

The final, hypothetical "Self-Consistent-Field" algorithm for optimizing the Spin Coupled wavefunction is therefore as follows: one solves the orbital equations with a trial spin function (and the corresponding energy E) and obtains

---

[11]Indeed, the corresponding F_{km} operators are null because $D(ku|kv) = 0$ for orthogonal orbitals when $k \neq m$.

an improved set of orbitals; then, he uses this new set of orbitals in the secular problem

$$\sum_l \left\{ \langle \psi_k | H | \psi_l \rangle - E \langle \psi_k | \psi_l \rangle \right\} c_l = 0 \tag{1.9}$$

(where the ψ_k's are the structures of Section (1.2)) in order to determine a better set of coupling coefficients, go back to the orbital equations and so on. In practice, as already mentioned, direct minimization of the energy functional is more efficient, just like in the HF optimization.

It is interesting, however, to note how the overlap properties of the orbitals determine the spin coupling. In order to show this we take a simple $2n$ electron model system in which our best orbital configuration turns out to be composed of a set of "orthogonal pairs"

$$\langle \phi_{2i-1} | \phi_{2i} \rangle = s_i \ i = 1, 2, ..N$$

$$\langle \phi_{2i-1} | \phi_{2j-1} \rangle = \langle \phi_{2i-1} | \phi_{2j} \rangle \simeq 0 \ i \neq j$$

each of which well *localized* so that we can neglect the inter-pair electronic repulsions. Then, it is possible to show that the spin equation simplifies to

$$\left\{ \sum_{i=1}^{n} (J_i - K_i P_i^\sigma) \Pi_{j=1, j \neq i}^{n} (1 - |S_j|^2) \right\} |\Theta_{SM}\rangle = E \left\{ \Pi_{j=1}^{n} (1 - |S_j|^2 P_j) \right\} |\Theta_{SM}\rangle$$

where P_i is the transposition of the i-th couple (i.e. $(2i - 1, 2i) \rightarrow (2i, 2i - 1)$) and J_i, K_i and S_i are the Heitler-London integral defined in Section (1.1). Then, the solution of this equation for the singlet state is the perfect-pairing Rumer function (the "Lewis structure") and the corresponding energy is a sum of HL contributions from each bond

$$E = \sum_{i=1}^{n} \frac{J_i + K_i}{1 + |S_i|^2}$$

In closing this Section it is worth to mention that, although at present the application of the SC method is restricted to few electrons, it is possible to freeze the "core" electrons of a many-electron system in doubly occupied MO orbitals and perform the SC optimization of the valence, most important part of the electronic configuration. Furthermore, the MO core can be *optimized* in the presence of the SC valence orbitals (see Karadakov et al.(1992) and reference therein).

1.6 The SCVB method

Much like what happens in the MO's theory one can introduce correlation in the mono-electronic SC wavefunction exciting the "occupied" orbitals in appropriate *virtual* orbitals, in such a way to build a Configuration Interaction (CI) wavefunction. The differences with the MO's theory are that now we have to introduce only the *dynamical* correlation and, further, that in our CI wavefunction the Configuration State Functions (the *structures* in this context) are non-orthogonal. Furthermore, since the SC function is a *very good* reference function for this excitation step, the resulting Valence Bond wavefunction turns out to be dominated by the SC contribution; thus, this property allows an accurate description of electronic structure while still preserving a clear physical picture of the underlying interactions (Cooper et al., 1987; Cooper et al., 1991).

There are at least two ways to generate the virtuals in SC framework. Here we consider the early, computationally simple approach developed by Gerratt and Raimondi (1980), which gave rise to the so-called Spin Coupled Valence Bond (SCVB) method. In the next Section we will consider a more recent improved version, usually known as the SCVB* method.

As already mentioned in the previous Section, the SC equations are rather different from the HF ones, being not pseudoeigenvalue equations. Thus, it is not straightforward to generate virtual orbitals using "excited" solutions of the problem. However, with the solution of SC problem at hand, it is possible to rewrite the Spin Coupled equations eq.(1.7) using the Lowdin's partitioning technique so that to isolate an effective monoelectronic operator for *each* orbital,

$$(F_{kk} - \epsilon_k) \, |\phi_k\rangle = \sum_{v,v \neq k} F_{kv} \, |\phi_v\rangle$$

$$F_{mk} \, |\phi_k\rangle = - \sum_{v,v \neq k} (F_{mv} - \epsilon_m \delta_{mv}) \, |\phi_v\rangle = - \sum_{v,v \neq k} G_{mv} \, |\phi_v\rangle \ \text{ for } m \neq k$$

In these formulas $\mathbf{G}$ is, in the language of the previous Section, an (adjoint) super-operator that acts in the space $\mathcal{H}_{N-1}$ obtained from $\mathcal{H}_N$ by striking out the k-th component. In other words, when the usual expansion of the orbitals on an atomic basis set is performed, the $\mathbf{G}$ operator becomes a $(N-1)\mathrm{x}(N-1)$ (super)matrix obtained from the (super)matrix $\mathbf{F} - \boldsymbol{\epsilon}$ by striking out the k-th (super)row and the k-th (super)column. Thus, solving for $|\phi_v\rangle$ the last equation and introducing the result in the first equation, one obtains

$$\left\{ F_{kk} - \sum_{v,m(v,m \neq k)} F_{kv} (\mathbf{G}^{-1})_{vm} F_{mk} \right\} |\phi_k\rangle = \epsilon_k \, |\phi_k\rangle$$

where $\mathbf{G}^{-1}$ is a kind of Green's operator in the $\mathcal{H}_{N-1}$ space that enters in the construction of an *effective potential* for the k-th orbital

$$V_k^{eff} = - \sum_{v,m(v,m \neq k)} F_{kv}(\mathbf{G}^{-1})_{vm}F_{mk}$$

(the similarities with the partitioning technique used in multichannel scattering theory, to be discussed later in Section (3.5), are remarkable. In that context the effective potential is known as *optical* potential since it is not necessarily self-adjoint and thus can absorb flux. In our case it is self-adjoint).

One can therefore write an eigenvalue problem

$$F_k^{(eff)}\ket{\phi} = \epsilon \ket{\phi} \tag{1.10}$$

where the *effective* (self-adjoint) *operator* $F_k^{(eff)}$ is the sum of the previous diagonal ("Hartree" operator) F_{kk} and the effective potential arising from the interaction of the electron described by the k-th orbital with the other electrons,

$$F_k^{(eff)} = F_{kk} + V_k^{(eff)}$$

The k-th "occupied" SC orbital, $\ket{\phi_k}$, obtained in the Spin Coupled optimization step, is therefore one of the solutions of eigenvalue problem of eq.(1.10) and, usually, but not always, is the one with the lowest (orbital) energy. The other solutions of eq.(1.10) are *virtual* orbitals that can be used to build the final non-orthogonal CI wavefunction, the SCVB function. The difference with the HF-MO theory is that, now, each virtual comes from an effective $N-1$ electron field, as it must be, and *not* from a N electron field, besides having its *own* specific electron field. Thus, the resulting SCVB expansion is, for the same accuracy, considerable shorter than conventional MO-CI expansions (see Cooper et al. (1987) and reference therein).

The SCVB function is obtained, just like in the MO theories, by performing excitations of the occupied SC orbitals into the virtuals obtained by diagonalization of the effective operators. Each SC orbital has its own *stack* of virtuals, the SC orbital and the virtual being orthogonal to each other *within* this stack. In other words, this method allows to decompose each orbital space, $\mathcal{H}_k$, in orthogonal one-dimensional subspaces, made up of the k-th SC orbital and its virtuals. Since the spaces $\mathcal{H}_k$ are clearly equal to each other we can say that we perform in this way different decompositions of the same one-electron space *adapted* to the particular molecular environment.

The excitations are usually "vertical", in the sense that each occupied orbital is excited into a virtual of its own stack, but clearly "crossed" excitation can

be done. In the case of vertical excitation, the final VB function becomes

$$\left|\Psi_{SM}^{N}\right\rangle = A \sum_{k} \left\{ c_{k}^{(0)} \left|\phi_{1}^{(0)}..\phi_{N}^{(0)}; \Theta_{SM;k}^{N}\right\rangle + \sum_{m}^{\alpha} c_{m;k}^{\alpha} \left|\phi_{1}^{(0)}..\phi_{m}^{(\alpha)}..\phi_{N}^{(0)}; \Theta_{SM;k}^{N}\right\rangle + \right.$$

$$\left. + \sum_{m,n}^{\alpha,\beta} c_{mn;k}^{\alpha\beta} \left|\phi_{1}^{(0)}..\phi_{m}^{(\alpha)}\phi_{n}^{(\beta)}..\phi_{N}^{(0)}; \Theta_{SM;k}^{N}\right\rangle .. \right\}$$

$$(1.11)$$

where $\phi_{m}^{(\alpha)}$ is the α-th orbital in the m-th stack ($\alpha = 0$ denotes the corresponding occupied SC orbital), the sums over greek indexes run over the virtuals and the spin coupling coefficient $c_{m;k}^{\alpha}$ are variationally determined by solving the corresponding (non-orthogonal) secular problem with an efficient VB code. It is worth to mention in this context that the virtual space of each SC orbital is, actually, the space on which the orbital variations $|\delta\phi_{k}\rangle$ of the previous Section were performed in order to give variational SC orbitals (see eq.(1.6)). Thus, it follows that each virtual satisfy a kind of Brilloun theorem when employed in vertical excitation

$$\left\langle A\left\{\phi_{1}^{(0)}..\phi_{m}^{(\alpha)}..\phi_{N}^{(0)}\right\} \left| H - E_{SC} \right| A\left\{\phi_{1}^{(0)}..\phi_{m}^{(0)}..\phi_{N}^{(0)}\right\} \right\rangle = 0$$

where E_{SC} is the Spin Coupled energy.

1.7 Perturbative optimization of virtual orbitals

The Valence Bond expansion of eq.(1.11) can be considerably shortened if foptmizationor each occupied SC orbital we *optimize* the virtual orbitals in such a way to lower the energy of the corresponding VB wavefunction. Needless to say, such "MultiConfiguration Self-Consistent Field" optimization of the wavefunction is beyond the current computational capabilities. However, it is possible to *approximately* (and cheaply) optimize a reduced set of orbitals in such a way that when these orbitals are used in the non-orthogonal CI wavefunction it turns out to be substantially improved (Raimondi et al., 1996). We describe here briefly the main ideas behind this method.

As is well known, correlation corrections are mainly brought by doubly excited configurations and, thus, one may focus on optimizing a function of the form

$$\left|\Psi\right\rangle = c_{SC} \left|\Psi_{SC}\right\rangle + \sum_{m,n} c_{mn} \left|\Psi_{mn}\right\rangle \qquad (1.12)$$

where one keeps fixed the Spin-Coupled $|\Psi_{SC}\rangle$ wavefunction and optimizes the virtuals $|\phi_{m}^{+}\rangle$ that enter in the double excited configurations

$$\left|\Psi_{mn}\right\rangle = \left|\phi_{1}..\phi_{m}^{+}..\phi_{n}^{+}..\phi_{N}\right\rangle$$

(when no superscript appear we refer to an occupied SC orbital). Furthermore, since we are interested in optimizing virtuals to be used subsequently in the (linear) variational optimization of the final VB function, we can minimize the *perturbative* expression of the energy, i.e. we can consider in eq.(1.12) the SC function like an "unperturbed" wavefunction and the doubly excited configurations like perturbative corrections to such wavefunction; these configurations then give the (second order) perturbative correction to the SC energy. The use of this perturbative expression of the energy, which reads

$$E^{(2)} = \sum_{mn} \frac{\left(H_{(0,mn)} - H_{(00)}S_{(0,mn)}\right)^2}{\left(H_{(0,0)}S_{(mn,mn)} - H_{(mn,mn)}\right)}$$

where $H_{(0,0)} = E_{SC}$

$$H_{(0,mn)} = \langle \Psi_{SC} | H | \Psi_{mn} \rangle$$

$$H_{(mn,mn)} = \langle \Psi_{mn} | H | \Psi_{mn} \rangle$$

$$S_{(0,mn)} = \langle \Psi_{SC} | \Psi_{mn} \rangle$$

$$S_{(mn,mn)} = \langle \Psi_{mn} | \Psi_{mn} \rangle$$

is particularly useful since it requires only "diagonal" and "first row" elements of the operators H and 1. In practice, the most recent version of the optimization code fixes the spin coupling coefficients at their SC level and uses an approximate Hessian matrix in a Newton-Raphson algorithm which ensures good convergence properties, while maintaining low the overall CPU time. Indeed, the approximate second derivatives require only density matrix elements up to third order, i.e. the same needed for a pure gradient driven optimization (Clarke et al., 1998a). Thanks to the good choice of the unperturbed wavefunction, the overall procedure turns out to work well in producing optimized virtuals while maintaining low the computational cost[12].

---

[12]It is worth to mention that the procedure outlined here can be employed to optimize a set of orbitals at time. It has become usual practice to optimize *pairs* of orbitals at time, and this is the method actually used in our work (see Part II).

Chapter 2

Single channel collision theory

In this and the next two chapters we will briefly review the collision theory. Only a short summary of this fascinating matter will be presented; the interested reader is referred to the excellent book of Taylor (1969) for an introduction to the topic and to the books of Levine (1969), Gianturco (1979) and J. Zhang (1999) for closer looks at molecular problems.

In this chapter we will consider the so-called single channel collision theory. Although this theory does not concern directly our work it allows for the introduction of some basic concepts of scattering theory, without the inessential complications that arise from the internal structure of the colliding partners. As a typical system we may consider two noble gas atoms that, for many purposes, are equivalent to two structureless particles. We remove from the beginning the center-of-mass motion, i.e. we take into account the linear momentum conservation law in order to work with the relative motion of the two partners. Thus the hamiltonian of the system is

$$H = \frac{\mathbf{p}^2}{2\mu} + V(\mathbf{x}) = H^0 + V(\mathbf{x})$$

where $\mathbf{p}$ is the momentum operator for the relative motion, μ is the reduced mass of the binary system and $V(\mathbf{x})$ is the interaction potential which is a function of the relative position vector operator $\mathbf{x}$; H^0 defined by this equation is the hamiltonian of the system in absence of interaction. The corresponding Hilbert space for the relative motion is denoted with $\mathcal{H}$.

2.1 Wave operators

A scattering event can be schematically divided in three steps:

- long before the collision takes place the atoms are far apart, do not experience any interaction and move according to the given "initial collision conditions";

- during "the collision time" the atoms undergo a very complicated motion that depends on the interaction potential acting on them;

- long after the collision the atoms move again freely and follow a "free" orbit determined by the collision.

In classical mechanics this means that as $t \to -\infty$

$$\mathbf{x}(t) \to \mathbf{x}^o(t) = \mathbf{b}_{in} + \mathbf{v}_{in}\, t$$

where $\mathbf{v}_{in}$ is the initial velocity vector and $\mathbf{b}_{in}$ is the position that the system would have at time $t = 0$ in absence of interaction; analogously, as $t \to +\infty$

$$\mathbf{x}(t) \to \mathbf{x}^o(t) = \mathbf{b}_{out} + \mathbf{v}_{out}\, t$$

where $\mathbf{v}_{out}$ is the final velocity vector and $\mathbf{b}_{out}$ is the position that the system would have had at time $t = 0$ if it had moved freely all the time. For each specified "in" asymptotic state (the vectors $\mathbf{b}_{in}$ and $\mathbf{v}_{in}$) there is an "out" asymptotic state (the vector $\mathbf{b}_{out}$ and $\mathbf{v}_{out}$) and *viceversa*; the one-to-one correspondence is given by the actual orbit of the system, $\mathbf{x}(t)$, which in turn is determined by the laws of motion. Every orbits with an "in" asymptote have an "out" asymptote, that is they are truly "scattering orbits"; however, they are not, usually, all the possible orbits of the system because there can be orbits in which the system is bound at all times: the bound and scattering orbits represent all the possible orbits of the system[1].

In quantum mechanics the situation is very similar: a *scattering* "orbit" (in the relevant Hilbert space) should resemble the "free" motion as $t \to \pm\infty$, i.e.

$$U_t \left| \psi \right\rangle \to U_t^0 \left| \psi_{in} \right\rangle = e^{-iH^0 t} \left| \psi_{in} \right\rangle \ \text{ as } t \to -\infty$$

where $\left| \psi_{in} \right\rangle$ is the "position" in the Hilbert space of system that the system would have at $t = 0$ in absence of interaction and

$$U_t \left| \psi \right\rangle \to U_t^0 \left| \psi_{out} \right\rangle = e^{-iH^0 t} \left| \psi_{out} \right\rangle \ \text{ as } t \to +\infty$$

where $\left| \psi_{out} \right\rangle$ is the position that the system would have had at $t = 0$ if it had moved freely at all times. The two vectors $\left| \psi_{in} \right\rangle$ and $\left| \psi_{out} \right\rangle$ are known as

---

[1]These consideration actually apply to "reasonable" potentials. See below for the quantum case.

(in/out) asymptotic states. We expect that for each "in" state $|\psi_{in}\rangle$ exists an "out" state $|\psi_{out}\rangle$ and that there is a one-to-one correspondence between them determined by the full evolution operator. Furthermore, as in the classical case, we expect that these *scattering* states are not all the possible states of the system, because the potential could support some bound states which cannot have asymptotes. However, the scattering and bound states should be all the possible states of the system. For reasonable potentials[2] this turn out to be the case; one can indeed prove some fundamental theorems which we are going to describe.

Asymptotic condition. For every $|\psi_{in}\rangle$ in the Hilbert space of the system there is a $|\psi_0\rangle$ such that

$$U_t |\psi_0\rangle - U_t^0 |\psi_{in}\rangle \ \to 0 \text{ as } t \to -\infty$$

and likewise for every $|\psi_{out}\rangle$ in $\mathcal{H}$.

This theorem in practice states that *every* state of the system can be an asymptotic state, i.e. the experimentalist can choose any arbitrary state to do scattering experiments. This may seem surprising because among the states of the systems there can be some bound states, which we know do not have asymptotes; however, one should reflect on the definition of the *asymptotic* state: it moves according to the *free* evolution operator and only when the time is let to go to infinity its orbit resembles the actual orbit of the system.

The vector $|\psi_0\rangle$ is the state at the time $t = 0$ which (uniquely) characterizes that particular orbit with the specified asymptote. It is obtained by the following limiting operation

$$|\psi_0\rangle = lim_{t \to -\infty} U_t^\dagger U_t^0 |\psi_{in}\rangle = \Omega_+ |\psi_{in}\rangle \tag{2.1}$$

which defines the *Møller operator* Ω_+ for the incoming asymptote; similarly one can introduce another Møller operator, Ω_-, for the outgoing asymptote

$$\Omega_- = lim_{t \to +\infty} U_t^\dagger U_t^0 \tag{2.2}$$

which relates the "out" asymptote to the actual state of the system at $t = 0$. The two Møller operators are *half collision* operators, in the sense they divide the duration of the process in two (infinite) time intervals. The role of the $t = 0$ instant of time (and that of the two operators) depends on the actual

---

[2]The results that follow are surely valid for continuous potentials that are less singular than $r^{-3/2}$ at the origin and fall off faster than r^{-3} at infinity (see Chapter 2 of the book of Taylor(1969)). However, these are *sufficient* conditions; some results can be proved under weaker conditions.

states involved. In some cases, like photodissociation experiments, one is able to produce a state at $t = 0$ which is well localized into the interaction region and the Ω_- operator truly characterize an *half* collision process. Adversely, in cross-beam experiments one produces a state in which the two atoms are initially far apart and with a momentum distribution directed toward the interaction region; for this initial state the action of the full evolution operator U_t *in the past* is equivalent to that of the *free* evolution operator U_t^0 and therefore it follows that

$$|\psi_0\rangle \simeq |\psi_{in}\rangle \tag{2.3}$$

(i.e. *for our particular choice of the initial state* $\Omega_+ \simeq \mathbf{I}$ [3]). In this case Ω_- clearly describes the *full* collision process.

The two Møller operators are limits of unitary operators and thus are *isometric*. In general, however, they are not *unitary,* because unitarity means that *every* state of the system has an (in/out) asymptote and this can only happen when the system does not have bound states[4]. The Ω_+ operator maps the space of the asymptotic states (the *entire* $\mathcal{H}$) onto a subspace, the space of states that have an *incoming* asymptote, $\mathcal{R}_+ = \Omega_+(\mathcal{H})$. Analogously, Ω_- maps $\mathcal{H}$ onto $\mathcal{R}_- = \Omega_-(\mathcal{H})$, the space of states with an *outgoing* asymptote. For a state in the appropriate space, $|\psi_0\rangle \in \mathcal{R}_\pm$, we may write

$$U_t |\psi_0\rangle \to U_t^0 \Omega_\pm^\dagger |\psi_0\rangle \text{ as } t \to \mp\infty \tag{2.4}$$

where we have used the isometric relation. Therefore when $|\psi_0\rangle \in \mathcal{R}_+ \cap \mathcal{R}_-$ we obtain a nice picture of the collision (see Fig.(2.1)): the system evolves along the orbit $U_t |\psi_0\rangle$ from an "in" asymptotic state $|\psi_{in}\rangle = \Omega_+^\dagger |\psi_0\rangle$ to an "out" asymptotic state $|\psi_{out}\rangle = \Omega_-^\dagger |\psi_0\rangle$, the two asymptotes being related by the *scattering operator S*

$$|\psi_{out}\rangle = \Omega_-^\dagger \Omega_+ |\psi_{in}\rangle = S |\psi_{in}\rangle \tag{2.5}$$

that represents the most important tool of scattering theory. To investigate its properties we continue on showing two more results.

Orthogonality. The space of the states with an "in" (out) asymptote, $\mathcal{R}_+ (\mathcal{R}_-)$ is orthogonal to the space spanned by the bound states of the system, $\mathcal{B}$. In other words, $\mathcal{R}_\pm \subset \mathcal{B}^\perp$.

---

[3]This means that with our choice we can neglect the distortion caused by the potential "in the past". There are situations, e.g. weak potentials and high collision energies, in which this approximation is good also for wavepackets well spread in space (or peaked in the momentum distribution); in these cases this approximation is known as the *Born approximation.*

[4]The isometric properties is expressed by the relation $\Omega^\dagger\Omega = 1$ while unitarity requires in addition that $\Omega\Omega^\dagger = 1$ holds. The latter means that $\Omega(\mathcal{H}) = \mathcal{H}$, i.e. that the operator is *suriettive.*
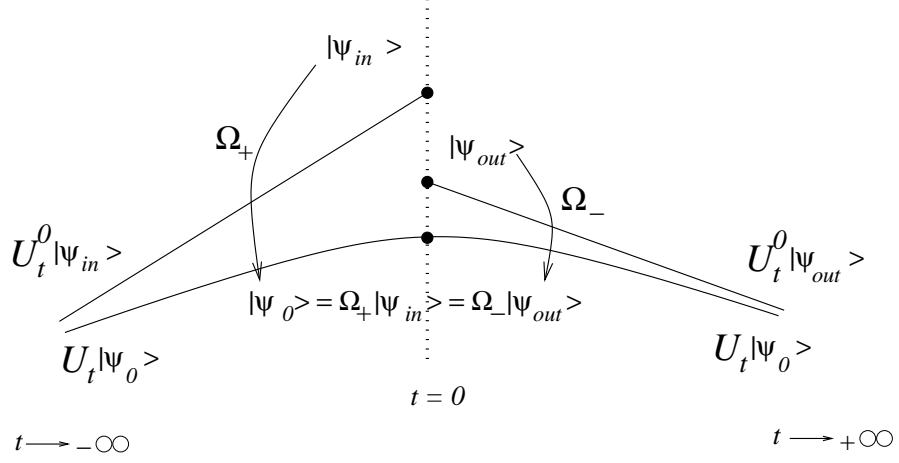
Figure 2.1: A pictorial description of a scattering "orbit". The vertical line represent the Hilbert space $\mathcal{H}$ and the dots mark the "position" of the relevant vectors.

This theorem states formally what we stressed previously: the bound states of the system cannot have asymptotes. Moreover, it shows that the *scattering* states must lye in the space spanned by the *continuum* eigenvectors of the spectrum of the hamiltonian operator H; only in that space one can describe a motion that extend to infinity.

Asymptotic completeness. The space of the states with "in" asymptote coincides with the space of the states with "out" asymptote, $\mathcal{R}_+ = \mathcal{R}_- = \mathcal{R}$, and they *are* the orthogonal complement of $\mathcal{B}$, $\mathcal{R} = \mathcal{B}^\perp$. In other words, $\mathcal{H} = \mathcal{B} + \mathcal{R}$.

This is the most important result (and the most difficult to prove, see discussion on p. 33 of Taylor(1969)) on which the S operator lays its foundation. From a physical point of view it states that *every* orbit with an "in" asymptote has an "out" asymptote (i.e. that such an orbit represents a *true* scattering event) and that the scattering and the bound orbits are *all* the possible orbits of the system. From a formal point of view this means that the Møller operators have a common image and therefore the S operator

$$S = \Omega_-^\dagger \Omega_+ \tag{2.6}$$

is a well defined operator which maps the space of in-asymptotes ($\mathcal{H}$) onto the space of out-asymptotes ($\mathcal{H}$) with a one-to-one correspondence. Since the Møller operators are isometric the scattering operator turns out to be

unitary[5]. This mathematical property has the very important meaning of *law of conservation of probability (particle number)* in a scattering event. Another very important conservation law, the *conservation of energy*, follows from the so-called *intertwining relation*

$$\Omega_{\pm} H^0 = H \Omega_{\pm} \tag{2.7}$$

which relates the *asymptotic* hamiltonian (or any function of it) to the *actual* one (or the same function of it). The conservation of energy takes the form

$$[S, H^0] = 0$$

where we recall that H^0 is the *free* hamiltonian: since S maps asymptotic states it commutes with the asymptotic hamiltonian. It should be noted that the intertwining relation (2.7) has importance in its own rights: for example, *every* (improper) eigenvector of the free hamiltonian gives rise to a corresponding (improper) eigenvector of the full hamiltonian[6]. This fact opens the way for the *time-independent* scattering theory, which is the subject of Section 2.3. At the moment, however, we can note the following: because of the asymptotic completeness one can construct a *basis* of $\mathcal{H}$ that is adapted to the decomposition of the space in scattering and bound states. For example, if the vectors $\{|\psi_n\rangle\}$ form a basis of $\mathcal{H}$ then the scattering vectors $|\psi_n+\rangle = \Omega_+ |\psi_n\rangle$, together with the bound states $\{|\phi_n\rangle\}$ of the full hamiltonian, form another basis of $\mathcal{H}$
,

$$\mathbf{I} = \sum_n |\phi_n\rangle \langle \phi_n| + \sum_n |\psi_n+\rangle \langle \psi_n+|$$

In particular, one may use the momentum eigenvectors $\{|\mathbf{p}\rangle\}$ of the free hamiltonian (or other eigenvectors) to write down two useful resolutions of the identity operator

$$\mathbf{I} = \sum_n |\phi_n\rangle \langle \phi_n| + \int d^3 p \, |\mathbf{p}+\rangle \langle \mathbf{p}+| = \sum_n |\phi_n\rangle \langle \phi_n| + \int d^3 p \, |\mathbf{p}-\rangle \langle \mathbf{p}-| \tag{2.8}$$

in terms of vectors that, in view of eq.(2.7), are *eigenvectors* of the *full* hamiltonian[7].

---

[5]The result is contained in the chain of mappings: $\Omega_-^{\dagger}$ is an operator extension of the *inverse* of Ω_- , $\Omega_-^{\dagger} \supseteq \Omega_-^{-1}$, which by definition maps the range of the operator back to its domain, in this case $\mathcal{H}$. Thus, if it happens that $\mathcal{R}_- \supseteq \mathcal{R}_+$ the chain of mappings is *suriettive*. For completeness, it should be said that the orthogonality theorem implies $\Omega_-^{\dagger}(\mathcal{B}) = \{0\}$, i.e. that $\mathcal{B}$ is the *kernel* of the operator $\Omega_-^{\dagger}$.

[6]Actually, this needs some care. We have seen that the Møller operators are well defined on *true* vectors of the Hilbert space $\mathcal{H}$.

[7]Eq.(2.7) shows why, in general, the Møller operators cannot be unitary. If they were unitary H would have the *same* spectrum of H^0 .

2.2 Cross sections

Collisions change the state of the system and therefore can modify the mean value of observables that otherwise would be constant. Gaseous systems reach the macroscopic equilibrium through this mechanism[8]. For example, in a gas of noble atoms every binary collision changes the magnitude and the direction of the velocity vectors of the atoms until they reach the equilibrium Boltzmann distribution[9]. Keeping this in mind, we consider a generic observable A compatible with the energy of the free system, i.e.

$$[A, H^0] = 0 \tag{2.9}$$

whose mean value on a scattering orbit is expected to become constant as $t \to \pm\infty$. Let $|\psi_0\rangle$ be a scattering state, i.e. $|\psi_0\rangle \in \mathcal{R}$, which originates from a given "in" asymptotic state, $|\psi_0\rangle = \Omega_+ |\psi_{in}+\rangle$. The mean value of the observable A at the time t is given by

$$< A >_t = \langle \psi_t | A | \psi_t \rangle = \langle U_t \psi_0 | A | U_t \psi_0 \rangle$$

Using eq.(2.4) and eq.(2.9) we can write

$$< A >_{-\infty} = lim_{t \to -\infty} \langle U_t \psi_0 | A | U_t \psi_0 \rangle =$$
$$lim_{t \to -\infty} \langle U_t^0 \psi_{in} | A | U_t^0 \psi_{in} \rangle = \langle \psi_{in} | A | \psi_{in} \rangle$$

and analogously

$$< A >_{+\infty} = lim_{t \to +\infty} \left\langle U_t^0 \Omega_-^\dagger \psi_0 \left| A \right| U_t^0 \Omega_-^\dagger \psi_0 \right\rangle = \left\langle \psi_{in} \left| S^\dagger A S \right| \psi_{in} \right\rangle$$

Thus, we see that the "collision change" of the value of the observable, ΔA_{coll}, is given by the following simple relation[10]

$$\Delta A_{coll} = \left\langle \psi_{in} \left| S^\dagger A S - A \right| \psi_{in} \right\rangle$$

When the system is not in a pure state one has to introduce a density matrix; in that case the above result can be rewritten as

$$\Delta A_{coll} = Tr\{\rho_{in}(S^\dagger A S - A)\} \tag{2.10}$$

---

[8]We are not claiming that this result is well understood...

[9]Note that we are talking about velocities in a *laboratory* reference frame. Every binary system has its own *center-of-mass* frame and in that frame only the direction of the velocity vector can change.

[10]Note also $S^\dagger A S - A = S^\dagger [A, S] = [S^\dagger, A]S$
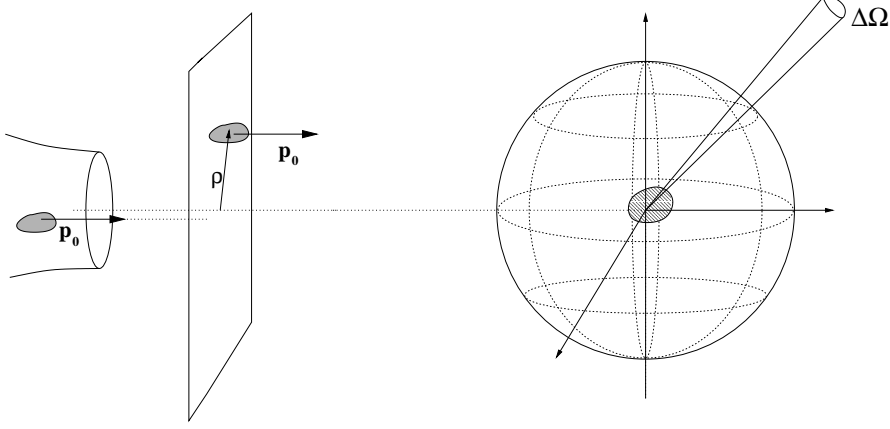
Figure 2.2: The idealized scattering experiment discussed in the main text. On the left the "ideal beam machine"; on the right the target.

where ρ_{in} is the "in" asymptotic density matrix of the system. These are the expected results considering eq.(2.5); however, one should note that they are valid under the "observability" condition expressed by eq.(2.9).

The use of a density matrix allows us to consider more realistic problems. In particular, in a still idealized scattering experiment a beam machine is able to produce the same initial state $|\psi_{in}\rangle$ over and over again; such state is well peaked in the momentum distribution around some value $\mathbf{p}_0$ but is *randomly* displaced in the plane perpendicular to the direction of propagation of the wavepacket (see Fig.(2.2) and Sections 3-d/e of Taylor (1969)). The corresponding density matrix is given by

$$\rho_{in} = n_{inc} \int d^2\rho\, e^{-i\rho\mathbf{p}} |\psi_{in}\rangle \langle\psi_{in}| e^{i\rho\mathbf{p}} \tag{2.11}$$

where n_{inc} is the number of particles incident on the target for unit surface. In eq.(2.11) the integral runs (perpendicularly to the incident direction $\widehat{\mathbf{p}}_0$) over an area that is much larger than the target dimensions and the displacement operators describe the "imperfections" of the beam machine; thus, the ρ vector is the analogue of the classical impact parameter. This density matrix is normalized to the number of incident particles, N

$$Tr\{\rho_{in}\} = n_{inc} \int d^2\rho = N$$

and therefore the resulting collision change of the observable A is the change in a system of N (non interacting) projectiles scattering off a target. Note that there is no need to consider stationary experiments: we consider N particles

($N \gg 1$ so that they are really randomly displaced) and let them scatter off the target, one at time, whenever we want. We define a generalized collision cross section

$$\sigma_{\Delta A} = Tr \left\{ \int d^2\rho e^{-i\rho \mathbf{p}} \left| \psi_{in} \right\rangle \left\langle \psi_{in} \right| e^{i\rho \mathbf{p}} (S^\dagger A S - A) \right\} \qquad (2.12)$$

such that the collision change of A is given by

$$\Delta A_{coll} = n_{inc} \sigma_{\Delta A}$$

The cross section defined in eq.(2.12) has the dimensions of [A] x [length]^2 and thus it is an effective area of the target for changing the value of the observable A.

To obtain an explicit expression of eq.(2.12) we need to know how the the momentum basis S matrix elements look like. Since the S matrix conserves energy, it must be an operator that acts "on the energy shell", i.e.

$$\left\langle \mathbf{p}' \right| S \left| \mathbf{p} \right\rangle = \delta(E' - E) s(\mathbf{p}' \leftarrow \mathbf{p})$$

where $E = p^2/2m$, $E' = p'^{\,2}/2m$ and s is some function which is arbitrarily defined out of the energy shell. We now observe, in addition, that in a scattering event the "out" state is always a superposition of a scattered state and the incoming state and therefore a more adequate decomposition of the S matrix elements is

$$\left\langle \mathbf{p}' \right| S \left| \mathbf{p} \right\rangle = \delta_3(\mathbf{p}' - \mathbf{p}) + \frac{i}{2\pi m} \delta(E' - E) f(\mathbf{p}' \leftarrow \mathbf{p}) \qquad (2.13)$$

where f, called *scattering amplitude*, is expected to contain no more delta functions (see Section 2.3). Furthermore, without loosing generality, we consider an observable that satisfies

$$[\mathbf{p}, A] = 0$$

This restriction is all but severe: the physically meaningful *free* particle observables cannot depend on the position of the system and the above relation tells us, indeed, that A is a function of the momentum only. In this case the resolution of A can be written as

$$A = \int d^3\mathbf{p} \, a(\mathbf{p}) \left| \mathbf{p} \right\rangle \left\langle \mathbf{p} \right| \qquad (2.14)$$

Now, when we use eqs.(2.13) and (2.14) in eq.(2.12) and take into account the fact that the initial state $\left| \psi_{in} \right\rangle$ is well peaked around some value $\mathbf{p}_0$, we obtain,

after considerable algebra,[11] the following expression

$$\sigma_{\Delta A} = \int d\Omega' a(\mathbf{p}') |f(\mathbf{p}' \leftarrow \mathbf{p}_0)|^2 - \frac{4\pi}{p_0} a(\mathbf{p}_0) \mathrm{Im} f(\mathbf{p}_0 \leftarrow \mathbf{p}_0) \qquad (2.15)$$

where $\mathbf{p}'$ is understood to have the same magnitude of $\mathbf{p}_0$ and the integral runs over the directions of the primed vector. If we set *by definition*

$$\sigma(\mathbf{p}_0) = \frac{4\pi}{p_0} \mathrm{Im} f(\mathbf{p}_0 \leftarrow \mathbf{p}_0) \qquad (2.16)$$

we can write the result in a more compact form

$$\sigma_{\Delta A} = \int d\Omega' a(\mathbf{p}') |f(\mathbf{p}' \leftarrow \mathbf{p}_0)|^2 - a(\mathbf{p}_0) \sigma(\mathbf{p}_0) \qquad (2.17)$$

We can now apply this formula to some specific observable A. We start considering the observable that corresponds to the number of particles whose momentum vector lays in a small angular cone $\Delta\Omega$ of our reference system. This observable is defined by

$$A = \int_0^\infty dp p^2 \int_{\Delta\Omega} d\Omega \, |\mathbf{p}\rangle \langle\mathbf{p}| \qquad (2.18)$$

that is, in eq.(2.14), by $a(\mathbf{p}) = 1$ if $\mathbf{p}$ lays in the specified cone and $a(\mathbf{p}) = 0$ otherwise.

We first consider the case where the cone does *not* contain the incident direction; in this case the initial value of the observable is null and therefore its change is the number of *scattered* particles in the specified direction. The relevant cross section is therefore

$$\sigma = \int_{\Delta\Omega} d\Omega' |f(\mathbf{p}' \leftarrow \mathbf{p}_0)|^2 \qquad (2.19)$$

or, in the limit $\Delta\Omega \to 0$,

$$\frac{d\sigma}{d\Omega}(\mathbf{p}' \leftarrow \mathbf{p}) = |f(\mathbf{p}' \leftarrow \mathbf{p}_0)|^2 \qquad (2.20)$$

This is the well-known expression of the *differential cross-section* in terms of the scattering amplitude. If in eq.(2.19) we extend the cone to the full

---

[11]The approach is strictly original work of the author. The following result, to the author's knowledge, seem to be absent in the literature. The derivation is somewhat long; however, we note that we use the same approximations of Section 3-e of Taylor(1969) except for the fact that we do *not* need to exclude the forward direction from our consideration.

solid angle (i.e. if we integrate (2.20) over all angles) we get the *total* cross-section, $\sigma^{tot}(\mathbf{p}_0)$: it gives the *total* number of *scattered* particles, but it does *not* correspond to any observable[12].

When the specified cone *contains* the incident direction the change in the corresponding observable is the *loss* of particles in the beam and it is given by

$$\sigma_{\Delta A} = \int_{\Delta\Omega} d\Omega' |f(\mathbf{p}' \leftarrow \mathbf{p}_0)|^2 - \sigma(\mathbf{p}_0)$$

or, in the limit $\Delta\Omega \to 0$,

$$\sigma_{\Delta A} = -\sigma(\mathbf{p}_0)$$

We therefore see that the quantity defined in eq.(2.16) is a measure of the attenuation of the beam; since the particle number is conserved we expect that this quantity is related to the total cross section defined above. Indeed, we can apply eq.(2.17) to the observable $A = \mathbf{I}$. In this case, considering eq.(2.10) and the *unitarity* of S[13], we know that $\sigma_{\Delta A} = 0$; therefore it follows

$$\sigma(\mathbf{p}_0) = \int d\Omega' |f(\mathbf{p}' \leftarrow \mathbf{p}_0)|^2 = \sigma^{tot}(\mathbf{p}_0)$$

With this interpretation of the quantity $\sigma(\mathbf{p}_0)$ our previous definition eq.(2.16) is known as *optical theorem*.

One further application of the formula (2.15) is for $\boldsymbol{A} = \mathbf{p}$, i.e. when the observable corresponds to the linear momentum of the system. In this case, using the above results, one can easily obtain the following (vectorial) cross-section:

$$\sigma_{\Delta A} = \int d\Omega' (\mathbf{p}' - \mathbf{p}_0) |f(\mathbf{p}' \leftarrow \mathbf{p}_0)|^2$$

The projection of this quantity onto the incident direction $\mathbf{p}_0$ defines the cross-section corresponding to the *loss of momentum* of the beam, i.e. the expression

$$\sigma_d = p \int d\Omega' (1 - \widehat{\mathbf{p}}\widehat{\mathbf{p}}_0) |f(\mathbf{p}' \leftarrow \mathbf{p}_0)|^2$$

defines the *momentum transfer* cross-section[14].

---

[12]The experimental reader may be horrified by this claim; such cross-section is much more easy to "observe" than the differential one. We are talking about the *quantum mechanical* observables. One cannot extend the integral in eq.(2.18): in that case one would get $A = \mathbf{I}$ and should consider *also* the forward direction (see below).

[13]Actually, we need only the isometric properties of S.

[14]In the momentum cross-section generally used one factors out the p term and thus obtain a quantity with the dimension of an area (see (Levine, 1969)).

2.3   The Lippmann-Schwinger equation

Up to now we have taken into explicit account the time in order to gain a physical picture of what happens when two atoms collide. More precisely, we have taken a *time dependent* point of view or, in other words, we have worked in the *time domain.* Historically the scattering theory developed in the late twenties and thirties in a *time independent* framework and only in the late fifties its formalism was properly justified by the time dependent approach outlined above (see Taylor(1969), Introduction). One of the main advantages of working in the latter framework is that it furnishes practical means for computing scattering observables. For a long time these were the *only* means to get informations on collision processes. Nowadays, the tremendous increase in the computational power of the last years has opened the way to the direct solution of the time dependent Schrödinger equation, but these time-independent means are still widely used and therefore we describe here their theoretical foundations[15]. Before starting to be buried by complicated formulas it should be stressed that we have to deal with the *energy domain*; the bridge between this and the former domain can be built in different ways but in any case is a *time-energy Fourier transform.*

We start considering the Møller operator Ω_+ (similar results apply to Ω_-)

$$\Omega_+ = lim_{t \to -\infty} U_t^\dagger U_t^0$$

and writing the time dependent operator inside the limit operation as an integral of its derivative

$$\Omega_+ = \mathbf{I} + i \int_0^{-\infty} U_t^\dagger V U_t^0 dt$$

We now apply it to an improper eigenstate of the *free* hamiltonian. In doing this we need some trick to handle the non definiteness of the integral which arises from the fact that the above operator is actually defined only for *proper* vectors. The trick is to insert the famous ϵ factor (Jauch, 1958)

$$\Omega_+ \left| En \right\rangle = \left| En \right\rangle + i \, lim_{\epsilon \to 0^+} \int_0^{-\infty} e^{\epsilon t} U_t^\dagger V e^{-iEt} \left| En \right\rangle dt$$

also used with the meaning of "adiabatic switching" (Lippmann and Schwinger,

---

[15]In our work we have used both the approaches (see Part II).

1950).[16] Using the result of Appendix A[17] we arrive at the following expression

$$\Omega_+ \ket{En} = \ket{En+} = (\mathbf{I} + G^+(E)V) \ket{En} \tag{2.21}$$

where the vector $\ket{En+}$ is here defined. As discussed at the end Section (2.1) it is an (improper) eigenvector of the full hamiltonian with same "initial" energy E and it is called *scattering eigenstate*. Since the time has been factored out (we have a stationary, although improper, state) this vector contains all the scattering informations for the chosen energy.

The operator $G^+(E)$ is defined by

$$G^+(E) = lim_{\text{Im}\lambda \to 0^+} G(\lambda) \, (\text{Re}\lambda = E) \tag{2.22}$$

and it is the Green's operator corresponding to the so-called *outgoing* boundary conditions; it is given by a limit of the operator

$$G(\lambda) = (\lambda - H)^{-1} \tag{2.23}$$

which is well defined (and analytic as a function of its argument) in any open set of the complex plane that does not include eigenvalues of H (proper or improper). It is the most important tool of the time independent theory; the reader is referred to Appendix A for a summary of its properties.

Eq.(2.21) expresses the action of the Møller operator on the energy shell and it allows us to introduce the "on shell" Møller operators

$$\Omega_+(E) = \mathbf{I} + G^+(E)V$$

which in turn allow us to write down a sort of "spectral resolution"

$$\Omega_+ = \int_0^{+\infty} dE \Omega_+(E) \delta(E - H^0) \tag{2.24}$$

We could have well defined a generalized "on-shell" Møller operator

$$\Omega(\lambda) = \mathbf{I} + G(\lambda)V \tag{2.25}$$

---

[16]Here we have used the symbol $\ket{En}$ to denote a general eigenvector; n is understood to be any necessary quantum "number" although it actually may be a continuous index (as for example in the case $\ket{En} = const \ket{\mathbf{p}}$ where it coincides with the direction of the momentum vector). If needed we take these vectors normalized on the energy scale, i.e.

$$\braket{E'n' | En} = \delta(E' - E)\delta_{n'n}$$

when n is countable and

$$\braket{E'n' | En} = \delta(E' - E)\delta(n' - n)$$

when it happens to be continuous.

[17]It is an *half Energy-Time* Fourier transform. It is at this point that we move to the energy domain.

from which
$$\Omega_{\pm}(E) = lim_{\mathrm{Im}\lambda \to 0\pm}\Omega(\lambda)\,(\mathrm{Re}\lambda = E) \tag{2.26}$$
Another useful related operator is the *transition operator*. It is defined by

$$T(\lambda) = V\Omega(\lambda) = \Omega^{\dagger}(\lambda^*)V \tag{2.27}$$

for the appropriate λ values (i.e. where $G(\lambda)$ exists); in particular we put for future reference[18]
$$T(E^+) = lim_{\epsilon \to 0+}T(E + i\epsilon) \tag{2.28}$$
Now we can use the Lippmann-Schwinger equation for $G(\lambda)$ reported in Appendix A to write down a corresponding equation for $\Omega(\lambda)$

$$\Omega(\lambda) = \mathbf{I} + G_0(\lambda)V\Omega(\lambda) \tag{2.29}$$

or

$$(\mathbf{I} - G_0(\lambda)V)\Omega(\lambda) = \mathbf{I}$$

where $G_0(\lambda)$ is the *free* particle Green's operator. This is the *Lippmann-Schwinger* equation for the on-shell Møller operators: it applies both to $\Omega_+(E)$ and $\Omega_-(E)$[19]. It is an equation for $\Omega(\lambda)$ in terms of the known free particle Green's operator and the potential. A corresponding equation holds for the transition operator defined above

$$T(\lambda) = V + VG_0(\lambda)T(\lambda)$$

or equivalently

$$(\mathbf{I} - VG_0(\lambda))T(\lambda) = V$$

Power series solutions of these equations, known as *Born series*, can be obtained recalling the geometrical series

$$(\mathbf{I} - A)^{-1} = \sum_{n=0}^{\infty} A^n$$

When they are truncated to definite orders they lead to different approximations, known as *(first) Born approximation*, second Born approximation and so on. However it should be noted that the geometrical series do not necessarily converge and, furthermore, even when they do it is not straightforward that the convergence is so rapid that their first or two terms are good approximations[20].

---

[18]Explicitly, $T(E^+) = V\Omega_+(E) = (\Omega_-(E))^{\dagger}V$.

[19]$\Omega_-(E)$ is defined accordingly to eq.(2.26) and satisfies a relation analogous to eq.(2.24).

[20]The "physical" Lippmann-Schwinger equations (i.e. those for Ω and T, involve the product of $G_0^+(E)$ and V; it follows that the Born approximation can be realistic when V and $G(E)$ are "small" in some sense, i.e. for weak potential or high energies.

A Lippmann-Schwinger equation can also be written for the scattering eigenstates,

$$|En+\rangle = |En\rangle + G_0^+(E)V|En+\rangle \tag{2.30}$$

which give rise to an integral equation for the scattering eigenfunctions, one of the most powerful means to deal with scattering problems. We return in the next section to its connection with the Schrödinger equation; for the moment we leave this section of barren mathematics going back to the physics. In particular, we have introduced "time-independent" operators but how can we get scattering information from them? The answer is in S operator and in particular in eq.(2.13) which introduced the scattering amplitude. To obtain that expression we need a spectral resolution analogous to eq.(2.24). It is simpler to work with the operator $S - \mathbf{I}$ which we manipulate as follow

$$\Omega_-^\dagger \Omega_+ - \mathbf{I} = \Omega_-^\dagger(\Omega_+ - \Omega_-) = \int_0^{+\infty} dE\,\Omega_-^\dagger(G^+(E) - G^-(E))V\delta(E - H^0)$$

where we have used the isometric property of the Møller operators and their spectral resolution. We now use the following formula

$$\frac{1}{2\pi i}(G^-(E) - G^+(E)) = \delta(E - H)$$

and the adjoint of the intertwining relation eq.(2.7) for Ω_- to get

$$S - \mathbf{I} = -2\pi i \int_0^{+\infty} dE\,\delta(E - H^0)\Omega_-^\dagger(E)V\delta(E - H^0)$$

where $\Omega_-^\dagger(E)V$ is the transition operator defined in eq.s(2.27, 2.28). Thus, we have the following "spectral resolution" of the S operator

$$S = \int_0^{+\infty} dE\,S(E)\delta(E - H^0) \tag{2.31}$$

where the "on shell" S operator is given by

$$S(E) = \mathbf{I} - 2\pi i\delta(E - H^0)T(E^+) \tag{2.32}$$

Taking momentum basis matrix elements of this expression we obtain eq.(2.13) if we put

$$f(\mathbf{p}' \leftarrow \mathbf{p}) = -m(2\pi)^2 \langle \mathbf{p}'|T(E_p^+)|\mathbf{p}\rangle \tag{2.33}$$

where $\mathbf{p}'$ and $\mathbf{p}$ are understood to correspond to the same energy E_p . We therefore see that the scattering amplitude is given by the on-shell matrix elements of the T operator; however, it is worth to note that they must be taken with the appropriate limit of eq.(2.28) at the chosen energy $E = \mathrm{Re}\lambda$, i.e. there is a different operator for each fixed energy. It is worth to note that the T operator(s) acts *also* "out of the energy shell" and in eq.(2.32) the energy projector ensures that S conserves energy.

2.4   The stationary scattering states

We are now ready to go slightly deeper in the time independent formalism. In the previous Section we introduced the scattering eigenstates as the solution of the Lippmann-Schwinger equation (2.30) which is, in practice, an integral equation for the function $\psi_{En}^{+}(\mathbf{x}) = \langle \mathbf{x} | \mathbf{p}+ \rangle$ (or other representations). We know that they are eigenstates of the full hamiltionan but we also know that this property does not characterize them entirely[21]. In this Section, therefore, we show the actual connection with the Schrödinger equation.

We first note that eq.(2.21) is actually the usual limit (i.e. $\mathrm{Im}\lambda \to 0^{+}$ with $\mathrm{Re}\lambda = E$) of the following equation

$$|En+\rangle = (\mathbf{I} + G(\lambda)V) |En\rangle \tag{2.34}$$

which can be rewritten as

$$(\lambda - H) |En+\rangle = (\lambda - H^0) |En\rangle \tag{2.35}$$

when one remembers the meaning of the Green's operator defined in eq.(2.23). Whenever λ has a non vanishing imaginary part, this equation has a unique solution, given formally by the previous expression eq.(2.34)[22]. When we take the above limit this equation reduces to the usual Schrödinger equation

$$(E - H) |En+\rangle = 0 \tag{2.36}$$

which we know to have a non unique solution. Thus, we see that the non-null imaginary part of the complex energy λ, i.e. the ϵ factor of the scattering theory, "contains" the boundary conditions that have to be applied to the Schrödinger equation to get *scattering* solutions.

In order to obtain these boundary conditions we look at the "boundaries", that is we consider what happens, in coordinate representation, when $R \to \infty$. Since the potential dies at the boundaries the Schrödinger equation reduces to the free particle equation

$$(E - H^0)\psi_{En}^{+}(\mathbf{x}) = 0 \text{ for } R \to \infty$$

and therefore the scattering eigenstate should be, at long-range, a superposition of free particle states of the same energy. The actual superposition is obtained

---

[21] The trouble is clearly in the degeneracy of the corresponding eigenspace.

[22] We may well re-obtain the Lippmann-Schwinger equation (2.30) by writing on the l.h.s. of eq.(2.35) $H = H^0 + V$, using the *free* particle Green's operator and taking the appropriate limit.

by taking coordinate matrix elements of eq.(2.30) and by using the asymptotic properties of the free Green's operator

$$\left\langle R\widehat{\mathbf{x}}\big|G_0^\pm(E_p)\big|\Phi\right\rangle \to -m(2\pi)^{1/2}\frac{e^{\pm ipR}}{R}\left\langle p\widehat{\mathbf{x}}\big|\Phi\right\rangle \qquad (2.37)$$

with $|\Phi\rangle = V|E\alpha+\rangle$. For example, for $|E\alpha\rangle = |\mathbf{p}\rangle$ the well-known result is

$$\psi_{\mathbf{p}}^+(\mathbf{x}) \to \frac{1}{(2\pi)^{3/2}}\left\{e^{i\mathbf{p}x} + f(p\widehat{\mathbf{x}} \leftarrow \mathbf{p})\frac{e^{ipR}}{R}\right\} \text{ for } R \to \infty \qquad (2.38)$$

where

$$f(p\widehat{\mathbf{x}} \leftarrow \mathbf{p}) = -m(2\pi)^2\left\langle p\widehat{\mathbf{x}}|V|\mathbf{p}+\right\rangle$$

is the scattering amplitude defined in eq.(2.33), when one remembers eq.(2.28). We could have well proceeded starting from eq.(2.21) and using the asymptotic behavior of the *full* Green's operator, i.e.

$$\left\langle R\widehat{\mathbf{x}}\big|G^\pm(E_p)\big|\Phi\right\rangle \to -m(2\pi)^{1/2}\frac{e^{\pm ipR}}{R}\left\langle p\widehat{\mathbf{x}}\big|\Omega_-^\dagger(E_p)\Phi\right\rangle \qquad (2.39)$$

which follow from eq.(2.37) and the Lippmann-Schwinger equation for G. In this case the relevant scattering amplitude would have turned out to be

$$f(p\widehat{\mathbf{x}} \leftarrow \mathbf{p}) = -m(2\pi)^2\left\langle p\widehat{\mathbf{x}}-|V|\mathbf{p}\right\rangle$$

which is equivalent to the previous expression in view of eq.(2.27).

Eq.(2.38) is the boundary condition that has to be applied to the solution of the Schrödinger equation (2.36) in order to get "scattering" solutions[23]. It clearly states that, asymptotically, such solutions must be a superposition of the incoming plane wave and a spherical outgoing *scattered* wave.

Actually, starting from this result, one can set up the following "spatial" description of the scattering process (see Taylor(1969), Chapter 10): the long range behavior of a *wave packet*[24] launched on the target centered in the origin of our reference system is given by a superposition of the incident wavepacket with a scattered one

$$\psi(\mathbf{x},t) = \psi_{in}(\mathbf{x},t) + \psi_{scatt}(\mathbf{x},t) \text{ for } R \to \infty$$

---

[23] With the same token, one can start with the Schrodinger equation and use standard Green's function techniques (see Morse and Feshbach (1953), Chapter 7) with the mentioned boundary conditions. The result is of course the Lippmann-Schwinger equation.

[24] The wavepacket is understood to be well peaked in the momentum distribution around a certain value $\mathbf{p}_0$.

where $\psi_{scatt}(\mathbf{x}, t)$ is proportional to the amplitude of the incident wavepacket at the *same* distance $R = |\mathbf{x}|$ but in the incident direction,

$$\psi_{scatt}(\mathbf{x}, t) = \frac{f(p_0 \widehat{\mathbf{x}} \leftarrow \mathbf{p}_0)}{R} \psi_{in}(R\widehat{\mathbf{p}}_0, t)$$

Therefore, well before that collision takes place ($t \ll 0$) the incident wavepacket moves on the negative $\widehat{\mathbf{p}}_0$ axis with a (group) velocity $\mathbf{v}_0 = \mathbf{p}_0/m$ and the scattered wave is absent, as it must be ($\psi_{in}(\mathbf{x}, t)$ attains significant values only around $\mathbf{x}_t \sim -\widehat{\mathbf{p}}_0 v_0|t|$). Adversely, for $t \gg 0$ the unscattered wavepacket is localized near $\widehat{\mathbf{p}}_0 v_0 t$ and the scattered one moves outwards in a shell of radius $v_0 t$.

The conditions needed for this description to be valid are the same used in Section 2.2. In particular the scattering amplitude must be a slowly varying function of its arguments, a condition *not* satisfied near a resonance; in this case, indeed, one observes a *resonant* scattered wave that appears with a certain *delay* time from its unscattered and non-resonant counterparts[25].

One further note on the long range behavior of a scattering state is needed. Since $\psi_{in}(\mathbf{x}, t)$ and $\psi(\mathbf{x}, t)$ have the same normalization some destructive interference phenomenon must occur between $\psi_{in}(\mathbf{x}, t)$ and $\psi_{scatt}(\mathbf{x}, t)$ in order to conserve probability (i.e. the "number of particles"). This is the reason for the existence of the optical theorem, eq.(2.16), that

> "...is characteristic of a wave theory, in which the reduction
> in intensity of a plane wave passing through a scattering medium
> is accounted for by destructive interference between the original
> wave and the secondary waves scattered in the direction of propa-
> gation..." (Lippmann and Schwinger, 1950).

Note also that, from a theoretical point of view, the Lippmann-Schwinger equation (2.30) or its direct counterpart, eq.(2.35), are much more useful than the Schrödinger equation with the appropriate boundary conditions. This is clearly because they entail such boundary conditions and these can be recovered, when needed, by taking the appropriate asymptotic limit.

---

[25]The situation is actually more complicated. One has to distinguish between the case in which the energy spread ΔE of the wavepacket is much less than the width of the resonance, Γ, and the case in which the opposite is true. In the former, the spatial spread of the wavepacket, $\Delta x \sim v_0/\Delta E$ is much greater than the "delay distance" $\Delta x_d \sim v_0/\Gamma$ and one can measure the (energy) *profile* of the resonance but not its delay time. In the latter one can measure the delay time, or "decaying rate of the resonance", but cannot measure the profile. See (Taylor, 1969), Sections 13-c/d for a clear discussion of the topic.

Chapter 3

Multichannel scattering theory

In the previous Chapter we have introduced some basic concepts of scattering theory considering the simplest case in which the collision partners do not have internal structure. We now move to the more interesting situation in which the partners have some internal structure. Every *molecular* collision system is of this kind: even in the simplest case of an atom scattering off a diatomics one cannot neglect the rovibrational structure of the molecule. Furthermore, it is clear that *all* the chemically interesting collision processes are of this kind: the *change* of internal structure due to a collision is at the heart of chemistry. These facts complicate the theory, but, ultimately, the price to be paid is well compensated by a clear physical picture of the chemically interesting processes.

Exactly as in the previous Chapter, we factor out the center of mass motion and denote with $\mathcal{H}$ the resulting Hilbert space of the system. H is the full hamiltonian in this frame,

$$H = K + V = \sum_i \frac{\mathbf{p}_i^2}{2\mu_i} + V\left(.., \mathbf{x}_i, ..\right)$$

where $\{\mathbf{x}_i\}$ is a suitable set of coordinates that factor out the center of mass position, $\{\mathbf{p}_i\}$ is the corresponding set of conjugate momenta and μ_i are the relevant reduced masses. For definiteness, we take the potential V vanishing in the limit of the full breaking of the system, i.e. $V \to 0$ when $R_i = |\mathbf{x}_i| \to +\infty$ for all i.

3.1   Arrangements and channels

The main difference in dealing with systems that have internal structure with respect to the previous single-channel case is the increase in the dimensionality of the problem. This fact, besides having several consequences in practical

applications, has some important consequence also from a theoretical point of view. First of all we have to abandon the idea of a *unique* scattering coordinate, that is of a unique coordinate that, when left to be increased, brings the system to the asymptotic situation. The reason is that, in general, we do not have *one* asymptotic situation any more: molecules can rearrange themselves, that is they can *react*. Furthermore, the increase of the number of degrees of freedom allows the flow of energy from one degree of freedom to another: in some cases this flow occurs only *temporarily,* i.e. only *during* the collision, while in other cases it may lead to permanent excitation/deexcitation of the collision partners.

These complications are best seen by taking as an example an isotopic variant of the system which is the subject of Part II. We consider the possible outcomes of a collision between LiH^+ and D, namely[1]

$$LiH^+ + D \rightarrow \begin{array}{l} LiH^+ + D \\ LiD^+ + H \\ Li^+ + DH \\ Li^+ + H + D \end{array}$$
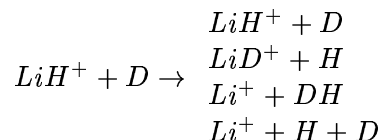
In the first equation the outcome is chemically equal to the reagents and the process seems to be analogous to that described in the previous Chapter. However, when we remember that the diatomicdiatomic has internal structure the possibility of exciting/deexciting the molecule should be taken into account. That is, the first equation describes also *inelastic* processes.

The successive equations refer, instead, to *chemical* transformations. In writing these equations we realize that several *asymptotic hamiltonians* are possible. For example, the "reagent side" (center-of-mass) hamiltonian reads as

$$H^{(1)} = \frac{\mathbf{P}_1^2}{2\mu_1} + h_{LiH^+}$$

where $\mathbf{P}_1$ is the momentum operator for the relative motion of D with respect to the center of mass of LiH^+, μ_1 is the corresponding reduced mass and

$$h_{LiH^+} = \frac{\mathbf{p}_1^2}{2m_1} + V_{LiH^+}(\mathbf{x}_1)$$

is the hamiltonian of the LiH^+ molecule, with $\mathbf{x}_1$ the diatomic vector operator, $\mathbf{p}_1$ its conjugate momentum and m_1 the corresponding reduced mass. On the "product side" we have in the third line, for example,

$$H^{(3)} = \frac{\mathbf{P}_3^2}{2\mu_3} + h_{DH}$$

---

[1]We are talking about *adiabatic* processes.

where now $\mathbf{P}_3$ and μ_3 are understood to be the "scattering" variables of the atom Li^+ with respect to the center of mass of the DH molecule and h_{DH} is molecular hamiltonian of HD. Analogously, we can obtain a similar expression for the other two-body process.

The fourth equation introduces a novel possibility of the multichannel theory, that is the fact that *many*-body processes have to be considered. In general they contain one or more molecular fragments, but in our three-atom example we have only the *full* break-up process. The corresponding hamiltonian is pure kinetic; in this case we have no more a physically advantageous choice of the coordinates and we can take any diatomic vector and the relative vector of the remaining atom with respect to the center of mass of the chosen "diatomic" as a possible set of coordinates[2].

Every asymptotic situation defines an *arrangement* which is characterized by a particular asymptotic hamiltonian. In this Section only we label the different arrangements by the first few letters, a, b, c, ..; the corresponding hamiltonians will be denoted by

$$H^{\mathrm{a}} = K^{\mathrm{a}} + h^{\mathrm{a}}$$

where K^{a} is the kinetic energy *of the scattering motion* in the a arrangement and h^{a} is internal hamiltonian of the arrangement. This, in turn, is given by the sum of the molecular hamiltonians of each fragment. For the full break-up process (like the $Li^+ + H + D$ arrangement of the previous example) the internal hamiltonian is absent and the kinetic term coincides with the full hamiltonian. The three "molecular" arrangements of a three atom system, i.e. those in which a molecule is present, and a useful labeling of them is shown in Fig.(3.1), together with a suitable set of coordinates.

The internal hamiltonians of each arrangement have one or more bound states[3]. Each bound state of these hamiltonians defines a *channel* in the specified arrangement. For consistency, the case $h^{\mathrm{a}} = 0$, i.e. the full break-up arrangement, also defines a channel. For example, the $LiH^+ + D$ arrangement has a certain number of roto-vibrational channels, labeled by the vibrational and rotational quantum numbers (v, j) of the LiH^+ molecule; in the (v, j) channel the D atom and the LiH^+ molecule in the specified roto-vibrational state move freely.

One therefore introduces a *channel space* $\mathcal{H}^{(\alpha, \mathrm{a})} \subset \mathcal{H}$ which is given by the

---

[2]This already tell us the difficulties in treating such processes. We note that, without factoring out the center of mass of the total system, the most democratic "individual" choice becomes possible.

[3]The situation in which h^{a} does not have bound states is excluded by definition: we are referring to asymptotically *stable* fragments and, therefore, such hypothetical arrangement belongs to the full break-up arrangement. From this point of view the h^{a}'s can be seen as the molecular hamiltonians projected onto the space spanned by their bound states.
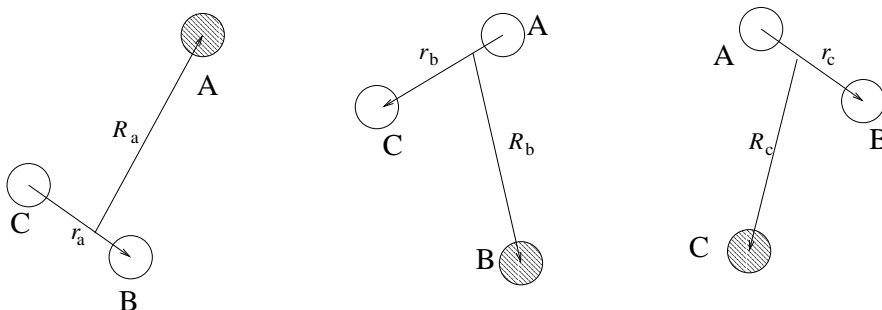
Figure 3.1: The "molecular" arrangements for the three atom system and a suitable set of coordinates. From left to right, the arrangements a, b and c.

space spanned by the vectors of the form

$$\left|\psi^{(\alpha,a)}\right\rangle = |\chi\rangle\,|\phi_\alpha\rangle$$

where $|\chi\rangle$ is a (general) vector that describes the translational motion in the arrangement a and $|\phi_\alpha\rangle$ is the α-th bound state vector of the internal hamiltonian h^a. Note that different channel spaces in the same arrangement are orthogonal with each other, but this is no longer true when different arrangements are considered; for example the full break-up arrangement *is* one channel and the channel space *is* the full space, i.e. it cannot be orthogonal to any channel space.

Every channel space is much like a room on a floor of a building: one can enter the room only if (s)he has enough energy. At a fixed total energy only a certain number of channel spaces is available for being used as asymptotic spaces. The corresponding channels are termed *open channels* (they are "available rooms"), in contrast to those that are forbidden at the given energy and that are called *closed channels*[4]. One of the possible situations for our three particle model system is depicted in Fig.(3.2): in this example we consider the case in which all the molecular fragments are stable and, moreover, bound states of the three atoms exist. The system could resemble the familiar X^1H_2O system (or also our title system in the first excited state), in which the arrangements describe the $H+OH$ and the H_2+O collision processes and the potential well supports many bound states. Other possibilities can be met in practice.

The free motion in each channel is described by the asymptotic hamiltonians introduced before, H^a, one for each arrangement. This means that, with

---

[4]Note, however, that the closed channel spaces, being subspaces of $\mathcal{H}$, can be "sampled" by the actual orbit of the system and therefore, in general, these channels *cannot* be excluded at all.
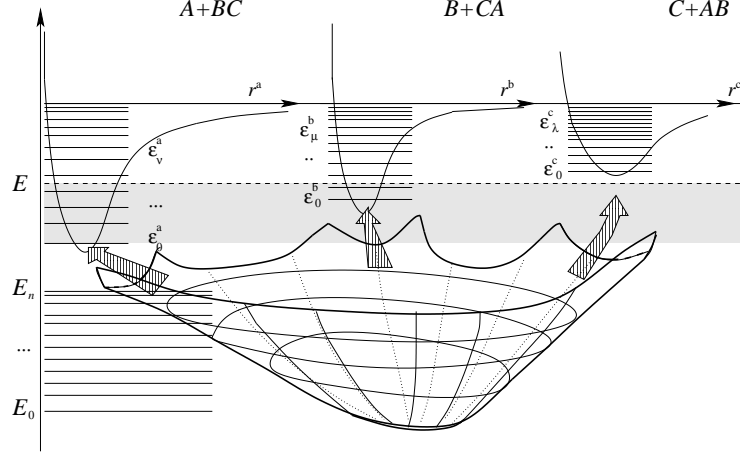
Figure 3.2: Pictorial representation of channel levels in the ABC system. On the top: the potential curves of the diatomic BC, CA and AB, with their energy levels. The shaded region indicates the channels that are open at energy E: in this case the c arrangement is closed. On the bottom: representation of the potential function of the ABC system with the indicated energy levels on the same energy scale as above.

respect to the situation of the previous Chapter, we will have to consider different free Green's operators $G_a(\lambda)$ that are the counterparts of the operator $G_0(\lambda)$ of the single channel case. This is not the only difference with the single channel case. There is also a qualitative difference: the *channel Green's operators* are much more complicated and usually not known.

These complications are already evident if we focus attention on the two-body arrangements. We know that the known, single channel Green's operator, G_0, describes the relative motion of the two fragments and we can argue that an expression of the channel Green's operator in terms of it should be feasible. That this is the case can be seen by using the spectral resolution of h^a, i.e.

$$G_a(\lambda) = \sum_\alpha G_0(\lambda - \epsilon_\alpha)p_\alpha^a + \int d\epsilon G_0(\lambda - \epsilon)\delta(\epsilon - h^a) \qquad (3.1)$$

where p_α^a is the projector onto the α-th bound state of h^a with energy ϵ_α and the integral runs over the continuous spectrum of h^a. Complications arise when we realize that we need to know the *full* spectral resolution of the internal hamiltonian if we wish to apply $G_a(\lambda)$ *out of channel spaces* and this depends

on the our knowledge of the dynamics described by h^α [5,6] . From now on, unless otherwise stated, we will drop the arrangement label.

3.2   Wave operators

We can now set up a time-dependent description of the collision process which parallels that given in Section (2.1). The description is somewhat complicated by the presence of the channels but a close analogy with the single channel case helps us not to lose sight of the ultimate goal, i.e. the understanding of the physics of the collision process.

Exactly as in Section (2.1) we expect that a scattering orbit should resemble a free motion as $t \to \pm\infty$. In this case, however, we have more than one possible "free" motion. From an experimental point of view, at the time of writing, we can only prepare a system in a definite arrangement. This is however only a practical limitation: we expect that the outcome of the collision process can be a superposition of free motions in different arrangements and, thus, we should expect that the same is true for the incoming motion. Therefore, a scattering orbit should have the following limiting behaviors:

$$U_t \ket{\psi_0} \to \sum_\alpha U_t^\alpha \ket{\psi_{in}^\alpha} \text{ for } t \to -\infty$$

and

$$U_t \ket{\psi_0} \to \sum_\alpha U_t^\alpha \ket{\psi_{out}^\alpha} \text{ for } t \to +\infty$$

where U_t is the full evolution operator, U_t^α's are the *channel evolution operators* and $\ket{\psi_{in}^\alpha}$, $\ket{\psi_{out}^\alpha}$ are the *channel components* of the "in" and "out" asymptotes respectively, which belong to the appropriate channel spaces defined in the previous Section. The sum runs over all channels of all arrangements. Although we have one channel evolution operator for each arrangement (each arrangement has its own *free* hamiltonian) we labeled them by a *channel* label. This turns out to be useful in describing scattering processes[7].

---

[5]For example, in the $LiH^+ + D$ arrangement of our system we have $h^{\rm a} = h_{LiH^+}$. The knowledge of the spectral resolution of this hamiltonian depends also on the knowledge of the scattering dynamics in the $Li^+ + H$ system.

[6]One remark about the continuous spectrum of the *internal* hamiltonian. Its lowest energy marks the *threshold* for the breaking of the arrangement into (sub)arrangements. For example, we can consider the $D+ABC$ arrangement in a 4-atom system $ABCD$, in which the ABC molecular hamiltonian is that of Fig.(3.2): only the bound states of ABC are channels of this arrangement; the other levels represent channels in a different arrangement, e.g. $D + A + BC$ and so on.

[7]As a matter of fact, each channel has a different translational behavior: for a given energy the more the internal excitation the less its translational content, i.e. the channel components of a definite arrangement move with different speeds.

Exactly as in the single channel space we expect a one-to-one correspondence between "in" and "out" asymptotes. In the previous Chapter this correspondence was given by the unitary scattering operator; now we have several channel components of the asymptotic state and therefore a *matrix* of scattering operators is expected to connect these components. Furthermore the actual scattering orbits are again expected to be orthogonal to the "bound orbits" and complementary to them, in the sense that, together, they should be *all* the possible orbits of the system.

These results are contained in the multichannel version of the theorems stated in Section (2.1), for which similar remarks about the potential apply. Here, we consider briefly these multichannel versions; the reader is referred to the previous Chapter for a deeper discussion on the general principles.

Asymptotic condition. For every $|\psi_{in}\rangle$ *in the channel space* $\mathcal{H}^\alpha$ there is a vector $|\psi_0\rangle$ such that

$$U_t |\psi_0\rangle - U_t^\alpha |\psi_{in}\rangle \quad \to 0 \text{ as } t \to -\infty$$

and likewise for every $|\psi_{out}\rangle$ in $\mathcal{H}^\alpha$.

In this case the same considerations of the single channel case apply. Here we note only that the vector $|\psi_0\rangle$, which we remember to be the actual state that characterizes uniquely that orbit with the desired asymptotic properties, is obtained by the appropriate (isometric) *channel Møller operator*

$$\Omega_\pm^\alpha = lim_{t \to \mp\infty} U_t^\dagger U_t^\alpha \tag{3.2}$$

We have a *different* Møller operator for each channel, also for channels belonging to the same arrangement: every limit is taken *in the appropriate channel space*, thus defining its own domain[8]. We can say that every Møller operator maps the channel space $\mathcal{H}^\alpha$ onto the space $R_\pm^\alpha = \Omega_\pm^\alpha(\mathcal{H}^\alpha)$ which is the space of the states with (in/out) asymptotes in the specified channel. These states are related by the following theorem:

Orthogonality theorem. The space of the states with an "in" asymptote in the channel α, $\mathcal{R}_+^\alpha$, is orthogonal to the space spanned by the bound states of the system, $\mathcal{B}$, and to the space of the states with an "in" asymptote in a different channel β. In other words, $\mathcal{R}_+^\alpha \subset \mathcal{B}^\perp$ and $\mathcal{R}_+^\alpha \perp \mathcal{R}_+^\beta$ if $\alpha \neq \beta$. Likewise for the $\mathcal{R}_-^\alpha$'s.

---

[8]This fact is somewhat hidden in the awkward notation of eq.(3.2) where we know that the channels of the same arrangement have the *same* evolution operator.

Here we find again the "non-belligerent" relation with the possible bound states of the system. The novelty is the orthogonality between the *actual* orbits that come from different channels. We have already noted in the previous Section that the channel spaces, in general, are not orthogonal to each other, so why should the actual orbits be orthogonal? As in Section (2.1) the reason is again in the definition of the asymptotic state: when we let the time to go to infinity the orbits resemble their free counterpart and *move accordingly to their free evolution operators*. It follows that, when the arrangements are the same, the states are orthogonal because they are different eigenstates of the molecular hamiltonian. On the other hand, when the arrangements are different there is at least one degree of freedom which is bound in one state and not bound in the other: this means that in the latter arrangement one interatomic distance will be "stretched" by the free motion, thus making the states orthogonal.

The orthogonality relations allow us to clearly define the *full* space of the states with an "in" or an "out" asymptote. For example, for the incoming asymptotes we can define

$$R_+ = \sum_\alpha \oplus R_+^\alpha$$

where the symbol $\oplus$ denotes the (internal) direct sum. A general vector $|\psi_0\rangle$ of this space is given by a superposition of *orthogonal* vectors, i.e.

$$|\psi_0\rangle = \sum_\alpha \Omega_+^\alpha \, |\psi_{in}^\alpha\rangle$$

and characterizes an orbit with the following limiting behavior

$$U_t \, |\psi_0\rangle \to \sum_\alpha U_t^\alpha \, |\psi_{in}^\alpha\rangle \ \text{ for } t \to -\infty$$

Furthermore, we can group together the isometric properties of the Møller operators and the orthogonality relations between their images with the following formula

$$(\Omega_\pm^\beta)^\dagger \Omega_\pm^\alpha = \delta_{\beta\alpha} \tag{3.3}$$

This formula clearly states the orthogonality for different channels. However, it is worth to note that the plus/minus signs in eq.(3.3) must be the same, otherwise an orbit with an "in" asymptote in the α channel can never end in the β channel, i.e. no $\alpha \to \beta$ processes are left.

We are left with the last, most important theorem.

Asymptotic completeness. The space of the states with "in" asymptotes coincides with the space of the states with "out" asymptotes, $\mathcal{R}_+ = \mathcal{R}_- = \mathcal{R}$, and they *are* the orthogonal complement of $\mathcal{B}$, $\mathcal{R} = \mathcal{B}^\perp$. In other words, $\mathcal{H} = \mathcal{B} + \mathcal{R}$.
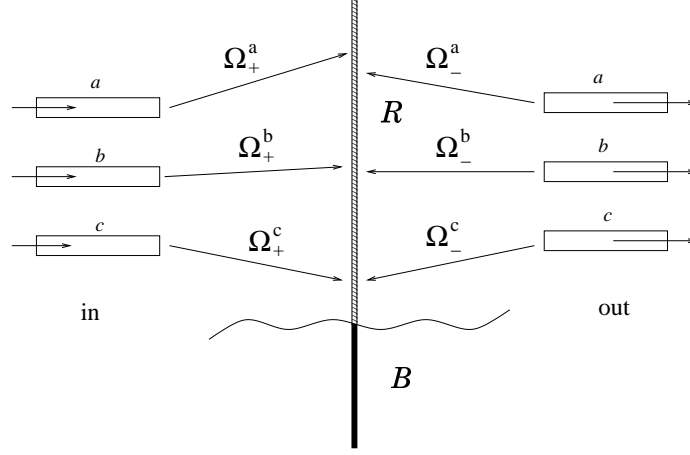
Figure 3.3: Pictorial representation of a collision in a three channel system. In the middle the wall represents the Hilbert space $\mathcal{H}$ with the indicated bound ($\mathcal{B}$) and scattering subspaces ($\mathcal{R}$). $\mathcal{R}$ can be thought to be a set of two computer disks, one arranged in sectors (the three R_+^α's) and the other arranged in cylinders (the three R_-^α's). The two disks exchange "information" by contact, thus making possible the flow of the system from every "in" channel to every "out" channel.

This exactly parallels the corresponding theorem of Section (2.1). It tells us that we can define a set of *scattering operators*

$$S_{\beta\alpha} = (\Omega_-^\beta)^\dagger \Omega_+^\alpha$$

which establish a connection between the "in" and the "out" asymptotic channel components

$$\left| \psi_{out}^\beta \right\rangle = S_{\beta\alpha} \left| \psi_{in}^\alpha \right\rangle$$

The previously mentioned one-to-one correspondence is expressed by the unitarity of the *matrix*, which takes the form

$$\sum S_{\gamma\beta}^\dagger S_{\gamma\alpha} = \sum S_{\beta\gamma} S_{\alpha\gamma}^\dagger = \delta_{\beta\alpha} \tag{3.4}$$

where the sum runs over all channels. The overall situation is depicted in Fig.(3.3) where the role of the channel components and that of the various spaces becomes evident.

Eq.(3.4) express the law of conservation of the number of particles; the conservation of energy follows, exactly as in the previous Chapter, from an *intertwining relation*

$$\Omega_\pm^\alpha H^\alpha = H\Omega_\pm^\alpha \tag{3.5}$$

and reads as

$$S_{\beta\alpha}H^\alpha = H^\beta S_{\beta\alpha} \qquad (3.6)$$

where now we have to take into account the fact that the final asymptotic hamiltonian can differ from the initial one.

We note that we could have well proceeded with a closer analogy with the single channel case. This is possible at the expense of introducing some more mathematics. Just to sketch this analogy we arrange the channel spaces $\mathcal{H}^\alpha$'s into one unique *asymptotic space* $\mathcal{H}_{asym}$. This is accomplished by building their (external) Hilbert direct sum

$$\mathcal{H}_{asym} = \sum_\alpha \oplus \mathcal{H}^\alpha$$

a general vector of which is a column vector with components $|\psi^\alpha\rangle$, that is

$$|\boldsymbol{\Psi}\rangle = \left(\begin{array}{c} .. \\ |\psi^\alpha\rangle \\ .. \end{array} \right)$$

In other words the previously defined channel components become the actual components of a vector in an "enlarged" space. This space is an Hilbert space with scalar product defined by

$$\langle\boldsymbol{\Psi}|\boldsymbol{\Phi}\rangle = \sum \langle\psi^\alpha|\phi^\alpha\rangle$$

where the sum runs over the channel components[9]. We can now arrange the channel evolution operators in a row vector, one component for each *channel*,

$$\mathbf{U}_t^0 = [....U_t^\alpha..]$$

and use the usual matrix multiplication rules. In this way the asymptotic limiting behavior of a scattering vector takes the form

$$U_t|\psi_0\rangle \rightarrow \mathbf{U}_t^0|\boldsymbol{\Psi}_{in}\rangle$$

and eq.(3.2) can be taken "as a whole", that is

$$\boldsymbol{\Omega}_\pm = lim_{t\to\mp\infty} U_t^\dagger \mathbf{U}_t^0$$

where $\boldsymbol{\Omega}_\pm$ is a row vector of operators, whose components are the channel Møller operators defined above. Eq.(3.3) allow us to write

$$\boldsymbol{\Omega}_\pm^\dagger \boldsymbol{\Omega}_\pm = \mathbf{1}$$

---

[9]If we define "canonical vectors" $|\Psi^\alpha\rangle = \{0.., |\psi^\alpha\rangle, ..0\}$ we may say that the "channels are orthogonal", i.e. $\langle\Psi^\alpha|\Phi^\beta\rangle = \delta_{\alpha\beta}$. However this is a mere consequence of the introduction of the asymptotic space.

where $\mathbf{\Omega}_{\pm}^{\dagger}$ is the column vector of the adjonts of the Møller operators and $\mathbf{1}$ is the unit operator of the asymptotic space $\mathcal{H}_{asym}$. This express the isometric property of the whole Møller operator. The scattering operator is now a true matrix

$$\mathbf{S} = \mathbf{\Omega}_{-}^{\dagger}\mathbf{\Omega}_{+}$$

which maps $\mathcal{H}_{asym}$ onto $\mathcal{H}_{asym}$ with one-to-one correspondence, being a unitarity operator

$$\mathbf{S}^{\dagger}\mathbf{S} = \mathbf{S}\mathbf{S}^{\dagger} = \mathbf{1}$$

Each element of it, $S_{\beta\alpha}$, relates the "in" channel α to the "out" channel β; that is, the column vector $\{S_{\beta\alpha}\}_{\beta}$ describes the outcome of a collision process that originates in channel α.

With the same token, the intertwining relation, eq.(3.5), takes the form

$$\mathbf{\Omega}_{\pm}\mathbf{H}^0 = H\mathbf{\Omega}_{\pm}$$

where $\mathbf{H}^0$ is the diagonal matrix of the channel hamiltonian operators H^{α}

$$\mathbf{H}^0 = \begin{bmatrix} .. & 0 & 0 \\ 0 & H^{\alpha} & 0 \\ 0 & 0 & .. \end{bmatrix}$$

and plays the role of *asymptotic hamiltonian*; the conservation of energy, eq.(3.6), can therefore be written in the compact form

$$[\mathbf{S}, \mathbf{H}^0] = \mathbf{0}$$

which exactly parallels that of the single channel case.

To close this section we note that the physically relevant observables are connected to the quantum operators through appropriate matrix elements of the $S_{\beta\alpha}$'s operators. Since this connection parallels that of the single channel case we move directly to the time-independent formalism knowing that our aim is, in any case, to obtain practical means for computing these matrix elements. We will turn later on the actual expressions which establishes the link between theory and experiments.

3.3 The Lippmann-Schwinger equation

Having developed the time-dependent formalism for the multichannel case we can introduce its time-independent version, on which much of the current work of research lays its foundation. With respect to the single channel case we have now to take into account the fact that each channel experiences its own potential. This *channel potential* vanishes in that regions of space in which the full

potential V approaches the internal potential of the channel in consideration[10]; that is, it is given by

$$V^\alpha = H - H^\alpha = V - v^\alpha$$

where v^α is the molecular potential of the specified arrangement. For example, in a model three atom system ABC in which V is a sum of pair potentials

$$V = V_{AB} + V_{BC} + V_{CA}$$

the channel potential for the channels of the $AB + C$ arrangement is given by

$$V^{C-AB} = V_{AC} + V_{BC} = V - V_{AB}$$

which is the potential that links the different fragments of the specified arrangement.

With this is mind we proceed, as in Section (2.3), by writing the (channel) Møller operator in integral form, applying it to an improper eigenvector of the channel hamiltonian H^α and performing the time integral. The result is

$$\Omega_+^\alpha \, |En; \alpha\rangle = |En; \alpha+\rangle = (\mathbf{I} + G^+(E)V^\alpha) \, |En; \alpha\rangle \qquad (3.7)$$

Here $|En; \alpha\rangle$ is an improper eigenvector with *total* energy E of the H^α operator, taken in the channel space $\mathcal{H}^\alpha$, and n is any quantum number needed to specify completely the state of the system (see also footnote 16 of Chapter (2)). The vector $|En; \alpha+\rangle$ is here defined and, in view of the intertwining relation, eq.(3.5), it is an eigenstate of the *full* hamiltonian with the same energy E which is called *stationary scattering state*.

Equation(3.7) introduces an "on shell" Møller operator

$$\Omega_+^\alpha(E) = (\mathbf{I} + G^+(E)V^\alpha) \qquad (3.8)$$

which allows us to write the following spectral resolution

$$\Omega_+^\alpha = \int dE \, \Omega_+^\alpha(E)\delta(E - H^\alpha) = \int dE \, \Omega_+^\alpha(E)\delta(E - \epsilon_\alpha - K^\alpha)$$

In writing this equation we have taken into account the fact that each channel Møller operator is defined on its channel subspace; furthermore, since K^α is a positive definite operator, the integral effectively runs in the range $E \geq \epsilon_\alpha$, i.e. when the channel in consideration is open.

Eq.(3.8) is again the usual limit $(\text{Im}\lambda \to 0^+$ with $\text{Re}\lambda = E)$ of the "generalized" channel Møller operator

$$\Omega^\alpha(\lambda) = (\mathbf{I} + G(\lambda)V^\alpha)$$

---

[10]As before, there is actually one different "channel" potential for each arrangement.

which satisfies a *Lippmann-Schwinger* equation analogue to eq.(2.29)

$$\Omega^\alpha(\lambda) = \mathbf{I} + G_\alpha(\lambda)V^\alpha\Omega^\alpha(\lambda)$$

where now the channel Green's operator takes the place of the free Green's operator and the channel potential takes the place of the potential.

Some differences with the single channel case arise when one introduces the transition operator. We now have a set of double labeled operators, $T_{\beta\alpha}$, which describe the transitions $\alpha \to \beta$ exactly as the scattering operators $S_{\beta\alpha}$ do. But, when we generalize eq.(2.27) to the multichannel case we are left with two *different* definitions for it. The first is known as the *post version* and is given by

$$\widetilde{T}_{\beta\alpha}(\lambda) = V^\beta\Omega^\alpha(\lambda) = V^\beta + V^\beta G(\lambda)V^\alpha$$

Its name arises from the fact that in it, when specialized to the Ω_+ case, we first take the system in the interaction region with the *initial* channel Møller operator *and then* we let it interact with the *final* channel potential. The *prior version* is instead

$$T_{\beta\alpha}(\lambda) = (\Omega^\beta(\lambda^*))^\dagger V^\alpha = V^\alpha + V^\beta G(\lambda)V^\alpha$$

and its name follows from analogous reasoning. The two operators differ for the difference of the two channel potentials

$$\widetilde{T}_{\beta\alpha}(\lambda) - T_{\beta\alpha}(\lambda) = V^\beta - V^\alpha$$

This may seem strange: we have two different operators, which is the correct one? The answer is that they differ for elements in which we are not interested in: as we should expect, we need only their matrix elements *on the energy shell* and the two operators give the *same* on-shell matrix elements [11]. However, they satisfy two different kinds of Lippmann-Schwinger equations

$$\widetilde{T}_{\beta\alpha}(\lambda) = V^\beta + \widetilde{T}_{\beta\alpha}(\lambda)G_\alpha(\lambda)V^\alpha$$

$$T_{\beta\alpha}(\lambda) = V^\alpha + V^\beta G_\beta(\lambda)T_{\beta\alpha}(\lambda)$$

because such equations involve also elements *out* of the energy shell. It seems that only the second of these equations resembles the single channel counterpart; however, an equation like the first one can be written also for the single channel case, as one can realize by taking $\alpha = \beta$ the label of the only channel in a single channel process.

---

[11] Indeed, $\langle E'm; \beta | V^\beta - V^\alpha | En; \alpha \rangle = \langle E'm; \beta | H^\beta - H^\alpha | En; \alpha \rangle$. However much care is needed in using the self-adjoint properties of an operator between *two* improper vectors (for example, the momentum operators are self-adjoint because in $\langle \psi | p | \phi \rangle$ a surface term vanishes when one consider at least one L^2 function).

Born series solutions can be hint for the Lippmann-Schwinger equation for the channel Møller operators and for that in terms of either versions of the transition operators; in particular, the first Born approximation of the two T versions differs again for the difference of the two channel potentials and, therefore, it leads to the same matrix elements *on the energy shell*.

The connection with the physically relevant cross-section is again given in terms of the S matrix. In particular, exactly as at the end of Section (2.3) we can obtain an expression for the "on-shell" S operators in terms of the transition operators. Using the same manipulations of Section (2.3) on the operators $S_{\beta\alpha} - \delta_{\beta\alpha}$ (in place of $S - 1$) we arrive at the following expression in terms of the *prior version* T operators

$$S_{\beta\alpha} = \int dE S_{\beta\alpha}(E)\delta(E - H^\alpha) \tag{3.9}$$

$$S_{\beta\alpha}(E) = \delta_{\beta\alpha} - 2\pi i\delta(E - H^\beta)T_{\beta\alpha}(E) \tag{3.10}$$

which can be written also in terms of the *post version* T operators since the projectors on either side of T ensure that they act on the energy shell. With the matrix notation introduced at the end of the previous Section, eq.s(3.9,3.10) can be rewritten as

$$\mathbf{S} = \int dE \mathbf{S}(E)\delta(E - \mathbf{H}^0)$$

$$\mathbf{S}(E) = \mathbf{1} - 2\pi i\delta(E - \mathbf{H}^0)\mathbf{T}(E)$$

where $\mathbf{T}(E)$ and $\mathbf{S}(E)$ are the matrix of operators $T_{\beta\alpha}(E)$ and $S_{\beta\alpha}(E)$ respectively and $\mathbf{H}^0$ has been defined in Section (3.2).

3.4   The stationary scattering states

Exactly as in Section (2.4) the Lippmann-Schwinger equation in terms of the stationary states can be shown to be equivalent to the Schrödinger equation with appropriate boundary conditions. The proof starts again by recognizing that the equation (3.7) or the following equation

$$|En; \alpha+\rangle = (\mathbf{I} + G(\lambda)V^\alpha)|En; \alpha\rangle \tag{3.11}$$

(which is the same in the limit $\text{Im}\lambda \to 0^+$ and $\text{Re}\lambda = E$) is equivalent to

$$(\lambda - H)|En; \alpha+\rangle = (\lambda - H^\alpha)|En; \alpha\rangle \tag{3.12}$$

Thus, this equation leads to a Schrödinger equation whose boundary conditions are obtained by considering the asymptotic form of the "scattered" term of

eq.(3.11) and by taking the limit *from above* in the complex energy plane. The purpose of this Section is to obtain such boundary conditions.

We begin by first noting that we can write the full Green's operator in term of any channel Green's operator, that is

$$G(\lambda) = G_{\rm b}(\lambda)(1 + V^{\rm b}G(\lambda)) = G_{\rm b}(\lambda)(\Omega^{\rm b}(\lambda^*))^{\dagger}$$

and in particular

$$G^+(E) = G_{\rm b}^+(E)(1 + V^{\rm b}G^+(E)) = G_{\rm b}^+(E)(\Omega_-^{\rm b}(E))^{\dagger}$$

(In these formulas we have taken into account the fact the G_β and V_β depend actually on the arrangement label and thus we have resorted to the "arrangement notation"). Then we use the asymptotic properties of the channel Green's operators. In doing this, we restrict attention to *two* body arrangements, that is we look at the scattered wave in a given two-body arrangement. In this case, we have already discussed a decomposition of the channel Green's operator in terms of the *free* Green's operator, eq.(3.1). This decomposition allows us to write

$$G^+(E) = \left\{ \sum_\beta G_0^+(E - \epsilon_\beta)p_{\rm b}^\beta + \int d\epsilon G_0^+(E - \epsilon)\delta(\epsilon - h) \right\} (\Omega_-^{\rm b}(E))^{\dagger} \quad (3.13)$$

where G_0 operates on the (unique) scattering coordinate of the arrangement b in consideration and $p_{\rm b}^\beta, h$ operate on the internal coordinates[12]. Therefore, we can multiply eq.(3.13) by the vector $\langle \mathbf{R} |$ (where $\mathbf{R} = R\widehat{\mathbf{X}}$ is the scattering coordinate of our "final" arrangement) and use the known asymptotic form of the free Green's function, eq.(2.37). In this case, however, we realize that we need also the asymptotic form of the Green's function for *negative* real values of the argument. Indeed, the closed channel terms in eq.(3.13) have *negative* translational energy. The requested asymptotic form is given by

$$\left\langle R\widehat{\mathbf{X}} \Big| G_0^\pm(E_P) \Big| \Phi \right\rangle \rightarrow -m(2\pi)^{1/2}\frac{e^{-PR}}{R}\widetilde{\Phi}(P\widehat{\mathbf{X}}) \text{ for } E_P = -P^2/2m$$

where

$$\widetilde{\Phi}(P\widehat{\mathbf{X}}) = \frac{1}{(2\pi)^{3/2}} \int d^3\mathbf{R}' e^{-P\widehat{\mathbf{X}}\mathbf{R}'} \left\langle \mathbf{R}' \big| \Phi \right\rangle$$

Thus, we see that the closed channels do not contribute to the asymptotic limit of the scattering states, being exponentially decaying, the faster the decaying the higher in energy is the channel level. We consider a total energy less than

---

[12]Note that in a *many* body arrangement one has no longer *one* "scattering" coordinate.

the threshold energy of the b arrangement, thereby having asymptotically only contributions from the (proper) channels. [13]

To complete the proof, we now consider a state that originates also from a two body arrangement and with (relative) momentum $\mathbf{P}$. We denote this state with $|\mathbf{P}; \alpha\rangle$, where α is the initial channel; its total energy content is given by $E = P^2/2m + \epsilon_\alpha$ and, for simplicity, is assumed to be *less* than the threshold for the breaking-up of the arrangement (see Footnote 6 in this Chapter). Moreover, we look for the full coordinate representation of the wavefunction and therefore project eq.(3.7) on the vector $\langle \mathbf{R}\mathbf{r}|$, where $\mathbf{R}$ has been defined before and $\mathbf{r}$ is the set of internal coordinates of the final arrangement which we are looking at. The final expression of the scattering wavefunction in the limit for $R \to \infty$ depends on whether or not we look at the initial arrangement. In the first case, i.e. when we look at the *elastic* and *inelastic* scattering contributions, we get

$$\langle \mathbf{R}\,\mathbf{r}|\mathbf{P}; \alpha+\rangle \to$$
$$\frac{1}{(2\pi)^{3/2}} \left\{ e^{i\mathbf{P}.\mathbf{R}} \phi_\alpha(\mathbf{r}) + \sum_\beta f(P_\beta \widehat{\mathbf{X}}; \beta \leftarrow \mathbf{P}; \alpha) \frac{e^{iP_\beta R}}{R} \phi_\beta(\mathbf{r}) \right\}$$

$$(3.14)$$

while in the second one, i.e. when we look at the *reactive* outcome, we obtain

$$\langle \mathbf{R}\,\mathbf{r}|\mathbf{P}; \alpha+\rangle \to$$
$$\frac{1}{(2\pi)^{3/2}} \left\{ \sum_\beta \left(\frac{\mu_\beta}{\mu_\alpha} \right)^{1/2} f(P_\beta \widehat{\mathbf{X}}; \beta \leftarrow \mathbf{P}; \alpha) \frac{e^{iP_\beta R}}{R} \phi_\beta(\mathbf{r}) \right\}$$

$$(3.15)$$

In both formulas the sums run over the *open* channels, where

$$P_\beta = \sqrt{2\mu_\beta (E - \epsilon_\beta)}$$

is the channel translational energy (with m_β the relevant reduced mass), $\phi_\beta(\mathbf{r})$'s are the channel eigenstates and $f(P_\beta \widehat{\mathbf{X}}; \alpha \leftarrow \mathbf{P}; \alpha)$ is the *scattering amplitude* for the indicated transition. This amplitude is given by

$$f(P_\beta \widehat{\mathbf{X}}; \beta \leftarrow \mathbf{P}; \alpha) = -(\mu_\beta \mu_\alpha)^{1/2} (2\pi)^2 \left\langle P_\beta \widehat{\mathbf{X}}; \beta \middle| T_{\beta\alpha}(E) \middle| \mathbf{P}; \alpha \right\rangle \qquad (3.16)$$

which can be written equivalently in terms of the *post version* T operator. In this equation the mass factors are introduced following ((Taylor, 1969),

---

[13]Indeed, we can show that theses contribution are negligible just outside of the strong interaction region. This property can lead to notable saving of CPU time in actual computation (see Section(10.3)).

Chapter 19) in that they ensure that the cross-sections have the same formal expression

$$\frac{d\sigma}{d\Omega}(\mathbf{P}_\beta; \, \beta \leftarrow \mathbf{P}_\alpha; \, \alpha) = \frac{P_\beta}{P_\alpha} \, |f(\mathbf{P}_\beta; \, \beta \leftarrow \mathbf{P}_\alpha; \, \alpha)|^2 \qquad (3.17)$$

in terms of the scattering amplitudes both for collisions with rearrangement and for collisions without rearrangement . Indeed the simple rule

$$\mathrm{cross-section} \; = \frac{\mathrm{scattered\ flux/solid\ angle}}{\mathrm{incident\ flux/area}}$$

leads to eq.(3.17) when one notes that the incident flux per unit area is given by

$$\mathrm{incident\ flux/area} \; = (2\pi)^{-3}\frac{P}{\mu_\alpha}$$

and the differential scattered flux is

$$\mathrm{diff.\, scattered\ flux} \; = (2\pi)^{-3}\frac{\mu_\beta}{\mu_\alpha}\frac{P_\beta}{\mu_\beta}|f|^2$$

Eq.s(3.14,3.15) are the boundary conditions that we were looking for. They clearly state that, asymptotically, the scattering states is a superposition of the incoming plane wave and outgoing spherical waves. Indeed, exactly as in Section (2.4) one can set up a "spatial" description of the scattering process that exactly parallels that of the single channel case. That is, if one properly prepares a wavepacket and launch it toward the target, long after the collision (s)he observe a superposition of the original wavepacket with a spherically spread one (Fig.(3.4)). Here we note only that in the multichannel case the various channel components of the scattered wavepacket moves with different speeds: the less the channel energy the more the velocity of the component. Therefore, in a deexcitation processe one observe a component *in advances* with respect to the incident wave[14].

3.5 The Close-Coupling approximation

In this Section we discuss in fairly general terms the widely used Close-Coupling approximation. This approximation scheme is today widely used both in inelastic and in reactive scattering calculations, either in the time-independent or in the time-dependent framework. Here we consider only its theoretical foundations and, possibly, its merits and limitations. The actual specialization to a case in which we are interested in will be discussed later, in Section (4.4).

---

[14]Much like in the single channel case, this picture is valid only "off-resonance".
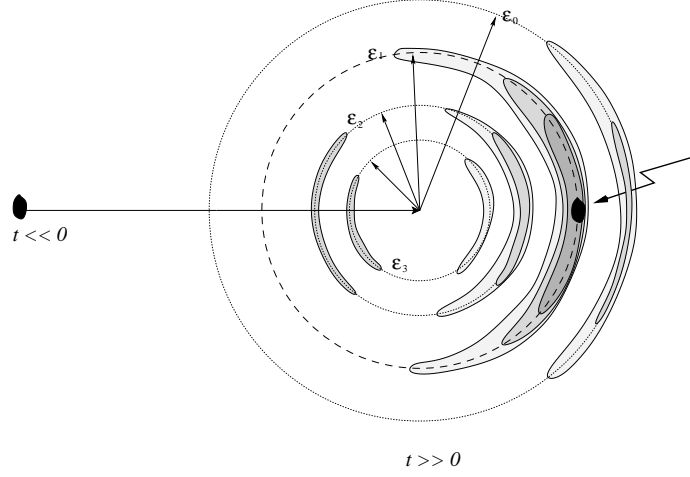
Figure 3.4: An inelastic event. The wavepacket long before (on the left) and long after (on the right) the collision. We have four open channels ($n = 0, .., 3$ with $\epsilon_0 < .. < \epsilon_3$) and the collision starts form channel 1. On the right the big arrow marks the incident wavepacket. The radius of the various circles are given by $v_n t$ where v_n is the "channel speed".

We introduce it using the *partitioning technique* in the time-independent formulation (Levine(1969), Part 3). This technique has the merit to give some physical insight to the procedure, thus allowing to establish the feasibility of the approximation as we will discuss at the end of this Section. However, we are not able to avoid the introduction of some more mathematics...which we hope will not obscure the physical content of the subject.

The partitioning technique consists in dividing the Hilbert space $\mathcal{R} \subset \mathcal{H}$ in two spaces, one that is of direct interest ($\mathcal{P}$) and the other that is of secondary importance ($\mathcal{Q}$). The aim is obtain an *exact* equation for the vectors projected onto the space $\mathcal{P}$ which implicitly takes into account the effect of the less important space $\mathcal{Q}$. In this way, approximate solutions to the scattering problem can be obtained by neglecting or modeling the influence of the $\mathcal{Q}$ space on the dynamics. In this sense its use is much like the use of a reduced density matrix (see for example Section (1.5)) in handling many body phenomena: one focuses attention on a part of the system and tries to model the interaction with the "bath".

Let us consider, for example, the collision of an atom with a diatomic molecule at an energy such that only the inelastic processes can take place. We may focus attention on the *open* channels which, ultimately, are the only channels that contribute to the asymptotic wavefunction. In this case we

consider the following projection operator

$$P = \sum_\alpha |\phi_\alpha\rangle \langle\phi_\alpha| \tag{3.18}$$

where ϕ_α's are the rovibrational eigenstates of the diatomic and the sum runs over the open channels and some low-energy closed channels. We can then define the $\mathcal{P}$ space as image of the projector (3.18), that is $\mathcal{P} = P(\mathcal{R})$, and the $\mathcal{Q}$ space follows from the image of the projector[15] $Q = 1 - P$. In this case we are interested in an *exact* equation for the scattering eigenstate projected onto the $\mathcal{P}$ space, that is

$$\langle \mathbf{R}\,\mathbf{r}| \, P \, |\mathbf{P}; \, \alpha_0+\rangle = \sum_\alpha F_{\alpha\leftarrow\alpha_0}(\mathbf{R})\phi_\alpha(\mathbf{r})$$

where the F's here introduced are the translational "channel components" of our wavefunction. Since in the asymptotic region $(R \to \infty)$ the exact wavefunction coincides with the projected one, we could obtain, in principle, all the scattering informations from this "reduced dimensionality" function.

In the following P and Q will be the projector operators onto $\mathcal{P}$ and $\mathcal{Q}$ respectively and A_{PP}, A_{PQ}, ...will be the "components" of the general operator A on the above mentioned spaces, that is $A_{PP} = PAP$, $A_{PQ} = PAQ$, and so on. For each operator we have four different components: the "on-diagonal" A_{PP} and A_{QQ} operates *in* $\mathcal{P}$ and $\mathcal{Q}$ respectively, while the "off-diagonal" A_{PQ} and A_{QP} operates from one space to the other. We work in fairly general terms with the "components" $PG(\lambda)$ and $QG(\lambda)$ of the Green's operator *onto* the $\mathcal{P}$ and $\mathcal{Q}$ space; if we want to solve the particular non-homogeneous problem

$$(\lambda - H)\,|\psi\rangle = |\phi\rangle$$

in term of the components $P\,|\psi\rangle$ and $Q\,|\psi\rangle$ it is then sufficient to apply the $PG(\lambda)$ and $QG(\lambda)$ operators on the vector $|\phi\rangle$.

The result we need is obtained from the system of equations

$$\begin{cases} (\lambda - H_{PP})PG(\lambda) - H_{PQ}QG(\lambda) = P \\ -H_{QP}QG(\lambda) + (\lambda - H_{QQ})QG(\lambda) = Q \end{cases}$$

which, in turn, follows from the equation $(\lambda - H)G(\lambda) = 1$ that defines the Green's operator. All the quantities of interest can be expressed in terms of the following "Q-Green's operator"

$$\widetilde{G}_Q(\lambda) = (\lambda - H_{QQ})^{-1} \tag{3.19}$$

---

[15]Since we deal only with the $\mathcal{R}$ space we write 1 for the identity operator in this space, although a more appropriate notation would be $1_\mathcal{R}$.

where, in practice, the hamiltonian H_{QQ} describes the "constrained" motion in the $\mathcal{Q}$ space. Eq.(3.19) allows us to solve for the components of interest and lead us to the equation

$$\begin{cases} (\lambda - H_P^{eff}(\lambda))G_{PP}(\lambda) = P \\ (\lambda - H_P^{eff}(\lambda))G_{PQ}(\lambda) = H_{PQ}\widetilde{G}_Q(\lambda)Q \end{cases} \qquad (3.20)$$

which states the map *to the* $\mathcal{P}$ *space* of the Green's operator, i.e. of $PG = G_{PP} + G_{PQ}$. The effective hamiltonian introduced in eq.(3.20) is given by

$$H_P^{eff}(\lambda) = H_{PP} + H_{PQ}\widetilde{G}_Q(\lambda)H_{QP} \qquad (3.21)$$

where the last term on the r.h.s. of the above equation is known as *effective* or *optical potential*

$$V_P^{opt}(\lambda) = H_{PQ}\widetilde{G}_Q(\lambda)H_{QP} \qquad (3.22)$$

We turn back to these operators below, just after having reordered these complicated formulas. Meanwhile we note only that the first line of eq.(3.20) tells us that the *in the* $\mathcal{P}$ *space* the *full* Green's operator can be computed with an *effective* hamiltonian

$$G_{PP}(\lambda) = (\lambda - H_P^{eff})^{-1}P$$

thus establishing an equivalence relation (in $\mathcal{P}$) between the exact hamiltonian and some effective one. Two other expressions for the QG component can be obtained

$$\begin{cases} G_{QQ}(\lambda) = \widetilde{G}_Q(\lambda)(1 + H_{QP}G_{PQ}(\lambda)) \\ G_{QP}(\lambda) = \widetilde{G}_Q(\lambda)H_{QP}G_{PP}(\lambda) \end{cases} \qquad (3.23)$$

where G_{PQ} and G_{PP} are given by eq.(3.20) in terms of the Green's operator of equation (3.19). As a whole, eq.s(3.20,3.23) express the full Green's operator in terms of a unique "variable", the Q-Green's operator, and therefore we call them "Q-expressions"[16]. Analogous relations can be obtained in terms of the "P-Green's operator"

$$\widetilde{G}_P(\lambda) = (\lambda - H_{PP})^{-1} \qquad (3.24)$$

that is

$$\begin{cases} (\lambda - H_Q^{eff}(\lambda))G_{QQ}(\lambda) = Q \\ (\lambda - H_Q^{eff}(\lambda))G_{QP}(\lambda) = H_{QP}\widetilde{G}_P(\lambda)P \end{cases} \qquad (3.25)$$

---

[16]It's worth to note that the Q-Green's operator "variable" can occur also implicitly through the Green's operator of the effective hamiltonian. The latter operator gives the solution of the first line in eq.(3.20) and can be used explicitly in the "Q-expressions" reported.

and

$$\begin{cases} G_{PP}(\lambda) = \widetilde{G}_P(\lambda)(1 + H_{PQ}G_{QP}(\lambda)) \\ \quad G_{PQ}(\lambda) = \widetilde{G}_P(\lambda)H_{PQ}G_{QQ}(\lambda) \end{cases} \tag{3.26}$$

and we call them "P-expressions".

Eq.s(3.20,3.21,3.22) are the key equations we were looking for: we have first introduced the Green's operator for the "constrained" motion *in the* $\mathcal{Q}$ *space* (the Q-Green's operator of eq.(3.19)) and then written an effective hamiltonian for the motion *in the* $\mathcal{P}$ *space* in which the constraints due to the use of the projected hamiltonian H_{PP} are exactly corrected for by an *effective potential*. To apply these results to a specific situation we use eq.(3.12), which we rewrite as

$$(\lambda - H)\,|\psi\rangle = (\lambda - H^\alpha)\,|\phi\rangle$$

We suppose for simplicity that $[P, H^\alpha] = [Q, H^\alpha] = 0$ and $Q\,|\phi\rangle = 0$; these conditions are satisfied, for example, in the scattering of an atom off a diatomic molecule discussed above, eq.(3.18)[17]. Then, we obtain

$$|P\psi\rangle = G_{PP}(\lambda)(\lambda - H^\alpha)\,|\phi\rangle$$

or with the help of eq.(3.20)

$$(\lambda - H_P^{eff}(\lambda))\,|P\psi\rangle = (\lambda - H^\alpha)\,|\phi\rangle \tag{3.27}$$

We see that equation (3.27) for the P component of the scattering eigenstate is formally identical to the Lippmann-Schwinger equation for the full eigenfunction in the $\mathcal{P}$ space. The only difference is that hamiltonian H_{PP} is modified by the presence of the *optical* potential defined in eq.(3.22). This *non-local* and *energy-dependent* potential operator express *implicitly* the role of the Q space on the dynamics. It allowed us to write down a closed equation for P component of the scattering eigenfunction, eq.(3.27), that, by a suitable choice of the $\mathcal{P}$ space, can be considerably simpler to solve than the original one. However, this potential is a dream more than a reality: it is usually not known unless we know the dynamics in the (complicated) Q space.

If we neglect the optical potential in eq.(3.27) we obtain a simple equation in terms of the unknown $|\psi_{cc}\rangle$

$$(\lambda - H_{PP})\,|\psi_{cc}\rangle = (\lambda - H^\alpha)\,|\phi\rangle \tag{3.28}$$

---

[17]Note that we could generalize the projector of equation (3.18) to an **R**-dependent case

$$P = \sum \left|\phi_\alpha^{\mathbf{R}}\right\rangle \left\langle\phi_\alpha^{\mathbf{R}}\right|$$

where $\left|\phi_\alpha^{\mathbf{R}}\right\rangle$ depends parametrically on **R** and reduces to $|\phi_\alpha\rangle$ when $R \to \infty$ as it is done in the *adiabatic* expansion. However in this case the commutation relation $[P, H^\alpha] = 0$ is no longer satisfied.

which involves only operators acting *in* the $\mathcal{P}$ space[18]. When the $\mathcal{P}$ space is chosen like in eq.(3.18) this approximation is known as the *Close-Coupling approximation* (CC). It is probably the current most widely used approach to the scattering problems: it has been here introduced in the time independent framework but it clearly applies also to the (equivalent) time-dependent case. In Section (4.4) we will consider the application of this equation to the problem addressed before of the scattering of an atom off a diatomic; in the meantime we try to get some ideas about the feasibility of this approximation which, in some sense, is expected to be good (at the energy considered) when the Q space plays a negligible role on the dynamics.

In order to see when this is case we look at the optical potential of eq.(3.22) which now consider on the physical energy axis

$$V^{opt}(E) \equiv lim_{\mathrm{Im}\lambda \to 0^+} V_P^{opt}(\lambda)\,(\mathrm{Re}\lambda = E) = H_{PQ}\widetilde{G}_Q^+(E)H_{QP}$$

Let H_{QQ} be an "usual" hamiltonian, with a discrete spectrum bound from below and a continuous spectrum that extends from a given energy E_{th} to infinity (see also Fig.(3.5)). We may distinguish three cases:

Case(a). If the total energy of the system is less than the threshold energy E_{th} for the continuous spectrum of H_{QQ} then the Q-hamiltonian H_{QQ} cannot describe any scattering motion. In this case, then, when the energy is *not* an eigenvalue of H_{QQ} we have

$$\widetilde{G}_Q^+(E) = \widetilde{G}_Q^-(E) = \widetilde{G}_Q^{pr}(E)$$

that is the Green's operator is continuous and self-adjoint (it coincides with its "principal value" $\widetilde{G}_Q^{pr}(E)$, see Appendix A). It follows that $V^{opt}(E)$ is self-adjoint and can be viewed as a pure "distortion potential". We can argue that this potential is small when H_{PQ} is "small" and/or when the energy is far from the singularities of the Q-Green's operator, that is from the spectrum of H_{QQ}.

Case(b). For $E > E_{th}$ we can write

$$\widetilde{G}_Q^+(E) = \widetilde{G}_Q^{pr}(E) - i\pi\delta(E - H_{QQ})$$

and then

$$V^{opt}(E) = V^R(E) - iV^I(E)$$

---

[18]With the solution of eq.(3.28) at hand one may write, if needed, an equation for the (component of the) exact wavefunction, that is

$$|P\psi\rangle = |\psi_{cc}\rangle + G_{PP}(\lambda)V_P^{opt}(\lambda)\,|\psi_{cc}\rangle = |\psi_{cc}\rangle + \widetilde{G}_P(\lambda)V_P^{opt}(\lambda)\,|P\psi\rangle$$

but this is as much as complicated as the original one.
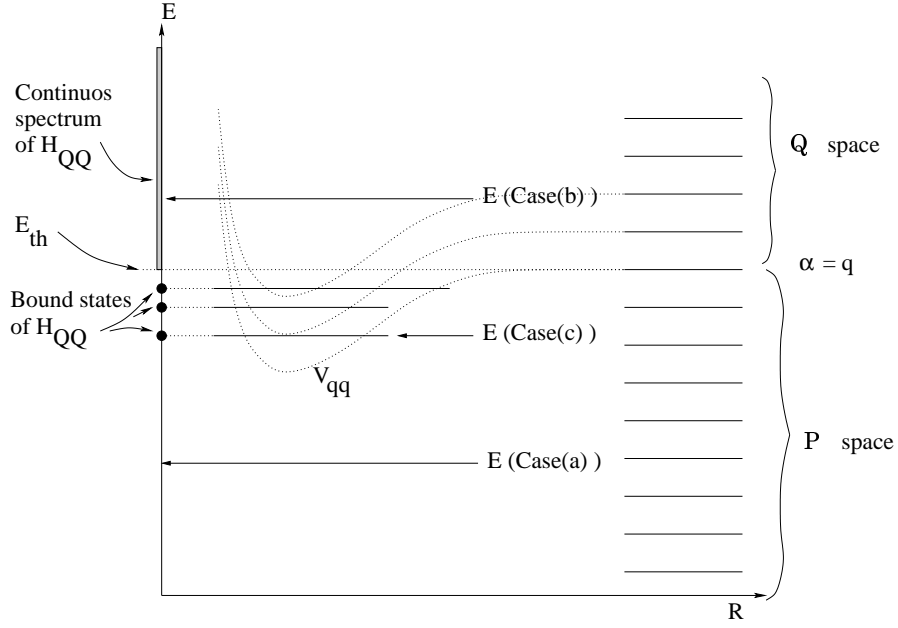
Figure 3.5: A model scattering system: an atom-molecule system in which the molecule has a pure discrete spectrum. The hamiltonian H_{QQ} is given by $T + QVQ + \sum_{\alpha \geq q} \epsilon_\alpha \left| \phi_\alpha \right\rangle \left\langle \phi_\alpha \right|$ and its "threshold energy", E_{th} , is given by ϵ_q. The V_α's are effective potentials for the channels α (either adiabatic or diabatic depending on the situation); usually their bound levels are good approximation to the bound states of H_{QQ}. The case (a), (b) and (c) are discussed in the text. The resonance phenomenon (case(c)) that arises form the internal structure of the colliding partners is called *Feshbach* resonance. In our case the atom-diatom system is temporarily trapped in a well of the interaction potential (i.e. it forms the quasi-bound state), the released translational energy being used to excite the molecule to an asymptotically closed level.

where $V^R(E)$ is a kind of "distortion potential" introduced before and

$$V^I(E) = \pi H_{PQ}\delta(E - H_{QQ})H_{QP}$$

is a *positive definite* operator. We therefore see that the optical potential has a non null negative imaginary part which play the role of an *absorbing* potential in that it determine the non-conservation of probability in time. This absorbing potential clearly takes into account the fact that, now, the $\mathcal{Q}$ space can contribute to the distribution of the scattering flux.

Case(c). When the energy is close to an eigenvalue of H_{QQ} our formalism goes into trouble since the Q-Green's operator (and the optical potential) has a polar discontinuity. This singularity is responsible of anomalous behavior of the scattering eigenfunction which, as we will show below, is associated with the presence of a *resonance*. In order to proceed we resort to the "P-expressions" introduced before, that do not suffer of any singularity. Before doing this, however, we note that very close to the chosen eigenvalue E_i of H_{QQ}, the Q-Green's operator can be well approximated by the term

$$\frac{1}{\lambda - E_i}\left|q_i\right\rangle\left\langle q_i\right|$$

where $\left|q_i\right\rangle$ is the corresponding eigenstate in the simple non-degenerate case. Therefore, we may focus attention on such state *defining* a new $\mathcal{Q}$ space as the corresponding eigenspace of the previously chosen hamiltonian H_{QQ}[19] . In this case the projected wavefunction onto the corresponding new $\mathcal{P}$ space is *more* than a close-coupling wavefunction in the sense that it takes into account all eigenstates of the previous H_{QQ} *except* $\left|q_i\right\rangle$. We will indicate the solution of the equation (3.28) with this choice of the $\mathcal{P}$ and $\mathcal{Q}$ space with $\left|\psi_d^\alpha+\right\rangle$ where "d" stands for *direct*[20]: in the language of perturbation theory this state proceeds without having the $\left|q_i\right\rangle$ state as an intermediate. Now, eq.(3.27) can be written in the form

$$\left|P\psi\right\rangle = G_{PP}(\lambda)(\lambda - H_{PP})\left|\psi_d^\alpha+\right\rangle$$

which with the help of the "P-expressions" eq.(3.26) can be rewritten as

$$\left|P\psi\right\rangle = \left|\psi_d^\alpha+\right\rangle + \widetilde{G}_P(\lambda)H_{PQ}G_{QQ}(\lambda)H_{QP}\left|\psi_d^\alpha+\right\rangle$$

In this form the second term on the r.h.s. contains the interaction with of the bound-state $\left|q_i\right\rangle$. The asymptotic behavior of this term is analogous

---

[19]That is, we now set $Q = \left|q_i\right\rangle\left\langle q_i\right|$ and $H_{QQ} = E_i Q$.

[20]We use the $+$ symbol since at the end we will take the usual limit $\mathrm{Im}\lambda \to 0^+$. More properly, one should use the λ "parameter".

to that of the first term; indeed the presence of the P-Green's operator on the left allows us to perform the same manipulation done in Section (3.4). The result is that the scattering amplitude (in any arrangement) is the sum of a *direct* and a *resonant term*: the first contribution arises from $|\psi_d^\alpha +\rangle$ and the latter comes from the "potential"

$$H_{PQ} G_{QQ}(\lambda) H_{QP}$$

(cfr eq.(3.11)). We have almost the desired result; we take the usual limit and write

$$G_{QQ}^+(E) = (E - H_Q^{eff}(E^+))^{-1} = (E^+ - E_i - \Delta_i(E) - i\Gamma_i(E))^{-1} Q$$

where

$$\Delta_i(E) = \left\langle q_i \middle| H_{QP} \widetilde{G}_P^{pr}(E) H_{PQ} \middle| q_i \right\rangle$$

is a real quantity and

$$\Gamma_i(E) = \pi \left\langle q_i \middle| H_{QP} \delta(E - H_{PP}) H_{PQ} \middle| q_i \right\rangle$$

is real and positive definite[21]. The final result for the resonant amplitude is therefore (cfr eq.(3.16))

$$f_{res} = -(m_\beta m_\alpha)^{1/2}(2\pi)^2 \frac{\left\langle P_\beta \widehat{\mathbf{X}}; \beta_d - \middle| H_{PQ} \middle| q_i \right\rangle \left\langle q_i \middle| H_{QP} \middle| \psi_d^\alpha + \right\rangle}{E - E_i - \Delta_i(E) - i\Gamma(E)}$$

where, as before, the subscript d refers to the "direct" process. As it is evident this expression *can* give rise to the famous Lorentzian shape of the resonance as a function of energy[22].

The three cases above described allow us some insight into the Close-Coupling approximation (see also Fig.(3.5)). It is surely reliable in case(a) when the total energy is well below the lowest eigenvalue of H_{QQ}; this represents the ideal situation for a CC calculation. In the other cases the reliability of the approximation depends critically on the "interaction" terms H_{PQ} and H_{QP} which, in turn, are system dependent. The CC approximation, however, can hardly be good in case(c): the only remedy left is to "enlarge" the $\mathcal{P}$ space in order to contain the (quasi) bound state.

---

[21] The projector appearing in this equation can be explicitly written is terms of the direct scattering states at the given energy, i.e.

$$\delta(E - H_{PP}) = \sum \left| \psi_d^{E\alpha} + \right\rangle \left\langle \psi_d^{E\alpha} + \right|$$

[22] It should be noted that this result is exact, that is it is valid also when the resonance is not "isolated". However, in the latter case this result is useless because the "direct" term is also wildly behaving.

Chapter 4

Computing scattering
observables

In this Chapter we review the basic approaches to computing scattering observables. It is clearly impossible to consider the *plethora* of methods developed up to now; the interested reader is referred to the recent book of J. Zhang (1999) and reference therein for a more comprehensive treatment of the subject. Rather, we outline here the general ideas and focus attention on those particular approaches that are relevant for the Part II of this work.

As we have already emphasized in the previous two Chapters we have at hand two basic approaches which differ for the choice of the "domain": in the time-dependent approach of Sections (4.2,4.3) one follows the time evolution of a properly prepared wavepacket and at the end extracts the relevant scattering observables on a broad energy range using the information at all times; in the time independent approach of Sections (4.4,4.5) one works directly on the energy domain by solving the scattering equations at a fixed total energy and he extracts the scattering amplitude from the asymptotic behavior of the stationary scattering states, for every fixed total energy.

This subdivision is a "traditional" one in the sense that in the last years several "hybrid" approaches have been developed; for example, one may work with *wavepackets* (i.e. superposition of scattering eigenstates with different energies) in a time-*independent* framework (Zhu et al., 1994a; Zhu et al., 1994b). We have chosen this coarse grained point of view since it closely resembles the *experimental* practice: on the one hand we have the stationary approach of the cross-beam experiments (e.g. see Scoles(1988)) and, on the other hand, we have the real-time photographs of the collision processes that come from the Femtochemistry world (Zewail(2000))[1].

---

[1]We can hardly be wrong if we state that the "Femtolands" of Zewail et al. at Caltech

4.1   Partial wave expansion

Before outlining the most common practical approaches to computing dynamical observables let us do few comments about conservation laws. Conservation laws are important not only from a theoretical point of view: actual calculations could not be done without taking into account the simplifications that arise from the symmetry properties of the collision system. Up to now we have only used the energy conservation law and, implicitly, the total (linear) momentum conservation, i.e. the invariance principles that arise from the homogeneity of time and space, respectively. There are at least two other symmetries that turn out to be useful in molecular collisions[2]. We will discuss first the total *angular* momentum conservation law and, then, we will briefly mention the conservation of *parity*.

For definiteness we consider a simple, spin-less, three atom system ABC. Its hamiltonian can be written in terms of the Jacobi coordinates $(\mathbf{R}, \mathbf{r})$ of one of the arrangements, for example $A + BC$, (we drop the arrangement label)

$$H = \frac{\mathbf{P}^2}{2\mu} + \frac{\mathbf{p}^2}{2m} + V$$

or equivalently

$$H = \frac{P_r^2}{2\mu} + \frac{\mathbf{l}^2}{2\mu R^2} + \frac{p_r^2}{2m} + \frac{\mathbf{j}^2}{2mr^2} + V \qquad (4.1)$$

where P_r and p_r are the *radial* momenta of the relative $(A - BC)$ and internal motion (BC) respectively, $\mathbf{l}$ is the orbital angular momentum of the relative motion and $\mathbf{j}$ is the "rotor" angular momentum of BC. The total angular momentum

$$\mathbf{J} = \mathbf{l} + \mathbf{j}$$

is conserved because H is a scalar operator, i.e. it is invariant under arbitrary rotations (we are considering an isolated scattering system).

In classical mechanics, taking into account this and the linear momentum conservation law, one can reduce the motion of our three atom system to a simpler 3x3-6=3 dimensional problem. That is, one factors out the overall translations and the overall rotations. In quantum mechanics the situation is somewhat different since the three components of the angular momentum operator do not commute and, thus, cannot have simultaneously a definite value, *except* when $J = 0$. This means that we cannot effectively factor out *three* coordinates by making use of the rotational invariance.

---

are already part of the History of Chemistry.

[2]We will not mention a third symmetry, the time-reversal, that is also useful in practice (it makes the "K matrix" real). It would be of great interest to discuss such invariance principle in its own right, but it is well beyond the scope of the present work...

Anyway, we can expand the state vector of our system in terms of $\{J^2,\ J_z\}$ eigenvectors

$$|\Psi\rangle = \sum_{J=0}^{\infty} \sum_{M=-J}^{J} \left|\Psi^{JM}\right\rangle \tag{4.2}$$

where the vectors $\left|\Psi^{JM}\right\rangle$ have definite values $\{J(J+1),\ M\}$ of the above mentioned obervables, and get independent equations of motion of each of them. This means that either in the Time-Dependent and in the Time-Independent approach the problem is considerably simplified. Furthermore, it is worth to note that the value M of the projection of the angular momentum operator depends essentially on the choice of the reference system and thus the fundamental (scalar) variables are independent of its value. For example, the rotational invariance implies the commutation relations

$$[\mathbf{S}, J_i] = 0 \ \text{ for } i = x, y, z$$

which identify the scattering $\mathbf{S}$ matrix as a scalar operator; from this follows that the matrix elements $\langle J'M'\alpha|S|JM\beta\rangle$ are diagonal in J *and* independent of M [3]. We feel, in this way, to have accomplished a "two-dimensional" reduction of the dimensionality of the problem.

There are at least two ways in which exploiting, in practice, rotational invariance[4]. In the *Space-Fixed Representation* one uses a complete set of eigenvectors of the operators

$$\{J^2,\ J_z,\ l^2,\ j^2\}$$

These vectors, denoted $|JMlj\rangle$, can be obtained by coupling the l, j angular momenta, i.e. using the known vector coupling rules

$$|JMlj\rangle = \sum_{m_l m_j} |lm_l jm_j\rangle \langle lm_l jm_j|JMlj\rangle \tag{4.3}$$

where $|lm_l jm_j\rangle$ are eigenvectors of $\{l^2,\ l_z,\ j^2,\ j_z\}$ and the Clebsh-Gordon (CG) coefficients are usually known in terms of $3j$ symbols

$$\langle lm_l jm_j|JMlj\rangle = (-)^{l-j+M}(2J+1)^{1/2} \begin{pmatrix} l & j & J \\ m_l & m_j & -M \end{pmatrix}$$

---

[3] A formal proof can be obtained by using the rising and lowering $J_\pm$ operators in the above mentioned commutation relations.

[4] The following discussion is based on the excellent works of Pack(1974) and Launay(1976) and on Appendix D of the book of J. Zhang(1999). It follows however the personal tastes of the author.
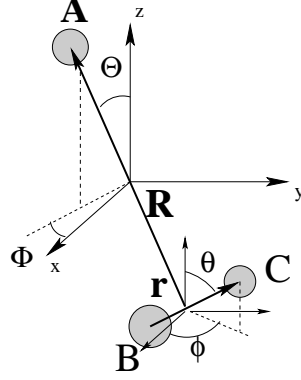
Figure 4.1: Coordinates of the A-BC system in a Space-Fixed reference frame.

The above sum, eq.(4.3), is actually a single sum since the CG coefficients vanish unless $m_l + m_j = M$; furthermore, from the triangular inequality it follows, for example, that for each (J, j) values l can take up $2Min(J, j) + 1$ values, i.e.

$$l = |J - j|, \ |J - j| + 1, ..J + j$$

In coordinate representation, introducing the unit vectors along $\mathbf{R}$ and $\mathbf{r}$, we can write

$$\left\langle \widehat{\mathbf{R}}\widehat{\mathbf{r}} \middle| JMlj \right\rangle \equiv \mathcal{J}_{lj}^{JM}(\Theta, \Phi, \theta, \phi) =$$
$$= \sum_{m_l m_j} (-)^{l-j+M} (2J+1)^{1/2} \begin{pmatrix} l & j & J \\ m_l & m_j & -M \end{pmatrix} Y_l^{m_l}(\Theta, \Phi) Y_j^{m_j}(\theta, \phi)$$

$$(4.4)$$

where (Θ, Φ) and (θ, ϕ) are the polar coordinates of $\mathbf{R}$ and $\mathbf{r}$ respectively (see Fig.(4.1)).

On the other hand, in the *Body Fixed Representation* one uses the complete set of eigenvectors of the operators

$$\{J^2, \ J_z, \ J_\zeta, \ j^2\}$$

where ζ is a body-fixed axis[5]. We choose, as usual, the ζ axis coincident with the $\widehat{\mathbf{R}}$ direction[6]. In particular, we define a Body-Fixed (BF) *reference frame*

---

[5]It is necessary for ζ to be *body-fixed*. Adversely, the corresponding operator cannot commute with J_z; the relation $[J_z, \ J_\zeta] = 0$ follows from the scalar nature of the operator $J_\zeta = \mathbf{J}\mathbf{n}_\zeta$ where $\mathbf{n}_\zeta$ is the unit vector of the axis ζ.

[6]This is the usual choice when one focuses on a particular arrangement, e.g. in non-reactive dynamical calculations. When all the arrangements are evenhandled (i.e. with the use of hyperspherical coordinates) the body-fixed axis is better chosen to be the vector normal to the plane of the three atoms.
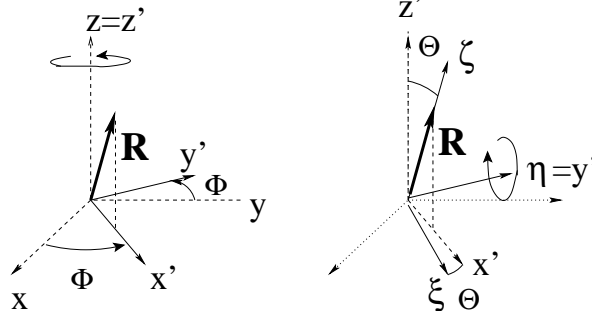
Figure 4.2: The BF reference frame is obtained by the SF one with two rotations: a Φ rotation around the z axis brings the (xyz) system in $(x'y'z')$ system; a Θ rotation around y' brings $(x'y'z')$ in $(\xi\eta\zeta)$.

$(\xi\eta\zeta)$ in such a way the η axis lies always on the xy plane of the Space-Fixed (SF) reference frame (xyz). For a given direction $\widehat{\mathbf{R}}$ of the relative position vector the BF frame can be obtained by rotating the SF frame of the Euler angles $(\Phi, \Theta, 0)$ (Fig.(4.2)).

In order to obtain a coordinate representation of the BF vectors, denoted with $|JM\Omega j\rangle$, we focus attention on a given direction $\widehat{\mathbf{R}}$, i.e. we consider the vector $\left\langle\widehat{\mathbf{R}}\middle|JM\Omega j\right\rangle$. This vector can be obtained by (inverse) rotation of the corresponding BF vector[7],

$$\left\langle\widehat{\mathbf{R}}\middle|JM\Omega j\right\rangle_{SF} = R^{-1}(\Phi, \Theta, 0)\left\langle\widehat{\mathbf{R}}\middle|JM\Omega j\right\rangle_{BF}$$

where R is the rotation operator of Messiah(2000)

$$R(\alpha, \beta, \gamma) = e^{-iJ_z\alpha}e^{-iJ_y\beta}e^{-iJ_z\gamma}$$

here written in terms of the SF components of $\mathbf{J}$. We can also write

$$\left\langle\widehat{\mathbf{R}}\middle|JM\Omega j\right\rangle_{SF} = \sum_{\Omega'=-J}^{J} D^J_{M\Omega'}(\Phi, \Theta, 0)^* \left\langle\widehat{\mathbf{R}}\middle|J\Omega'\Omega j\right\rangle_{BF} \qquad (4.5)$$

where the D^J's are the usual rotation matrices of Edmonds(1957) and the vectors $\left\langle\widehat{\mathbf{R}}\middle|J\Omega'\Omega j\right\rangle_{BF}$ no longer depend on $\widehat{\mathbf{R}}$ since the relative position vector

---

[7]We use the SF and BF pedices, when needed, to remember us the corresponding frame and, in particular, the axis which the angular momentum projection refers to. If we imagine to have a machine that produces a SF state, the actual meaning of a BF vector is that of a state prepared by a *rotated machine*. In absence of pedices the vectors refer always to the SF frame.

has a fixed orientation in the BF frame (its polar coordinates in this frame are $(0, 0)$). Now, the vectors $\left\langle \widehat{\mathbf{R}} \middle| J\Omega'\Omega j \right\rangle_{BF}$ are eigenvectors of j^2 with value j and of J_ζ with component Ω' *and* Ω simultaneously! Thus they must be of the form[8]

$$\left\langle \widehat{\mathbf{R}} \middle| J\Omega'\Omega j \right\rangle_{BF} = const_J \, \delta_{\Omega\Omega'} \left| j\Omega \right\rangle_{BF}$$

Thus, using this expression in eq.(4.5) we obtain

$$\left\langle \widehat{\mathbf{R}} \middle| JM\Omega j \right\rangle \equiv \left\langle \widehat{\mathbf{R}} \middle| JM\Omega j \right\rangle_{SF} = \sqrt{\frac{2J+1}{4\pi}} D^J_{M\Omega}(\Phi, \Theta, 0)^* \left| j\Omega \right\rangle_{BF} \qquad (4.6)$$

or in "full coordinates" representation

$$\left\langle \widehat{\mathbf{R}}\widehat{\mathbf{r}} \middle| JM\Omega j \right\rangle = \sqrt{\frac{2J+1}{4\pi}} D^J_{M\Omega}(\Phi, \Theta, 0)^* Y^\Omega_j(\theta', \phi')$$

where the correct normalization factor has been used and where (θ', ϕ') are the polar coordinates of $\mathbf{r}$ in the BF frame.

Taking into account the definitions of the D^J's and Y 's functions one may also write

$$\left\langle \widehat{\mathbf{R}}\widehat{\mathbf{r}} \middle| JM\Omega j \right\rangle = \sqrt{\frac{2J+1}{4\pi}} D^J_{M\Omega}(\Phi, \Theta, \phi')^* Y^\Omega_j(\theta', 0)$$

a formula which can also be obtained with a slightly different definition of the BF frame $(\xi\eta\zeta)$. This last formula is particularly interesting since it factors out the "external angular coordinates" (Θ, Φ, ϕ') from the (unique) angular internal coordinate θ'; that is, one may rewrite the angular momentum components of eq.(4.2) in the form

$$\left\langle \mathbf{R}\mathbf{r} \middle| \Psi^{JM} \right\rangle = \sum_{\Omega=-J}^{J} D^J_{M\Omega}(\Phi, \Theta, \phi')^* \Psi^{JM\Omega}(R, r, \gamma) \qquad (4.7)$$

where $\gamma \equiv \theta'$ is the angle between $\mathbf{R}$ and $\mathbf{r}$ and $\Psi^{JM}(R, r, \gamma)$'s are functions of the three internal variables only. We therefore see that for given (J, M) values we have $2J + 1$ functions of the 3 internal coordinates: the reduction of dimensionality is somewhat lower in quantum than in classical mechanics.

The SF and BF representations are related by a unitary transformation (note that, just like in the SF case, for given (J, j) values in eq.(4.6) there

---

[8]It is worth to note that the argument given here is entirely general since it does not depend on the internal angular momentum, e.g. it is applicable also to the case of two scattering molecules. Thus, in same way, one can obtain the eigenstates of a symmetric top rigid rotor (Landau, 1996).

are $2Min(J, j) + 1$ values of Ω, ranging from $-Min(J, j)$ to $Min(J, j)$). This transformation can be easily obtained by an argument similar to that used before, i.e.

$$\left\langle \widehat{\mathbf{R}} \Big| JMlj \right\rangle_{SF} = \sum_{\Omega=-J}^{J} D^J_{M\Omega}(\Phi, \Theta, 0)^* \left\langle \widehat{\mathbf{R}} \Big| J\Omega lj \right\rangle_{BF}$$

where now (see eq.(4.4))

$$\left\langle \widehat{\mathbf{R}} \Big| J\Omega lj \right\rangle_{BF} = \sum_{m_l m_j} (-)^{l-j+\Omega} (2J+1)^{1/2} \begin{pmatrix} l & j & J \\ m_l & m_j & -\Omega \end{pmatrix} Y_l^{m_l}(0, 0) \, |jm_j\rangle_{BF}$$

with

$$Y_l^m(0, 0) = (-)^{m_l} \sqrt{\frac{2l+1}{4\pi} \frac{(l-m)!}{(l+m)!}} P_l^m(1) \equiv \delta_{m0} \sqrt{\frac{2l+1}{4\pi}}$$

since $P_l^m(x) = (1 - x^2)^{m/2} d^m P_l(x)/dx^m$ and $P_l(1) = 1$. It therefore follows

$$|JMlj\rangle = \sum_{\Omega} U^{Jj}_{l\Omega} \, |J\Omega lj\rangle$$

with

$$U^{Jj}_{l\Omega} = (-)^{l-j+\Omega} (2l+1)^{1/2} \begin{pmatrix} l & j & J \\ 0 & \Omega & -\Omega \end{pmatrix}$$

and where the sum runs over the allowed Ω values.

In practice one may use either the SF or the BF representation. The differences between the two are mainly due to the form of the kinetic and potential matrices in these representations. The kinetic operator in eq.(4.1) is diagonal in the SF representation since it involves explicitly the l^2 and j^2 operators, while in the BF representation, remaining diagonal in j, couples Ω with $\Omega \pm 1$ (see for example Pack(1974)). On the other hand, the potential matrix has a "full" complicate structure in the SF representation[9] while in the BF representation it is diagonal in Ω since the potential is invariant for arbitrary rotation around the $\mathbf{R}$ direction. Thus, we can say that in the SF representation the coupling is brought by the potential, while in the BF representation only the j coupling is due the potential, the Ω coupling being brought by the motion.

The choice of one or the other representation depends on the particular approach. Here we note only that the BF equations are simpler then the SF ones at short-range, where the coupling is mainly due to the potential, while at long-range they have a residual kinetic Ω coupling that falls off like R^{-2}

---

[9]Apart, of course, being diagonal in (J, M).

[10] . On the other hand, the possibility of working with $3D$ Ω-component wavefunctions, eq.(4.7), is very appealing in view of using methods other than Finite Basis expansion for representing the wavefunction[11]. Furthermore, the BF representation is better suited for doing dynamical approximations. For example, one may neglect the Ω coupling in the kinetic energy term and obtain a set of $2Min(J,j)+1$ independent equations (*Centrifugal Sudden* or *Coupled States* approximation). These approximations are reviewed in the excellent work of Kouri(1979).

When one takes into account also the *parity* conservation law one more simplification is obtained. Indeed, the $\{JM\}$ subspaces are divided into two subspaces according to the parity transformation properties of the vectors. The basis vectors of the SF representation are already eigenvectors of the parity operator Π since this operator commutes with the set of commuting observables that defines the SF representation[12]

$$[\Pi, j^2] = [\Pi, l^2] = 0$$

In particular, $\Pi\,|JMlj\rangle = \epsilon\,|JMlj\rangle$ with $\epsilon = (-)^{j+l}$ and therefore the SF basis can be divided in two parity sets according to the parity of $j + l$. On the other hand, the parity operator *anti*-commute with the J_ζ operator of the BF representation since it is a *pseudoscalar*

$$\Pi J_\zeta = -J_\zeta \Pi$$

Thus, in order to exploit the parity symmetry in the BF representation one has to combine the Ω and $-\Omega$ components; since $\Pi\,|JM\Omega j\rangle = (-)^J\,|JM-\Omega j\rangle$ the resulting parity adapted vectors are defined by (Launay, 1977)

$$\left|JM\overline{\Omega}j\epsilon\right\rangle = \sqrt{\frac{1 + \delta_{\overline{\Omega}0}}{2}}\left\{|JM\Omega j\rangle + \epsilon(-)^J\,|JM-\Omega j\rangle\right\}$$

where $\overline{\Omega} = 0, 1, ..Min(J,j)$ if $\epsilon = (-)^J$ and $\overline{\Omega} = 1, ..Min(J,j)$ if $\epsilon = (-)^{J+1}$.

The partial wave expansion of the wavefunction of eq.(4.2) leads to corresponding partial wave expansion of the scattering attributes (Arthurs and

---

[10]This means that some kind of BF$\rightarrow$SF transformation is needed. For this reason inelastic CC calculations are usually done in the SF representation.

[11]Indeed, the use of the BF representation has become the method of choice for Time Dependent calculations.

[12]The parity operator commutes with the SF components of **J**, $[J_i, \Pi] = 0$, since the angular momentum is an *axial* vector operator (note on the contrary that usual vectors like **r** and **p** change sign under inversion). Comprehensive accounts of tensor theory and its relation to quantum mechanics can be found in the books of Landau(1997; 1996) and in that of Messiah(2000).

Dalgarno, 1960). Thus, in the general (two-body) differential cross section of eq.s(3.16,3.17)[13]

$$\frac{d\sigma}{d\Omega}(\mathbf{P}_\beta; \beta \leftarrow \mathbf{P}_\alpha; \alpha) = \frac{P_\beta}{P_\alpha} |f(\mathbf{P}_\beta; \beta \leftarrow \mathbf{P}_\alpha; \alpha)|^2 \qquad (4.8)$$

with

$$f(\mathbf{P}_\beta; \beta \leftarrow \mathbf{P}_\alpha; \alpha) = -(\mu_b \mu_a)^{1/2} (2\pi)^2 \langle \mathbf{P}_\beta; \beta | T_{\beta\alpha}(E) | \mathbf{P}_\alpha; \alpha \rangle \qquad (4.9)$$

one may use the usual angular momentum representation of the plane wave vector

$$|\mathbf{p}\rangle = \frac{1}{(\mu p)^{1/2}} \sum_{l,m} |E_p lm\rangle Y_l^m(\widehat{\mathbf{p}})^*$$

to get

$$|\mathbf{P}_\alpha; \alpha\rangle = \frac{1}{(\mu_a P_\alpha)^{1/2}} \sum_{l,m_l} |E_\alpha lm_l\rangle Y_l^m(\widehat{\mathbf{P}})^* |jm_j v\rangle$$

(where $(jm_j v)$ labels the rotovibrational state of the molecule in the generic a arrangement of our three atom system and E_α is the corresponding kinetic energy) in which (l, j) can be coupled as in the SF representation to give the following vector

$$|\mathbf{P}_\alpha; jm_j v\rangle = \frac{1}{(\mu_a P_\alpha)^{1/2}} \sum_{J=0}^\infty \sum_{M=-J}^J \sum_{l=|J-j|}^{J+j} |EJMljv\rangle$$
$$\langle JMlj | lM - m_j jm_j \rangle Y_l^{M-m_j}(\widehat{\mathbf{P}})^*$$

where now $|EJMljv\rangle$ is a "free" vector of total energy E. Inserting this expression in eq.(4.9) and using the rotational invariance one obtains

$$f(\mathbf{P}_\beta; j'm'v' \leftarrow \mathbf{P}_\alpha; jmv) = -\frac{(2\pi)^2}{(P_\beta P_\alpha)^{1/2}} \sum_{J=0}^\infty \sum_{M=-J}^J \sum_{l,l'} Y_{l'}^{M-m'}(\widehat{\mathbf{P}}_\beta) Y_l^{M-m}(\widehat{\mathbf{P}}_\alpha)^*$$
$$\langle l'M - m'j'm' | JMl'j' \rangle \langle JMlj | lM - mjm \rangle T_{(l'j'v';ljv)}^J(E) \qquad (4.10)$$

both for non-reactive and for reactive transitions (each set of quantum number refers to the corresponding arrangement). The $T_{(l'j'v';ljv)}^J(E)$ is a matrix element of the $\mathbf{T}$ operator of the previous Chapter and is related to an "operational" S matrix

$$S_{(l'j'v';ljv)}^J(E) = \delta_{ab}\delta_{ll'}\delta_{jj'}\delta_{vv'} - 2\pi i\, T_{(l'j'v';ljv)}^J(E)$$

---

[13]We use the labels a and b for the initial and final arrangements, respectively. Furthermore, $\alpha = (jm_j v)$ and $\beta = (j'm'_j v')$ label the initial and final channels, intented to be in the a and b arrangements respectively.

which *differs* from the "on-shell" S matrix defined in Section (3.4) in that a further delta function of energy has been factored out. Thus, thanks to rotational invariance, the scattering amplitude is a *single* sum in J and the differential cross section is given in the form

$$\frac{d\sigma}{d\Omega}(\mathbf{P}_\beta; j'm'v' \leftarrow \mathbf{P}_\alpha; jmv) = \frac{1}{P_\alpha^2}\left|\sum_{J=0}^{\infty}\{..\}\right|^2$$

where $\{..\}$ denotes the sums in the previous amplitude expression eq.(4.10). If one then defines the *degeneracy-averaged* differential cross-section

$$\frac{d\sigma}{d\Omega}(\mathbf{P}_\beta; j'v' \leftarrow \mathbf{P}_\alpha; jv) = \frac{1}{2j+1}\sum_{mm'}\frac{d\sigma}{d\Omega}(\mathbf{P}_\beta; j'm'v' \leftarrow \mathbf{P}_\alpha; jmv)$$

he finds that the corresponding integral cross-section

$$\sigma(j'v' \leftarrow jv|E) = \int \frac{d\sigma}{d\Omega}(\mathbf{P}_\beta; j'v' \leftarrow \mathbf{P}_\alpha; jv)d\Omega$$

is given by a *single* sum over J values[14]

$$\sigma(j'v' \leftarrow jv) = \sum_{J=0}^{\infty}\sigma^J(j'v' \leftarrow jv)$$

where the *partial cross section* σ^J's are sums of square modulus of T-matrix elements

$$\sigma^J(j'v' \leftarrow jv) = \frac{\pi}{P_\alpha^2}\frac{(2J+1)}{(2j+1)}\sum_{ll'}\left|T_{(l'j'v';ljv)}^J(E)\right|^2$$

This expression has some attractive features for analysing a scattering outcome, since it links in some rough sense the scattering probabilities with the scattering cross-sections. For example, in the case of a reactive collision we have $-2\pi iT_{ij} = S_{ij}$ and then, using the unitarity property of S one may define a reaction probability $(j, v) \rightarrow (j'v')$ for each J and for fixed initial orbital angular momentum l (the "impact parameter") as

$$P_{j'v' \leftarrow ljv}^J = \sum_{l'}\left|S_{(l'j'v';ljv)}^J(E)\right|^2 \leq 1$$

and the "true" *reaction probability* $(j, v) \rightarrow (j'v')$ for fixed J as the average over the allowed initial impact parameters

$$P_{j'v' \leftarrow jv}^J = \frac{1}{2Min(J, j) + 1}\sum_{ll'}\left|S_{(l'j'v';ljv)}^J(E)\right|^2$$

---

[14]It is remarkable how the four-fould initial summation reduces to a single sum over J values when we look for a scalar observable.

In this way the partial wave scattering cross-section can be written also in terms of scattering probabilities[15]

$$\sigma^J(j'v' \leftarrow jv) = \frac{\pi}{(2\pi P_\alpha)^2} \frac{(2J+1)(2Min(J,j)+1)}{(2j+1)} P^J_{j'v' \leftarrow jv}$$

where $\pi(2J+1)(2Min(J,j)+1)/(2j+1)/(2\pi P_\alpha)^2$ is a geometrical factor and $P^J_{j'v' \leftarrow jv}$ is a reaction "efficiency".

4.2 The Time-Dependent approach

[16]Thanks to important devolpements in the computational practice, like the use of the Fast Fourier methods and that of Negative Imaginary absorbing potential, Time-Dependent (TD) methods have been recently attracted the attention of more and more researchers. The reason is simple: the TD method is a straightforward solution of the initial value time-dependent Schrödinger equation, gives a clear physical picture of a collision event and is easily extended to explicitly time-dependent problems. Furthermore, from a computational point of view, since it fixes an initial condition it solves for *one* "column of **S** matrix" and *several* energies at time and thus scales more favoraubly with the dimension of the problem than the traditional Time-Independent method. However, if a complete state-to-state analysis of the collision process is needed difficulties arise.

As a first step in solving the Time-Dependent Schrödinger Equation (TDSE) one decides at the outset the working picture. In what follows we implicitly assume to work in the Schrödinger picture, but it should be noted that works in other pictures (like in the Interaction picture) have appeared.

As a second step one chooses a particular set of coordinates[17]. In the previous Section we have used the Jacobi set of coordinates of one of the possible arrangements of our model three atom system. This is a very simple choice and it gives rise to the simple hamiltonian of eq.(4.1). However, it should be recognized that such a choice treats preferentially one arrangement. Thus, although the *total* reaction probabilities are not affected by this "coordinate problem" (for reason to be explained later in the next Section), it gives rise to

---

[15]Thus, the previously noted simple J sum can be easily understood: the (degeneracy averaged) scattering cross-sections are related to the probabilities, i.e. to particular squares modulus of the component wavefunctions in eq.(4.2).

[16]This discussion is heavily based on the book of J. Zhang (1999) and on a previous review article of Balakrishnan et al. (1997). References to original works will be given only in special occasions.

[17]Of course, this is valid both for Time-Dependent and for Time-Independent calculations.

some problems when reactive state-to-state transition are to be computed[18].
On the other hand, one may choose to work with hyperspherical coordinates
(Smith, 1962; Whitten and Smith, 1968; Kuppermann, 1975; Johnson, 1980)
which have the advantage of treating in a even fashion all the arrangements:
the reactive problem is, in practice, transformed to an inelastic problem having
one scattering coordinate (the hyperradius) and the products at different values
of the hyperangles. In this case, however, the corresponding hamiltonian is no
longer simple and, from a computational point of view, requires a long-range of
integration to give rise to convergent observables; indeed, the single scattering
coordinate describes both the relative motion of the fragments in a given
arrangement and the vibrational motion of the molecule in that arrangement.

Having done the above mentioned choices we are ready to outline the ba-
sic problems of a Time-Dependent calculation, which can be summarized as
follows:

- the representation of the wavefunction $|\Psi\rangle$;

- the evaluation of $H|\Psi\rangle$;

- the time-propagation

(a fourth problem will be subject of the next Section). They clearly originate
from the nature of the problem (which we now consider taking into account
the results of Section (4.1)): we have a first order time differential problem for
a "proper" wavevector

$$H\left|\Psi_t^{JM}\right\rangle = i\frac{d\left|\Psi_t^{JM}\right\rangle}{dt} \quad \left|\Psi_{t=0}^{JM}\right\rangle = \left|\Psi_0^{JM}\right\rangle$$

whose formal solution (for time-independent problems)

$$\left|\Psi_t^{JM}\right\rangle = e^{-iHt}\left|\Psi_0^{JM}\right\rangle$$

needs to know the result of the action of a function of H on the wavevector.

The problem of representing the wavefunction is striclty related to the
choice of the coordinate set. Having decided for one kind of coordinates one
fixes the form of the hamiltonian operator and consequently looks for the rep-
resentation of the wavefunction more suited for evaluating the action of the
operator. In order to represent the wavefunction one may use either a "grid
description" or a "channel description" or a mixture of the two, in the sense

---

[18]It should be noted that with the recent introduction of the so-called Reactant-Product-
Decoupling approach the situation has been substantially improved.

that one uses the first description for some degrees of freedom and the second for other degrees of freedom.

In a "grid description" $\{\langle x_p|\Psi\rangle\}$ one represents the wavevector on a finite set of grid points in coordinate or momentum space, sufficiently close to each other in order to correctly represent the wavefuction and its properties, thereby paralleling the ordinary "continous" representations like $\Psi(x) = \langle x|\Psi\rangle$ or $\Psi(p) = \langle p|\Psi\rangle$. The grid must be chosen large enough "to contain the dynamical event", i.e. in the usual Initial State Selected Dynamics (ISSD) the grid must contain the interaction and the asymptotic regions. The grid parameters depend on the system at hand: a grid in a spatial coordinate of lenght L and with average separation between points of Δx can represent the conjugate momemtum with a precision $\sim 1/L$ up to a maximum $\sim 1/\Delta x$.

In a "channel description" $\{\langle i|\Psi\rangle\}$ one expandes the wavevector over an appropriate basis set, thereby transforming the TDSE in a set a coupled equations for the expansion coefficients. This is the so-called *Finite Basis Representation* and its use is very similar to the well known LCAO expansion in *ab-initio* calculations. In this case the choice of the basis set depends on the problem at hand, and in particular on the coordinate set chosen at the outset. In jacobi coordinates, rotations and vibrations of the reagent molecule can be treated by expanding the wavevector over a set of (proper) eigenfunctions of the diatomic. Continuos sets (i.e. improper eigenvectors) are handled with difficulties and therefore the use of such an expansion is limited to that region of the configurational space which can be described well by this "bound reagent set". This region should be large enough to contain the dynamical event, much like what happens with the grid description or, in other words, the vibrational basis must allow the reaction to occure. Usually, the FBR is not applied to all coordinates since the unbound motion on the scattering coordinate is best handled with a grid.

One can (and in practice does) switch betwenn channel and grid descriptions, since some operators are best evaluated in one representation and other operators in the other representation. For example, for what concerns the angular variables, the orbital and the rotational operators are best evaluated in a FBR like the ones described in the previous Section, while on the other hand the potential is diagonal in the coordinate representation. With the same token, the radial operator is best handled in a "momentum basis set" and the potential in the radial coordinate representation: the difference with the previous case is that now both representations are continuos in origin and thus, in practice, they both give rise to grid descriptions (but in different spaces).

In order to explain better how one switches between the two representations let us go slightly deeper in the grid description. The use of a grid is equivalent to a particular (truncated) expansion of the wavefunction: the values of the

wavefunction at grid points are the coefficients in the expansion of the wave-function over a basis set made up of functions *localized* on the grid points. This is the so-called *Discrete Variable Representation* (DVR), introduced by Light and coworkers (Light et al., 1985; Vill et al., 1982) in opposite to the previous FBR. A DV Representation is realized when one fixes an oridinary basis set $\{|\phi_i\rangle\}$ and a quadrature rule such that the scalar product between basis elements becomes

$$\langle\phi_i|\phi_j\rangle = \sum_p w_p \phi_i^*(x_p)\phi_j(x_p) = \delta_{ij}$$

where x_p are the quadrature points on the x space and w_p are the weights of the quadrature rule. Then, the expansion of the wavevector over the basis set $\{|\phi_i\rangle\}$

$$|\Psi\rangle = \sum_i |\phi_i\rangle \langle\phi_i|\Psi\rangle$$

can be rearranged, approximating the scalar products with the quadrature rule, as a sum over quadrature points

$$|\Psi\rangle = \sum_i \sum_p |\phi_i\rangle w_p \phi_i^*(x_p)\Psi(x_p) = \sum_p \Psi(x_p) |\xi_p\rangle \qquad (4.11)$$

where

$$|\xi_p\rangle = w_p \sum_i |\phi_i\rangle \phi_i^*(x_p)$$

is a basis vector associated to the x_p grid point. This vector is localized on the grid point since the quantity

$$\xi_p(x) = \langle x|\xi_p\rangle = w_p \sum_i \phi_i(x)\phi_i^*(x_p)$$

is, in the same approximation, the representation of a Dirac delta function

$$w_p \sum_i \phi_i(x)\phi_i^*(x_p) = w_p \langle x| \left\{ \sum_i |\phi_i\rangle \langle\phi_i| \right\} |x_p\rangle \sim w_p\delta(x - x_p)$$

and thus it is, in practice, a function very peaked on the grid point. The accuracy of the representation of this Delta function depends on the truncation error in the Finite Basis set which, in turn, is related to the accuracy of the quadrature rule: starting with an arbitrary set of grid points, these determine a maximum number of finite basis elements because, clearly, the orthogonality relations prevent one from having more functions than grid points. In turn,

the truncation error in the DVR (and in the corresponding FBR) is due to the empty space between grid points and outside the boundaries of the grid.

It follows that the FBR→DVR and the converse DVR→FBR transformations are simply given by

$$\langle x_p | \Psi \rangle = \sum_i \phi_i(x_p) \langle i | \Psi \rangle$$

$$\langle i | \Psi \rangle = \sum_p w_p \phi_i^*(x_p) \langle x_p | \Psi \rangle$$

where $\{\langle x_p | \Psi \rangle\}$ and $\{\langle i | \Psi \rangle \equiv \langle \phi_i | \Psi \rangle\}$ are the DVR and FBR representations, respectively, and $\{\phi_i(x_p)\}_{pi}$ and $\{w_p \phi_i^*(x_p)\}_{ip}$ are the matrices that perform the above mentioned transformations.

One commonly used DV representation is that defined by the uniform quadrature rule and the plane wave basis set (which is not an ordinary Finite Basis). This representation defines the discretization of the Fourier transform operation. With a finite (periodic) grid of period L and spacing Δx the allowed momentum values are given by the Born-von Karman conditions and the corresponding basis elements are ($n = L/\Delta x$ is the effective number of grid points, being x_0 and x_n equivalent, $\phi(x_0) = \phi(x_n)$)

$$\phi_{k_m}(x) = \frac{1}{\sqrt{L}} e^{ik_m x} \quad \Delta k = k_{m+1} - k_m = \frac{2\pi}{L}$$

They satisfy ($w_p \equiv \Delta x$)

$$\langle \phi_{k_l} | \phi_{k_m} \rangle = \frac{\Delta x}{L} \sum_{p=1}^n e^{i(k_m - k_l)x_p} = \frac{\Delta x}{L} \sum_{p=1}^n \left(e^{i\frac{2\pi}{L}(m-l)\Delta x} \right)^p = \delta_{lm}$$

since

$$\sum_{p=1}^n r^p = \left\{ \begin{array}{ll} n & r = 1 \\ \frac{r^n - 1}{r - 1} r & r \neq 1 \end{array} \right. \quad \text{and} \quad r^n = e^{i2\pi(m-l)} = 1$$

In this case[19]

$$|\Psi\rangle = \sum_{p=1}^n \Psi(x_p) |\xi_p\rangle$$

---

[19] The reality of the DVR basis functions can be obtained with a symmetric choice of the "first Brillouin zone". That is, for an odd number n of grid points we select $k_m = m\Delta k$ (with $m = 0, \pm 1, .., \pm(n-1)/2$) and for an even number of points $k_m = m\Delta k/2$ (with $m = \pm 1, \pm 3, .. \pm (n-1)$). Clearly, this kind of choice allows an even representation of the momentum space in both directions.

$$\langle x | \xi_p \rangle = \frac{\Delta x}{L} \sum_n \left(e^{i\frac{2\pi}{L}(x - x_p)} \right)^n = \frac{\Delta x}{L} \frac{sin\left\{ \frac{n\pi(x - x_p)}{L} \right\}}{sin\left\{ \frac{\pi(x - x_p)}{L} \right\}}$$

This kind of grid representation has the advantage of being DVR *both* in the coordinate *and* in the momentum representation since each "Finite Basis element" is, at the same level of approximation, a Dirac delta function in momentum space. However, it is uniformely spread in space and thus the use of a DVR more densely arranged in the interaction region can be preferred for some applications.

Anyway, the numerical solution of the TDSE, either with FBR or DVR descriptions of the wavevector, amounts to approximate the configuration space with a subspace (e.g. the finite grid) and, therefore, according to Section (3.5), the full hamiltonian should be corrected with an optical potential term that accounts for the neglect of the complementary space[20]. This is not only a problem of principles: in practice, for example, the use of a grid with finite size is equivalent to place an infinite repulsive potential on the grid boundaries on which the wavefunction unphysically bounces off[21]. The solution of this problem was an important devolpement in the area of TDQM calculations and followed the systematic investigation of Neuhauser and Baer (1989) of the *Negative Immaginary Potentials* (NIP). In practice, a NIP located in the asymptotic regions (i.e. "at the boudaries of the grid") is added to the interaction potential in order to absorb the wavefunction *after* it has been analyzed for extracting the relevant scattering informations. In this way, one avoids artificial reflections from the boundaries, although introduces a reflection effect from the NIP, which can be substantial in the low energy regime.

The evaluation of the action of the hamiltonian operator on the wavefunction depends strictly on the representation of the wavefunction. The problem is considerable simplified when an operator is diagonal in the chosen representation; if it is not the case (and this is always true for some operator!) one may change representation or perfom a kind of vector-matrix multiplication. In a FBR representation one has to perform a multiplication between the vector representation of the wavefunction and the matrix representation of the operator. In a DVR the evaluation of a (non-diagonal!) operator is accomplished by computing and storing the result of the action of the operator on the DVR basis set. For example, momentum operators in coordinate DVR representation can be evaluated by knowing the derivatives $d^n \xi_p(x)/dx^n$ of the

---

[20]This is true in the time *independent* framework where the optical potential depends on energy. In this case we may argue that the correction should be a time dependent potential.

[21]With the "Fourier-DVR" described above, because of the periodicity conditions, one observes the wavepacket turning around the grid. Analogously, with a reagent vibrational basis one observes an anomalous re-forming of the reagent molecule.

basis element $\xi_p(x)$, as can be easily obtained by eq.(4.11)[22]. An execption to this rule is the above mentioned Fourier-DVR: in this case one has actually *two* DVR representations, one in the coordinate space and the other in the momentum space, and thus he uses the *Fast Fourier Transform* (FFT) algorithm to switch from one representation to the other, in order to evaluate each operator in its simplest diagonal form[23]. Needless to say, the introduction of the FFT in the practice of TDQM calculations by D. Kosloff and R. Kosloff (1983) was another great development in the Time Dependent approach.

Focusing now on the last problem, the "time differential" one, we may say that there are several way to perform the propagation in time of the solution, starting with the simple second order approximation of the time derivative of the TDS equation and ending with the complicated Lanczos iteration scheme. Here we consider briefly only two very common approaches. The first is the *Split Operator* method which represents a short-time, unitary approximation of the evolution operator (Feit et al., 1982; Feit and J. Fleck, 1984a; Feit and J. Fleck, 1984b)

$$e^{-i\Delta t(H^0+H^1)} = e^{-i\frac{\Delta t}{2}H^0}e^{-i\Delta t H^1}e^{-i\frac{\Delta t}{2}H^0} + O(\Delta t^3) \qquad (4.12)$$

where $H = H^0 + H^1$ is any useful decomposition of the hamiltonian operator, or a part of it which one wishes to "split" further. In the case of non commuting operators this is clearly an approximation but it is very good for short time propagation steps and, furthermore, has the advantage of being explicitly unitary. One straightfoward application of this method is its use in conjunction with the Fourier-DVR representation of the wavefunction and the FFT algorithm for switching between the coordinate the momentum representations. For example, in one dimension, one may choose $H^1 = p^2/2m$ and $H^0 = V(x)$ (or the converse) and evaluate the first operator on the r.h.s. of eq.(4.12) in coordinate representation, move to the momentum representation to evaluate the second operator and finally go back to the coordinate representation for the third operator. In this case one has to perform two Fast Fourier Transforms for each time step and simple scalar multiplication operations. In $3D$ calculations the situation is somewhat more complicated. Working in reagent jacobi coordinates we can employ a mixed channel-grid description and split the hamiltonian operator in the following form

$$H^0 = \frac{P_r^2}{2\mu} + h \quad H^{(1)} = \frac{\mathbf{l}^2}{2\mu R^2} + \frac{\mathbf{j}^2}{2mr^2} + V_{int}$$

---

[22]It is worth to note in this context the conceptual advantage of working with a DVR: if we had stopped our reasoning with the introduction of a generic grid the only way to compute "derivatives" would have been by using a finite-difference approximation.

[23]Note that the FFT algorithm scales as $NlogN$, while the above DVR computation scales as N^2 (although there would need a less number of points with a suitable DVR).

where h is the vibrational hamiltonian of the reagent diatomic and $V_{int} = V - v$ is the corresponding interaction potential. Thus, the first exponential operator is best evaluted in the $\{\langle P_q v \Omega j | \Psi \rangle\}$ representation where the (momentum) grid description is used for the relative motion and the channel description is used for the other variables. The resulting vector can be transformed in the $\{\langle R_l r_m \Omega j | \Psi \rangle\}$ representation (in which the DVR is used for the two radial coordinates) and the action of the second exponential operator evaluated for each $\{R_l r_m\}$ grid point by diagonalizing the effective potential matrix

$$\left\langle R_{l'} r_{m'} \Omega' j' \left| H^{(1)} \right| R_l r_m \Omega j \right\rangle = \delta_{ll'} \delta_{mm'} U_{\Omega'j',\Omega j}(R_l, r_m)$$

which is already diagonal in the radial coordinates and which can be computed and stored at the outset for each couple of radial points. Then, one goes back to the first representation and so on. Essentially this kind of procedure has been used by D. Zhang and J. Zhang to perform $3D$ calculations in the $H + O_2$ atom-diatom case and $6D$ calculations ($J = 0$) for the $H_2 + OH$ diatom-diatom case (Zhang and Zhang, 1994a; Zhang and Zhang, 1994b).

An alternative method, suitable for the long propagation time is the *Chebichev expansion* of the long-time propagator (Tal-Ezer and Kosloff, 1984)

$$U(t \leftarrow t_0) = e^{-i(t-t_0)H}$$

In this kind of approximation one uses the good truncation properties of the Chebichev polynomials and writes

$$e^{-i(t-t_0)H} = e^{-i(t-t_0)E_m} \sum_{n=0} A_n(\Delta E(t - t_0)) T_n(-i H_{norm})$$

where H_{norm} is a "normalized" hamiltonian operator with spectrum in the range $(-1, +1)$, E_m is the mean value and ΔE the range of the original spectrum, T_n are the Chebichev polynomials and A_n are defined by

$$A_n(x) = (2 - \delta_{n0}) i^n J_n(x)$$

where J_n are Bessel functions of the first kind. This kind of approximation can be viewed as a wise reorganization of the truncated exponential series

$$e^{-i(t-t_0)H} = \sum_{n=0}^{\infty} \frac{[-i(t - t_0)]^n}{n!} H^n$$

and its formal powerful is essentially due to the same reasons for which the exponential function in pocket calculators is evaluated by Chebichev expansion.

4.3 Scattering observables from TD calculations

Having described how to solve the Time Dependent Schrödinger equation we now consider briefly the problem of extracting scattering information from the time evolution of the wavepacket. Much like in the formal theory outlined in the previous two Chapters, this step needs a *Time-to-Energy* mapping which allows us to get the scattering attributes on the *energy* shell from the *time* evolution of the system. Here we consider only the so-called Initial State Selected Dynamics, in which one fixes at the outset the initial internal state of the collision system and obtains scattering cross sections for the processes that start from that initial state and simultaneously for several energies, because the initial translational wavefunction spreads over the energy spectrum. This is not the only way to obtain scattering informations. A less detailed analysis of the process can be obtained by applying the Time Dependent version of the Miller's ideas about the *direct* and *exact* calculations of canonical (and microcanonical) rate constants (e.g. see Miller (1998)). While looking for developing a *Quantum* Transition State Theory, Miller recognized that *chemical* rate constants (i.e. state-to-state rate constants averaged over initial states and summed over final states) do not require to know the detailed state-to-state informations that are "washed out" by the final averages, simply because, as he was able to show, the required averages can be computed *directly* by looking at the reactive "flux" (Miller, 1974; Miller et al., 1983). Although this subject is very fascinating we mention only that the corresponding theory can be cast both in the Time Dependent and in the Time Independent approaches; an application with TD methods can be found in the work of Light and D. Zhang (1998).

The above mentioned Time-to-Energy mapping in the ISSD is given by the following (half) Fourier transform

$$\int_0^{+\infty} e^{iEt} \left|\Psi_t\right\rangle dt = lim_{\epsilon\to 0^+} \int_0^{+\infty} e^{-\epsilon t} e^{i(E-H)t} \left|\Psi_0\right\rangle dt \equiv iG^+(E)\left|\Psi_0\right\rangle \quad (4.13)$$

which has been formally evaluated by introducing the famous ϵ converging factor[24]. Now, with the use of the Lippmann-Schwinger equation for G (see Sections (2.3) and (3.3)),

$$G^+(E) = G_b^+(E)(1 + V_b G^+(E)) = G_b^\dagger(E)(\Omega_-^b(E))^\dagger$$

we are left with the Ω_- operator of the (arbitrary) "final" arrangement b: as already noted in the single channel case[25], under suitable conditions on the

---

[24]The first integral actually converges to an improper vector. The introduction of the converging factor allows one to define the operator that perfoms the time integral.

[25]See the discussion in Section (2.1) on the meaning of the $t = 0$ instant of time in the theorem of the Asymptotic Condition and in particular eq.(2.3).

initial state vector $|\Psi_0\rangle$, the operators Ω_-^β's contain the desired scattering informations.

In order to see this, we multiply the above expression by the vector $\langle \mathbf{R}_b\beta|$, where $\mathbf{R}_b = R\widehat{\mathbf{R}}_b$ is an asymptotic value of the scattering coordinate in the b arrangement (i.e. $R \to \infty$) and $\beta = \{j_\beta, v_\beta\}$ is the rovibrational set of quantum numbers necessary to specify completely the state of the system. In this way, we can use the asymptotic expansion of the channel Green's operator to get

$$\int_0^\infty e^{iEt} \langle \mathbf{R}_b\beta | \Psi_t\rangle \, dt = i \left\langle \mathbf{R}_b\beta \middle| G^+(E) \middle| \Psi_0 \right\rangle \sim -i(2\pi)^{1/2} \mu_b \frac{e^{iPR}}{R} \left\langle P\widehat{\mathbf{R}}_b\beta - \middle| \Psi_0 \right\rangle \tag{4.14}$$

where P is determined by the conservation law, $E = P^2/2\mu_b + \epsilon_\beta$, in which ϵ_β is the $\beta = \{j_\beta, v_\beta\}$ channel energy. Now, *if the initial wavepacket $|\Psi_0\rangle$ is well localized in the asymptotic region of the* a *arrangement and with momentum distribution directed toward the interaction region* (a sort of "asymptotic condition") we can write

$$|\Psi_0\rangle = \sum_{c,\gamma} \int dE' \, |E'\gamma c+\rangle \left\langle E'\gamma c+ \middle| \Psi_0 \right\rangle \sim \int dE' \, |E'\alpha a+\rangle \left\langle E'\alpha a \middle| \Psi_0 \right\rangle \tag{4.15}$$

where γ is the appropriate set of initial quantum numbers in the c arrangement needed to specify (along with the total energy E') the state of the system. Here the above mentioned asymptotic condition has been used in the form

$$|\Psi_0\rangle = \Omega_+^\alpha |\Psi_{in}^\alpha\rangle \sim |\Psi_{in}^\alpha\rangle$$

along with the orthogonality theorem of Section (3.2). As already emphasized in the single channel case, this approximation holds in this case because, *with our wavepacket*, the *full* evolution of the state vector *back* in time is equivalent to the evolution of the *free* channel evolution operator.

We are almost at the desired result. We write for simplicity

$$\left| P\widehat{\mathbf{R}}_b, j_\beta, v_\beta \right\rangle = \frac{1}{(\mu_b P)^{1/2}} \left| E\widehat{\mathbf{R}}_b, j_\beta, v_\beta \right\rangle \equiv \frac{1}{(\mu_b P)^{1/2}} |E\beta\rangle$$

$$\text{where now } \beta = \{\widehat{\mathbf{R}}_b, j_\beta, v_\beta\}$$

and insert in eq.(4.14) the spectral resolution of the initial wavepacket (eq.(4.15)) obtaining

$$\left\langle P\widehat{\mathbf{R}}_b, j_\beta, v_\beta - \middle| \Psi_0 \right\rangle = \frac{1}{(\mu_b P)^{1/2}} \int dE' \left\langle E\beta - \middle| E'\alpha+ \right\rangle \left\langle E'\alpha \middle| \Psi_0 \right\rangle =$$

$$= \frac{1}{(\mu_b P)^{1/2}} \int dE' \left\langle E\beta \middle| S_{\beta\alpha} \middle| E'\alpha \right\rangle \left\langle E'\alpha \middle| \Psi_0 \right\rangle$$

Here the relevant S matrix element can be written in term of the "on-shell" S matrix (eq.(3.10))

$$\langle E\beta | S_{\beta\alpha} | E'\alpha \rangle \equiv \langle E\beta | S_{\beta\alpha}(E) | E'\alpha \rangle = \delta(E' - E)\{\delta_{\alpha\beta} - 2\pi i \langle E\beta | T_{\beta\alpha}(E) | E\alpha \rangle\}$$

and finally in terms of the "operational" S matrix defined in the previous Section which appears in the last term between brackets, i.e.

$$S_{\beta\alpha}(E) = \delta_{\alpha\beta} - 2\pi i \langle E\beta | T_{\beta\alpha}(E) | E\alpha \rangle$$

Therefore, we arrive at the following, very important result

$$\int_0^\infty e^{iEt} \langle \mathbf{R}_\beta j_\beta v_\beta | \Psi_t \rangle \, dt = -i(2\pi)^{1/2} \mu_b \frac{e^{iP'R}}{R} \frac{1}{(\mu_b P)^{1/2}} S_{\beta\alpha}(E) \langle E\alpha | \Psi_0 \rangle$$

$$\beta = \{\widehat{\mathbf{R}}_b, j_\beta, v_\beta\}$$

from which a number of other useful expressions can be obtained (see Chapter 7 of the book of J. Zhang (1999)). This is the working formula, although in practice it is used on the J components of the state vector with a simple redifinition of the "projection" vector $\langle \mathbf{R}_\beta \beta |$ (the actual constants depend on the choice of this vector). It was introduced in a different form by Balint-Kurti et al. (1990) and Zhang (1995). In practice, it allows one to obtain the relevant S matrix elements from the knowledge of the "weights" of the energy components in the initial wavepacket[26] by simply computing the half time-energy Fourier transform of the amplitude of the wavepacket in the relevant asymptotic region[27]. One considers a definite initial state and, from a single calculation, obtains the desired S matrix elements for the processes $\alpha \rightarrow \beta$ (α fixed, β arbitrary) for all the energies well represented in the initial wavepacket.

It is worth to note at this point that the time-propagation of the wavepacket performed in a TDQM calculation is contained, in virtue of eq.(4.13), in the Green's operator $G^+(E)$, i.e.

$$\int_0^{+\infty} e^{iEt} | \Psi_t \rangle \, dt = iG^+(E) | \Psi_0 \rangle$$

---

[26] These weights, $a(E) = \langle E\alpha | \Psi_0 \rangle$, can be chosen at the outset with an appropriate preparation of the initial wavepacket. Usually, one chooses a gaussian wavepacket for the translational motion and thus the $a(E)$ can be readily computed from the momentum representation of this initial state vector.

[27] It should be noted that the application of this formula is not straightforward as it may seem. One problem is how far apart one should project the wavefunction, which could require the use of a very large grid. A second problem arises with the coordinate chosen: for example, if one uses a reagent jacobi set of coordinates the projection onto final states requires a sort of interpolation of the product wavefunctions in reagent coordinates or, *viceversa*, the interpolation of the wavepacket in product coordinates.

whereas the initial conditions (for several collision energies) are contained in the wavepacket. Beacuse of the meaning of the the Green's operator, the result of Fourier transforming the time evolution of the wavepacket can be obtained also by solving the *inhomogeneous* problem

$$(E - H) |\Psi_E\rangle = |\Psi_0\rangle$$

(where the unknown $|\Psi_E\rangle$ is the previous $G^+(E) |\Psi_0\rangle$ vector) with the usual outgoing boundary conditions[28]. This is the Time Independent Wavepacket Schrödinger Equation (Zhu et al., 1994a; Zhu et al., 1994b) which, as it stands, has already one advantage with respect to the conventional time independent methods described in the next two Sections: it allows one to "fix" the initial collision conditions (i.e. it allows to solve for "one column" of the S matrix). In practice, one can express directly the Green's operator for *several* energies using the Chebichev expansion technique with a little more effort than in the single energy case.

The methods described up to now furnish, at least in principle, a complete state-to-state analysis of the collision process. Much like in the Miller's flux approach to computing chemical rate constants, if one is interested only in *total* reaction probabilities/cross-sections one may look at the total flux going through a surface in the relevant product region. Without going into details we note only that this flux is related by the continuity equation to the reaction probability and, for stationary states[29] , it can be computed through any arbitrary surface. Thus, one may use reagent jacobi coordinate to perform the time propagation and compute the total flux going through a surface adapted to the reagent coordinates. In this way one can avoid the "coordinate problem" mentioned in the previous Section. It is worth to mention here that the formal flux operator relative to a given surface s is obtained by defining the operators that project the state vectors onto the spatial regions divided by s, which we denote P and $Q = 1 - P$. Indeed, the flux operator F_s is simply the time derivative of P (or Q depending on the verse of the surface normal)

$$F_s = \frac{dP}{dt} = i[H, P] = i[H^0, P]$$

where H^0 is the free-particle hamiltonian (P commutes with the potential).

---

[28]This is an equation for an "improper" vector: eq.(4.14) tells us its asymptotic behaviour, i.e. a pure outgoing spherical wave. Indeed, the initial wavepacket is localized in space and thus, in the asymptotic region, the equation reduces to an ordinary Schrodinger equation for improper vectors.

[29]These states can be formally obtained by the Time to Energy mapping of the kind discussed before.

Using the definition of P

$$P = \int_{P_s} d\mathbf{R} d\mathbf{r} \, |\mathbf{R}\mathbf{r}\rangle \, \langle \mathbf{R}\mathbf{r}|$$

where the integral extends over the relevant region P_s one gets the known flux formula in coordinate representation.

4.4 The Close-Coupling equations

We now consider briefly the Time Independent approach. In particular we focus on the simple inelastic ("subreactive") dynamics which allows us to definitely choose one of the possible sets of jacobi coordinates. Reactive problems can be handled in a "similar" fashion by making use of the hyperspherical coordinates (at least in principle).

The standard approach is to solve the Time Independent Schrödinger Equation (TISE) of the previous Chapter (see Section (3.4))[30]. One begins expanding the unknown scattering eigenvector on a suitable basis set that describes the internal motion of the colliding system and thus transforms the TISE in a set of coupled equations for the (simpler) expansion coefficients, just like what happens with the use of FBR in TD calculations. Since one can handle only finite basis sets, one must truncate the orginal complete basis set thereby "closing" the coupled equations. This is the close-coupling approximation described formally in detail in Section (3.5). It is clearly the same approximation of using FBR in TD calculations, though the name "Close-Coupling" (CC) refers invariably to the time independent approach.

In Section (3.5) we introduced the CC approximation using a fixed rotovibrational basis set of the target molecule; now we take into account the results of Section (4.1) and use a cleaver basis set in order to exploit the rotational invariance. Before doing so, it is worth to note that we use in this way what is called a *diabatic* basis: it remains fixed for every value of the scattering coordinate. An alternative approach is the use of an *adiabatic* basis, that is a basis that "adapts" itself during the collision process: one defines the basis that diagonalizes the effective potential at the expense of introducing non-adiabatic (kinetic) coupling terms. The adiabatic and diabatic descriptions of the scattering process in this context closely parallel the analogous descriptions in the electron-nuclear separation problem: in the (electronic) adiabatic representation one diagonalizes the electronic hamiltonian at the expense of introducing kinetic non-adiabatic couplings (at least in principle), while in the diabatic

---

[30] Of course, one may well solve the Lippmann-Schwinger equation.

representation he works with a diagonal kinetic operator and a non diagonal potential.

We consider each partial wave at time and use the Space Fixed Representation[31] of Section (4.1) for building the SF rovibrational basis set $\{|JMljv\rangle\}$ starting from the uncoupled rotovibrational basis vectors defined by

$$h\,|jm_jv\rangle = \epsilon_{vj}\,|jm_jv\rangle$$

in which

$$h = \frac{p_r^2}{2m} + \frac{\mathbf{j}^2}{2mr^2} + v(r)$$

is the hamiltonian of the target molecule. In this way, we use a FBR for all the coordinates involved except the radial coordinate

$$\Psi^{JM}(\mathbf{R},\mathbf{r}) = \sum_{ljv} \frac{F_{ljv}^{JM}(R)}{R}\left\langle \widehat{\mathbf{R}}\mathbf{r}\Big| JMljv\right\rangle$$

where $F_{ljv}^{JM}(R)/R = \langle R|\left\langle JMljv\big|\Psi^{JM}\right\rangle$ (the introduction of the factor $1/R$ simplifies the evaluation of the radial momentum operator). Therefore, we obtain a set of coupled differential equations for the "channel components" F's of the scattering eigenfunctions (we drop the $\{JM\}$ label)

$$\left\{\frac{d^2}{dR^2} + k_{jv}^2 - \frac{l(l+1)}{R^2}\right\} F_{ljv}(R) = -2\mu \sum_{l'j'v'} V_{ljv;l'j'v'}^J(R)\, F_{l'j'v'}(R)$$

where

$$k_{jv}^2/2\mu = E - \epsilon_{jv}$$

is the channel translational energy (positive for open channels and negative for closed channels) and $V_{ljv;l'j'v'}^J(R)$ is the potential matrix in the channel basis. This last matrix is computed at the outset, usually starting from the "vibrational couplings"

$$V_{v'j';vj}(R,\gamma) = \int_0^\infty dr\, \chi_{v'j'}^*(r) V(r,R,\gamma)\chi_{vj}(r)$$

where γ is the jacobi angle $cos^{-1}(\mathbf{Rr})$ and $\chi_{vj}(r)$'s are the radial components of the target eigenvectors[32]

$$\langle \mathbf{r}|jvm\rangle = \frac{\chi_{vj}(r)}{r}Y_j^m(\widehat{\mathbf{r}})$$

---

[31] That is, we consider the CC equations in the SF representation. Anologous equations can be written in the BF representation.

[32] One often neglects the rotational dependence of the vibrational functions, i.e. he separates rotational and vibrational motions by approximating $(2mr^2)^{-1} \sim (2mr_e^2)^{-1} = B_e$ or, more properly, by a vibrational dependent rotational constant B_v.

The angular dependence of the vibrational couplings is usually expressed in terms of Legendre polynomials

$$V_{v'j';vj}(R, \gamma) = \sum_{\lambda} V^{\lambda}_{v'j';vj}(R) P_{\lambda}(cos\gamma)$$

and the angular coefficients (operators) are used to build the final potential matrix by making use of the complicated formulas that express $\langle JMj'l'|P_{\lambda}|JMjl \rangle$ in terms of $3j$ and $6j$ symbols.

In matrix form we can collect the channel components in a column vector $\mathbf{F}^J$ and write

$$\left\{ \frac{d^2}{dR^2} + \mathbf{k}^2 - \mathbf{V}^J - \frac{\mathbf{l}^2}{R^2} \right\} \mathbf{F}^J = 0 \qquad (4.16)$$

where

$$(\mathbf{k}^2)_{l'j'v';ljv} = \delta_{ll'}\delta_{jj'}\delta_{vv'}k_{jv}^2$$

$$(\mathbf{l}^2)_{l'j'v';ljv} = \delta_{ll'}\delta_{jj'}\delta_{vv'}l(l+1)$$

and $\mathbf{V}^J$ is the potential matrix introduced before. In principle, one solves this equation with the regularity condition *at the origin*

$$\mathbf{F}^J(R) = 0$$

(which follows from the fact that each F is actually a radial component of the wavefunction) and the scattering boundary condition *in the asymptotic region*. This boundary condition is the partial wave expansion of the "three-dimensional" boundary condition of eq.(3.14), i.e.

$$F^J_{ljv}(R) \to \frac{1}{\sqrt{k_{jv}}} \left\{ \delta_{ll_0}\delta_{jj_0}\delta_{vv_0}e^{-i(k_0 R - l_0\frac{\pi}{2})} - S^J_{ljv;l_0j_0v_0}e^{i(k_{jv}R - l\frac{\pi}{2})} \right\} \quad \text{as} \quad R \to \infty$$

$$(4.17)$$

for the open channel components $(k_{jv}^2 > 0)$ and $F_{ljv}(R) \to 0$ for the closed channel ones $(k_{jv}^2 < 0)$[33]. In this equation we have used $\{l_0j_0v_0\}$ for the entrance channel quantum numbers, i.e. for the initial collision condition $(k_0^2/2\mu$ is the corresponding collision energy) and we have denoted with $S^J_{ljv;l_0j_0v_0}$ the corresponding element of the "operational" S matrix defined in Section (4.1). In principle, the study of the collision process from the internal state $\{j_0v_0\}$ is reduced to the solution of the previous equations for each value of J and all the allowed l_0 values for each fixed J: the scattering observables can then be obtained by their partial waves expansions as outlined in Section (4.1).

---

[33] Actually, the spherical waves are Riccati-Hankel functions $\widehat{h}^{(\pm)}_l$, which have the property $\widehat{h}^{(\pm)}_l(x) \to e^{\pm i(x - \frac{l}{2}\pi)}$ when $x \to \infty$ and which reduce to exponentially decaying functions in the closed channel case $(x \to ix)$. The "asymptotic" value at which the scattering function resembles a superposition of Riccati-Hankel functions is usually smaller that that needed for the $e^{\pm ikR}$ behavior.

4.5   The Log-Derivative matrix

The Close Coupling equations of eq.(4.16) can hardly be solved in practice as they stand. The reason is simple. If we use M channels they represent a set of M coupled second order differential equations, among which the regularity condition at the origin selects M well behaved solutions. These M independent solutions contain a number N_o of scattering solutions (which depends on the number N_o of open channels) and $M - N_o$ unphysical solutions. The physical solutions should be chosen accoring to the boundary conditions of eq.(4.17) but, in practice, these conditions are difficult to impose because one always solves the equations starting from the known value of the function at the origin[34].

This problem is solved by considering the whole set of M independent solutions left us by the regularity conditions. They can be arranged in a matrix $\mathbf{\Psi}$ (in which each column vector is a vector solution) that satisfies the matrix equation

$$\left\{ \frac{d^2}{dR^2} + \mathbf{k}^2 - \mathbf{V}^J - \frac{\mathbf{l}^2}{R^2} \right\} \mathbf{\Psi} = \mathbf{0} \tag{4.18}$$

Of course, if $\mathbf{\Psi}$ is a matrix solution we can multiply it to the right by an arbitrary (non-singular) matrix and still get a solution matrix: indeed, the right multiplication perfoms a (non-singular) linear combination of the solution vectors.

We may now define the *Log-Derivate* matrix[35]

$$\mathbf{Y} = \mathbf{\Psi}' \mathbf{\Psi}^{-1}$$

that is invariant for non singular combinations of the solution vectors and holds all the invariant properties of the solutions. This is the key quantity: we can re-write the previous equation in term of the unknown $\mathbf{Y}$ matrix and get the (first-order) Riccati matrix equation

$$\frac{d\mathbf{Y}}{dR} + \mathbf{W} + \mathbf{Y}^2 = \mathbf{0}$$

where $\mathbf{W} = \mathbf{k}^2 - \mathbf{V}^J - \mathbf{l}^2/R^2$. Now, we can solve this matrix equation, starting from the condition $\mathbf{Y}^{-1} = \mathbf{0}$, up to the asymptotic region where the potential is vanishing small and the solution resembles that of the free particle problem.

---

[34] This problem doesn't arise if we resort to the Lippamann-Schwinger equation, which entails the boundary condition. However, its numerical solution turns out to be very difficult.

[35] It is the multichannel version of the log-derivative function usually introduced in one-dimensional scattering problems (see for example Messiah(2000)). In that case it factors out the normalization constant which is inessential for computing the scattering phase shifts from the asymptotic behaviour of the eigenfunction.

In order to see how this asymptotic solution looks like we turn back to the channel Schrödinger equation (eq.(4.18)) with $\mathbf{V} = \mathbf{0}$ whose *general* solution can be written in "standard form" as

$$\mathbf{\Psi}^{\infty}(R) = \mathbf{J}(R) - \mathbf{N}(R)\mathbf{K}$$

Here the $\mathbf{J}$ and $\mathbf{N}$ matrices can be defined as follows ($z_i = k_i R$ are dimensionless quantities):

$$\text{Open channels :} \quad \begin{aligned} (\mathbf{J}(R))_{ij} &= \delta_{ij} \frac{1}{\sqrt{k_i}} \left(\tfrac{\pi}{2} z_i\right)^{1/2} J_{l_i+1/2}(z_i) \\ (\mathbf{N}(R))_{ij} &= \delta_{ij} \frac{1}{\sqrt{k_i}} \left(\tfrac{\pi}{2} z_i\right)^{1/2} Y_{l_i+1/2}(z_i) \end{aligned} \tag{4.19}$$

$$\text{Closed channels :} \quad \begin{aligned} (\mathbf{J}(R))_{ij} &= \delta_{ij} \frac{1}{\sqrt{k_i}} \left(z_i\right)^{1/2} I_{l_i+1/2}(z_i) \\ (\mathbf{N}(R))_{ij} &= -\delta_{ij} \frac{1}{\sqrt{k_i}} \left(z_i\right)^{1/2} K_{l_i+1/2}(z_i) \end{aligned} \tag{4.20}$$

where J_n, Y_n are the Bessel functions of the first and second kind and I_n, K_n are modified Bessel functions of the first and third kind as defined by M. Abramowitz and I.A. Stegun (1972): they are the general solutions of the (scalar) "free" equations for open and closed channels respectively[36],[37]. The $\mathbf{K}$ matrix introduced here is the whole set of constants that combine the basis solutions. It holds the scattering informations in its "open-open" block $\mathbf{K}_{oo}$. Indeed, this block is related to the (operational) S matrix by a Caley transform

$$\mathbf{S} = (1 + i\mathbf{K}_{oo})(1 - i\mathbf{K}_{oo})^{-1} \tag{4.21}$$

as the reader can easily check starting with the Hankel/S form of the asymptotic solution

$$\mathbf{\Psi} = \mathbf{H}^{(-)} - \mathbf{H}^{(+)}\mathbf{S}_{aug}$$

where $\mathbf{S}_{aug}$ is an "augemented" S matrix (whose open-open block is the previous $\mathbf{S}$ matrix) and $\mathbf{H}^{(\pm)} = -\mathbf{N} \pm i\mathbf{J}$ (see also eq.(4.17)).

It follows, then, that the asymptotic $\mathbf{Y}$ matrix, here denoted $\mathbf{Y}^{\infty}$, reads as

$$\mathbf{Y}^{\infty}(R) = (\mathbf{J}(R) - \mathbf{N}(R)\mathbf{K})'(\mathbf{J}(R) - \mathbf{N}(R)\mathbf{K})^{-1}$$

---

[36]We have used *real* valued k_i to refer to $\sqrt{2\mu(E - \epsilon_i)}$ for the open channels and to $\sqrt{2\mu(\epsilon_i - E)}$ for the closed ones. Furthermore, it should be noted that with our definition the wronksian for each channel is unity both for open and for closed channels, i.e. in matrix form $W\{\mathbf{J}, \mathbf{N}\} = \mathbf{I}$.

[37]The J, N solutions are "standing wave" solutions, just like $sin(kr)$ and $cos(kr)$ are standing solutions of the $l = 0$ case. We could have well used the ougoing/incoming spherical solutions (the "Hankel solutions").

where $\mathbf{K}$ is an arbitrary matrix of constants. This $\mathbf{K}$ matrix can be obtained by the "matching condition" $\mathbf{Y}(R_\infty) = \mathbf{Y}^\infty(R_\infty)$ (for any $R = R_\infty$ sufficient far from the interaction region), that is by solving the simple linear problem

$$\{\mathbf{N}(R_\infty)' - \mathbf{Y}(R_\infty)\,\mathbf{N}(R_\infty)\}\,\mathbf{K} = \{\mathbf{J}(R_\infty)' - \mathbf{Y}(R_\infty)\,\mathbf{J}(R_\infty)\} \qquad (4.22)$$

As already mentioned, once it is obtained one gets scattering observables by making use of the Caley transform, eq.(4.21), to have the "operational" S matrix.

It is worth to note at this point that the Riccati equations are very different from Ordinary Differential Equations (ODE), as can already be argued by looking at our initial condition $\mathbf{Y}^{-1} = \mathbf{0}$. We can see this clearer considering the Riccati equation for one *free* channel without centrifugal potential (i.e. $\mathbf{W} \to k^2$): its solution $y = cotg(kR)$ is singular at each R point such that $kR = \left(\frac{1}{2} + n\right)\pi$, $n = 0, 1, \dots$ Thus, in order to propagate the solution from the initial condition at the origin, one has to adopt special techniques based on "local boundary conditions" (Mrugala and Secrest, 1983; Manolopulos, 1986; Alexander, 1984; Alexander and Manolopulos, 1987). One could also consider the Riccati equation for the inverse log-derivative matrix $\widetilde{\mathbf{Y}} = \mathbf{Y}^{-1}$

$$\frac{d\widetilde{\mathbf{Y}}}{dR} + \widetilde{\mathbf{Y}}\mathbf{W}\widetilde{\mathbf{Y}} + \mathbf{1} = \mathbf{0}$$

and switch between $\mathbf{Y}$ and $\widetilde{\mathbf{Y}}$ whenever one of the two matrices reaches a singluar point: this method, combined with the ODE integrator to be described in Chapter 10, has approximately the same accuracy at the same expense of computational time of the traditional log-derivative algorithms.

In concluding this Section we note some symmetry properties of the relevant matrices. First of all the Caley transform of eq.(4.21) is a one-to-one mapping between self-adjoint and unitary operators (whitout -1 as proper eigenvalue). It is a well known map in spectral theory and allows us to state that the $\mathbf{K}_{oo}$ matrix is self-adjoint since the S matrix is unitary. We can say more. The time-reversal invariance allows us to consider real $\mathbf{\Psi}$ matrices without lose of generality. For the same reason we can consider the Riccati matrix equation as a real and symmetric equation whose initial condition is also symmetric: thus, the $\mathbf{Y}$ matrix can be considered to be a real and symmetric matrix. It follows that also the "augmented" $\mathbf{K}$ matrix is real and symmetric, as the reader can check by using eq.(4.22) along with the wronskian relation of the footnote 36 on pag. 111.

Part II

The LiH_2^+ system

Chapter 5

Overview

In this Chapter we review the molecular astrophysics relevant to the present work and introduce our system, the LiH_2^+ system, showing its possible importance in the early Universe chemistry. We begin in Section (5.1) with a brief history of the Universe evolution, as it turns out from the widely used Big Bang theory. In Section (5.2) we focus attention on the recombination and post-recombination era which saw the birth of chemistry and set the stage for the subsequent evolution of the Universe. The Lithium chemistry is reviewed in Section (5.3) while the LiH_2^+ system is introduced in Section (5.4), in which we show its connection with the Lithium network.

5.1   Universe evolution

We briefly review here the history of the Universe by looking at the crude diagram of Fig.(5.1) in which only "recent events" are shown. The diagram represents the arrow of time and is based on the data collected in Table 1 of the review article of Lepp and Stancil (1998). The actual dating of events is correct in red-shift units (the "z" parameter) while is somewhat uncertain in the usual time units. This is because the actual dates of the Universe evolution events depend on the cosmological model adopted while the red-shift z is an "observed" quantity, although at present we can observe objects only up $z \sim 5$. As it is well known, the red-shift is the fractional reduction of the frequency of light that comes from a moving source: it is related to the velocity of the moving source through a Doppler-like relation

$$z + 1 = \sqrt{\frac{c + v}{c - v}} \longrightarrow \frac{v}{c} + 1 \text{ when } v \ll c$$

and to the distance from the source by the Hubble's law, which (in the recent Universe) reads as

$$v = H_0 d$$

where $H_0 = 40 - 70\,kms^{-1}Mpc^{-1}$, the "parsec" ($pc$) being the astronomical unit of distance ($1\,pc = 3.623\,ly \sim 3x10^{16}m$). The relation between z and t is given by

$$dt/dz \propto -(1 + z)^{-2}(1 + \Omega_0 z)^{-1/2}$$

where Ω_0 (the "closure parameter") is 1 for a flat Universe. The data of Fig.(5.1) corresponds to $\Omega_0 = 1$ and $H_0 = 50\,kms^{-1}Mpc^{-1}$.

The events of the first few seconds of life of the Universe do not concern our work: this is matter of particle physics which, with the current energy obtainable in particle accelerators, has confirmed the present theories up to $10^{-10}\,s$ after the Bing Bang[1].

We begin our history at about 200 s after the Big Bang, when the adiabatic cooling due to expansion allowed the formation of the first composite nuclei (D, He). Only the lightest nuclei were formed in this *nucleosynthesis* process, because of the lack of a stable nucleus with atomic mass five. Slightly heavier elements were formed in rare collisions between the D, T, ^3He and ^4He nuclei: they are ^6Li, ^7Li and ^7Be which complete the Standard Big Bang Nucleosynthesis (SBBN) scenario. These nuclei were free of electrons, as the matter was mantained ionized by the still high temperature, either through termal collisions and (high energy) photoionization. At that time the Universe was filled with a homogeneous barion-photon fluid and matter and radiation were strongly coupled. Indeed, the background radiation field could exchange energy in a continuous fashion with the charged particles present (mainly through Compton/Thomson scattering on electrons) much like what happens between the radiation field and the wall of a(n ideal) black-body containing it. The temperature drop due the continuos expansion broke this equilibrium: for example, for temperatures below $T \sim 10^5\,K$ the thermal motion becomes ineffective in ionizing hydrogen atoms and for He^+, He the "critical temperatures" are even higher. This means that when the neutral hydrogen formation was completed at about $z \sim 1300$ the Universe underwent a phase transition from a charged (plasma-like) system to a neutral one[2]. The radiation then *decoupled* from the

---

[1] The highest attainable energies are $\sim 90\,GeV$ in the LEP accelerator at the CERN center of Geneva, Switzerland (to be substitued with the LHC collider that will work at $\sim 7\,TeV$) and $\sim 1\,TeV$ in the Tevatron accelerator at the Fermi National Accelerator Laboratory, Batavia, IL.

[2] Two notes about this "decoupling" process: (i)the mean energy of radiation is $E_\gamma \sim 3k_B T$ and that of the matter is $E_m \sim 3/2k_B T$, thus the radiation plays a primary role in ionizing the matter; (ii)the temperature at $z = 1300$ was about $3500\,K$, that is it was well below the "critical temperature" mentioned above; this is because every recombination process has
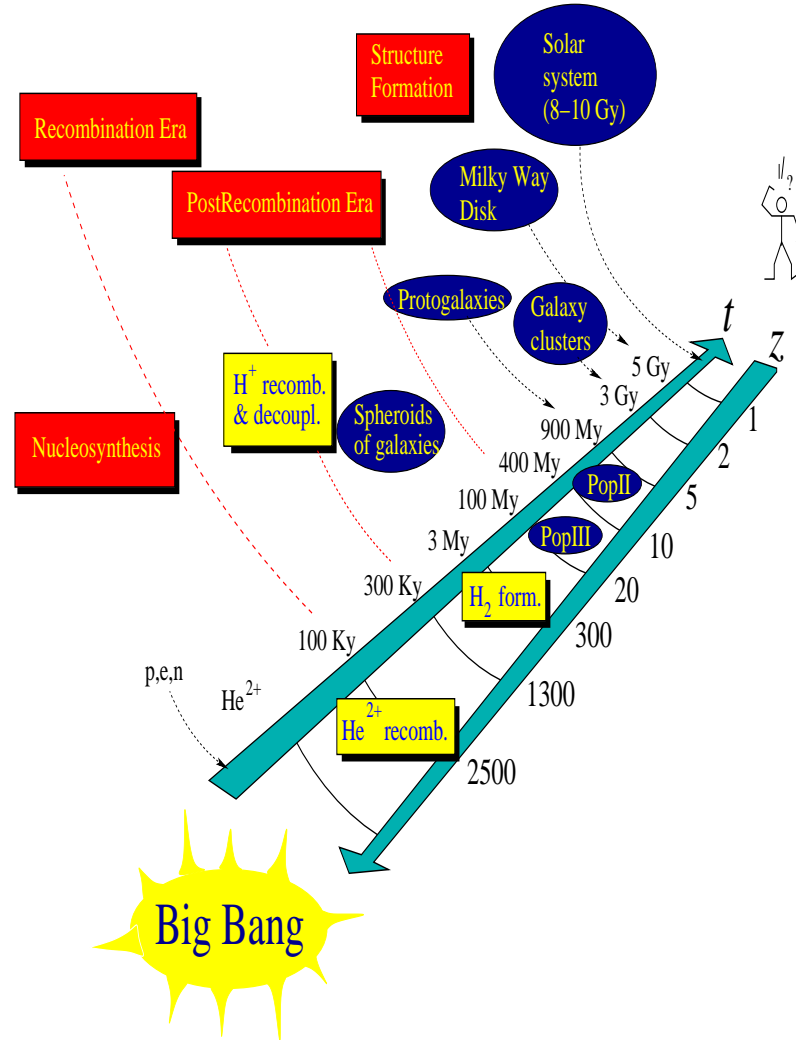
Figure 5.1: The arrow of time: some representative events of the evolution of the Universe.

matter and begun its independent evolution: this period marks the istant at which the Cosmic Background Radiation (CBR) interacted with matter for the last time, apart for very weak subsequent interactions: the CBR conserved its original (equilibrium) spectrum, modified only by the adiabatic expansion.

This period, $z = 6000 - 1000$, which begun with the netralization of He and ended with the partial neutralization of Li is known as *recombination era*,

a *negative* entropy contribution and, therefore, is substantially delayed with respect to the epoch in which the temperature reached its critical (enthalpic) value.

although the term is somewhat misleading because at this time nuclei and electrons combined for the first time. The chemistry of the recombination era and of the subsequent *post-recombination era* was very simple: only few elements were present, while dust grains, cosmic rays, interstellar radiation field and stellar UV emissions had yet to appear. The chemical evolution was, thus, determined by binary collisions and low-energy photon processes.

The formation of the first generation of stars (Population III or simply PopIII) at about $z \sim 20 - 12$ changed abruptly the situation. These stars originated from the collapse of the early clouds which is thought to have begun at about $z \sim 100 - 20$. In their high temperature interiors, they produced for the first time the heavy elements, the so-called "metals". Futhermore these stars produced solar winds, ultravacuum UV radiations and shock waves (with their death) that spread over the interstellar medium, thereby complicating the "simple" situation of the previous epoch. This is the epoch of structure formation in which the Universe reached its present aspect, together with our Milky Way, our Solar System and our Earth.

The chemical and physical evolution of the late Universe was(is) very complicated, in particular in the star forming regions. From a chemical point of view dust grains are thought to have played a key role in this evolution, since they allowed many reactions that otherwise would have been forbidden. For example, only in this epoch the simple reaction

$$H + H \rightarrow H_2$$

became possible on the grains surface.

5.2   The post-recombination era

The recombination and post-recombination era are a somewhat unique area in astrophysics, because the current impossibility of observing "objects" of this epoch. Our knowledge of these era relies on the current knowledge of non-equilibrium chemistry, physical cosmology, hydrodynamics and only occasionaly can be indirectly tested on the Universe we see today. Much of the work in this area is a judicious use of available rate constants and computational power in chem-physical simulations of a composite gas, subject to the initial SBBN concentrations of nuclei together with the general relativity theory of gravitation in an expanding Universe.

In this Section we consider briefly two main topics in this research area: the "average" evolution of the chemical species across this era and the onset of the collapse within the gas that determined the end of the post recombination era leading to the formation of the first generation of stars. Since the pioneering

works of Saslaw and Zipoy (1967) and of Peebles and Dicke (1968) the role of
molecules in the Universe evolution has been recognized. Molecules set scale of
the first objects and might have helped to amplify galaxy formation and lead
to large-scale structure. Molecular formation in the early Universe has been
the subject of several theoretical studies (Palla et al., 1983; Lepp and Shull,
1984; Stancil et al., 1996; Bougleux and Galli, 1997; Galli and Palla, 1998; Puy
and Signore, 1999). Here we focus attention on the above mentioned review
article of Lepp and Stancil in the book of Hartquist and Williams (1998) and
on the recent work of Galli and Palla (1998).

5.2.1 Early Universe chemistry

In their recent work Galli and Palla (1998) followed the evolution of 21 molec-
ular species from $z = 10^4$ to $z = 0$ in a homogeneous and isotropic gas (the
Universe matter in the Friedman cosmological model). They included 87 gas-
phase reactions and critically discussed some of them.

Starting with the abundances predicted by the SBBN model the fractional
abundances of the molecular species were followed until they reached their
asymptotic limit at $z \sim 100$. Indeed, at that time the reaction rates fell below
the speed of the expansion of the Universe and the molecular concentration
"froze out". From that time the gas would have remained in that state unless
some perturbation was introduced. As already noted, perturbations appeared
at $z \sim 100-20$ as collapse of overdense clouds and, later at $z < 20$, as reheating
due to UV stellar radiation. Therefore, the data of the above mentioned works
are applicable down to these red-shifts, where they set the initial conditions
for the next stage of the evolution of the Universe.

The chemistry of the post-recombination epoch started at $z \sim 1300$ with
the formation of the molecular ions HeH^+ and He_2^+ through *radiative associ-
ation*[3]

$$He + H^+ \rightarrow HeH^+ + \gamma$$

$$He + He^+ \rightarrow He_2^+ + \gamma$$
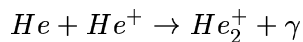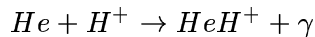
The ions, however, were depleted by two *dissociative recombination* reactions

$$HeH^+ + e^- \rightarrow H + He$$

$$He_2^+ + e^- \rightarrow He + He$$

---
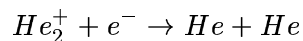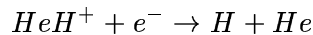
[3]The radiative association is the major route for the formation of the first neutral and
ionic molecular species in rarefied dust-free environments where densities are too low to allow
for the more common ternary association $A + B + M \rightarrow AB + M$. Here the third body M
absorbs the energy released by the AB system in the continuum-to-bound transition. Also
the *associative detachment* $A + B \rightarrow AB^+ + e^-$ plays an important role.

thus increasing the rate of neutralization of He^+ and H^+. Furthermore, the photodestruction at $z \sim 1300$ was particularly efficient and therefore chemistry really began with the formation of the first H_2 molecules. H_2 could not be formed by radiative association since the lack of dipole moment forbids the continuum-to-bound transition. Two different routes led to the molecule formation, each initiated by slow radiative processes,

$$H + e^- \rightarrow H^- + \gamma$$

$$H^- + H \rightarrow H_2 + e^-$$

and

$$H^+ + H \rightarrow H_2^+ + \gamma$$

$$H_2^+ + H \rightarrow H_2 + H^+$$
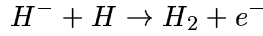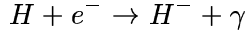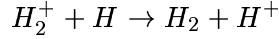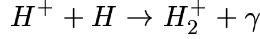
(also the reaction $HeH^+ + H \rightarrow H_2^+ + He$ contributed to the H_2 formation for $z > 500$, since the H_2^+ product of this reaction could enter the charge-exchange process with H). The so-called H_2^+ sequence was important for $z > 100$ while the so-called H^- sequence became dominant for $z < 100$ when photodetachment of H^- was reduced by the decline of the CBR.

The chemistry of He is summarized in the above mentioned reactions while that of D was very similar to that of hydrogen, except for the fact that HD can be produced also by direct radiative association thanks to its (very low) dipole moment. The Lithium chemistry played only a minor role in the evolution of the early matter since the very low initial abundance of Li nuclei ($\sim 10^{-9}$ with respect to H^+, in contrast to D^+ and He^{2+} that were $\sim 10^{-1}$ times the hydrogen abundance) prevented the Lithium species to really affect the other molecular abundances. However, as we shall see in the following, Lithium species could really play an important role in astrophysics.

Let us now go slightly deeper in the evolutionary model of the early matter in order to get some ideas of the order of magnitude of the relevant quantities. The evolutionary model consists of a set of coupled differential equations coupling the chemical species, the background radiation field and the (matter) temperature T_m,

$$\frac{dn_i}{dt} = k_f n_j n_k - k_d n_i + .. \tag{5.1}$$

$$\frac{dT_m}{dt} = -2T_m \frac{dR}{Rdt} + \frac{2}{3kn}[(\Gamma - \Lambda)_{scatt} + (\Gamma - \Lambda)_{mol}] \tag{5.2}$$

The first equation represents the canonical rate of formation of the specie i, where k_f and k_d are the formation/destruction rates and n_i is the number density of specie i. The initial conditions are taken from the SBBN model and usually expressed in terms of fractional abundances with respect to the (most

abundant) H species. The total atomic hydrogen density is taken to be (see for example (Stancil et al., 1996))[4]

$$n_H = 8.02 \cdot 10^{-6} \Omega_b h^2 (1+z)^3 cm^{-3}$$

where $\Omega_b \sim 1$ and $h \sim 0.5$, depending on the cosmological model adopted. This quantity corresponds to $2.0 \cdot 10^{-3} cm^{-3}$ in the "compressed" Universe of $z = 1000$ and to $0.018 \, cm^{-3}$ at the end of the post-recombination epoch ($z = 20$). These values are to be compared with the standard gas density at $273.15 \, K$, i.e. $n = 1.35 \cdot 10^{22} \, cm^{-3}$!

The radiation temperature diminishes following the relation[5]

$$T = T_0(1+z) \text{ where } T_0 = 2.726 \, K$$

and is considered to be in equilibrium, as the perfect black-body spectra of the CBR suggests. Therefore, the number density of photons with frequency between ω and $\omega + \delta\omega$ is given by the Planck distribution law

$$n(\omega, \delta\omega) = \frac{8\pi}{(2\pi c)^3} \frac{\omega^2 \delta\omega}{e^{\beta\hbar\omega} - 1} = 8\pi \frac{\overline{\nu}^2 \delta\overline{\nu}}{e^{\beta\hbar\omega} - 1}$$

(where $\beta = (k_B T)^{-1}$ and $\overline{\nu} = \omega/(2\pi c)$) from which the energy density follows

$$u(\omega, \delta\omega) = \frac{\hbar}{\pi^2 c^3} \left(\frac{k_B T}{\hbar} \right) \frac{\eta^2 \delta\eta}{e^\eta - 1} \text{ with } \eta = \frac{\hbar\omega}{k_B T}$$

In Fig.(5.2) we report the last mentioned distribution function at four significative values of z; in Table (5.1) we report some relevant data about these z values. From left to right we report the radiation temperature, the wavenumber of the approximate maximum in the energy distribution (the values corresponds to $\eta = 3$ which is very close to the maximum) and the corresponding energy and photon number densities in a spectral range $1 \, cm^{-1}$ wide; finally, in the last column we report the above mentioned total hydrogen number density.

---

[4]The $(1+z)^3$ dependence follows from the expansion of the Universe, which is linear in z because of the Hubble's law.

[5]As already noted in the previous Section the CBR underwent to simple adiabatic cooling after hydrogen recombination. Thus, the evolution of the radiation temperature can be obtained by the Wien law for the frequency peak of the energy density distribution

$$\frac{\omega}{T} = \frac{\omega_0}{T_0}$$

knowing the present radiation temperature T_0: the mentioned relation follows from $\omega = (1+z)\omega_0$.
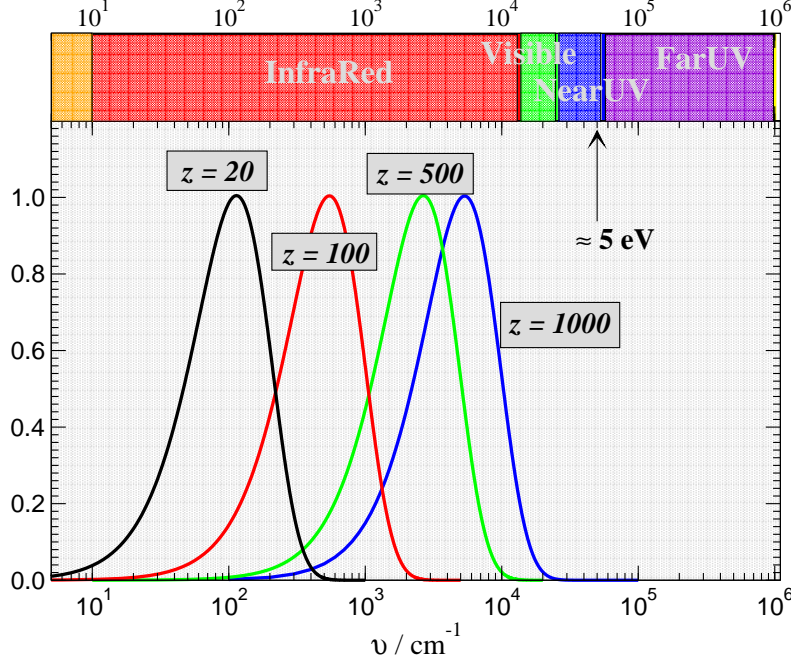
Figure 5.2: Energy density distributions (normalized with respect to their maximum value) of the Cosmic Background Radiation in four moments of the post-recombination era.

z	T/K	$\overline{\nu}_0/cm^{-1}$	$\delta u_0/eV\ cm^{-3}$	$\delta n_0/cm^{-3}$	n_H/cm^{-3}
1000	2728.7	5689.66	$3.01*10^7$	$4.26*10^7$	$2.0*10^3$
500	1365.7	2847.64	$3.77*10^6$	$1.07*10^7$	252.1
100	275.3	574.01	$3.09*10^4$	$4.34*10^5$	2.1
20	57.2	119.26	$2.77*10^2$	$1.87*10^4$	0.018

Table 5.1: Some relevant quantities at four significative z values.

The matter temperature evolves because of the expansion (the first term in Eq.(5.2))[6] and because of the interaction between matter and radiation: the $(\Gamma - \Lambda)_{scatt}$ term represents the net transfer of energy in Compton scattering of CBR photons on electrons, while the $(\Gamma - \Lambda)_{mol}$ is the molecular heating/cooling. The $(\Gamma - \Lambda)_{mol}$ can become an effective heating(cooling) source for the matter if the rate of collisional de-excitation is faster(slower) than the radiative decay; however, in general, the contribution of this term is small.

---

[6]The adiabatic expansion of a monoatomic gas ($E = 3/2\,k_B T$) is given by $dT/T = -2/3\,dV/V$ where $dV/V = 3dR/R$, R being the radius of the spherical Universe.

Nevertheless, this term is important for the collapse of the early clouds that we are going to describe.

5.2.2 Molecules in the collapse of early clouds

The model of an isotropic gas filling up the Universe is very useful in studying the average composition of the early matter, but it is clearly untenable. As a matter of fact, although very homogeneous on a large scale, our Universe is quite inhomogeneous, having local overdense zones (galaxies and clusters of galaxies) separated by almost empty regions, where the number of atoms can be as low as 1 per a cubic meter. In the Big Bang framework one has to postulate the existence of small deviations from homogeneity, i.e. of regions in which a significantly overdense portion of the early matter starts to collapse under the effect of self-gravity and, ultimately, can form gravitationally bound objects. In particular, the star formation process is one of the possible outcomes of a falling down cloud.

One of the main problems that a collapsing cloud has to face at is its *cooling*: without a cooling mechanism that works taking away the energy excess, the collapse will end in a stationary state in which *pressure* (i.e. the atomic and molecular motion) counterbalances *gravity*. In particular, in the low-temperature gas of the late post-recombination era a cooling mechanism involving only hydrogen and helium atoms is quite inefficient, because of the lack of low-lying energy levels. For this reason it has been long recognized that, even at a fraction of $10^{-4} - 10^{-5}$ of the total atomic hydrogen abundance, *molecules* trigger the collapse. The mechanism is known as *radiative cooling* and has been introduced at the end of the previous Section: in practice, molecules are collisionally excited and radiatively de-excited, thereby taking away the energy as light quanta. This mechanism was proved to be efficient even when H_2 only was considered, but it is clearly more efficient when HD and LiH are taken into account: indeed, despite their lower abundances, these two molecules have more closely spaced energy levels and greater radiative efficiency of H_2[7].

The characteristic quantity in this context is the *molecular cooling function* which for a molecule M in the initial state i is given (in steady-state level populations) by

$$\lambda_M^i = \sum_{X, j > i} n_X k_{i \to j}^X P_{j \to i}^{rd} \Delta e_{ij}$$

where X represents a collisional partner, $k_{i \to j}^X$ is the relevant collisional rate

---

[7]It is worth to note that radiative rotational transitions in H_2 are of *quadrupole* type ($\Delta j = \pm 2$) and thus they (i) need a higher collision energy to be started and (ii) give rise to a weaker emission efficiency than in the case of HD and LiH.

constant, $P_{j \to i}^{rd}$ is the radiative de-excitation rate and Δe_{ij} is the (absolute) energy gap between level i and level j; analogously, we can define a *molecular heating function*

$$\gamma_M^i = \sum_{X, j > i} \Delta e_{ij} P_{i \to j}^{re} k_{j \to i}^X n_X$$

where now $P_{i \to j}^{re}$ is the radiative excitation rate. The radiative rates can be given in terms of the Einstein coefficients,

$$P_{j \to i}^{rd} = A_{ji} + B_{ji} u_{ji}$$
$$P_{i \to j}^{re} = B_{ji} u_{ji}$$

where u_{ji} is the energy density of the radiation per unit frequency corresponding to the $i \to j$ transion. The total cooling and heating functions are then given by

$$\lambda_M = \sum_i x_i \lambda_M^i$$
$$\gamma_M = \sum_i x_i \gamma_M^i$$

where x_i is the fractional population of level i, and the *net cooling function* by

$$\Lambda_M = \lambda_M - \gamma_M$$

The net cooling function clearly depends on the temperature and on the density of the collisional partners: it is an increasing function of the temperature, due the increasing ability of the molecules to be excited in higher levels, and it is a decreasing function of the density of the collisional partners, since the higher the density the higher is the rate of collisional de-excitation prior to radiative transfer[8]. Galli and Palla (1998) computed the cooling functions of LiH, HD and HH in the low density limit using the available data to date. The Figure 2 in their Appendix shows that LiH cooling dominates up to $100\,K$, followed by HD in the temperature range $100 - 2000\,K$ and, ultimately, by H_2 for $T > 2000\,K$[9].

5.3 The LiH in the Early Universe

There is considerable uncertainty on the abundance of LiH in the early Universe. This is somewhat unpleasent since Li bearing species have some importance for the astrophysical community. Thanks to its high dipole moment,

---

[8]It is worth to mention that the above formulas should be corrected, when needed, by the enthalpic contribution of the chemical reactions.

[9]We should mention, however, the fractional abundances of these species as they turned out from their work for $z < 20$: $f(H_2) \sim 10^{-6}$, $f(HD) \sim 10^{-9}$ and $f(LiH) \sim 10^{-19}$.

LiH could be the first "object" of the early Universe to be observed and, indeed, a very preliminary search for primordial *LiH* molecules has been started (de Bernardis et al., 1993). Dubrovnich (1993) and Maoli et al. (1994) have suggested that Thomson scattering of CBR photons by primordial molecules with large dipole moments may have attenuated second order angular CBR anisotropies, thereby leaving their imprint on the CBR spectrum. This imprint may be observable if sufficient molecular abundances were produced. On the other hand, it is important to assess the feasibility of such experiments since the total Lithium abundance turns out to be a *discriminant* for the nucleosynthesis models. Furthermore, the role of *LiH* in the cooling mechanism of the early clouds, if any, depends clearly on the molecular abundance.

The pioneering computations of Lepp and Shull (1984), using an estimated value for the radiative association rates, gave the LiH/H_2 abundance ratio at low red-shift to be as high as $10^{-6.5}$; with $H_2/H \sim 10^{-6}$ the fractional abundance of LiH would be $10^{-12.5}$. Subsequently, and independently, Dalgarno et al. (1996) and Gianturco and Gori-Giorgi (1996; 1997) computed accurate rate constants for the radiative association process from ground-state atoms, both for LiH and for LiH^+. Gianturco and Gori-Giorgi (1996; 1997) also examined the possibility of producing LiH from an excited $Li(2p)$ atom and found the relevant rate six order of magnitudes larger than that involving $Li(2s)$ atoms. These first-principle results gave rise to a much smaller abundance of primordial LiH (Dalgarno et al., 1996; Galli and Palla, 1998). In their work, Galli and Palla (1998) further noted that the LiH abundance fell below that of LiH^+, since the formation of the molecular ion is controlled by the radiative association process $Li^+ + H \rightarrow LiH^+ + \gamma$ and Lithium remains ionized even at low red-shifts. All the recent works agree on a very low final LiH abundance, thereby preventing any possibility of observing primordial LiH. *However, we should recognize that the LiH/LiH^+ abundances depend also on the reactive interactions with the other primordial species.*

Very little is known about the exoergic reaction of LiH with the most abundant atoms

$$LiH + H \rightarrow Li + H_2$$
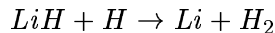
(Galli and Palla (1998) used an estimated rate constant of $2 \cdot 10^{-11} \, cm^3 s^{-1}$). This has prompted the *ab-initio* study of the underlying interactions and the first-principle determination of the rate constant: Clarke et al. (1998b) evaluated the ground-state PES and studied the collinear dynamics, both quantum mechanically and classically. They found surprisingly that the reactivity is *dynamically* prevented by the very narrow channel corresponding to the H_2 formation. Bodo et al. (2001) found that the subreactive interaction is very simple *but* dominated by the H_2 formation, showing that even the inelastic

dynamics cannot prescind from the reactive one. Lee et al. (1999) found that the excited $H_2(n = 0) + Li(2p)$ channel is already open at zero collision energy and is directly accessible from the $LiH(n = 0) + H(1s)$ *via* non-adiabatic transition to this first excited state. These data stimulated recent far-wing experiments on this system (Bililign et al., 2001). Martinez (1997) tested its Multiple-Spawning Ab-Initio-Molecular-Dynamics approach around the conical intersection of the $Li(2p) + H_2$ system.

The dissociative recombination rate, i.e. the rate of the process

$$LiH^+ + e^- \rightarrow Li + H$$
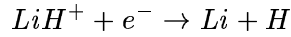
has been estimated to be $k = 3.8 \cdot 10^{-7} (T/K)^{-0.47} cm^3 s^{-1}$ and only very recently has been measured to be $3.8 \pm 1.4 \cdot 10^{-7} cm^3 s^{-1}$ at $300\,K$, i.e. about 10 times the estimated value (Khron et al., 2001).

All the (positive) ionic reactions have only estimated rate constants; Galli and Palla (1998) used in their model the following reactions with the indicated rate constants

$LiH + H^+ \rightarrow LiH^+ + H$	$k \sim 10^{-9} cm^3 s^{-1}$
$LiH + H^+ \rightarrow Li^+ + H_2$	$k \sim 10^{-9} cm^3 s^{-1}$
$LiH^+ + H \rightarrow LiH + H^+$	$k = 10^{-11} e^{-679000K/T} cm^3 s^{-1}$
$LiH^+ + H \rightarrow Li + H_2^+$	$k = 10^{-9} e^{-66400K/T} cm^3 s^{-1}$
$LiH^+ + H \rightarrow Li^+ + H_2$	$k = 3 \cdot 10^{-10} cm^3 s^{-1}$

where the exponential terms arise from enthalpic considerations. Strangely enough the reaction

$$LiH + H^+ \rightarrow Li + H_2^+$$
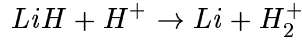
has been omitted.

On the other hand, much work has been done in evaluating the contribution of He to the LiH cooling function. The collisional process

$$LiH(n, j) + He \rightarrow LiH(n', j') + He$$
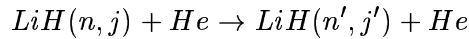
has been largely studied (Gianturco et al., 1997b; Gianturco et al., 1997a; Bodo et al., 1998b; Bodo et al., 1998a). The reliability of the interaction potential has been questioned by Taylor and Hinde (1999); however, their new potential has been proved to be somewhat less satisfactory in reproducing the only available (high energy) experimental results than the previous one (Bodo et al., 2000) and several experiments have been suggested to solve the controversy.

The H contribution to the LiH cooling function, as already said, has been proved difficult to assess, because of the competing H_2 formation reaction (Bodo et al., 2001); although the reactive outcome could turn out negligible, the inelastic dynamical results must come from full 3D *reactive* calculations.

Also in this case, the H^+ contribution to the LiH cooling function has not been determined. In this context it is worth to mention that the low red-shift fractional abundance of $H^+(f \sim 10^{-4})$ is much lower than the corresponding abundances of H ($f \sim 1$) and He ($f \sim 10^{-1}$) but the charge-dipole interaction acting between the strongly dipolar molecule and the proton can give rise to very large cross-sections ($10^4 - 10^5$ times a typical neutral cross-section), thereby offsetting the lower abundance of H^+.

All the above considerations on the ionic species motivated our interest in the LiH_2^+ system, which we shall present in the following Section: it is the relevant system for studying both the ionic Lithium (sub)network and the inelastic processes

$$LiH(n, j) + H^+ \rightarrow LiH(n', j') + H^+$$

$$LiH^+(n, j) + H \rightarrow LiH^+(n', j') + H$$
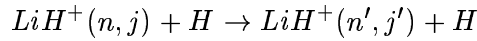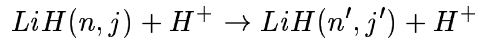
i.e. the interactions of LiH/LiH^+ with the abundant H^+/H species. We hope that this work will contribute to shed light to the entangled ionic (sub)network of the Lithium chemistry in the early Universe and, possibly, to furnish starting material to computing accurate rate constants that, in turn, could be of help for the astrophysical community.

5.4 The LiH_2^+ system

Very little is known about LiH_2^+. A preliminary work of Hobza and Schleyer (1984) speculated somewhat on its connection with the neutral LiH_2 system in order to interpret ionization experiments (Wu, 1979). Subsequent accurate calculations around the C_{2v} (ground-state) equilibrium structure were done by Searles and Nagy-Felsobuki (1991): the system was found to be weakly bound by the polarization forces acting between Li^+ and H_2. This equilibrium structure was also inferred in previous studies on the inelastic $Li^+ + H_2$ dynamics (Lester, 1971; Barg et al., 1976) which could be compared with beam experimental results (see the introductory Chapter of the collection edited by Bernstein (1979) and reference therein).

Here we approach the system in its full dimensionality by looking at the lower lying electronic states in order to determine its relavance with the reactive and non-reactive ionic processes described in the previous Section.

We report in Fig.(5.3) the correlation diagram for the energy levels of our system in order to see the relation between the asymptotic fragmentation channels. On the right hand side we have reported the channel fragments in terms of the LiH/LiH^+ species while on the left we have drawn the energy levels in the range of coordinates corresponding to H_2/H_2^+ molecules. The three
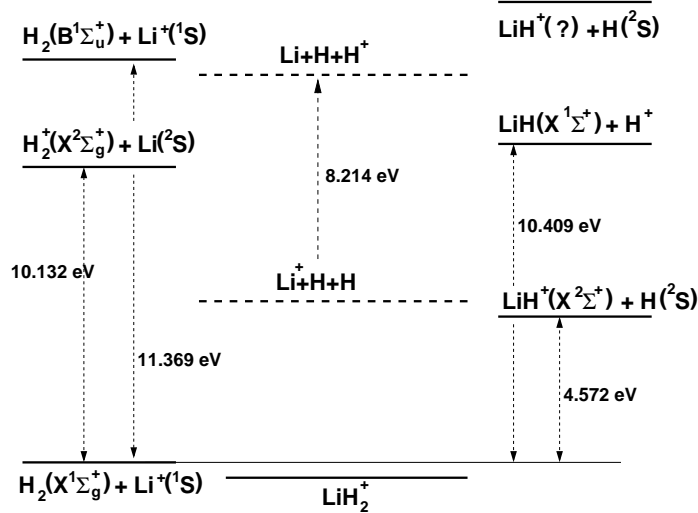
Figure 5.3: Correlation diagram for LiH_2^+ and its asymptotic states. Triatomic fragmentation arrangements are also displayed. See text for details.

atom break-up channels are displayed (as dashed lines) in the middle of the diagram, because of the relevance for the ground-state process (see Chapter 8). What is readily evident from the diagram is the large energy gap between the ground electronic state of $LiH + H^+$ and that of $LiH^+ + H$ by one side and $H_2 + Li^+/H_2^+ + Li$ on the other side. This is due the large difference between the ionization potentials of the Li-bearing species and those of H, H_2. On the other hand the energetic difference between the second and third state is much smaller; indeed, their three atom asymptotes $(Li + H^+ + H)$ are degenerate because they only differ for the simple exchange of charge between the hydrogens. We left unspecified the third asymptote for reasons to be explained below (see Chapter 7). Anticipating the results of the following Chapters we can say here that these features remain substantially unchanged in the interaction region: we will see two well separated lowest-lying states, while the second and the third electronic states interact because of the charge-exchange process between the two hydrogen atoms. Thus we will exclude non-adiabatic interactions between the first two states and we will focus on the adiabatic processes occuring on the corresponding PESs; we will neglect the interaction between the first and the second excited states.

The situation is summarized in the pictorial representation of the system of Fig.(5.4) as it turns out from the present work. In this picture we report also the relevant topological features of the PESs: the above mentioned polarization well of the ground-state $Li^+...H_2$ and two much deeper wells in the first excited
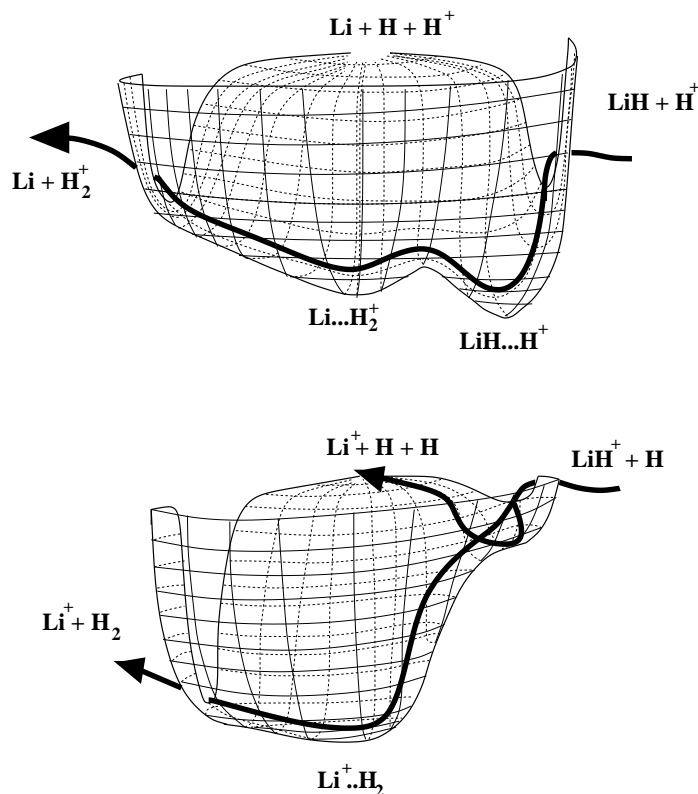
Figure 5.4: Pictorial view of the potential energy surfaces for the two lowest electronic states of LiH_2^+.

state. These last wells are of electrostatic origin too: on the reagent side $(LiH + H^+)$ we have a charge-dipole well which turns out to be the deepest, while on the product side $(Li + H_2^+)$ we have a charge-induced dipole well. The third electronic state, here not reported, turns out to be purely repulsive.

In this work we intentionally focus on the singlet manifold since we expect that the triplet one (which "touches" the $LiH^+ + H$ and $Li + H_2^+$ asymptotes, apart from the three atom dissociation limits) is purely repulsive, because of the non-bonding nature of the exchange interaction between the two valence electrons. Furthermore, we expect that the spin-orbit coupling that trigger the possible singlet-triplet transition is small for such light atoms and, thus, our singlet states should not be affected by the triplet manifolds. It should be emphasized, however, that spin multiplicity must be taken into account in dynamical considerations; for example, only 1/4 of the $LiH^+ + H$ collisions has a chance to go on the singlet manifolds.

For completeness we note that the data reported in Fig.(5.3) were extracted

from a combination of experimental/theoretical data. All the results reported
there refer to adiabatic transitions, with the exception of the process involving
the $H_2(X^1\Sigma^+) \to H_2(B^2\Sigma^+)$ transition where we have instead used the verti-
cal difference (Huber and Herzberg, 1979; Stwalley and Zemke, 1993; Moore,
1971); for the LiH^+ molecule we used our computed values. We collect the
relevant molecular parameters in Table (5.2).

	D_e/eV	D_0/eV	R_e/a_0
H_2	4.710	4.478	1.401
H_2^+	2.792	2.648	1.997
LiH	2.515	2.429	3.015
LiH^+	0.138	0.111	4.107

Table 5.2: Molecular parameter of the relevant diatomics. See text for details.

With this we close this long introductory Chapter which, starting with the
Big Bang, leaves us with the Big Deal: the LiH_2^+ system.

Chapter 6

A MultiReference Valence Bond approach

In Chapter 1 we introduced a modern Valence Bond approach to computing electronic energies. The method described there is based on a *single refer-ence* wavefunction, the Spin Coupled wavefunction, with which the electron correlation is introduced by vertical excitation on suitable virtual orbitals (see Sections (1.6) and (1.7)). As already emphasized in Chapter 1, one great ad-vantage of the method is the possibility of gaining a clear physical picture of the underlying interactions while maintaing a high degree of accuracy. However, much like in MO theories, to treat excited state problems and near-degenaracy effects a *multireference* approach should be more appropriate. In this Chap-ter, therefore, we will consider a MultiReference Valence Bond approach which parallels the well-known MultiReference approach of the MO theory. The nov-elty is that, as we will show in Section (6.1), we can *optimize* Spin-Coupled wavefunctions that work as reference functions to introduce correlation in the ground and in the excited states. In this way we can extend the appealing features of the SC method to the *excited* states while maintaining an overall high accuracy.

The realization of this procedure to compute ground and excited PESs was an important step in our work on the LiH_2^+ system, since, for example, the very important channel $LiH + H^+$ lays in the first excited PES of the system. All the *ab-initio* calculations described in this work were carried out using this method.

6.1 SC wavefunctions for excited states

In this Section we describe an approximate but very simple method to optimize excited state Spin Coupled wavefunctions. The method has the advantage of being easily implementable and of preserving the physical transparency that characterizes the SC theory.

Before treating in some details this method let us make a few remarks about the excited states. Why do excited state problems need more care than ground-state ones? Besides other things (see for example Bruna et al. (1987)) there is a basic problem in treating excited states. The method described in Chapter 1, like the MO-CI method (either in the HF-SCF or in the MC-SCF versions) or the Coupled-Cluster one, relies on the previous *variational* optimization of a simple wavefunction which is expected to contain the basic features of the exact wavefunction. The spirit of such procedure is based on the recognition that the Schroedinger equation can be obtained by a variational principle, i.e. that the solutions of the stationarity condition of the energy functional

$$\delta E = \delta \langle \Psi | H | \Psi \rangle = 0 \qquad (6.1)$$

under the normalization condition

$$1 = \langle \Psi | \Psi \rangle \qquad (6.2)$$

are the stationary states. This is true when the trial space is the entire Hilbert space, but it is clearly "almost" true when the trial space is a good approximation to the entire Hilbert space[1]. Thus, one expects that a solution of a variational problem is a good starting point to obtain an accurate wavefunction[2].

The variational principle can be applied to *any* state: if one is able to localize a *stationary* point of the energy functional the solution is expected to be a good starting point for some state of the system. The trouble with the excited states is that, in practice, we are able to localize efficiently only the *minima* of the energy functional and, thus, the variatonal principle is

---

[1]One might object that the (non-linear) space spanned by the single determinantal HF wavefunction is rarely a good approximation to the Hilbert space. One, however, should remember that the HF energy accounts almost always for more than 95% of the exact energy of system. The trouble, as it is well known, is that the remaining 5% *is the realm of chemistry*.

[2]With the exception of the Coupled-Cluster method, in all the methods mentioned above the improvements are achieved by a further application of the variational principle, that is they are *variational methods*.

useful only for the ground-state reference optimization[3]. Therefore, an excited variational solution can be obtained "in practice", with the knowledge of the ground state $|\Psi_0\rangle$, only by adding to the normalization condition (6.2) the orthogonality constraint

$$0 = \langle \Psi | \Psi_0 \rangle \qquad (6.3)$$

This condition allows us to obtain a solution for the first excited state as a *minimum* of the functional (6.1) and can be easily generalized to other excited states. If we do not know the exact ground state $|\Psi_0\rangle$ but only an approximation $|\Phi_0\rangle$, as it is always the case, it is still possible to obtain an approximation to the first excited state by replacing the condition (6.3) with

$$0 = \langle \Psi | \Phi_0 \rangle \qquad (6.4)$$

In this case, as it is well known (see for example Messiah (2000), Chapter XVIII), the stationary solution $|\Phi_1\rangle$ (which we assume to be normalized) is not orthogonal to $|\Psi_0\rangle$, but given

$$\varepsilon_0 = 1 - |\langle \Psi_0 | \Phi_0 \rangle|^{\,2}$$

it follows that

$$|\langle \Psi_0 | \Phi_1 \rangle|^{\,2} \leq \epsilon_0$$

and then

$$E[\Phi_1] \geq E_1 - \varepsilon_0 (E_1 - E_0)$$

where E_0 and E_1 are exact ground and first excited energies, respectively. From this it follows that an increasingly better approximation can be obtained whenever the approximate ground-state function is closer to the exact one.

This is the starting point of our approach: we are not directly interested in such approximation but we recognize that it can be useful also when, as it is in our case, the variational solution $|\Phi_1\rangle$ is used as a reference for the introduction of the correlation directly into this first excited state, as well as in the ground state[4].

Our aim is to preserve the appealing feautures of the Spin-Coupled VB method and therefore we use the ground-state Spin-Coupled wavefunction as

---

[3]To be clear, to the best of author's knowledge there is no evidence, for example, of a HF solution which corresponds to a *saddle* point of the energy functional, except when the symmetry of the system gives a simple structure to the saddle point. The only case in which a saddle point of the functional can be easily reached is the trivial case in which the trial space is linear: this is why the CI solutions can be used to approximate more than one electronic state.

[4]The higher energy excited states can be managed in a similar manner by a straightforward extension of the above considerations, although alternative "orthogonalization" approaches turn out to be equally valid (see below).

an approximate ground-state function and search for a function with the same shape, that is, we consider both $|\Psi\rangle$ and $|\Phi_0\rangle$ in equation (6.4) to be as in eq.(1.5) on pag. 24. We are not interested in the exact variational problem, which would consist of the application of the SC optimization (see Section (1.5)) under the general additional condition (6.4). Rather, we consider a simplified version where the same SC optimization procedure employed for the ground state is used on another still properly bound function. In this context, the only situations to be considered are those in which the excited state should be described by an orbital configuration different from that of the ground-state: adversely, the different solutions of the secular spin problem (eq.(1.9) on pag. 36) automatically satisfy equation (6.4) and are already included in the expansion of eq.(1.11). This is the key observation: we can try to satisfy the orthogonality condition

$$\langle\Psi|\Phi_0\rangle = \sum_{P\in S_N} \langle\psi_1\psi_2..\psi_N|P^r|\phi_1\phi_2..\phi_N\rangle \langle SM'|P^\sigma|SM\rangle = 0 \qquad (6.5)$$

(where $\{|\psi_i\rangle\}$ and $\{|\phi_i\rangle\}$ are, respectively, excited and ground-state orbitals and P belongs to the symmetric group S_N) *whatever* the spin functions employed for the two states and, of course, for eq. (6.5) to be valid it is sufficient that

$$\langle\psi_1\psi_2..\psi_N|P^r|\phi_1\phi_2..\phi_N\rangle = 0 \qquad (6.6)$$

for any chosen $P \in S_N$. This problem has a lot of solutions (see also Fig.(6.1)): given $X = \{|\phi_i\rangle\}_{i=1,N}$ the set of ground-state orbitals and $A = \{|\phi_i\rangle\}_{i=1,k} \subseteq X$ a chosen subset (the *active* one) of k elements, it is sufficient for $N - k + 1$ excited state orbitals $\{|\psi_i\rangle\}_{i=1,N-k+1} = A^*$ to span the orthogonal complement of A. Indeed, only a one-to-one mapping between $X \setminus A$ (the *inactive* set) and A^* could lead to a non-vanishing overlap but this is forbidden by the different numbers of the elements in the two sets. Obviously, we can consider different values of k (i.e. change the dimension of the active orbital set in the ground state) and we can consider different possible choices of the active space for each k. For each k there are $\begin{pmatrix} N \\ k \end{pmatrix}$ possible choices of the active space; this means that there are

$$\sum_{k=1}^{N} \begin{pmatrix} N \\ k \end{pmatrix} = 2^N - 1$$

different possibilities to satisfy condition (6.4) only using simple constraints on the orbitals. In this way, we obtain a trial space that is *flexible* and *simple* enough to be employed in practical calculations. As an example, for $N = 2$, we can consider an orbital $|\psi_1\rangle$ orthogonal to the two ground state orbitals, or two orbitals orthogonal to $|\phi_1\rangle$ or $|\phi_2\rangle$; for $N = 3$, we can consider one orbital
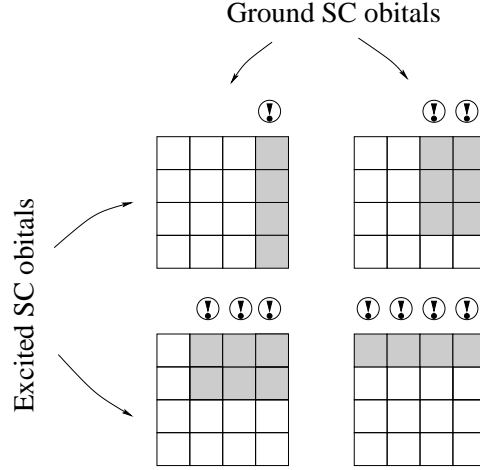
Figure 6.1: Schematic representation of the orthogonalization schemes. Overlap matrices between ground (orizontal axis) and excited (vertical axis) SC orbitals in a 4-electron system. The dark areas mark the matrix elements constrained to be zero, i.e. the orthogonality constrains. The symbols in circles indentify the "active" space. From left to right, from top to bottom the $[N : 1]$, $[(N - 1) : 2]$, ..$[1 : N]$ schemes (see the main text).

$|\psi_1\rangle$ orthogonal to the three ground state orbitals, two orbitals $|\psi_1\rangle$ and $|\psi_2\rangle$ orthogonal to one of the three pairs of ground state orbitals, or, finally, three orbitals orthogonal to one of the ground state orbitals.

We can take into account all these possibilities, optimizing one spin-coupled wavefunction for each of them and keeping the ones that yield the minimum energy to study low-lying excited states. In practice, we need only some of these combinations: for example, we can usually distinguish a given number of core orbitals that are not substantially altered in passing from the ground to the excited state and thus we can discard the "high energy" orthogonalization schemes which do not contribute to the first excited states (e.g. we can neglect *a priori* a situation in which all the excited orbitals are orthogonal to one specific core orbital since this would correspond to a core excitation).

In practice, the introduction of the orbital constraints turns out to be very simple: we change the basis set from the pure atomic to a projected one that is adapted to the decomposition of the one-electron space into an active space and its orthogonal complement. In this way the orthogonality constraints on orbitals are converted into an unconstrained, but limited, expansion of the excited state orbitals in the projected basis set. In two typical cases (see below) good results are obtained with a "$[N : 1]$" (N orbitals orthogonal to

one ground state orbital) and a "$[1 : N]$" (one orbital orthogonal to the ground state orbitals) orthogonalization schemes; for such situations a proper ordering of the orbitals and a Gram-Schmidt orthogonalization are sufficient (of course, in the same orthogonalization procedure the N linearly dependent functions are eliminated). It is worth noting at this point that the excited SC orbitals are subjected only to the orthogonality constraints and therefore their shape turns out to be variationally determined by the problem at hand.

6.2 The MRVB scheme

Having obtained one or more reference functions we can now optimize the virtual orbitals as described in Section (1.7) by taking the new SC functions as references for building the "perturbed" wavefunction. In doing this we realize that, in the optimization process of the virtuals, we have to employ some orthogonality constraints on them in order to avoid the wavefunction of eq.(1.12) on pag. 39 to collapse onto the ground state one. The actual constrains to be imposed depend on the particular orthogonalization scheme that generated the excited Spin-Coupled function. As a general prescription, in performing vertical excitation of the SC orbitals into virtuals, one has to use for the virtual orbital the *same space* used for the original "occupied" orbital of the state involved.

For example, let us consider an excited SC wavefunction that comes from the $[N : 1]$ scheme; in this case all the excited orbitals are orthogonal to the (unique) active orbital of the ground-state and, thus, every virtuals must be optimized in the orthogonal complement of the active space. On the other hand, let us consider the case in which the excited SC function comes from the $[1 : N]$ scheme and let us write the function as

$$|\Psi_{SC}^{exc}\rangle = A\left\{|\phi_1\rangle .. |\phi_{N-1}\rangle .. |\xi_N\rangle |SM\rangle\right\}$$

where $|\xi_N\rangle$ is the (unique) orbital constrained to be orthogonal to the active space. In the excitation process $|\phi_1\rangle \rightarrow |\phi_1^+\rangle$ the virtual is allowed to spread over the full space, while in the process $|\xi_N\rangle \rightarrow |\xi_N^+\rangle$ the virtual must be subject to the orthogonality condition with the active space.

With these general prescriptions a MultiReference Valence Bond procedure can be easily set up (Fig.(6.2)):

- optimize the ground-state Spin-Coupled wavefunction.

- optimize one or more excited-state SC wavefunctions. In doing this a number of physically reasonable orthogonalization schemes should be considered, although for a large-scale calculation one can look only at a number of key geometries.
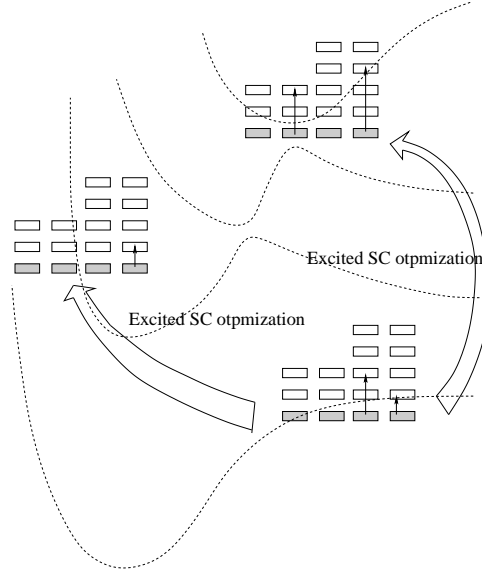
Figure 6.2: Pictorial representation of the MRVB scheme. Dark areas mark the occupied SC ground and excited orbitals, with their "stacks" of virtuals. Possible vertical excitations are indicated with thin arrows.

- for each SC wavefunction optimize a set of virtual orbitals, using the appropriate constrains described above.

- perfom the vertical excitation of the "occupied" SC orbitals into the previously optimized virtuals, in such a way to generate the VB structures.

- solve the secular problem corresponding the non-orthogonal Configuration Interaction wavefunction that mixes the previosly obtained VB structures.

In the following we consider some applications of the scheme just described. The applications to the LiH_2^+ system is of direct relevance for this work; as a matter of fact, all the *ab-initio* calculations described in this work were done as described in the following Section. The application to the awkward $C^2\Sigma^+$ state of the BeH molecule shows how the MRVB method can be used in such pathological situations.
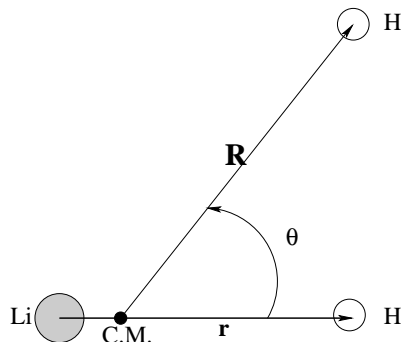
Figure 6.3: Jacobi coordinates for the $LiH+H^+$ scattering system.

6.3   Application to the $[LiH_2]^+$ system

6.3.1   The calculations in the subreactive region

As a first computational example of the newly developed approach, we consider here the sub-reactive interaction of a proton with the LiH species. We report only a short summary of the calculations performed: a full description of the complete potential energy surface (PES) will be the subject of Section (7.1), while the work in progress on the energy transfer dynamics of the $[LiH + H]^+$ system will be summarized in Chapter 10. The overall energetics of the system has been already discussed in Section (5.4).

In this Section we describe some potential energy curves obtained by moving the proton toward the center of mass (CM) of the LiH target treated as a rigid rotor at its equilibrium geometry ($r_e = 3.1042\ a_0$). We examine the behavior of the interaction for some values of the orientation of the approach (the angle θ of the Jacobi coordinate system shown in Fig.(6.3)) as a function of the scattering coordinate. The basis set employed in the calculations consists of $Li[10s4p2d/5s3p2d]$ and $H[7s2p1d/5s2p1d]$ contracted Gaussian functions and it has been already adopted in previous studies involving the LiH specie (Clarke et al., 1998b).

The Spin Coupled wavefunction of the system ground state turns out to have the form

$$|\Phi_0\rangle = A\left\{|\phi_{1s}\rangle\,|\phi'_{1s}\rangle\,|\phi_{H_a}\rangle\,|\phi_{H_b}\rangle\,|SM\rangle\right\} \qquad (6.7)$$

where $|\phi_{1s}\rangle, |\phi'_{1s}\rangle$ is a pair of orbitals localized on Li representing the $1s^2$ core of the atom and $|\phi_{H_a}\rangle, |\phi_{H_b}\rangle$ is a pair of atomic orbitals localized on the hydrogen atoms (Fig.(6.4)). Thus, we see that the ground state of the system naively describes the physical configuration $LiH^+ + H$ with the positive charge localized on the Li atom.

Figure 6.4: Contour plot of the (valence) Spin Coupled ground-state orbitals on the molecular plane. Distances are in atomic units.

In order to optimize reference Spin Coupled wavefunctions for the first excited state, we tried different orthogonalization schemes and, for the geometries considered, we obtained very good results by using only one excited reference configuration. The best scheme turned out to be the $[N:1]$ scheme, i.e. that in which four excited orbitals are maintained orthogonal to one of the ground state orbitals. The best *active orbital* was found to be that with the *highest* orbital energy[5]: this orbital coincides with the $1s(H)$ orbital of the projectile when $R \gtrsim r_e$ and becomes the $1s(H)$ orbital of the target when $R \lesssim r_e$. The Spin Coupled wavefunction of this state therefore has the form

$$|\Phi_1\rangle = A\left\{|\phi_{1s}\rangle \left|\phi'_{1s}\right\rangle |\phi_H\rangle \left|\phi_{2s(Li)}\right\rangle |SM\rangle\right\} \tag{6.8}$$

where $|\phi_{1s}\rangle, \left|\phi'_{1s}\right\rangle$ is the pair of core orbitals of the Li atom, $|\phi_H\rangle$ is the $1s$ orbital centered on the hydrogen atom closest to the Li site and $\left|\phi_{2s(Li)}\right\rangle$ resembles the (distorted) $2s$ orbital of the Li atom in the isolated LiH molecule (Fig. (6.5)). We thus note that, except for the region where $R \lesssim r_e$, this wavefunction describes exactly the physical situation of a proton colliding with the LiH molecule. It is worth to mention at this point that the same qualitative result is obtained by considering the orthogonalization scheme $[1:N]$ in which it is not necessary to choose the active ground state space. This last scheme
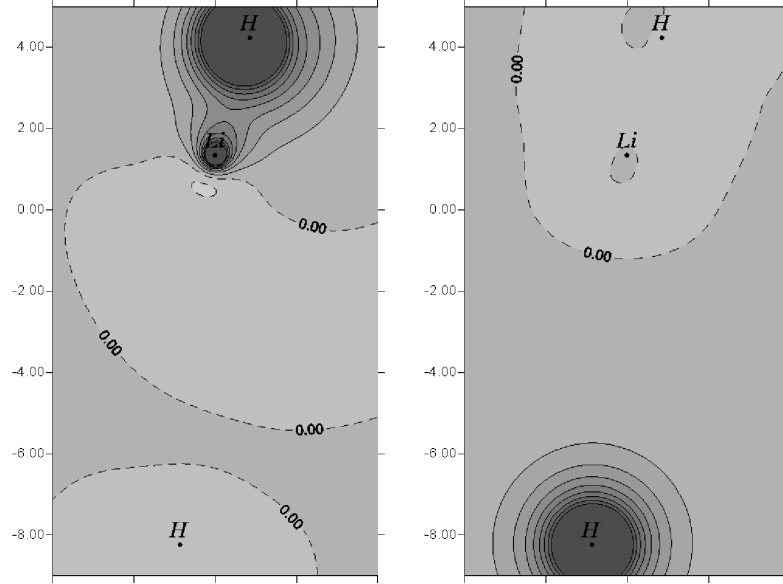
---

[5]The orbital energy was defined in Section (1.5).
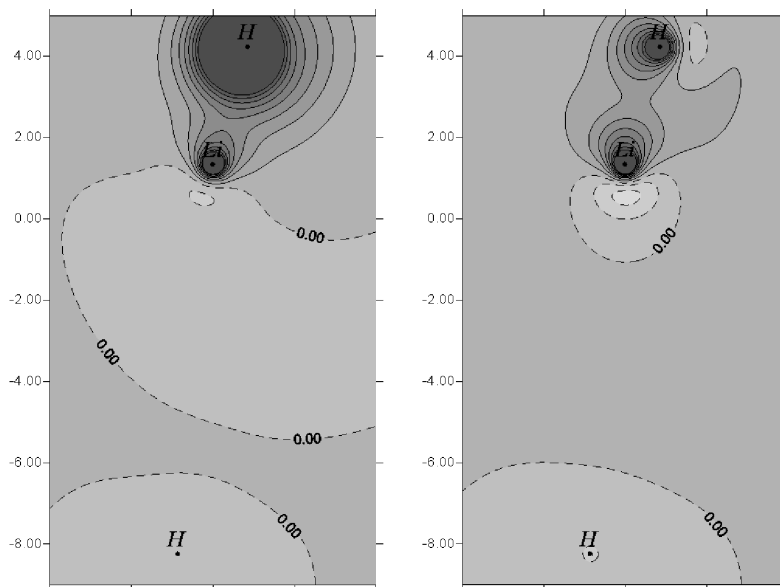
Figure 6.5: Contour plot of the (valence) Spin Coupled excited-state orbitals on the molecular plane. Distances are in atomic units.

is slightly better within a small cone around the target hydrogen atom corresponding to the entrance channel for the reaction $LiH + H^+ \longrightarrow Li + H_2^+$ as it will be discussed in the following Subsection.

We report in Fig.(6.6) the two simple Spin Coupled energy curves for the ground and the first excited states together with the results of Full-CI calculations corresponding to the same basis set. It is evident from this figure that there is a very good qualitative accordance between the two calculations: in particular the irregularity at short range appearing in the Full-CI surface cut is well reproduced in the corresponding Spin Coupled curve. An analysis of the SC wavefunction shows that such point corresponds to the change of character of the highest occupied SC orbital in the active space (from $H(1s)$ centered on the projectile to $H(1s)$ on the target). We therefore can conclude that the irregularity mentioned above, located in a narrow cone around the Li site, is the activation barrier of the exchange reaction $LiH_a + H_b^+ \longrightarrow LiH_b + H_a^+$. It is obvious that a single reference configuration wavefunction is not apt to correctly describe this region of the PES, thus a slightly refined SC Valence Bond wavefunction, that will be described below, was employed for the non-orthogonal CI calculations.

Dynamical correlation contributions to the ground and excited state energies were introduced by optimizing a selected number of virtual orbitals. For
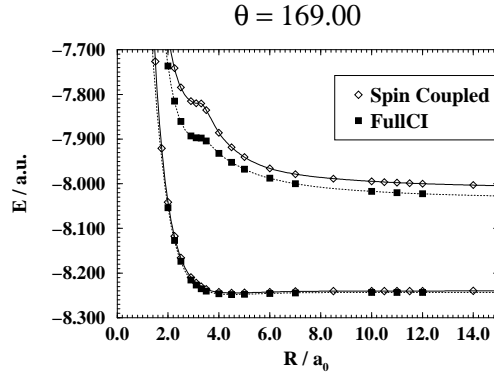
Figure 6.6: Spin-Coupled energy curves for $[LiH - H]^+$ system, with the LiH distance at its equilibrium value. Full-CI calculations corresponding to the same basis set are also reported (filled-in squares).

the ground state, one pair of core virtuals and three pairs of valence virtuals were considered: in the latter case one pair was made up of orbitals of a' symmetry while the other two pairs of a symmetry were forced to take up "x" and "y" character (we call xy the molecular plane). A similar procedure were used to describe the excited states but, in this case, the virtual orbitals were expanded into the orthogonal complement of the active orbital in order to preserve the orthogonality to the Spin Coupled ground state. The final Spin Coupled Valence Bond wavefunction was constructed as a Configuration Interaction between the two reference functions and all the singly and doubly excited configurations of appropriate symmetry, obtained by vertical promotions to the optimal virtuals previously calculated. In order to correctly describe the region of the proton exchange reaction, we used additional configurations obtained by single replacements of the valence orbitals of the SC excited state with the SC orbitals of the ground state. In this way the final SCVB wavefunction was able to describe both the configurations $LiH_a + H_b^+$ and $LiH_b + H_a^+$ representing the interacting states at small R values. By adding a set of ionic configurations, where double occupancy of the orbitals is included, the total number of configurations of the final SCVB wavefunction turned out to be 84, which corresponds to 125 Valence Bond structures, when one includes the spin degrees of freedom.

The results obtained with this wavefunction are shown in Fig. (6.7), where the potential energy surface cuts for some of the orientations of the impinging projectile are compared with the Full-CI data mentioned above. A first perusal shows that the SCVB and the Full-CI PES proceed parallel to one another over all the configuration space sampled by our calculation. In particular, it is worth
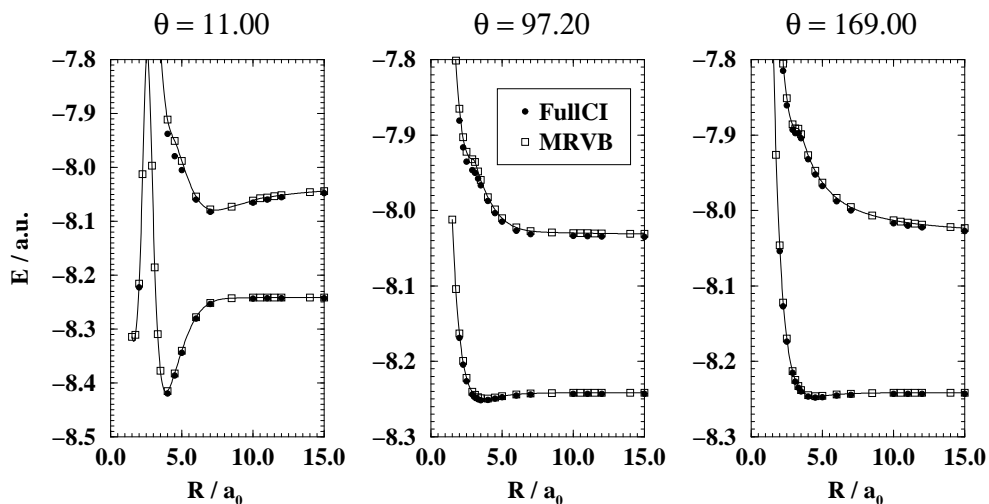
Figure 6.7: Cuts of the MRVB energy surface regarding the ground and the first excited states for $r(LiH) = r_e$ at some values of θ. Full-CI calculations corresponding to the same basis set are also reported (filled-in circles).

noting the good agreement between the two calculations in the charge-exchange region, a feature that suggests our description of the third electronic state (for clarity not reported here) to be a good one in this region. On the whole, the differences between the MRVB and the Full-CI values are of the order of $2.0 \cdot 10^{-3}$ and $4.0 \cdot 10^{-3}$ E_h for the ground state and for the excited state, respectively. It is important to note at this point that, even with the small basis set employed, the Full-CI expansion resulted to be much longer than the MRVB one, involving 1654650 determinants. Therefore, the computational cost of such MRVB calculation is extremely convenient when compared to the Full CI.

6.3.2 The calculations in the reactive region

In order to explore the reactive configurational space, the procedure outlined in the previous Subsection should be slightly refined in order to describe at the same level of accuracy the full Potential Energy Surface along a reactive pathway. Indeed, we found that as the $Li - H$ distance increases and the $H - H$ distance decreases the $[N : 1]$ orthogonalization scheme described above becomes higher in energy than a $[1 : N]$ scheme. In this case, no choice was left for the active space and we obtained at the outstart the Spin-Coupled function

for the reaction products:

$$|\Phi_2\rangle = A\left\{ |\phi_{1s}\rangle \left|\phi'_{1s}\right\rangle |\phi_{2s(Li)}\rangle \left|\phi_{\sigma_g(H_2^+)}\right\rangle |SM\rangle \right\} \tag{6.9}$$

in which the $\left|\phi_{2s(Li)}\right\rangle$ orbital came from the orthogonality constraint with the ground-state function (6.7) and the $\left|\phi_{\sigma_g(H_2^+)}\right\rangle$ orbital was the novel product of the optimization procedure. Therefore, in the present system we added at the MRVB wavefunction described above one more reference function and a set of 4 pairs of virtuals to correctly sample the reactive configurational space. Moreover, we decided to consider full (vertical) excitation of the occupied orbitals into the virtual ones. In this way the total number of configuration used was 321, corresponding to 617 structures when the spin degree of freedom are taken into account. The same basis-set described above has been employed here.

In Fig.(6.8) a collinear $Li\,\overset{r_1}{-}H\,\overset{r_2}{-}H$ sample calculation along a reactive path is compared with FullCI calculations. In the left panel the energy of the three references (6.7,6.8,6.9) has been reported to show the role of the different SC functions in the various configurational subspace. In the right panel, for the same path, the MRVB results are compared with the Full-CI one. We see that, with the previously described refinements of the subreactive wavefunction, the MRVB function is accurate over the full configurational space.

A detailed description of the collinear PESs and a preliminary analysis of the full dimensional PESs will be given in Sections (7.2,7.3).

6.4 The $C\,^2\Sigma^+$ state of the *BeH* system

The $C^2\Sigma^+$ state of the *BeH* system is the first excited state of $^2\Sigma$ symmetry of the molecule and is well known (Herzberg, 1950) to arise from an avoided crossing between the diabatic highly repulsive ground state $Be(1s^2 2s^2;^1 S) + H(1s;^2 S)$ and the bonding excited state $Be(1s^2 2s2p;^3 P) + H(1s;^2 S)$. The presence of near-degeneracy effects of the atomic *Be* renders the actual description of the system more complicated. Such effects arise, schematically, from the interaction between the $Be(1s^2 2s^2;^1 S)$ and the $Be(1s^2 2p^2;^1 S)$ states so as to require for the *BeH* molecule a minimal set of configurations of the form

$$\left\{ 1s_{Be}^2 2s_{Be}^2 1s_H \right\} + \lambda \sum_{i=x,y,z} \left\{ 1s_{Be}^2 2p_{Be,i}^2 1s_H \right\} \tag{6.10}$$

The SC wavefunction of the ground state mimics this description with the configuration

$$\left\{ 1s_{Be}^2 \sigma_{Be}^- \sigma_{Be}^+ 1s_H \right\}$$
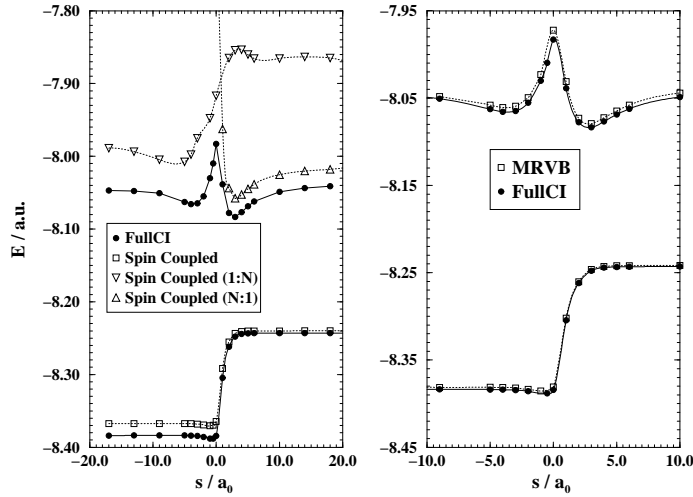
Figure 6.8: Comparison between VB and Full-CI results along a rectilinear reactive path. In abscissa the path is defined by ($r_1 = r_{LiH}^e$, $s = r_2$) for positive s and ($s = r_1$, $r_2 = r_{H_2^+}^e$) for negative s. SC energy curves are reported in the left panel and MRVB results in the right one. Energies and distances are given in a.u..

where $\sigma^{\pm} \approx 2s_{Be} \pm \mu \, 2p_{Be,z}$ take into account the term $i = z$ in eq. (6.10). As already described by Gerrat and Raimondi (1980), this configuration is appropriate for all the interatomic distances r, changing abruptly its spin counterpart around $r = 5.0 \, a_0$. Indeed the Spin Coupled wavefunction possesses a configuration which is suitable for both the ground state and the excited $C^2\Sigma^+$ state: when r is greater than $5.0 \, a_0$, the orbitals $\{\sigma^+, \sigma^-\}$ are paired to give a singlet or a triplet (in the ground state and in the excited states respectively) which couples with the spin of the remaining valence orbitals to give the two resultant doublet states; conversely, when r is smaller than $5.0 \, a_0$ the same spin-coupling competes to the orbital pairs $\{\sigma^+, 1s_H\}$. For such system the lowest energy orthogonalization scheme turned out to be $[1 : N]$, i.e. the case in which one orbital is expanded in the orthogonal complement of the ground state orbitals, and led in a natural way to the configuration

$$\left\{ 1s_{Be}^2 2s_{Be} \pi_{Be} 1s_H \right\}$$

apt to describe the $A^2\Pi$. The lowest energy Σ reference configuration obtained is optimal for the $^4\Sigma$ state dissociating to $Be(1s^2 2s 3s;^3 S) + H(1s;^2 S)$ which actually turned out to properly describe the higher states of Σ symmetry, a feature which however remains beyond the scope of the present work. In this case, therefore, the presence of molecular symmetry forced us to symmetry-
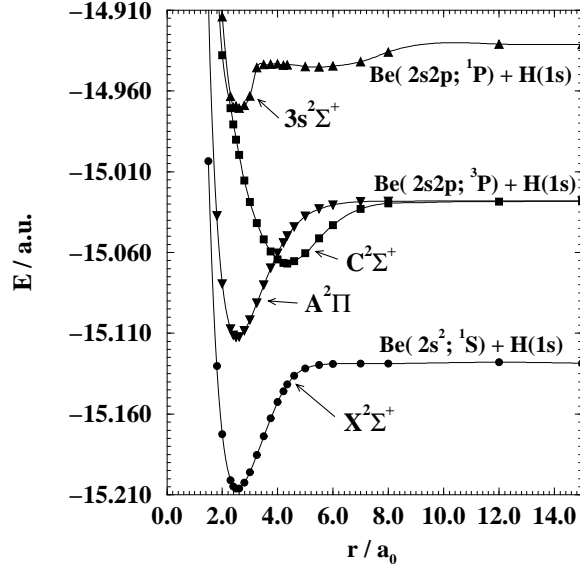
Figure 6.9: MRVB energy potential curves for low-lying states of the *BeH* system. The filled-in circles show the computed points . All energy and distance values are in a.u..

adapt the final reference configuration. This could be easily achieved by single replacements of the π orbital of the $A^2\Pi$ state with ground-state valence orbitals by a strategy similar to that used in the case described in the previous Section for the region of the proton exchange. Indeed the pair of configurations

$$\left\{ 1s^2_{Be}\sigma^+_{Be}2s_{Be}1s_H \right\}, \left\{ 1s^2_{Be}\sigma^-_{Be}2s_{Be}1s_H \right\}$$

correctly describes the state under investigation, both in the bonding (combination with the minus sign) and in the repulsive (combination with the plus sign) regions. Therefore, the appropriate multireference Σ-VB wavefunction was built via the resulting four-configuration reference space, while the virtuals were optimized with the two X, A Spin Coupled reference functions. The use for the Σ manifolds of the orbitals optimized for the Π state is justified by the similarity in energy and character of the $A^2\Pi$ and $C^2\Sigma^+$ states, both arising from the $Be(1s^2 2s2p;^3 P)$ state of atomic Be; this assumption fails in the proximity of the equilibrium geometry of the $A^2\Pi$ state, where the optimized virtual orbitals resulted to be specific for this state and seemed not to be optimal for the repulsive region of the $C^2\Sigma^+$ state.

In practice, the virtuals were optimized for each pair of valence electrons of the ground $X^2\Sigma^+$ and excited $A^2\Pi$ states. For each pair of the ground state

electrons, orbitals of symmetry s, p_x, d_{xy} were optimized; by proper rotation, the latter were transformed to p_y, $d_{x^2-y^2}$ symmetry. By considering vertical single and double excitations of the appropriate symmetry and some ionic configurations, the multireference VB wavefunction of $^2\Sigma^+$ symmetry included 236 configurations. A single reference VB wavefunction consisting of 223 configurations (for one of the basis functions belonging to a single component of the Π irreducible representation), was adopted for the $A^2\Pi$ state. To remove asymptotic discrepancies between $C^2\Sigma^+$ and $A^2\Pi$ functions, a Spin Coupled Σ^+ configuration optimized within the $S = 3/2$ manifold and properly dissociating to $Be(1s^2 2s 2p;^3 P) + H(1s;^2 S)$ was added. This total wavefunction contained 388/380 structures for the Σ^+ and $^2\Pi$ symmetries respectively if the core orbitals were paired and 928/917 if the full spin space of five electrons was considered. There were no quantitative differences between the two approaches at all the internuclear distances examined. The basis set is the same as that employed by P.S.Bagus et al. (1973), D.L.Cooper (1984) and C.Henriet et al. (1986), in which the STO were replaced by STO-6G functions.

The potential energy curves obtained for the $X^2\Sigma^+$, $C^2\Sigma^+$ and $A^2\Pi$ states are reported in Fig.(6.9); the higher energy states ($B^2\Pi$, $3\Sigma^+$, $4\Sigma^+$), not reported here, are in good qualitative accordance with the calculations of C.Henriet et al. (1986), I.D.Petsalakis et al. (1992) and F.B.C.Machado et al. (1998), the quantitative discrepancies being due to our description of these states at a more approximate level, i.e. without inclusion of proper SC reference configurations and virtual orbitals specifically optimized to describe such states. From the asymptotic energy values the $Be(^3P \leftarrow^1 S)$ term turns out to be 2.726 eV, to be compared with the experimental value of 2.725 eV. The resulting well depths for the $X^2\Sigma^+$,$C^2\Sigma^+$ and $A^2\Pi$ states are 2.112(2.161) eV, 1.046(1.048) eV and 2.295(2.400) eV respectively, where the experimental values are quoted in brackets. These results for the $X^2\Sigma^+$ and $A^2\Pi$ states are undoubtedly of lower quality with respect to today *state-of-the-art* results, but a complete investigation of such states in their equilibrium regions does not concern the present analysis: we mention only the fact that the correct description of the $C^2\Sigma^+$ state eliminates the previously observed small hump in the $X^2\Sigma^+$ one (Gerratt and Raimondi, 1980), in agreement with MO-CI calculations (Bagus and Moser, 1973; Cooper, 1984; Henriet and Verhagen, 1986; Larsson, 1984; Larsson, 1985). An optimal description is reached for the $C^2\Sigma^+$ state in the minimum region. This is confirmed by the above mentioned dissociation energy value and by the values of the equilibrium distance $r_e = 2.295(2.301)$ Å and of the first ($J = 0$) vibrational term $\Delta G_{1/2} = 1004(997)\,cm^{-1}$, the last obtained by numerical Numerov integration of the radial Schroedinger equation. To the best of our knowledge, only D.L.Cooper (1984) has reached a comparable accuracy regarding this state by means of valence electron Full-CI

calculations. As expected, in the repulsive region there is a little evidence of the avoided crossing with the $3s\Sigma^+$ Rydberg state, probably due to our choice of the virtual space.

Chapter 7

The interaction forces

In this Chapter we will summarize the most important results that we have extracted from our *ab-initio* calculations of the electronic structure of the title system. We will analyze the details of the interaction potential of the LiH_2^+ system in the view of establishing a connection with the dynamic processes analyzed in Chapter 5. We shall follow a chronological approach, analyzing first the sub-reactive surface and then the reactive ones. Finally we will summarize some important conclusions that can be drawn by only looking at the energy landscape outlined.

Through the following, when discussing reactive paths, we will take the convention that LiH/LiH^+ are the reactants of the processes unless otherwise stated.

7.1 The sub-reactive surfaces

In this Section we consider the first of the potential energy surface that we produced at the very early stage of our work. At that time the main objective was to obtain the interaction potential that acts between the LiH moiety and a colliding proton. The idea was to use it in a *non*-reactive dynamical calculation in order to help to estabilish the possibility of producing detectable rovibrationally excited LiH molecules (Maoli et al., 1994). We were interested in the collisional heating/cooling efficiency of LiH since we recognized that the strong, long-range interaction acting between the dipolar molecule and the charged projectile would result in cross-sections much larger than others previously computed in our group (Gianturco et al., 1997a; Bodo et al., 2000). Thus, the study was limited to the *sub*-reactive configurational space, i.e. we considered the orientational dependence of the interaction for a few number of geometries of the target molecule chosen to be close to the equilibrium one.

Only after this study we realized that a fuller understanding of the system was necessary and therefore we moved first to the collinear reactive geometries and then to the full dimensional evaluation of the PESs of the system.

The Jacobi coordinates that we employed for the construction of the subreactive surface is shown in Fig.(6.3) and the details of the MRVB calculations are given in Subsection (6.3.1). We generated the surface on a dense numerical grid whose range in these Jacobi coordinates is as follows: the distance between the center of mass of the molecule and the projectile, R, varies between $1.75\,a_0$ and $15.0\,a_0$ for a total of 21 points on an slightly irregular grid; r, the internuclear separation in the LiH molecule varies from $2.3\,a_0$ to $4.3\,a_0$ in five points chosen to be inside the range determined by the two turning points of the $\nu = 4$ vibrational level of LiH; finally θ, which is the angle between R and r, ranges from $11°$ to $169°$ in twelve points corresponding to the abscissas of the Gauss-Legendre quadrature. Although the computed grid of points is apt to describe better the excited state correlating with the asymptotic fragments $LiH + H^+$, we can also extract some information on the behavior of the ground state that leads to the fragmentation into $LiH^+ + H$ (the r_{eq} value for the LiH molecule is $3.014\,a_0$ while the value for the LiH^+ is $4.101\,a_0$).

In the following we first look at the orientational anistropy that, roughly speaking, controls the efficiency of the rotational energy transfer and subsequently we consider the vibrational dependence of the interaction.

7.1.1   The rotational coupling

When we keep the internuclear distance of the target at a fixed value we recover the behavior for a rigid-rotor potential (RR) energy surface that shows the coupling between the R and the θ coordinates. When the internuclear distance is fixed at the equilibrium value of the target the RR potential is, in many cases, a rough approximation to a (ground-state) vibrationally adiabatic potential; thus it can help to understand the low-energy dynamical processes that proceeds with a vibrationally adiabatic dynamics (Gianturco, 1979). We briefly consider here the Rigid Rotor potentials of the two target (LiH/LiH^+).

An overall view of the first two electronic states for $r = r_{eq}(LiH)$ in cilindrical coordinates is shown in Fig.(7.1) where we can see that the two states are well separated by a $\sim 5\,eV$ energy gap. Thus, the asymptotic energy gap noted in Section (5.4) (see in particular Fig.(5.3)) is not substantially altered by the interaction, at least in the configurational space spanned by the present calculations. The importance of this large energy gap between the two PESs will be considered later in connection with the possibility of a charge-transfer reaction.

The Rigid Rotor excited surface is markedly determined by the dipole-
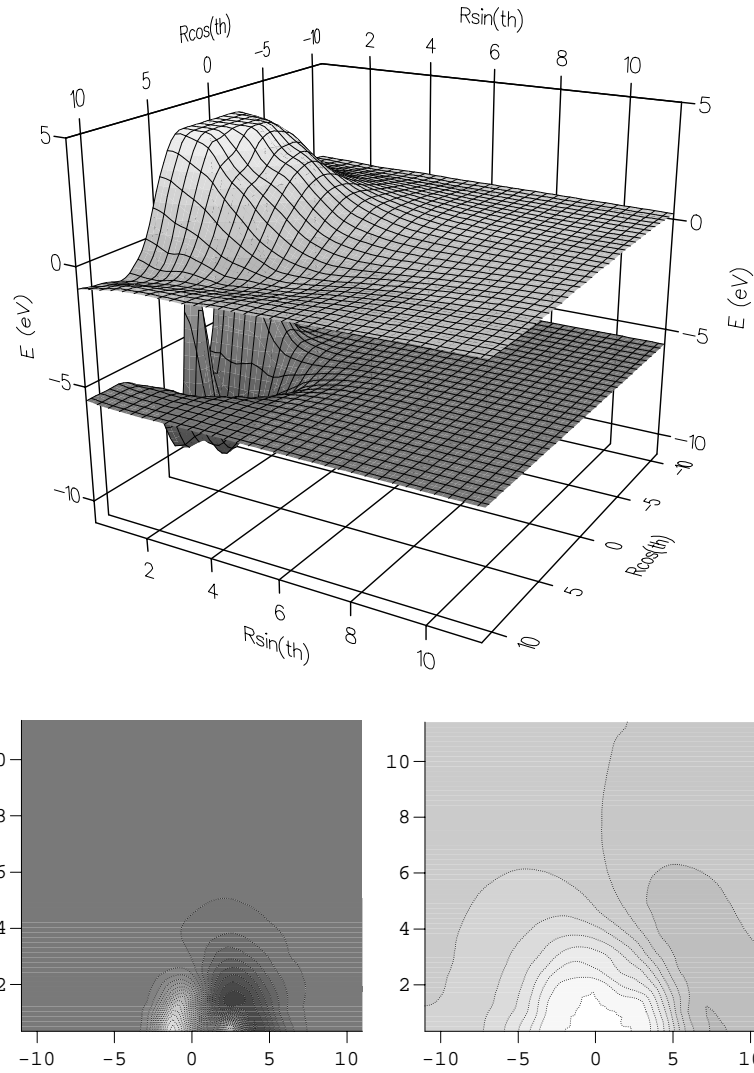
Figure 7.1: Three dimensional view of the two surfaces as a function of cylindrical coordinates where $x = R sin\theta$ and $y = R cos\theta$. The internuclear distance r is that of LiH at its equilibrium geometry. In lower panels contour plots of the two surfaces are displayed.

charge electrostatic interaction (see lower right panel of Fig.(7.1)). This is best seen in Fig.(7.2), where we report the coupling potential as a function of the
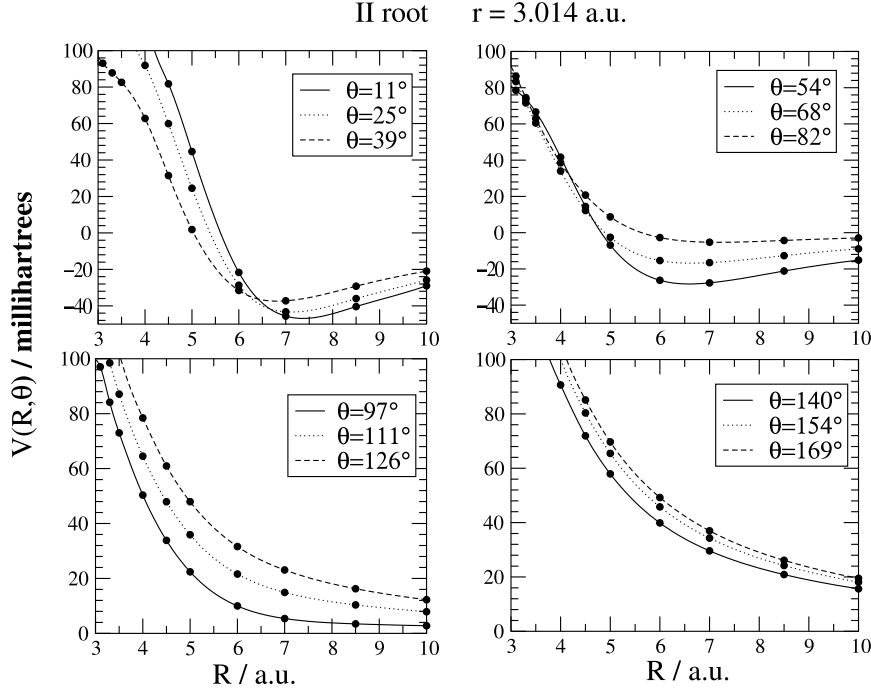
Figure 7.2: Behavior of the *interaction* potential in the excited electronic state as a function of the two coordinate θ and R. The internuclear distance r is that of LiH at its equilibrium geometry hence kept fixed at $3.014\,a_0$.

main radial coordinate for different values of the orientational angle. We see that the most stable structures occur in the small angle region of the upper left panel, while beyond $\theta \sim \frac{\pi}{2}$ the interaction becomes essentially repulsive as it is driven by the dominant dipole-charge interaction proportional to $P_1(cos\theta)R^{-2}$. It therefore follows that the corresponding anisotropy is rather marked and extends over the whole angular region examined by the calculations. The minimum structure, expected for the linear configuration, turns out to be quite deep: from the graph we obtain $\sim 46\,mE_h$, that is $\sim 1.25\ eV$ which is about half the dissociation energy of the target molecule, $D_e(LiH) \sim 2.5\ eV$.

The corresponding Rigid Rotor potential for the ground electronic state is presented in Fig.(7.3) where now the r value is fixed at $4.3\,a_0$, which is closer than the previous one to the equilibrium value of the LiH^+ fragment. We note that the well in the small angular cone located around the target hydrogen is
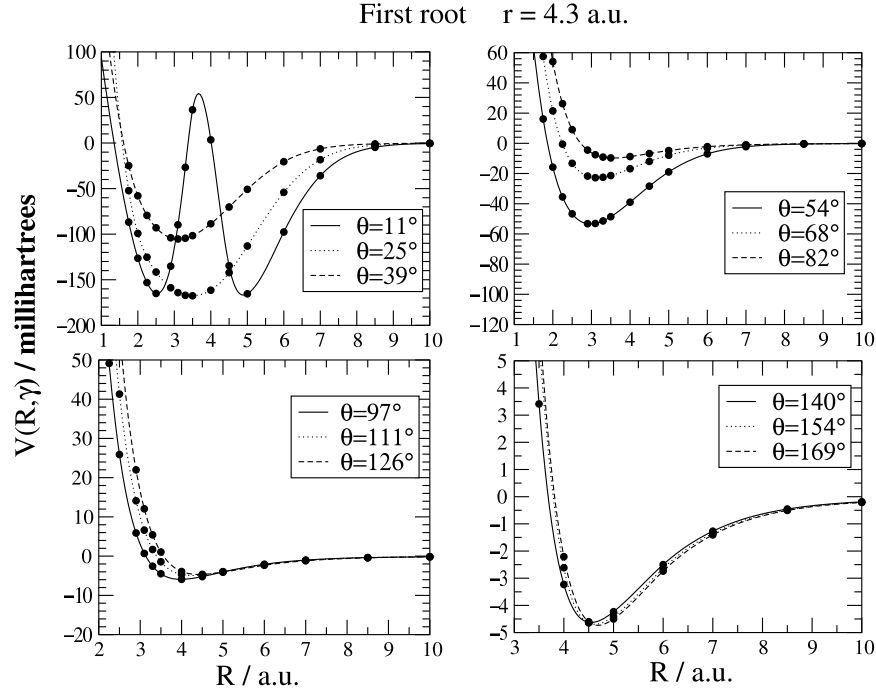
Figure 7.3: Same calculations as in Fig.(7.2) but for the lower surface and for $r = 4.30\,a_0$.

very deep and narrow (upper panels)[1]: the minimum is $\sim 4.6\ eV$ below the asymptote, a value that compares favorabouly with the formation of an H_2 molecule ($D_e \sim 4.7\ eV$) when one takes into account the low binding energy of LiH^+ ($D_e \sim 0.1\ eV$). The $H - H$ distance at the minimum turns out to be very close to that of the isolated hydrogen molecule and thus, taking also into account the nature of the wavefunction (see Section (6.3.1)), we may argue that this is the entrance channel for the reaction $LiH^+ + H \rightarrow Li^+ + H_2$. On the other hand, in the Lithium cone the shape and strength of the interaction is rather different: the surface is almost flat, with a residual weak well of ~ 0.1 eV on the Lithium side at a $Li - H$ distance of about $4.5\,a_0$ (to be compared with the structure of LiH^+). A somewhat similar situation has been recently found in the corresponding neutral system, LiH_2 (Bodo et al., 2001).

---

[1]Note that the cusp in the upper left panel is due to the $H - H$ repulsive interaction. This is amplified by the lightness of the H atom which places the center of mass of the target very close to the Lithium atom.

7.1.2   The vibrational dependence

The full PES discussed here also includes the explicit dependence of the interaction on the internuclear distances of the *LiH* molecule. It is the effect of the change of r which explicitly gives us the vibrational coupling produced within each surface. A pictorial example of such quantity is given by the results reported in the four panels of Fig.(7.4) where we can note the following:
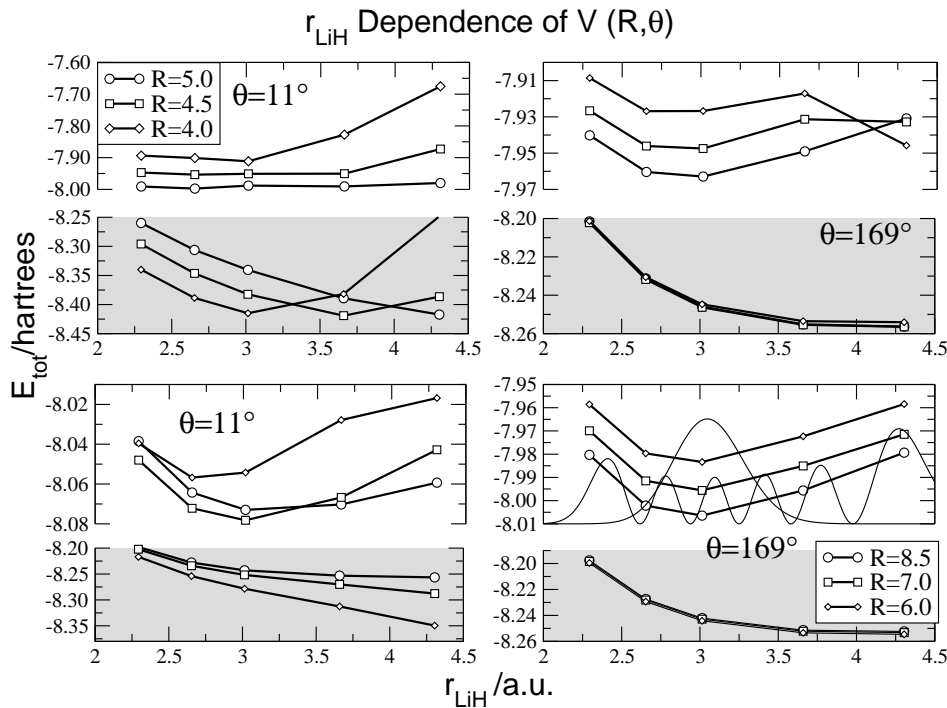
Figure 7.4: Computed vibrational dependence of the two PES's as a function of relative distances R and for two different relative orientations: $\theta = 11°$ (left panels) and $\theta = 169°$ (right panels). Each couple of panel refers to different values of the distance R (lower in the upper panels and higher in the lower ones) and in each couple of panel the upper plot represent the excited state and the lower one the ground state (in gray).

1. Both the surfaces attain their asymptotic behaviour in a rather short range region, i.e. as the distance between the projectile atom and the molecule increase, the dependence of the *intermolecular* potential on the molecular stretching motion becomes weaker. This indicates, as

often noted (Gianturco, 1979), the chiefly short-ranged nature of the vibrational-to-translational (V-T) coupling terms;

2. The asymptotic behaviour is reached faster on the Lithium side of the target. This a sort of "light atom effect" due to the fact that the center of mass of the molecular target is very close to the heavy Li atom. In other words, the stretching of the internuclear distance moves outward the H atom much more than the Li one.

3. The upper PES shows a V-T coupling that remains stronger as the angle varies and that it is also non-negligible at the larger distances (displayed in the lower panels). The charge-dipole interaction obviously plays here a dominant role in creating a more marked V-T coupling;

4. In the lower right panel, we have also shown the $n = 0$ and $n = 5$ vibrational wave functions of the isolated LiH molecule. For distances of the order of $8.0\,a_0$, and for the $\theta = 169°$, we see that we can almost neglect the coupling coming from the residual interaction between the LiH molecule and the proton. The monotonic long range electrostatic interaction simply causes our calculated potential to be an intermolecular LiH potential shifted by the charge-dipole contribution, which is only weakly affected by the vibrational motion. This is not true for the $\theta = 11°$ orientation for which a much more pronounced effect is observed (see Section (7.2)).

What the calculations, therefore, indicate is the existence of rather marked couplings between R and r over the range of the examined coordinates and thus the presence of an overall interaction which should produce dynamical outcomes with sizable flux going into rovibrationally excited molecular states. To make a more precise connection with the dynamics in the $LiH + H^+$ system we consider here in detail the vibrational coupling matrix elements, i.e. the terms

$$V^{nn'}(R, \theta) = \int_0^\infty dr\, \chi_n^*(r) V(r, R, \theta) \chi_{n'}(r) \tag{7.1}$$

(where the χ's are the vibrational eigenfunctions of the target molecule) which enter in the Close-Coupling equations in the usual multipolar expanded form

$$V^{nn'}(R, \theta) = \sum_\lambda V_\lambda^{nn'}(R) P_\lambda(cos\theta)$$

(see Section (4.4)). Since for a long-range potential like the one we are employing here, the true asymptotic values are never reached by the *ab-initio*

calculation, we used a linear square fitting to get the correct asymptotic limit. We adopted the following analytic form of the interaction at long range

$$V(r, R, \theta) = V_\infty(r) + \frac{\alpha_0(r)}{2R^4} P_0(cos\theta) +$$
$$+ \frac{D(r)}{R^2} P_1(cos\theta) + \left(\frac{Q(R)}{2R^3} + \frac{\alpha_2(r)}{2R^4} \right) P_2(cos\theta)$$

in which V_∞, α_0, α_2, D and Q are respectively the energy, the spherical and anisotropic polarizability, the dipole and the quadrupole moments of the molecule. All these terms were determined by a linear square fitting of the outer three R points of the computed *ab-initio* potential for each value of θ and r. We report in Fig.(7.5) the behavior of the above quantities as a function of r when compared against experimental values in the ground vibrational state taken from M. Rerat (1992). In particular the asymptotic value of the potential $V_\infty(r)$ has been compared to the diatomic potential of an isolated LiH which has been calculated with a full-CI calculation with the same basis set as that employed for our calculations.

Once we have obtained a complete representation of the interaction potential in all the configurational space spanned by θ and R, we still lacked an equally good description of the potential dependence upon the LiH internuclear distance r. To obtain a reliable representation also in the r coordinate we used an extrapolation procedure already adopted in the corresponding neutral system[2] (Bodo et al., 2001). Briefly, we recognized that the interaction potential

$$V_{LiH-H^+}(r, R, \theta) = V(r, R, \Theta) - V_{LiH}(r)$$

in the limit $r = 0$ reduces to the simple "united-atom" diatomic curve

$$V_{LiH-H^+}(0, R, \theta) = V_{BeH^+}(R)$$

and therefore we added one more point in the r coordinate by computing the BeH^+ curve. This point has been used in a spline interpolation, which was subsequently joined to a long-range (in r) multipolar expansion of the type

$$\frac{A(R, \theta)}{r^p} + \frac{B(R, \theta)}{r^q}$$

where the exponents p, q were determined by the long-range behaviour of the interactions (i.e. the $H - H^+$ and the $Li - H^+$ interactions, for which we

---

[2]Today such extrapolation is no longer necessary since the full dimensional PES is now available (see Section (7.3)). However, it turned out useful for the preliminary analysis of Chapter 10.
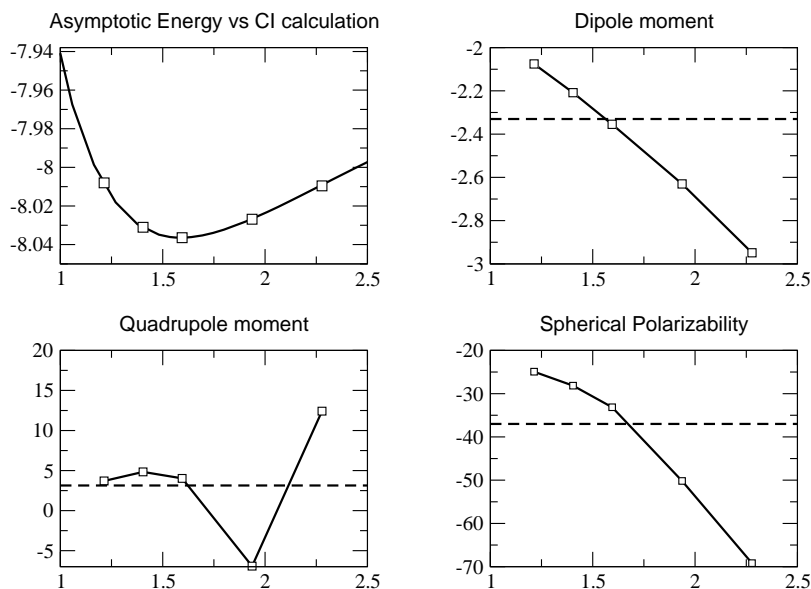
Figure 7.5: Fitted values of the multipoles of *LiH* compared with experimental data (dotted lines). In the upper -left panel the asymptotic potential is compared with a CI calculation of isolated *LiH* (solid line). Distances are in Å and other quantities in atomic units. The FullCI curve of the upper left panel has been energy shift by about $4\,mE_h$.

chose $p = 4$ and $q = 6$) and the coefficients A, B were determined by ensuring a smooth joining with the spline of the inner region. Some of the *ab-initio* points with the extrapolated potential are shown in Fig.(7.6), where we also reported the vibrational wavefunction for $n = 15$ to give an idea of the extension of the integrals (7.1) to be performed[3].

The coupling elements are reported in Fig.(7.7) in cylindrical coordinates centered on the *LiH* center of mass. The vibrational couplings converge rapidly toward small values with increasing the difference in the vibrational quantum numbers: while the V^{00} is identical to the rigid-rotor potential the off-diagonal couplings V^{01}, V^{02} and V^{03} are orders of magnitude smaller. The vibrational couplings are on average rather short ranged meaning that a certain degree

---

[3]As we will see in Chapter 10 we *need* such high vibrational levels since, as already noted, the depth of the interaction well is about one half the D_e of the target molecule.
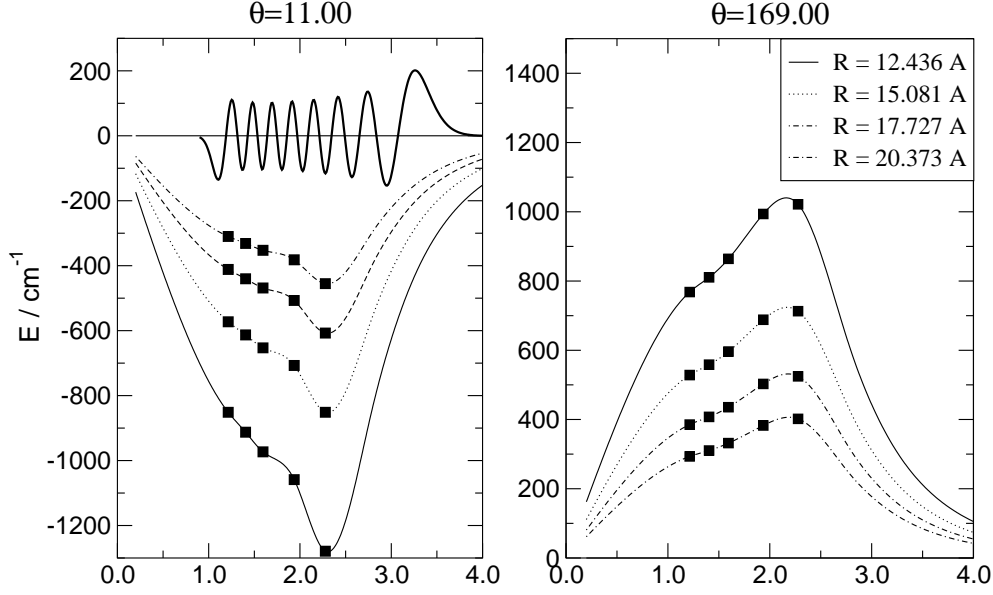
Figure 7.6: The r extrapolation. The dependence of the interaction is shown for two values of the jacobi angle and several value of the scattering coordinate. Distances are in Å.

of vibrational coupling exists only in or near the well region of the potential. A closer examination of the $V_\lambda^{nn'}$ terms of the coupling potential suggests, instead, that the long range coupling is quite substantial and mainly due to the $V_{\lambda=1}^{nn'}$ term that, in fact, turns out to be the dominant among the others for each value of n and n'. As it can be seen from Fig.(7.8), the $\lambda = 1$ term is the largest both in inner region of the well and in the asymptotic one where the potential reduces to the contribution

$$V^{nn'}(\theta, R) \sim V_1^{nn'}(R)\, P_1(cos\theta) \sim \frac{D_{nn'}}{R^2} P_1(cos\theta) \text{ for } R \to \infty$$

where the off-diagonal coupling is proportional to the (vibrational) dipole transition moment

$$D_{nn'} = \int_0^\infty dr \chi_n^*(r) D(r) \chi_{n'}(r)$$

The presence of such large term in the expansion of the potential makes the rotational coupling very large; since it couples directly the Δl, $\Delta j = |\lambda| = 1$
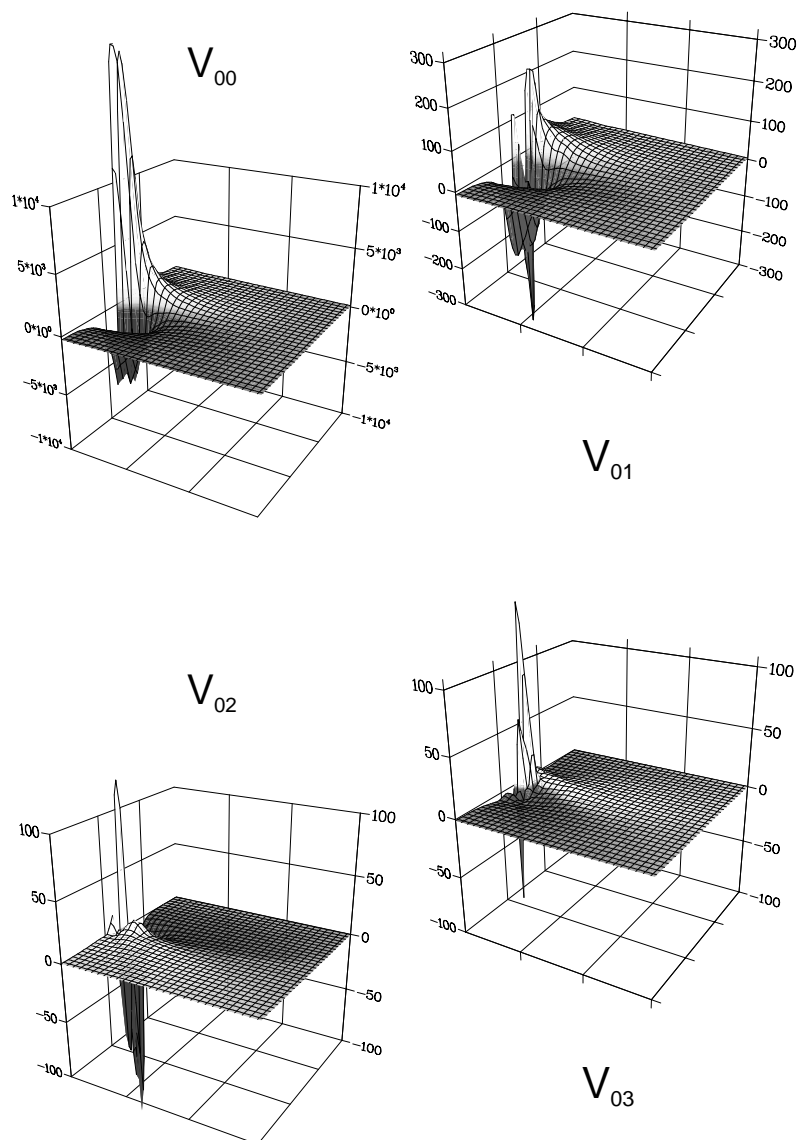
Figure 7.7: Coupling elements for the lowest vibrational levels in cylindrical coordinate centered around *LiH* center of mass.

transitions we expect an evident effect on the $\Delta j = \pm 1$ transitions. The actual situation is somewhat more complicated (see Chapter 10).
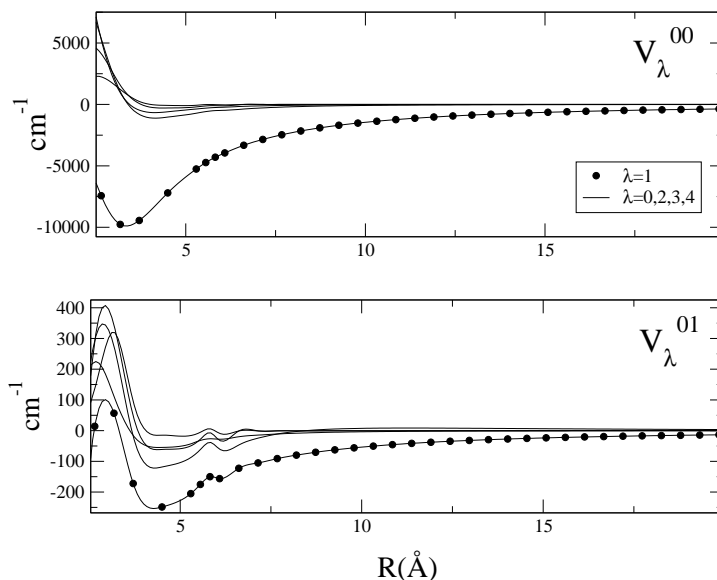
Figure 7.8: V_λ's as a function of R for the lowest adiabatic potential coupling elements.

7.1.3 The charge transfer reaction

We have mentioned in Section (5.4) that the difference between the LiH and H ionization potentials (respectively 7.9 eV and 13.6 eV) causes a large energy gap between the two lowest-lying electronic states; we have seen (see for example Fig.(7.1)) that, at least in the subreactive space spanned by the calculation described in this Section, the two PESs remain well separated also in the interaction region. As a consequence of these features and of the electronic nature of the system (Section (6.3.1)), we therefore expect that the behavior of the electronic densities in the two adiabatic roots is quite different.

A pictorial view of such differences is given in Fig.(7.9) , where we report the variation of the Mulliken charge populations on the three atomic centers as a function of orientation and of the relative atom-molecule distance R. The internuclear coordinate has been kept fixed at the equilibrium value of LiH in order to simplify the presentation. We only report in the figure two of the orientations we have examined since the behavior of the Mulliken populations changes rather smoothly across the angular range.

When looking at the ground electronic state (two lower panels) we see that the system is qualitatively well described, in both orientations, by the conven-
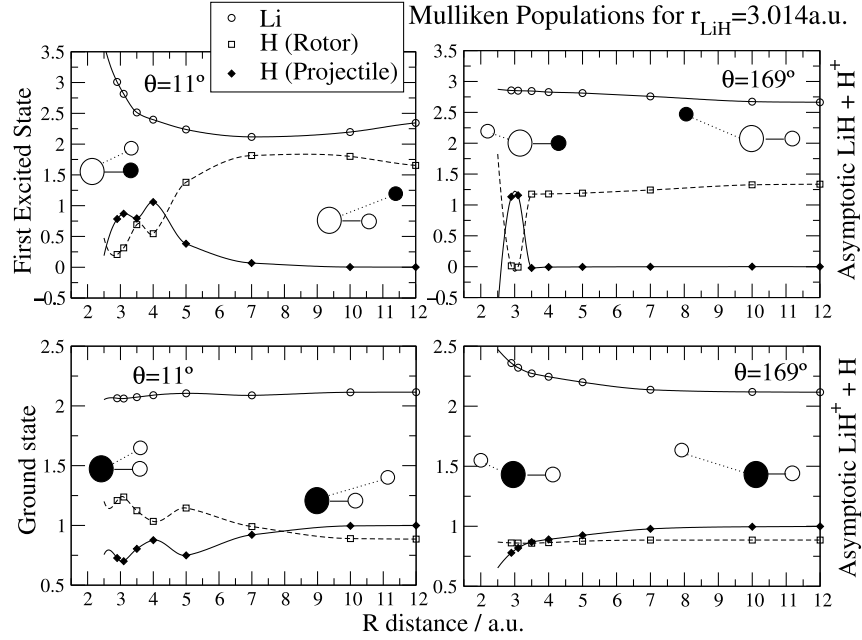
Figure 7.9: Computed Mulliken populations (negative charges) as a function of R and for two orientations ($\Theta = 11°$, $169°$). The two lower panels refer to the first root while the upper ones to the second root. The r value was chosen to be that of LiH at its equilibrium geometry. The black circles in the triatomic schemes are indicating the atoms on which most of the positive charge is localized. Energies are in cm^{-1}.

tional formula $Li^+ \cdots H_2$, where the charge is located on the lithium atom over the whole range of relative distances. Therefore the small angle region closer to the expected C_{2v} geometry of the ground state of the $[LiH_2]^+$ complex shows an arrangement of charges that corresponds to a sort of $Li^+ \cdots H_2$ situation. The behavior of the excited state is quite different and is shown in the upper panels of Fig.(7.9); one sees there more clearly the effects of electronic distortion during the approach of the proton. In the small-angle region the system undergoes a marked and rapid charge variation as one of the H atom is added to the complex: thus while in the asymptotic region the arrangement corresponds to that of a proton and a neutral LiH molecule, during the collision the positive charge is transferred to the H atom previously belonging to the LiH molecule. In the large-angle region the charge exchange between the two H atoms is more clear and takes place in a small range of R values, while the lithium atom remains nearly neutral. In this latter case one can think of a flow of electronic charge between the two H atoms via a sort of *through-bond*

charge migration. Between 2.5 and $3.5\,a_0$, in fact, the two hydrogen atoms exchange one unit of charge and reach fairly rapidly a situation where H^+ is removed from a neutral LiH system. This situation is the direct consequence of a strong non-adiabatic interaction with the *third* electronic state and it is the cause of the observed *bumps* in the high energy region of the $LiH - H^+$ potential when the proton approaches the target on the Lithium side (see right panel in Fig.(6.7); the bump, either a conical intersection or an avoided cross-ing, is located at $\sim 3\ eV$ above the asymptotic $LiH + H^+$ limit)[4] . As we shall see better in the following Section, the third root of the system correlates *asymptotically* with an excited state of LiH in the presence of a proton charge, when the internuclear distance in the LiH moiety remains close to the equilib-rium one; however when r is increased the second excited state changes nature and becomes essentially an excited state of LiH^+ (in the presence of a neutral hydrogen atom) in which the positive charge is localized on the *hydrogen side.* Thus, we can argue that in the interaction region this *diabatic* state interacts strongly with the *diabatic* $LiH + H^+$ state that characterizes the interaction potential here described in almost the whole range of coordinates examined.

The above analysis and in particular the fact that Li is not exchanging charge, shows that the chemical reaction leading to a charge-transfer process between the ground state of LiH^+ and LiH is prevented by the large energy gap separating the two surfaces at least for intra-molecular distances close to the near-equilibrium geometry of the molecular partners. In conclusion, this qualitative analysis, although still preliminary, can lead us to say that the charge-transfer process

$$LiH^+ + H \rightleftharpoons LiH + H^+$$
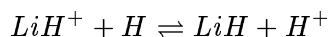
is not likely to be effective during the dynamics of LiH_2^+. We will turn back to these consideration in Section (7.4). We note, here, that the strong interactions that we have seen in this Section can be hardly discussed whitout proper consideration of the reactive configurational space. Therefore, we now move to the simple *reactive* collinear situation.

7.2   The collinear reactive surfaces

We will consider here the reactive potential energy surfaces for the system by looking at the collinear geometry of the partners relative approach. In particular, we will focus attention on the *Li-H-H* geometry which seems the most favorable for the reactions to occur. Although a full 3D surface for the

---

[4]It is worth to note that the bump is much more pronounced when the LiH molecule is streched.

reactive interaction is now completed, we will show below that the analysis of the collinear situation is already capable of providing us with a lot of insights into the microscopic aspects of the relevant reactions.

Ground and first excited state
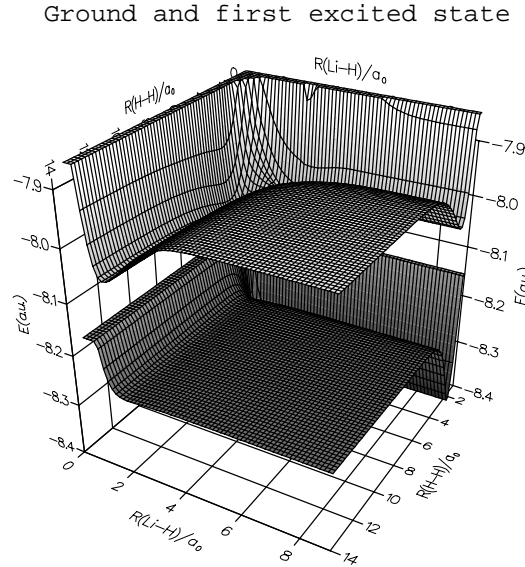
Figure 7.10: First and second roots in three dimensions as a function of $R(Li-H)$ and $R(H-H)$. The points are obtained from the analytical fitting of the *ab-initio* values (see text).

From the analysis of the previous Chapters (see in particular Fig.(5.3) on pag.128 and Subsection (6.3.2)) we deduce that the ground-state surface represents the interaction potential relevant for the study of the adiabatic processes

$$LiH^+ + H \longrightarrow \begin{matrix} Li^+ + H_2 \\ Li^+ + H + H \end{matrix} \qquad (7.2)$$
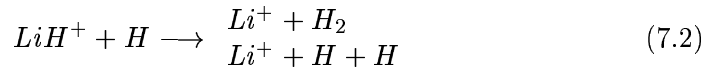
which will be the subject of the reduced dimensionality quantum dynamical treatment of Chapter 8. In eq.(7.2) the three body (3-B) break-up channel has been considered because, as already mentioned, the very low binding energy of the LiH^+ molecule makes it already accessible at a collision energy of a few tenths of eV.

With the same token the first excited PES is relevant for the adiabatic reaction

$$LiH + H^+ \longrightarrow Li + H_2^+ \qquad (7.3)$$
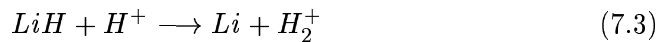
which will be the subject of Chapter 9. Since in this case the asymptotic partners experience strong electrostatic forces (due to the strong dipole of the *LiH*
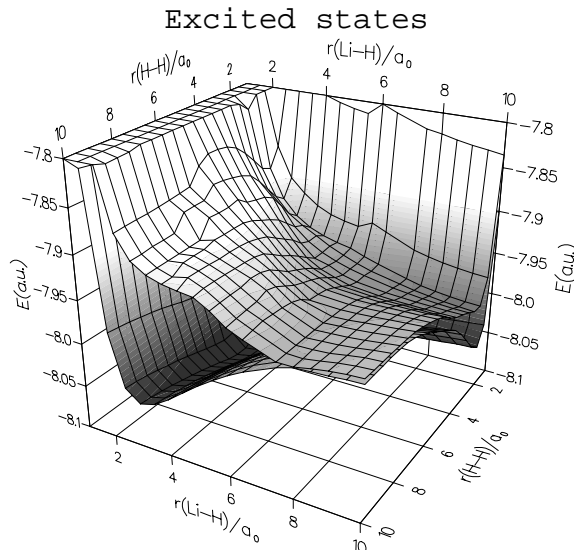
Figure 7.11: Second and third roots in three dimensions as a function of *R(Li-H)*
and *R(H-H)*. The points are the raw *ab-initio* values.

molecule and the substantial polarizability of the *Li* atom), the mentioned
potential is characterized by the dipole-charge and charge-induced dipole in-
teraction terms. Indeed, we have already seen in Fig.(6.8) two deep potential
wells that could support several triatomic bound states and, as we shall see,
will have a marked influence on the dynamics.

The reactive surfaces that we will discuss in the following were calculated
on a rather dense grid of the two inter-atomic distances. We computed the
potentials on a regular grid ranging from $1.0\,a_0$ to $11.0\,a_0$ for the *LiH* inter-
atomic distance and from $0.5\,a_0$ to $10.0\,a_0$ for the *HH* distance. A single point
calculation was performed every $0.5\,a_0$ throughout this region; the step-size
has been halved in a small region around the saddle point of the first excited
state, that is for $2.0\,a_0 \leq r_{LiH} \leq 5.0\,a_0$ and for $1.0\,a_0 \leq r_{HH} \leq 4.0\,a_0$.

An overview of the computed PESs is presented in Fig.(7.10) and in Fig.(7.11).
In the first one, we show a 3D representation of the PESs for the first two elec-
tronic states. In particular, we report the analytical fitting obtained from the
ab-initio points (see below) that show the main features of the potentials: the
two electronic states are well separated in energy and have a very different
topology. Indeed, as we shall see better in the following, only the first excited
state presents a non-trivial shape, having a saddle point between the two deep
wells located in the asymptotic channels. In Fig.(7.11) the first and second ex-

cited PESs (only the *ab-initio* points this time) are reported: although we are not interested in the highest state here showed, we note that the two surfaces come into contact in the asymptotic three-body break-up region and that the upper surface remains mainly repulsive.

In what follows we will consider some details of the potentials along with the fitting procedure used to obtained analytical representations of them, that in turn were used in the dynamical calculations of the next two Chapters. Before doing this we focus attention on an interesting feauture that occurs in the *first excited* state.

7.2.1 A curious fact

The possible non-adiabatic processes between the two lowest energy states have been already introduced in Subsection (7.1.3) where, taking into account the energy gap and the different nature of these states, we argued that multisurface events can hardly be effective in the dynamics of our system. We will see in the following that similar conclusions can be drawn from the reactive calculations and we will discuss their implications at the end of this Chapter. For the moment we focus attention on the *first* and the *second excited* electronic state for which non-adiabatic interactions should be expected. Indeed, as already noted in Section (5.4), a simple inspection to the three body break-up arrangement reveals that the dissociating state $(Li + H + H^+)$ is doubly degenerate due to the presence of the charge, thus bringing the two lowest *excited* potential surfaces into contact (see Fig.(7.11)). The previous analysis of Subsection (7.1.3) already revealed that deeply in the interaction region of the subreactive configurational space the two excited states are somewhat interacting, because of the charge-exchange process that takes place between the two hydrogen atoms (see the bump in the right panel of Fig.(6.7)). Thus we expect a strong interaction between the mentioned states.

The location and characterization of the seam of the possible conical intersection is an interesting matter, but it is beyond the scope of this work. Here we note another interesting aspect that arises in the asymptotic LiH potential energy (as considered within the LiH_2^+ system) because of the above mentioned degeneracy in the three-body break-up arrangement. This effect has been rarely noted in literature, although it occurs in similar systems, like the *ground-state* of HeH_2^+ (Sathyamurthy, 2000). In practice, a lower electronic state, in which the charge appears exchanged onto the two H atoms, arises whenever one stretches the LiH bond in the presence of an isolated H^+. In Fig.(7.12) we report (in the left panel) the relevant diatomic curves for the isolated LiH moiety and (right panel) the first lower lying curves of the LiH_2^+ PES obtained by stretching the LiH distance and fixing the HH distance at
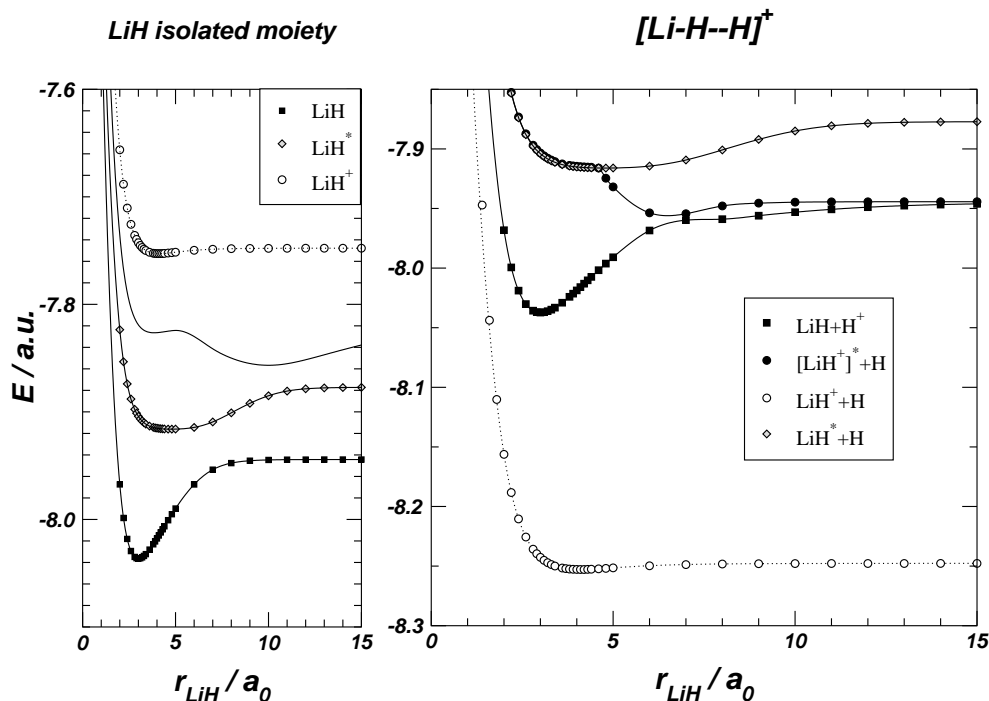
Figure 7.12: Potential energy curves for an isolated LiH and for the asymptotic situation in LiH_2^+ when $r_{HH} \to \infty$. Total energies and lengths in atomic units.

a very large value ($50\,a_0$ in the collinear $LiHH$ configuration). The potential energy curve of the ground state of the right panel is simply the ground state of LiH^+ (white circles) which is being energy-shifted by the presence of a neutral hydrogen atom at infinite distance. The potential energy curve of the first excited state in the right panel can be imagined to arise from two diabatic curves, one is that of the isolated LiH molecule (black squares) and the other is that of an electronically excited state of the isolated LiH^+ molecule (not shown in the figure, but very high in energy); this last state is the first excited state of the LiH^+ molecule and dissociates asymptotically as $Li + H^+$. Because of the presence of a shallow polarization well located at about $7.5\,a_0$, this state, when considered in the presence of an isolated hydrogen atom, becomes lower in energy than that of the LiH with an isolated H^+ and thus gives rise to a double minimum structure in the first excited asymptotic potential of the title system. At shorter range, instead, it becomes higher in energy than the state which correlates with the $A^1\Sigma^+$ state of LiH and therefore the nature of the second excited of LiH_2^+ state depends much on the geometry at hand. This

is the reason why in Fig.(5.3) we left an unspecified label for that asymptotic situation. Since this asymptotic interaction disappears in the interaction region (where the different electrostatic character of the two states is enhanced by the reduced distances) in the following we will neglect such interaction. Indeed, our purpose is to obtain some information on the low energy processes occurring in the first excited states for which we could safely assume that an electronically adiabatic picture is sufficiently accurate for a preliminary study.

7.2.2 The ground state

The ground-state potential energy function given by our calculations presents a very simple structure, arising mainly from the two-body contributions. Indeed it was a relatively simple matter to fit the 3-body (3B) non-additive term, given by

$$V_{3B}(r_{LiH}, r_{HH}) = V(r_{LiH}, r_{HH}) - V_{\mathrm{LiH}^+}(r_{LiH}) - V_{\mathrm{H}_2}(r_{HH}) - V_{\mathrm{LiH}^+}(r_{LiH} + r_{HH})$$

where the last term represents the potential acting between the lithium atom and the outer H atom. The diatomic potentials were chosen according to the properties of the ground-state electronic wavefunctions. Since the charge is always located on the Li atom the diatomic potentials corresponding to the two LiH were chosen to be that of LiH^+. The asymptotic potentials were obtained from additional calculations at larger distances, one at $r_{LiH} = 15\,a_0$ for the H_2 curves and the other at $r_{HH} = 50\,a_0$ for the LiH curves.

The parameters of the H_2 potential turned out to be $D_e = 4.612\,eV$ and $r^e = 1.421\,a_0$; it supports 14 vibrational bound states, of which the lowest one has a dissociation energy of $D_0 = 4.348\,eV$. For the LiH^+ potential we computed $D_e = 0.138\,eV$, $r^e = 4.107\,a_0$ and 5 vibrational levels, the lowest-lying yielding $D_0 = 0.111\,eV$.

We fitted the 3B with the following functional form,

$$V_{3B}(r_1,\,r_2) = V_{SR}(r_1,\,r_2) * (1 - f) + V_{LR}(r_1,\,r_2) * f$$

where r_1 and r_2 now correspond to r_{LiH} and r_{HH} respectively. Here V_{SR} is the short range potential, f is a "shape" function of the form

$$f(r_1, r_2) = \frac{1}{1 + e^{r_1 - \rho_1}} \frac{1}{1 + e^{r_2 - \rho_2}}$$

(with ρ_1 and ρ_2 fixed respectively to $7.0\,a_0$ and $9.0\,a_0$) and V_{LR} is the long-range tail of the 3B potential,

$$V_{LR}(r_1, r_2) = -\frac{1}{2(r_1 + r_2/2)^4}\left(\alpha_{\mathrm{H}_2}(r_2) - 2\,\alpha_{\mathrm{H}}\right)$$
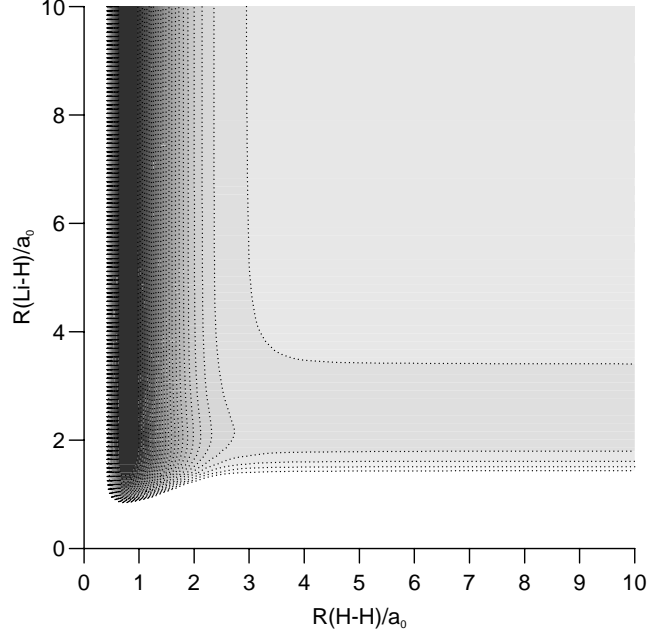
Figure 7.13: Contour plot of the ground state PES for the $Li - H - H$ geometry. Darker areas correspond to minima in the potential.

in which α_{H_2} is the polarizability curve of the hydrogen molecule and α_H is the polarizabilty of the hydrogen atom (4.50 in atomic units); for the first curve we used an analytic fitting of the data of Hyamas et al. (1994), further corrected to ensure the right asymptotic behaviour. The short range potential, V_{SR} is the term that was actually fitted: we wrote it as

$$V^{SR}(r_1, r_2) = \sum_{n,m=0}^{4} b_{nm} L_n(r_1) L_m(r_2) * e^{-\beta_{nm}(r_1 + r_2)} \qquad (7.4)$$

(where L_n 's are Laguerre polynomials). We optimized the 50 parameters $\{b_{nm} \} \bigcup \{\beta_{nm} \}$ minimizing the square deviation by using the efficient Levenberg-Marquadt method (Press et al., 1986). Since for $\beta_{nm} = 0.5$ the basis functions reduce to products of ordinary Laguerre functions, we used the coefficients of a preliminary linear optimization as guess for the non-linear optimization. The resulting fitting was fairly good having a standard deviation of 0.009 eV .

In Fig.(7.13) we report a contour map of the fitted PES. As already mentioned, the surface is fairly uneventful and shows one deep and narrow channel corresponding to the H_2 molecule formation and a shallow and broad channel

corresponding to LiH^+ formation[5].

7.2.3 The first excited state

The first excited surface has a more complicated structure than the ground-state, mainly because of the different electrostatic forces which are now acting between the reagents and between the products. Here a 3B potential were obtained by considering the charge located on one of the two H atoms:

$$V_{3B}(r_{LiH}, r_{HH}) = V(r_{LiH}, r_{HH}) - V_{\mathrm{LiH}}(r_{LiH}) - V_{\mathrm{H}_2^+}(r_{HH}) - V_{\mathrm{LiH}^+}(r_{LiH} + r_{HH})$$

In this formula V_{LiH} is the LiH curve (the *diabatic* curve in Fig.(7.12)) and V_{LiH^+} is the diatomic curve of LiH^+ in its first electronic excited state, which dissociates as $Li+H^+$. Our LiH curve turned out to have $D_e = 2.466\,eV$, $R = 2.977\,a_0$ and supports 25 vibrational states, the first one with a dissociation energy of $D_0 = 2.392\,eV$. The H_2^+ molecule turned out to have $D_e = 2.779\,eV$, $R = 1.998\,a_0$ and support 18 vibrational states the first one with $D_0 = 2.637\,eV$.

Since in this case the 3B term has very important contributions coming from the long-range tails of the interaction we wrote it in the form

$$V_{3B}(r_1, r_2) = V_{SR}(r_1, r_2) * f_1 * f_2 + V_{LR}^{(1)}(r_1, r_2) * (1 - f_1) + V_{LR}^{(2)}(r_1, r_2) * (1 - f_2)$$

where

$$f_1 = \frac{1}{1 + e^{0.5 * r_1 + r_2 - \xi_2}} \quad f_2 = \frac{1}{1 + e^{r_1 - \xi_1}}$$

and

$$V_{LR}^{(1)}(r_1, r_2) = -\frac{\mu_{\mathrm{LiH}}(r_1)}{(0.5 * r_1 + r_2)^2}$$

is the dipole potential term obtained from the data of Hyamas et al. (1994) and $V_{LR}^{(2)}$ is the analogous polarizability contribution (we used $\alpha_{\mathrm{Li}} = 176.0\,a.u.$ as obtaneid from our asymptotic potentials). The shape function f_1 switches on the dipole contribution when $0.5\,r_{\mathrm{LiH}} + r_{\mathrm{HH}} \geq \xi_1$, while f_2 switches on the polarization term only at large Li-H distances (for the dipole term it should be noted that the behaviour of dipole curve as a function of $r(LiH)$ ensures

---

[5]We computed and fitted also the ground state PES of the other collinear arrangement $H - Li - H$, because of its possible relevance on the Collision Induced Dissociation of the next Chapter. In that case we used an evenly spaced grid $r_{LiH_a} \geq r_{LiH_b} \in [1.0\,a_0,\ 11.0\,a_0]$ with a step size of 0.5 a_0. A simple linear fitting with ordinary Laguerre functions was sufficient to achieve a very small standard deviation: 0.001 eV with $5 * 5$ Laguerre functions. Indeed, the surface is very simple: it is obviously symmetric and shows only a shallow well due to the weak polarization charge interaction between LiH^+ and H.

Figure 7.14: Left panel: potential energy curves for different $R(LiH)$ values along the $R(HH)$ coordinate. Solid lines are the analytical fitting functions, while the open circles show the raw ab-initio points. The dashed line is the asymptotic H_2 potential. Right panel: long range region joining the *ab-initio* points and the fitting asymptotic function.

that the contribution vanishes for large *Li-H* distances). The variables ξ_1 and ξ_2, and those entering in the expansion of the short-range contribution, were subjected to the same optimization procedure used for the ground-state PES, the only difference being that the short-range term were written as

$$V_{SR}(r_1, r_2) = V_0 + \sum_{n,m=0}^{5} b_{nm} L_n(\rho_n^{(1)}) L_m(\rho_m^{(2)}) * e^{-0.5*(\rho_n^{(1)} + \rho_m^{(2)})} \qquad (7.5)$$

where

$$\rho_n^{(1)} = \beta_n \left(\frac{r_1}{r_{\text{LiH},e}} - 0.5 \right) \text{ and } \rho_n^{(2)} = \beta_n \left(\frac{r_2}{r_{\text{H}_2^+,e}} - 0.5 \right)$$

($r_{M,e}$'s being the equilibrium distances of the diatomic molecules). In this case the origin of the coordinates of the Laguerre functions was slightly shifted to better model the interaction region. It turned out that the final fitting function had to be slighlty modified in the (extrapolated) short range region (i.e. $\rho^{(i)} \ll 0$) to avoid anomalous behaviour of the analitycal PES.
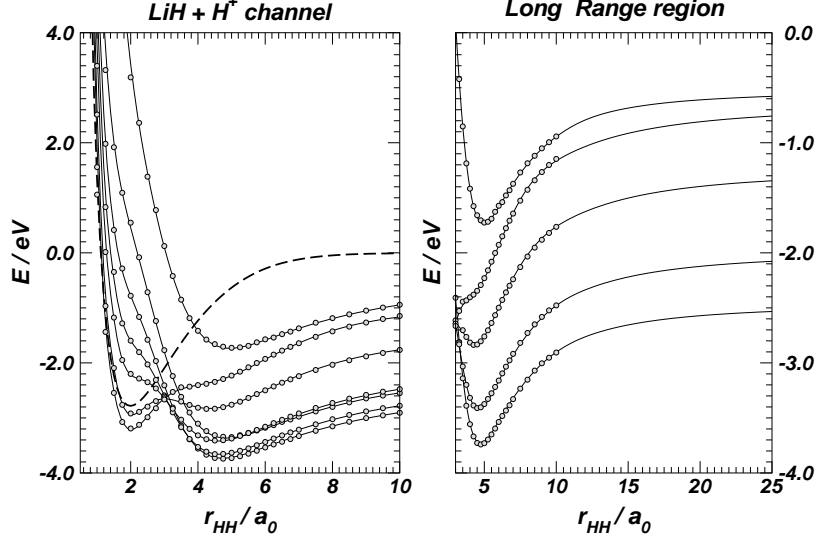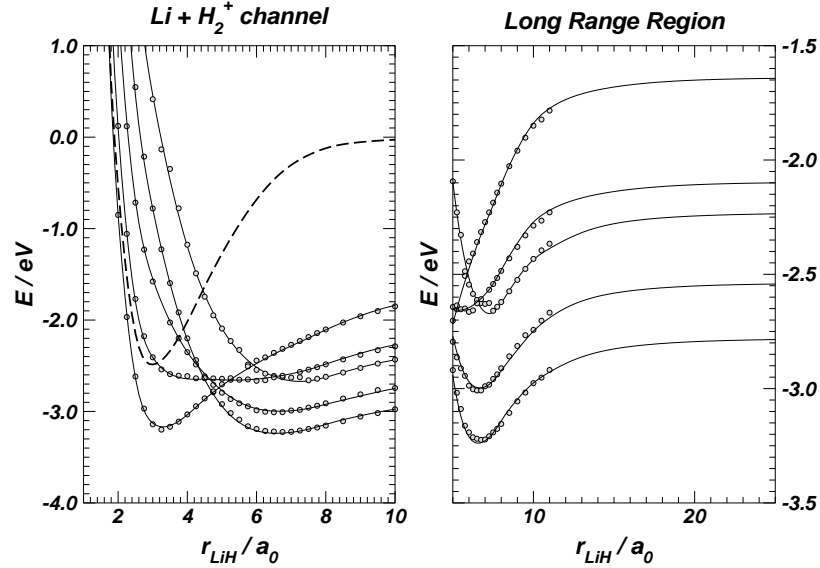
Figure 7.15: Left panel: potential energy curves for different $R(HH)$ values along the $R(LiH)$ coordinate. Solid lines are the analytic fitting functions, open circles are the raw *ab-initio* points and the dashed line is the asymptotic LiH potential curve. Right panel: long range region joining the *ab-initio* points and the fitting asymptotic function.

We optimized a total of 53 parameters using the data points with energy less than $1.0 \, eV$ (with the zero of the potential put in the triatomic dissociation limit). The resulting fit turned out to have a standard deviation of 0.018 eV. Fig.(7.14) and Fig.(7.15) show a comparison between the fitted PES and the original *ab-initio* data, both for the entrance channel and for the exit channel of the reaction eq.(7.3). In the right panels we report an enlarged view of the regions to show how smoothly the long-range term was added to the potential of the "*ab-initio*" region. Finally, in Fig.(7.16) we report a contour plot for the fitted surface of the upper electronic state. It presents an interesting topology caused mainly by the strong electrostatic forces which are now acting at large and intermediate distances between the fragments. As is evident from the figure, the surface presents two well localized minima and a saddle point. The minimum in the reactants region (along r_{HH}) is at an energy of $\sim -1.26 \, eV$ with respect to the $LiH + H^+$ arrangement and of about $\sim -3.74 \, eV$ with respect to the dissociation limit $(Li + H + H^+)$; the other is $\sim -0.46 \, eV$ in reference to $H_2^+ + Li$ and $\sim -3.24 \, eV$ to the dissociation limit. The "barrier" is located at $-2.655 \, eV$ respect to the dissociation limit. The two
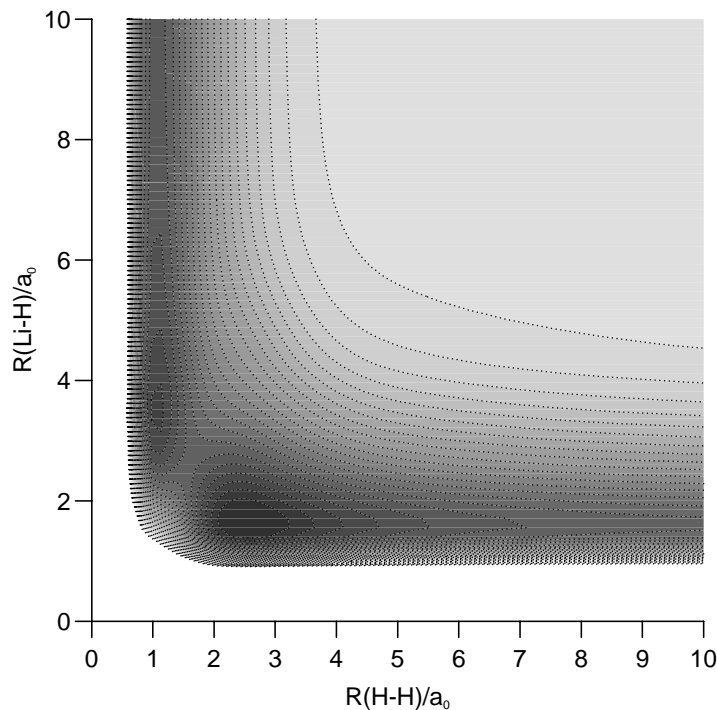
Figure 7.16: Contours for the first electronic state in the $Li - H - H$ geometry. Darker areas correspond to minima on the potential energy surface.

LiH and H_2^+ asymptotes are respectively $-2.47\,eV$ and $-2.78\,eV$ in reference to the dissociative threshold and therefore the barrier is 0.185 eV *lower* in energy than the $LiH+H^+$ asymptote and 0.125 eV *higher* than the $Li+H_2^+$ one. This is clearly illustrated by the minimum energy path on this surface, reported schematically in Fig.(7.17). One should note however that the position of the "left" asymptote is different from what is shown in the figure since the cut of it is taken in a region where the dipole charge contribution is still not negligible and thus it lowers the real asymptote of about $0.13\,eV$.

It is interesting to note that the transition state involves a geometry in which the LiH and the HH bonds are markedly "stretched" ($r_{LiH} \sim 5.0$ a_0 and $r_{HH} \sim 3.0$ a_0) and thus one should expect enhancing of the reaction probability when vibrationally excited LiH (or H_2^+ for the reverse reaction) is involved, while one should find a more limited reaction efficiency when starting with LiH (H_2^+) in its vibrational ground state. Apart from these simple considerations, however, the topology of the surface is such that only a direct treatment of the dynamics could give us more quantitative details.
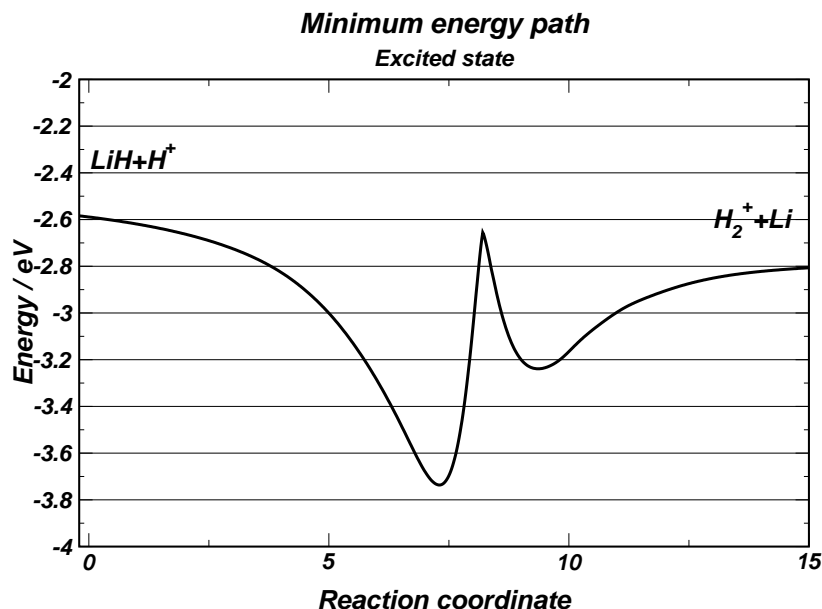
Figure 7.17: Minimum energy path for the first electronically excited state.

7.3 The 3D reactive surfaces

In this Section, we present an overview of the full 3D reactive surface for which we have just completed the huge amount of calculations required. At the end of the calculations a simple count of the data collected resulted in a total of 11341 *ab-initio* energy values for each electronic state[6]. It needs some time to put in order and fit this huge amount of data; at the time of writing, we are only at the very early stage of such procedure and therefore we present here just a preliminary analysis.

The coordinates used to sample the configurational space are depicted in Fig.(7.18). For a fixed Θ we computed the PESs on a $r_{LiH} - r_{HH}$ grid similar to that employed for the collinear $Li - H - H$ study of the previous Section. We considered one Θ angle every *10°* starting from $\Theta = 10°$ and ending with $\Theta = 120°$ (*12* grids); in the large angle region, where the dipolar repulsive interaction of the excited surface prevents any reaction, we computed only the $\Theta = 140°$ and *160°* PESs.

Our choice of the coordinates clearly does not make any use of the simmetry

---

[6]This data refers also to the collinear geometries of the previous Section, but not to the calculations in the subreactive region.

of the system and thus the results in the large angle region ($\Theta > 90°$) are somewhat redundant (although the actual geometries can be hardly superimposed). From a computational point of view, we took advantage of the fact that the time needed for each single point calculation was very low (about 10-15 min on a RISC6000 processor with 512Mb of RAM, in a multiuser environment).
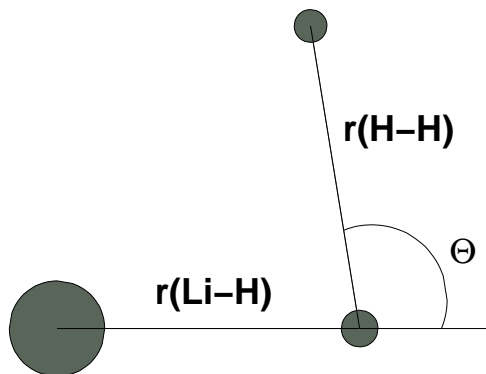
Figure 7.18: Reactive cordinates used in the calcualtion of the 3D surface

7.3.1 The general trend

When increasing the Θ angle of Fig.(7.18) from the zero value of the collinear geometry the PESs do not change substantially their qualitative behaviour, as can be seen from Fig.(7.20) on pag.176 where we report the $r_{LiH} - r_{HH}$ cut of the PESs for $\Theta = 50°$.

The interaction in the ground electronic state is dominated by the two-body contributions and in particular by the strength of the $H - H$ bond. Therefore we see that the ground-state PES is almost flat with one very deep and narrow channel corresponding to the formation of the H_2 molecule. On the other hand, in the excited electronic state the features of the surface arise mainly from the strong electrostatic interactions between the two partners, which are of course of the charge-dipole type in the $LiH + H^+$ channel and of the charge-induced dipole type in the $Li + H_2^+$ channel. In this case, however, because of the anistropy of the dipolar contribution we observe a marked difference in the strength of the interaction when varying the Θ angle; this feature ultimately leads to a repulsive contribution when $\Theta \gtrsim 90°$.

When we consider the large angle region ($\Theta \gtrsim 120°$) some structure arises (Fig.(7.21) on pag.177) which is due to our choice of the coordinate system. Indeed, for the ground-state we observe the appearence of a repulsive barrier between the two asymptotic channels; this is clearly due to the steric effect

of the Lithium atom that prevents the projectile hydrogen atom to reach the target H when we fix the Θ angle at a large value. For the excited state the situation is somewhat more complicated because of the presence of the previously mentioned charge-exchange process (see for example Section (7.1.3)). We
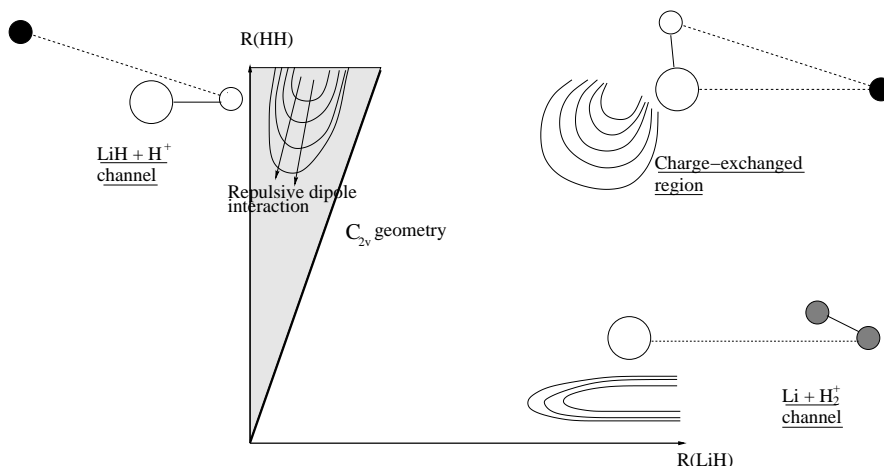
Figure 7.19: Schematic representation of the large angle region.

may analyze this region of the PES with the help of the diagram of Fig.(7.19) where we report a schematic representation of the PES for $\Theta = 160°$ along with some relevant geometries. When $\Theta > 90°$ our configurational space spans also the symmetric C_{2v} subspace; for a fixed Θ it is a simple matter to show that this subspace reduces to the rectilinear path of equation

$$r_{HH} = -2cos\Theta r_{LiH}$$

shown in Fig.(7.19) as a bold line. The dashed region above this line corresponds to the entrance $LiH + H^+$ channel (hindered by the repulsive dipole-charge interaction) and close to the r_{LiH} axis we have, as always, the exit $Li + H_2^+$ channel. In between these areas there is a "charge-exchange" region in which the initially charged projectile has exchanged its charge with the target hydrogen atom in order to form the more stable LiH moiety. This is the origin of the minimum evident in the central panel of Fig.(7.21).

We will turn below on the possible implications of such features on the dynamics of the system; for the moment let us briefly describe the low energy structures that characterize the bound states of the LiH_2^+ molecule.
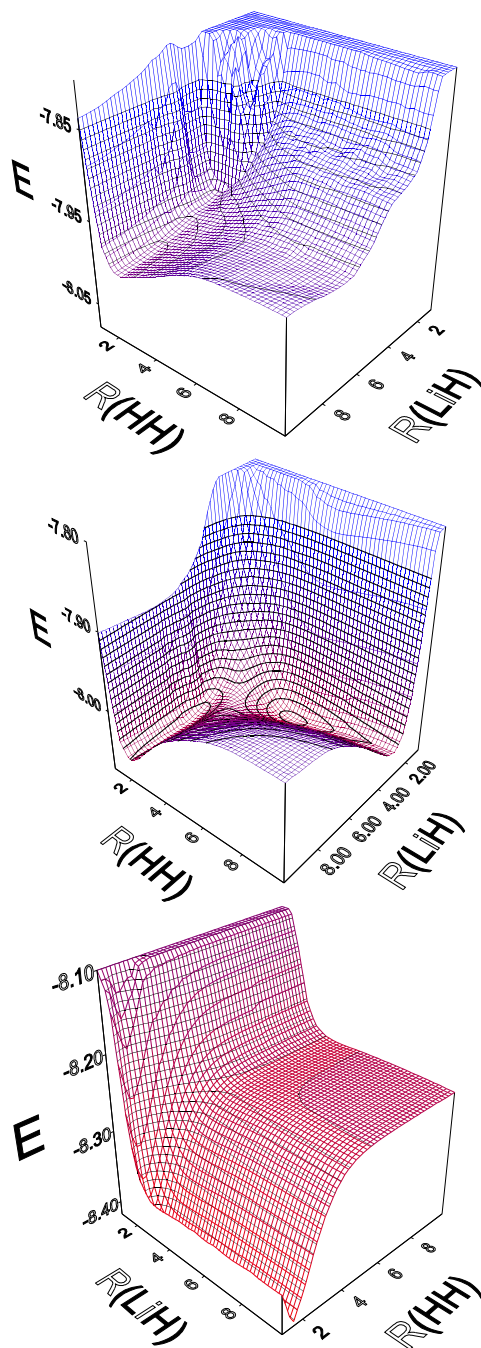
Figure 7.20: The three lowest PESs for $\Theta = 50°$.
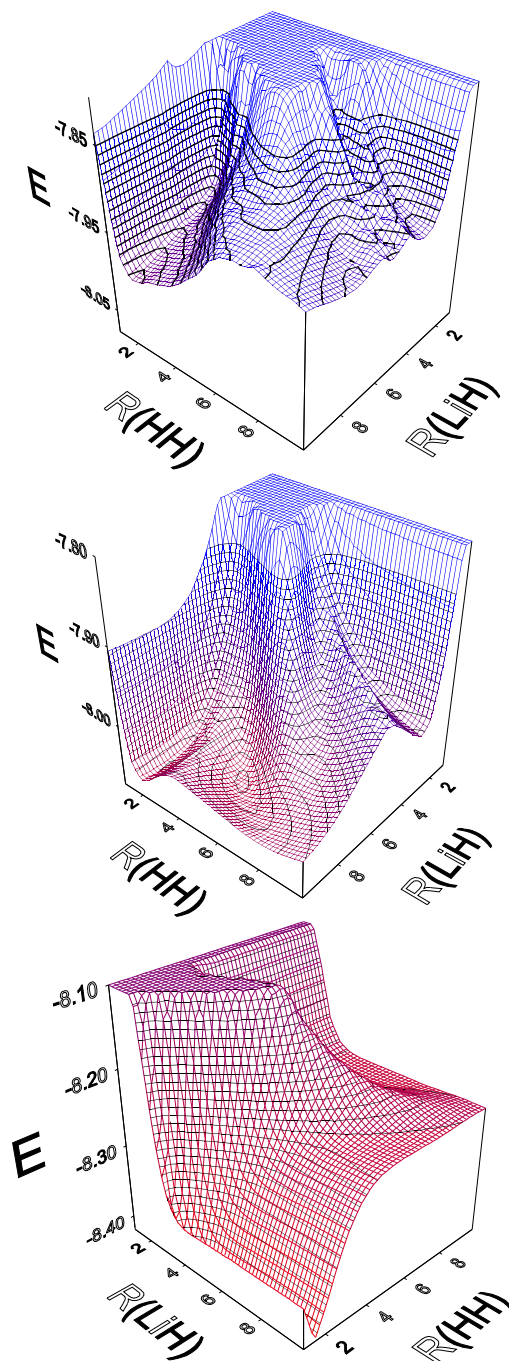
Figure 7.21: The three lowest PESs for $\Theta = 160°$.

7.3.2   The stable structures

We can obtain some preliminary informations on the equilibrium structures of the system by looking at the profiles obtained while fixing the value of one of the two internuclear distances of our grid at the equilibrium value of the relevant molecule. For the ground-state we have already noted that the interaction is mainly due to the formation of the H_2 molecule and, thus, fixing $r_{HH} = r_e(H_2)$ we may infer with a good approximation the equilibrium geometry of the complex. In the excited state the situation is somewhat different but we noted in the collinear arrangement that the two deep wells were "pre-reaction" wells, characterized by a substantially unchanged equilibrium distances of the relevant reagent molecule. Thus, although at a more approximate level, the same kind of profiles of before can be of help in understanding the nature of the interaction.
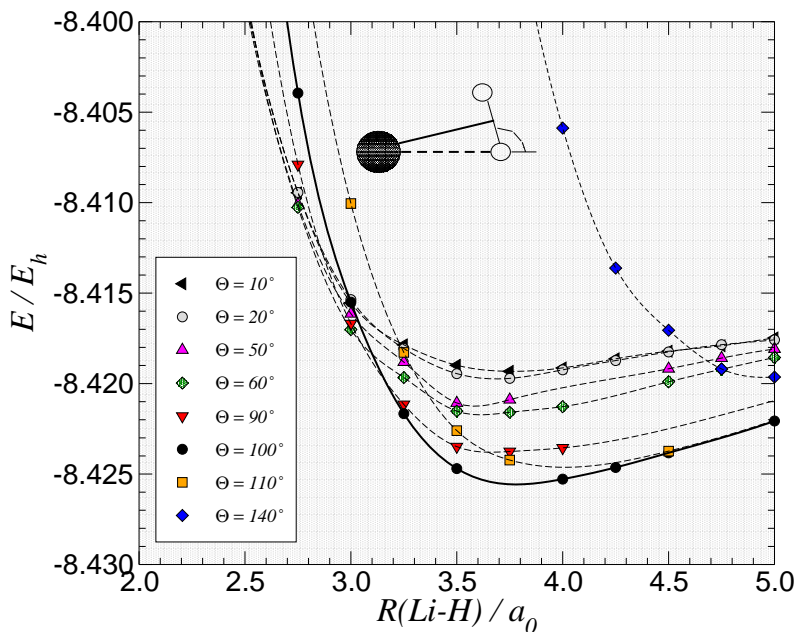
Figure 7.22: Cuts of the ground-state PES for $R(HH) = 1.5\,a_0$ and for different Θ values.

In Fig.(7.22) on pag.178 we report some curves obtained with $r_{HH} = 1.5\,a_0$, i.e. we consider the interaction of an approaching Li^+ atom for different orientation of a rigid H_2 molecule. We see that the shallow well of the collinear geometry becomes deeper and deeper when Θ is increased until it reaches the minimum for $\Theta = 100°$. A closer inspection of the corresponding geometry of the molecule reaveals that at the minimum we have, with a good approxima-

tion, a C_{2v} structure. Indeed, the equilibrium structure of the ion obtained by D.J Searles et al. (1991) corresponds in our coordinates to $r_{LiH} = 3.860\,a_0$ and $\Theta = 100.6°$, i.e. very close to that shown in Fig.(7.22). The binding energy is $D_e \sim 9\,mE_h = 0.245\,eV$, which is very close to that of D.J Searles et al. ($D_e = 0.258\,eV$). It is worth to note, however, that the *linear* saddle point is only $\sim 6\,mE_h = 0.163\,eV$ above this value.
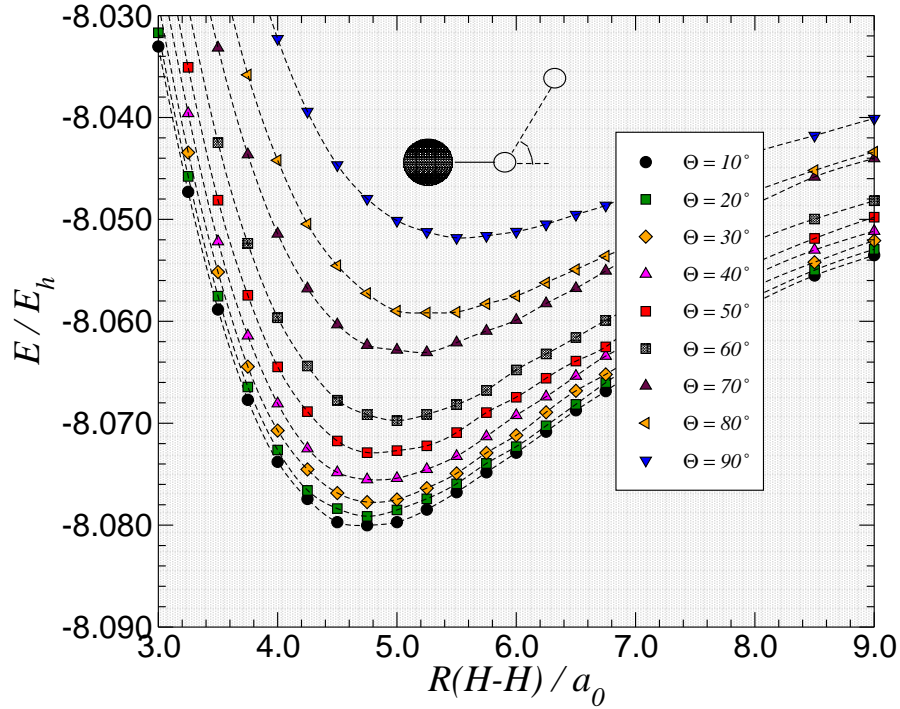
Figure 7.23: Cuts of the first excited PES for $R(LiH) = 3.0\,a_0$ and for different Θ values.

In the first excited state we have two wells. When we fix the LiH distance at the value $r_{LiH} = 3.0\,a_0$ we recover the expected behaviour of a dipolar interaction (see Fig.(7.23)); that is the collinear equilibrium geometry is a *true* minimum of the system and it turns out to be the absolute one. At the end, when we fix the HH distance at the value $r_{HH} = 2.0\,a_0$ we obtain surprisingly that the collinear equilibrium geometry is a saddle point between two symmetry related minimum structures with $\Theta \sim 10°$, located at about $2\,mE_h = 0.054\,eV$ below such saddle point (see Fig.(7.24) on pag.180). Note also in Fig.(7.24) the minimum that appears for $\Theta = 160°$ at $r_{LiH} \sim 8.5\,a_0$ which corresponds to the *same* structure of above[7].

---

[7] Just to have an idea of the strength of the interaction the binding energies of some bonds
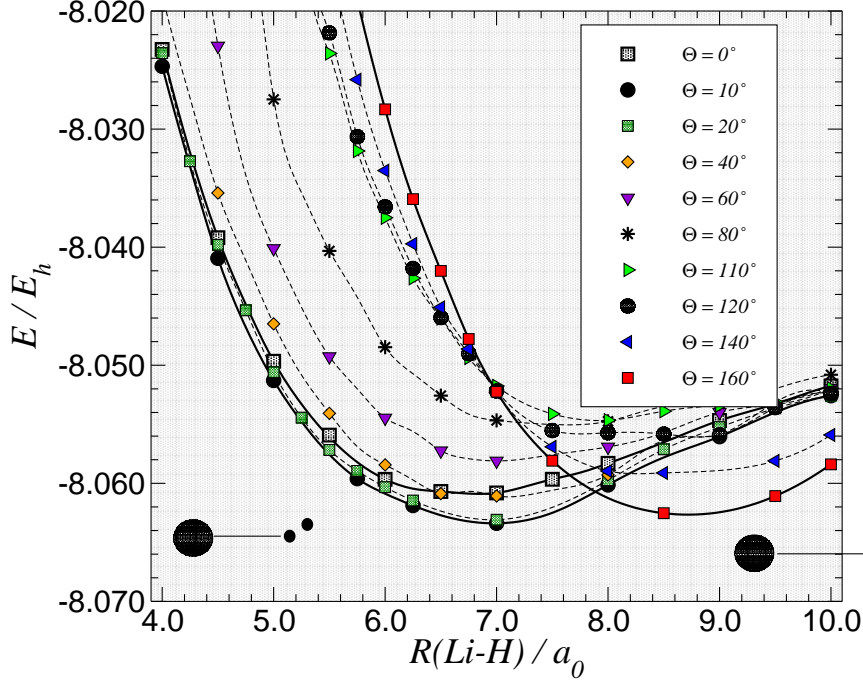
Figure 7.24: Cuts of the first excited PES for $R(HH) = 2.0\,a_0$ and for different Θ values.

7.3.3   The reaction pathways

We discuss here in some details the *excited state* PES focusing attention on the possible reaction paths that could take place on this surface. The ground-state PES, as already noted several times before, has a trivial topology and the 3D results here presented add only the repulsive "steric" barrier to the topology of the potential discussed in Section (7.2).

As expected, starting from the collinear geometry the saddle point of each cut PES becomes higher and higher in energy when Θ increases. That is, the collinear saddle point is a *true* saddle point of the surface[8]. The behavior of the saddle point can be seen in Fig.(7.25) on pag.181 where the relevant portion of the various surfaces is displayed. In upper panel of this figure, the saddle point moves toward larger r_{LiH} distances (y axes in the figure) when increasing Θ below *90°*. This means that for $\Theta > 0°$, not only the collision energy has to increase to overcome the barrier, but also the degree of vibrational excitation

are: $D_1(p^+ - e^-) = 13.6\,eV$, $D_e(H_2) = 4.76\,eV$, $D_e(C - H) \sim 4\,eV$, $D_e(H_2O..H_2O) \sim 0.22\,eV$ and $D_e(LiH..He) \sim 0.025\,eV$.

[8]This is only a qualitatively result that can be extracted by looking at the data.

of *LiH* must increase to overcome the saddle point. When we futher increase
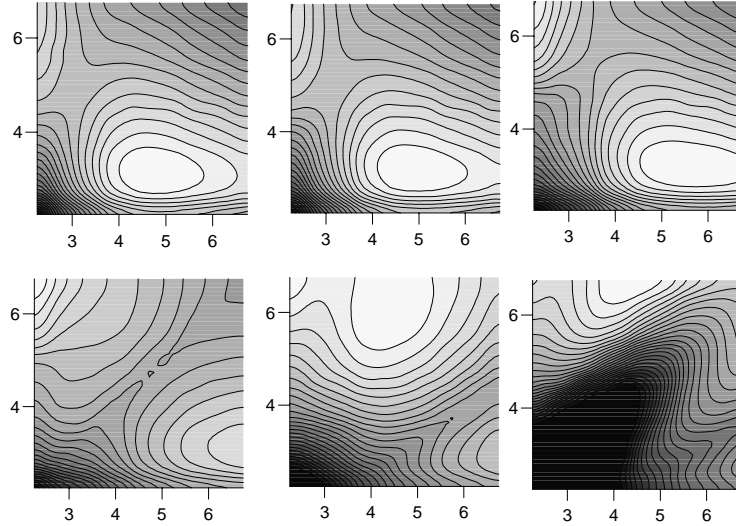
Figure 7.25: Saddle point evolution for a variation of the angle. From left to right, from top to bottom the angles are: *10°, 50°, 90°, 120°, 140°, 160°*. Distances are in a.u.. The y axis is the *R(Li-H)* distance.

Θ beyond *90°* the saddle point coalesces on the repulsive C_{2v} barrier until for large Θ a second saddle point appears that correponds to the barrier for the charge-exchange process (see Fig.(7.19) and Fig.(7.21)). Therefore, we may argue that, from a classical point of view, two mechanisms are possible for the reaction. At low energy only a small angular cone (the dipole allowed one) is effective for the reaction to occur: in this case the proton scatters off the hydrogen side of the target molecule and we expect the product appears *backward* with respect to the incident H^+ beam (back-scattering),

$$LiH_a + H_b^+ \rightarrow Li + H_a H_b^+$$
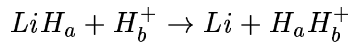
At higher energy, instead, the reaction may occur following "two steps", a charge-exchange process followed by a dipole-driven one, as indicated by the equation

$$\begin{cases} H_b^+ + LiH_a \rightarrow LiH_b + H_a^+ \\ LiH_b + H_a^+ \rightarrow Li + H_b H_a^+ \end{cases}$$
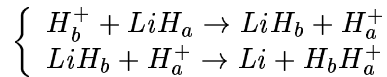
(In Fig.(7.19) this corresponds to a clockwise path on a large circle). In this case we expect that the product appears in the *forward* direction with respect

to the incident proton beam (a sort of harpooning mechanism). In quantum mechanics we cannot distinguish these two paths because the two protons are indistinguishable; however, the forward-backward nature of the process could be estabilished and the interference pattern between the two paths could be observed.

These conclusions would be at least plausible if the dynamics proceed in a *direct* way. However, the deep pre-reaction wells suggest (and the treatment of Chapter 9 confirms) that the dynamics is dominated by the formation of long-lived metastable states which *delete memory* of any actual mechanism. In other words, the long time of survival of the metastable states allows the system to perfom complete rotations before its breaking-up and, thus, the products are expected to appear in random directions (see for example D.R. Hershbach (1987)).

7.3.4   Avoided crossing or conical intersection?

Another interesting point pertaining to the excited state is its possible interaction with the third one: as we have already seen, non-adiabatic interactions should be not significative between the groud and the first excited state, but could play an important role between the first and second excited state.

The two surfaces interact strongly in the triatomic dissociation region (as already noted for the collinear geometries) where the dissociation limit is double degenerate. The problem of the asymptotic interaction between the two states has already been described above in Subsection (7.2.1) and is due to the mixing between the ground and first excited states of LiH with an excited state of LiH^+ in the presence of an hydrogen atom. In the interaction region we are not able to discuss accurately the question of the location and caracherization of the seam of the possible conical intersection since the third state was not calculated by an optimized reference function. However as the Fig.(7.26) shows the two surface are indeed very close to each other on the line that locates the C_{2v} subspace in our coordinate system (see also Fig.(7.19)) . What remains to estabilish is (i) if the surfaces actually cross and (ii) how the crossing point moves with the Θ angle[9].

7.4   Forbidden reaction pathways

As it is evident from the three-dimensional representation of the first two electronic states which we plot again for the collinear $Li - H - H$ geometry in

---

[9]In this context it is worth to note that the two relevant states have the same symmetry in the C_s group (^1A) and in the C_{2v} subspace belong to the $^1A_1$ and $^1B_2$ representation respectevely.
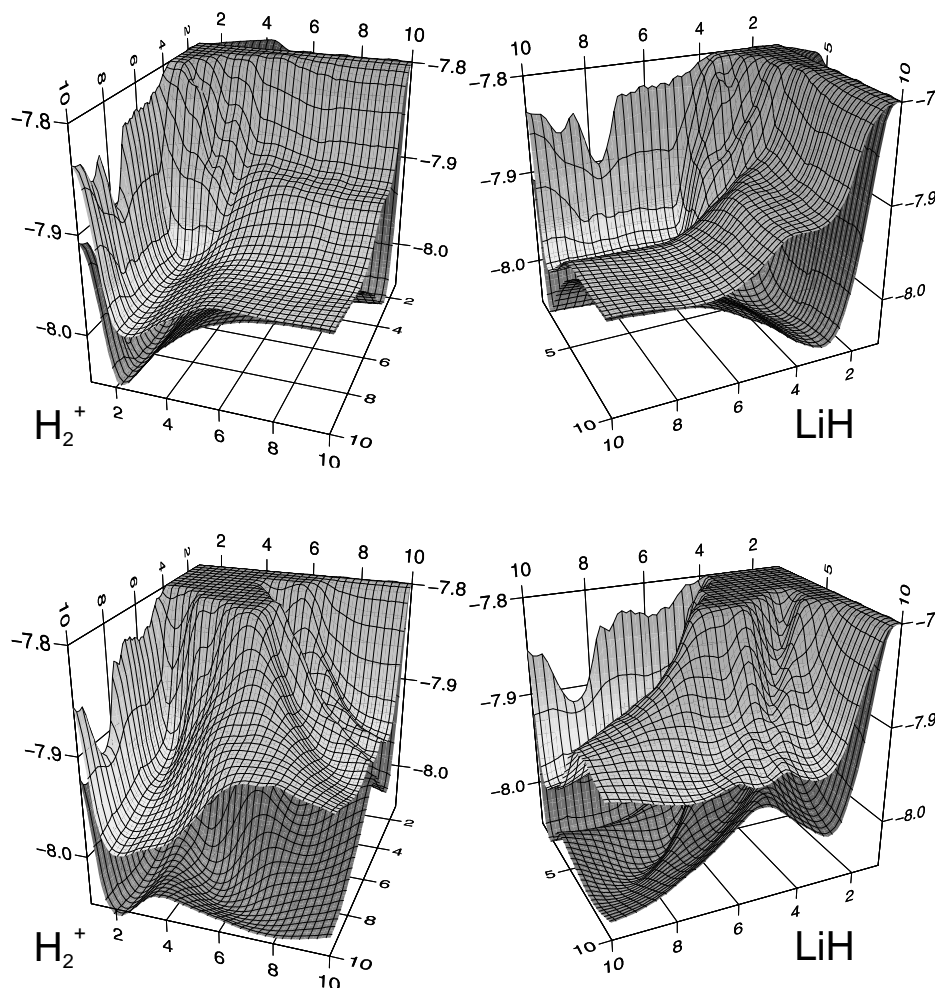
Figure 7.26: 3D representation of the first and second excited state for $\Theta = 90°$ (upper panel) and for $\Theta = 160°$ (lower panel). The two figures in each panel are exacly the same but the visual angle is changed to permit a better visualization of the two asymptotic states.

Fig.(7.27), the ground and the first excited states remain quite well separated in energy through the reactive regions. This feature was first noted in the configurational region sampled by the sub-reactive surfaces described earlier in Section (7.1) and then was confirmed by the full dimensional 3D reactive calculations described in the previous Section and by the C_{2v} calculations shown
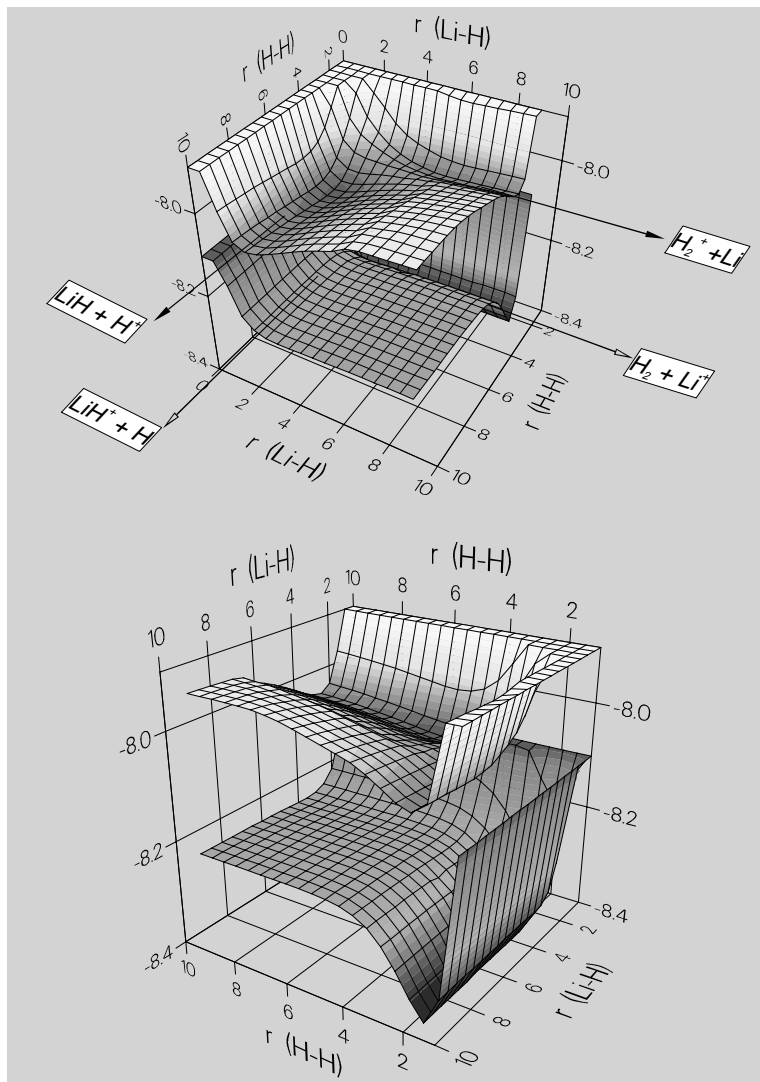
Figure 7.27: 3D view of the PES's for the first electronic states in the $\Theta = 0°$ geometry as a function of the two internal coordinates. The two plots differ only from the point of view of the relative perspective. All quantities are in atomic units.

in Fig.(7.28)[10]. This suggests that parts of the chemistry of the neutral and

---

[10]In similar system the seam of the conical intersection or the avoided crossing region is found in the critical C_{2v} geometry, where the charge-exchange process can take place; in our system this process indeed takes place in this geometry but it occurs between the first two *excited* states.
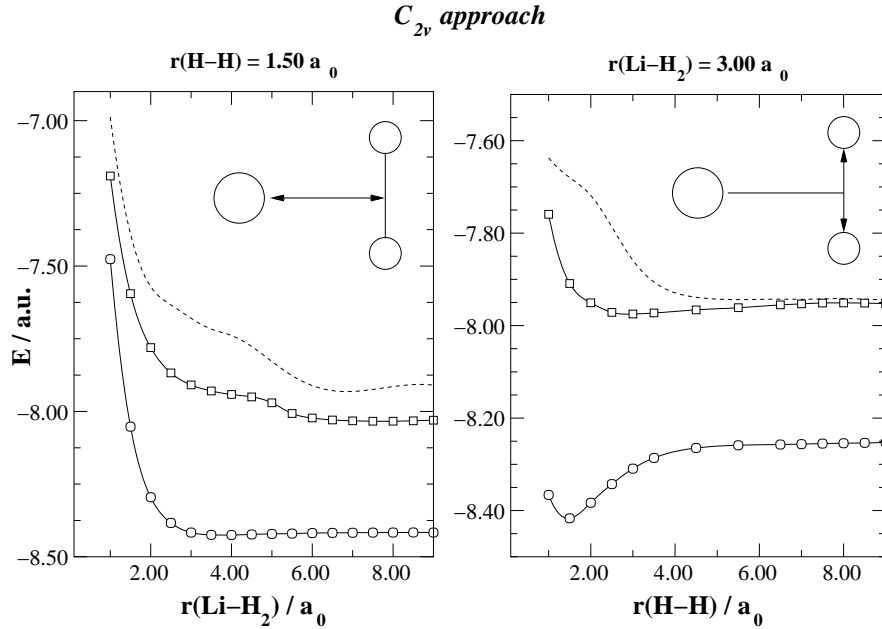
Figure 7.28: The computed potential energy curves for the complex breakup process along the C_{2v} symmetry path. Dashed lines are for the third state.

ionic species of lithium hydride have to be revised since most of the reaction paths that were expected to be efficient are probably adiabatically forbidden. The reason is that the two states show no intersections or non-adiabatic interactions in the whole configurational space, that is *there is no evidence of electronic funnels which can connect the upper state to the lower one*. In other words, there is no way in which a wavepacket "living" on one of the two surface can *flow* into the other *unless we envisage the intervention of the photon field* but this event seems to be rather unlikely.

Indeed, let us explain somewhat in detail this last point with an order-of-magnitude estimate of the relevant rate. Let us consider a multisurface event that goes from the first excited state to the ground state through a *spontaneous* emission process; the rates for the photon stimulated processes can be obtained from the rate of the spontaneous one. Now, if we look for the probability that along an excited state "trajectory" the system relaxes to its ground state, the probability of spontaneous emission is:

$$\frac{dP}{dt}(i \to f) = \frac{\mu_{fi}^2}{3\pi\hbar c^3} \left| \omega(i \to f) \right|^3$$

where μ_{fi} is the polarization-orientation averaged transition moment and ω is the frequency of the transition. In atomic units we can use the above expression and obtain

$$\frac{dP}{dt}(i \to f) \sim \mu_{fi}^2 \times \Delta E(i \to f)^3 \times 1.7 \cdot 10^9 \ s^{-1}$$

where we can consider a ΔE of the order of $5\,eV$ $(0.2\,E_h)$ and μ_{fi} to be about unity in a small volume of configurational space where the H^+ scatters near the LiH molecule and zero elsewhere. We could therefore consider l as the representative dimension of that small area of the configurational space in which the transition has a non-negligible probability of taking place. In this case the cross section of the "active" trajectories is l^2 and the probability of having a transition is $l \times (dP/dl)$ i.e. $lv^{-1} \times (dP/dt)$ where v is the relative velocity of the colliding systems. Therefore, the total cross section for a radiative reaction can be estimated to be: $\sigma \sim l^3/v \times dP/dt$ and the corresponding kinetic constant is $k \sim l^3 dP/dt$. In our case we can use the above formulas and set $l \sim 1.0 \div 10.0\,a_0$ to obtain a very crude estimate for $k \sim 2 \cdot 10^{-18} \div 2 \cdot 10^{-15}\,cm^3 s^{-1}$. Thus, the radiative reaction rates turn out to be well below the estimates provided by the recent literature for the non radiative processes (Bougleux and Galli, 1997)[11].

Let us now to focus on the reactions

$$LiH + H^+ \to LiH^+ + H \tag{7.6}$$

$$LiH + H^+ \to Li^+ + H_2 \tag{7.7}$$

$$LiH + H^+ \to Li + H_2^+ \tag{7.8}$$

$$LiH^+ + H \to Li + H_2^+ \tag{7.9}$$

$$LiH^+ + H \to Li^+ + H_2 \tag{7.10}$$
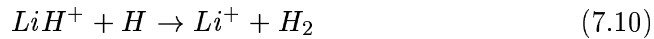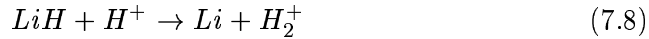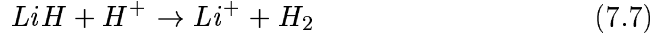
that are generally employed in the evolutionary models of the primordial Universe (see Chapter 5). A pictorial view of the possible reactions is presented in Fig.(7.29) where we draw schematically the energy levels of the various asymptotes involved and some arrows connecting them in order to represent the reaction pathways.

---

[11] The rates for the stimulated processes are N times the spontaneous rate, where N is the number of photons in the active volume of dimension l^3. Using the Planck distribution in the high temperature regime corresponding to $z = 1000$ we obtain a photon density (at an energy of $5\,eV$) of $n = 23.9\,cm^{-3}$ for a spectral range $1\,cm^{-1}$ wide; thus, this number is $N = 3.54\,10^{-21}$ which is extremely low even when the spectral range is increased by a factor of $10^3 - 10^4$. It is worth to note in this context that the relevant stimulated processes are actually three-body processes, $A + B + \gamma$, in which the density of photons comes from the black-body distribution law.
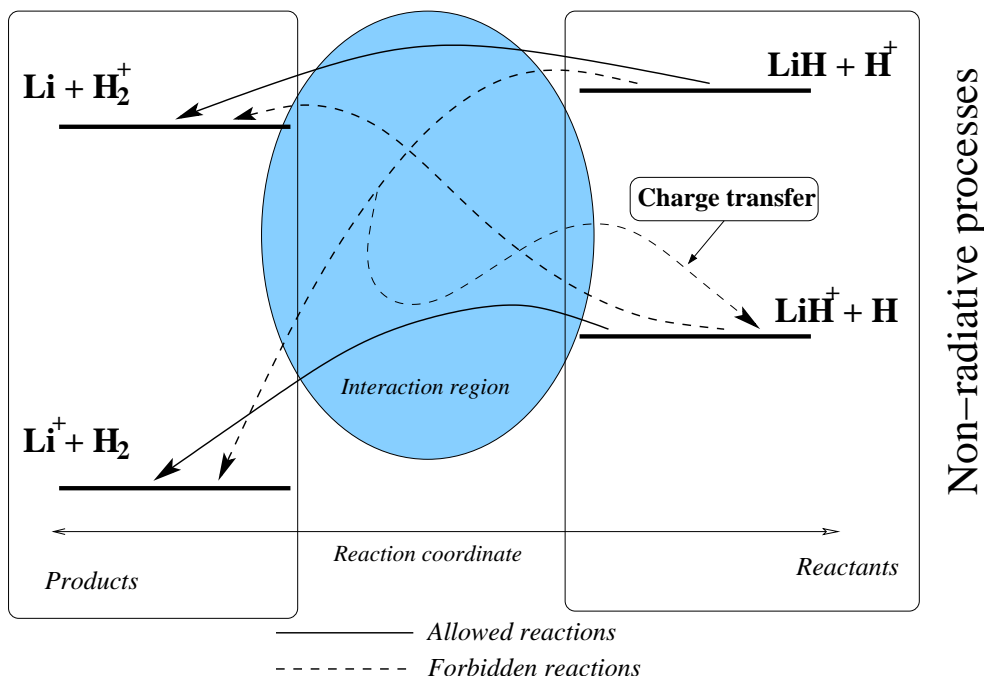
Figure 7.29: Allowed and forbidden adiabatic reaction pathways in LiH_2^+.

First of all, we may state that the charge transfer processes (CT) in equation (7.6) and in its inverse, although very common in highly polar systems, appears not to take place between the *ground-states* of the molecules involved. The CT process involves in fact the interchange between the asymptotic states $LiH^+ + H$ and $LiH + H^+$ that belong to the ground and first excited states respectively, a process that has been excluded above.

If we consider now the process which can lead to the destruction of LiH through formation of neutral molecular hydrogen (equation (7.7)) we can, as before, exclude this reaction from those relevant to the depletion of LiH from the primordial gas since, like the charge transfer reaction, in order to take place it requires a crossing between the electronic surfaces of the ground and first excited states.

Furthermore, among the processes that involve the H_2^+ molecular ion (the equations (7.8,7.9) and their inverse processes) the reaction that produces LiH^+ needs a jump between the two lower-lying PESs and therefore has to be considered forbidden. The other process seems, instead, to be particularly interesting because the surface connecting the reactants to the products (see Figure 7.16 on page 172) has a complex topology and will be subject of Chapter 9.

It is worth to mention at this point that reaction (7.10) appears to be inefficient in forming H_2 too, despite its high exoergicity, since it is strongly limited by the competing production of the dissociation product $(Li^+ + H + H)$ even in the singlet spin state considered in this work. We will consider in detail this aspect in the following Chapter.

Chapter 8

Collision Induced Dissociation of LiH^+

In this and in the next Chapter we will consider a reduced dimensionality quantum time-dependent treatment of the adiabatic processes left to us by the considerations of Section (7.4). There are several reasons why we planned the collinear calculations which, owing to the fact that they cannot produce any observable in the three-dimensional (real) space, are to be considered out of date when compared to $3D$ calculations (even with $J = 0$):

- At that time the full interaction potential was not available.

- We planned this preliminary analysis because the relevant processes were somewhat unusual. As a matter of fact, the CID process has received attention only in exact 2D and in *approximate* 3D quantum calculations (such as of the IOS type) and, on the other hand, reactions with long-range potentials like of the dipole-charge type has never been reported.

- Even if the $3D$, $J = 0$ calculations can be routinely done today they tell us very little from a quantitative point of view. The reason is that many partial waves contributes to the cross-sections in all but the very low collision energy regime, expecially when long-range potentials act between the collision partners.

In this Chapter we will consider the ground state adiabatic process in the two possible collinear geometries, while the excited state reaction in the $Li - H - H$ geometry will be the subject of the next Chapter.
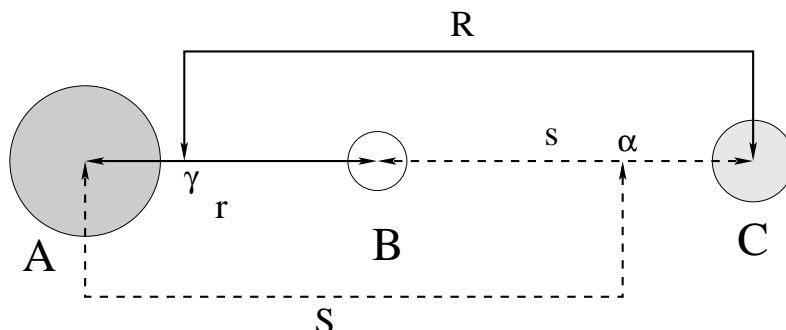
Figure 8.1: Jacobi coordinates for the collinear reaction $AB + C \rightarrow A + BC$. R and r are the reactants's Jacobi coordinates while S and s are the products' Jacobi coordinates. γ is the center of mass of AB and α is the center of mass of BC.

8.1   TD calculations

For the $AB + C$ collinear calculations to be discussed in these two Chapters we used the *reactants'* Jacobi coordinates of Fig.(8.1) in terms of which the hamiltonian reads as

$$H = \frac{P^2}{2M} + \frac{p^2}{2m} + V$$

where m is the reduced mass of the reagent molecule AB, M is the reduced mass of the $C - AB$ scattering system and p, P are the momenta conjugate to r, R of Fig.(8.1) respectively. As it is well known (see for example the book of R.D. Levine and R.B. Bernstein (1987)) the treatment is much more simplified if one *scales* the coordinates

$$Q_1 = \alpha R, \ \ Q_2 = \alpha r$$

choosing α in such a way that the kinetic energy term assumes a very simple form which we write in terms of the velocities $Q_i' = dQ_i/dt$, i.e.

$$H^0 = \frac{1}{2}\mu(Q_1'^2 + Q_2'^2)$$

where μ is some kind of *reduced mass* of the three-atom system. The usual choice for α is

$$\alpha = \left(\frac{M}{\mu}\right)^{1/2} = \left(\frac{m}{\mu}\right)^{1/2} \text{ with } \mu^2 = \frac{m_A m_B m_C}{m_A + m_B + m_C}$$

where m_A, m_B and m_C are the masses of the atoms involved. Without going into details we note that with the introduction of these mass-scaled coordinates

the dynamics of our system becomes equivalent to that of a point particle of mass μ subject to the potential $V(Q_1, Q_2)^1$. Since these coordinates are given explicitly by

$$
\begin{cases}
Q_1 = \alpha \left(\frac{m_A}{m_A + m_B} r + s \right) \\
Q_2 = \alpha r
\end{cases}
$$

where s is defined in Fig.(8.1) as the product internal coordinate, the new coordinate system is *skewed* with respect to the "chemical coordinate" system defined by r and s, the skewing angle being $tg^{-1}(m_B/\mu)$, where m_B is the mass of the atom *transferred* during the reaction.

In this Chapter we consider the ground electronic state of both the collinear geometries, $Li - H - H$ and $H - Li - H$. The surfaces in the corresponding skewed coordinates are reported in Fig.(8.2). The two directions of approach of the H projectile are markedly different simply because only the $\Theta = 0°$ orientation can lead to the formation of H_2. This last geometry shows an extremely exoergic pathway that is due to the large difference in the binding energy between products and reactants as one can easily see in Fig.(8.3) where we report the asymptotic potential profiles for LiH^+ and H_2 with their vibrational levels and density probabilities. On one side the LiH^+ molecular ion with its low binding energy ($D_e = 0.138$ eV), supporting *5* vibrational bound levels, has to be compared with the molecular structure of H_2 with *15* bound vibrational levels. (Taking into account the ZPE, the exoergicity of the reaction results to be 4.241 *eV*). Another striking aspect of the PES is the narrowness of the product channel, a feature that will strongly influence the dynamics as we shall see below. This is due to both to the electronic structure of the HH bond and to the light nature of the nuclei involved. The skewing angle that characterizes this surface is 48.6° because of the external position of the Li atom. A completely different situation occurs when the H atom impinges on the other side of the molecular ion; in this case the surface is, indeed, clearly symmetric, almost flat and with a shallow well due to the relatively weak polarization interaction between LiH^+ and H. In this case the skewing angle is of 82.8° degrees because this time the exchanged atom is the heaviest one.

---

[1]Similar coordinates can be introduced starting from the *products'* Jacobi coordinates and lead to an analogous expression for the kinetic energy operator in terms of *products'* coordinates. Thus, one of the main advantage of such scaling procedure is that in this way a reaction process reduces (asymptotically) to a simple rotation of the representative point of the system. Actually, the introduction of mass-scaled coordinates is the first step in defining the *hyperspherical* coordinates in which the arrangements appear at different values of the *hyperangle* (see for example B.R. Johnson (1980; 1983a; 1983b)). In our simple case the hyperspherical coordinates are simply the polar coordinates in the (Q_1, Q_2) plane.
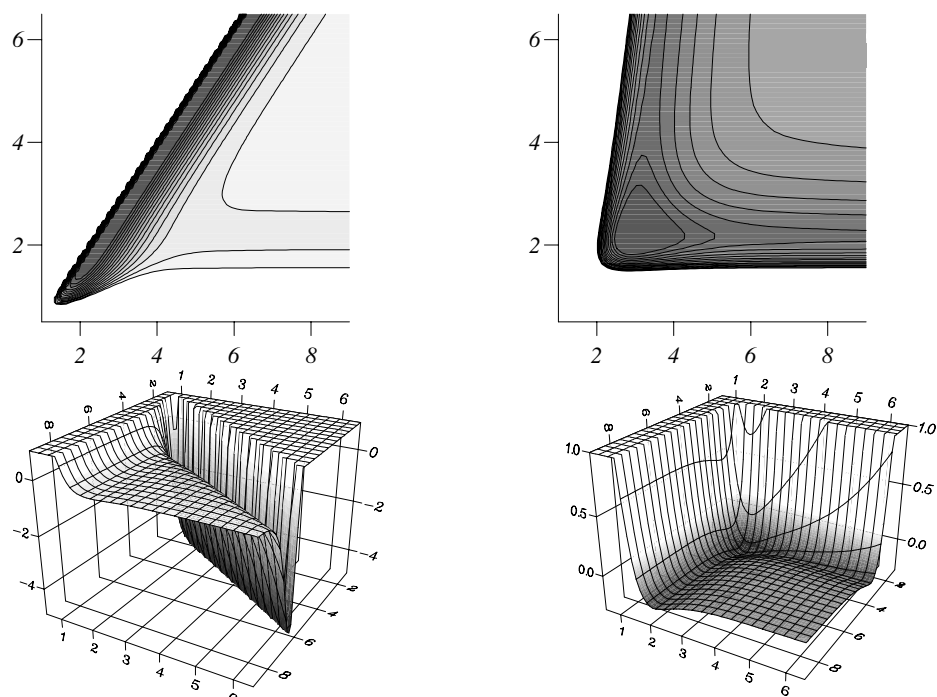
Figure 8.2: The two reactive PES's for the collinear collisions Li-H-H (left) and H-Li-H (right) in the ground state. On the left the energy ranges from *-5.0 eV* to *1.0 eV* while on the right from *-0.5 eV* to *0.5 eV*. In the upper panels the abscissae correspond to the mass scaled translational $[LiH - H]$ coordinate (Q_1), while the ordinates give is the mass scaled vibrational $[Li - H]$ coordinate (Q_2) (both distances are in Å).

8.1.1   Computational method

As one can see from Fig.(8.3), the triatomic dissociation threshold is here very low, due to the small binding energy of LiH^+, and thus the triatomic dissociation channel becomes open at a very low collision energy (0.111 *eV* for the ground vibrational level). The presence of reactive and dissociative channels within the same range of energies poses some conceptual and pratical problems in treating the dynamics. The difficulties arise when one uses an expansion over target states and are due to the presence of a non-orthogonal double continuum in the asymptotic basis functions associated with the full break-up: the continuum eigenfunctions of the LiH^+ would be needed to describe *both* the reaction forming H_2 and the full triatomic dissociation process (Diestler, 1979).

The presence of this double continuum requires that one should resort to the

Asymptotic molecular partners
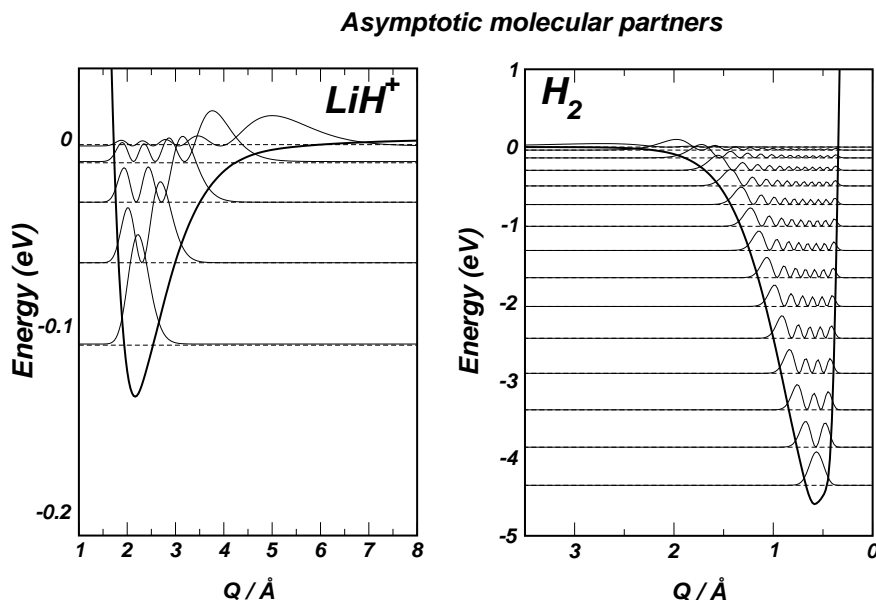
Figure 8.3: Asymptotic potentials of LiH^+ (left) and H_2 (right) referred to the dissociation limit as a function of mass scaled internal coordinates. Vibrational levels and probability densities are displayed.

use of hyperspherical coordinates that correctly describe on an equal ground both the dissociative and "reactive" continua, simply using a basis set made up of eigenstates of the "surface hamiltonian". This approach has the advantage of giving a complete description of the scattering process with a complete S matrix, but it should be mentioned that in the hyperspherical coordinates the propagation can be inefficient and time-consuming for a many channels problem (see the exploratory work of Kaye and Kuppermann (1981; 1985; 1988)). Most of the previous studies on the collision-induced dissociation involved a time independent scheme in hyperspherical coordinates which rely on a DVR representation of the scattering eigenfunction with the proper boundary conditions. In these studies (where a reactive channel was also present), only the collinear geometry has been investigated by Sakimoto and collaborators (1994; 1996; 1997) and by Onda and Sakimoto (1999). When the reactive arrangement can be neglected, instead, a full 3D calculation becomes feasible: both a semi-classical (Sakimoto, 1999; Sakimoto, 2000) and a quantum mechanical IOS description have been applied (Nobusada and Sakimoto, 1997; Nobusada and Sakimoto, 1998; Sakimoto, 1998) to simple systems like $He + H_2$.

Since we are not interested in the kinetic energy distributions of the three atoms (that would be given in terms of a complete S matrix), a grid description of the wavefunction is sufficient to obtain the *total* dissociation probabilities by computing all the bound-to-bound probabilities. Thus we used a full grid Time-Dependent scheme.

In our approach the initial wavefunction was taken to be the product of a minimum-uncertainty Gaussian wavepacket for the relative translational motion and a vibrational eigenfunction of LiH^+ (obtained by Numerov integration of our asymptotic Hamiltonian). The initial wavepacket, located well into the reagent asymptotic region (~ 10 Å), were chosen narrow enough to allow us to examine a wide range of collision energies with a single propagation without loosing accuracy in its representation on the chosen spatial grid. In particular, we employed seven different wavepackets (see Fig.(8.4)) each with an average
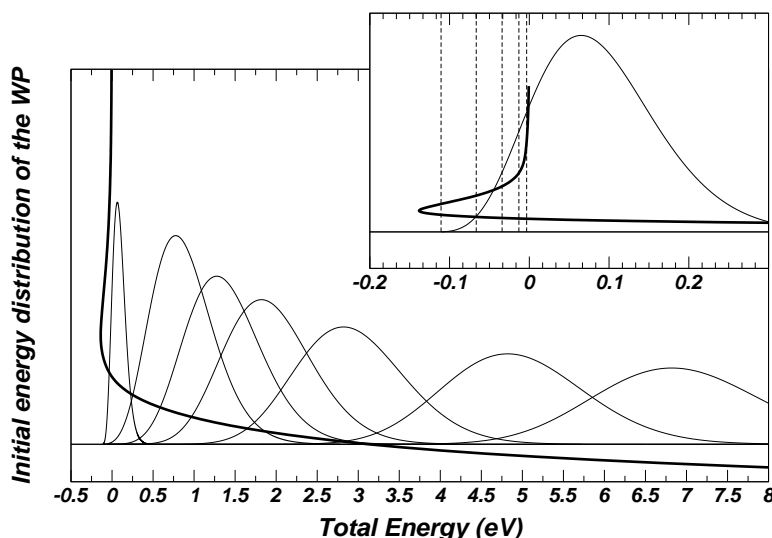
Figure 8.4: Distribution of energies for the seven wavepackets used in the calculations. The energy scale is the total energy with respect to the dissociation threshold of the three atoms. The thick solid line is the asymptotic potential of LiH^+. The inset shows the well region of this molecule with its bound vibrational levels.

width $\delta x = 0.125$ Å except for the lowest energy for which δx was chosen to be 0.27 Å to ensure that the resulting wavepacket had only momentum components directed towards the interaction region. The lowest energies considered were those at the triatomic dissociation threshold (as one can see in the inset in Fig.(8.4)) while all the other wavepackets were confined to energy regions

above the dissociation threshold. The time evolution of the wavepacket was carried out using the Split Operator method combined with the Fast Fourier Transform algorithm to evaluate efficiently the action of the kinetic energy part of the Hamiltonian on the wavefunction. The grid had to be dense enough to adequately represent all momentum components in the wavepacket. In particular we had to correctly represent the large energy gain due to the deep well ($\sim 4.5\,\text{eV}$) in the product region together with the collision energy. We therefore used different grid spacings depending on the collision energy: the finest-grained one was built with 384 points in 14 Å for the Q_1 coordinate (from 1 to 15 Å) and of 256 points in 8.5 Å for the Q_2 coordinate (from 0.5 to 9 Å). These parameters were sufficient to represent up to 20 eV in the entrance channel and up to 37 eV in the product channel. The propagation was carried out using a very short timestep (0.01 fs) to correctly account for the large potential energy difference experienced by the wavepacket when it enters the product channel. The calculation was continued until the 0.01% of the wavefunction was absorbed by the absorbing potentials placed at the grid boundaries. The absorbing potentials used were two cubic ramps of the functional form

$$V_{NIP} = \left\{ \begin{array}{cc} -iV_0 \left[\frac{q-(q_N-\Delta q)}{\Delta q} \right]^3 & q_N - \Delta q \leq q \leq q_N \\ 0 & \text{elsewhere} \end{array} \right.$$

where q_N is the grid boundary point, Δq is the width of absorbing region and V_0 is the strength of the absorbing potential. V_0 was set to the value of the mean kinetic energy of the wavepacket and the spread of the absorbing potential was set to 5 Å along Q_1 and to 3 Å along Q_2. All the parameters used were chosen after several test calculations and represent well stable solutions for all the considered dynamical quantities.

8.1.2 Bound-to-bound and dissociation probabilities

A complete grid representation of the wavefunction do not suffer the problems associated with the existence of a double continuum and thus it was possible to extract total dissociation probabilities from our 2D time-dependent calculations. One can, in fact, calculate the $i \rightarrow f$ state-to-state probability $P_{f \leftarrow i}$ using the usual Time-Energy mapping

$$\left| \int_0^\infty e^{iEt} \langle R_\infty | \left\langle f \Big| \psi_t^{(i)} \right\rangle dt \right|^2 = 2\pi\mu^2 a(E) \, P_{f \leftarrow i}(E) \tag{8.1}$$

Here $\left| \psi_t^{(i)} \right\rangle$ is the wavepacket at time t (initially prepared in state i), $|f\rangle$ is an asymptotic eigenfunction of the products (or of the reagents) and $|R^\infty >$

is a Dirac delta function of the scattering coordinate in the product (reagent) arrangement (located well inside into the asymptotic region) so that the spatial integral in (8.1) is actually to be performed on a dividing surface (on a line for 2D) placed into the relevant asymptotic region. As usual, the quantity $a(E)$ is the weight of the energy component E in the initial wavepacket.

If one chooses to represent the wavepacket in the *reagent* skewed coordinates, the calculation for the sub-reactive transitions is easily accomplished. For the product transitions, however, one has to transform the wavefunction into the mass scaled Jacobi coordinates of the products before evaluating the spatial integral in equation (8.1). Hence, we interpolated the wavefunction values on the original grid points by using the Fourier-based DVR basis set implicitly assumed in our calculation: the wavefunction at a given point in the product region $A(Q_1, Q_2)$ can in fact be obtained by

$$\psi(A) = \sum_{p}^{N_1 N_2} \psi(Z_p)\xi_p(A) \tag{8.2}$$

where $Z_p(Q_1^p, Q_2^p)$ is a point of the skewed grid, N_1 and N_2 are the grid dimensions and the basis functions are

$$\xi_p(A) = \frac{1}{N_1}\frac{sin\left\{\frac{N_1\pi(Q_1-Q_1^p)}{L_1}\right\}}{sin\left\{\frac{\pi(Q_1-Q_1^p)}{L_1}\right\}} \frac{1}{N_2}\frac{sin\left\{\frac{N_2\pi(Q_2-Q_2^p)}{L_1}\right\}}{sin\left\{\frac{\pi(Q_2-Q_2^p)}{L_2}\right\}} \tag{8.3}$$

with L_1 and L_2 being the periods of the grid in two dimensions (i.e. the grid lengths plus one more spacing for each direction) . Thus, we could represent the wavefunction over a line sufficiently far from the interaction region and which coincided with the vibrational coordinate of the products. It is worth to note at this point that the contribution from the various basis functions defined by equation (8.3) is very localized in space and thus we could evaluate the wavefunction at a given point A (on the product analysis line) summing up in equation (8.2) only the contributions from the points Z contained in a square centered in A. The size of the square was limited to the first nearest 100 grid points. Different test calculations were carried out to correctly place the analysis line and to determine the optimal length and spacing of it. We used a sufficiently long line to correctly represent the highest vibrational wavefunction of H_2 and the grid spacing used in the evaluation of the integral (8.1) was taken to be comparable to that of the two dimensional grid. We checked the numerical stability of the final transition probabilities to changes in the parameters which characterize the analysis line by preparing a wavepacket in the exit channel as a superposition of vibrational functions of the products
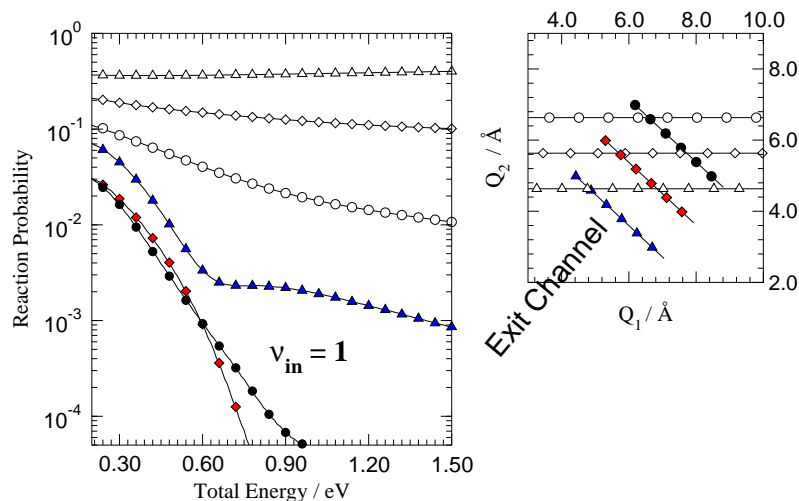
Figure 8.5: Left panel: computed reaction probabilities. Right panel: position of the analysis lines employed. Filled-in symbols refer to the method described in the text, open symbols are for the usual flux approach.

and evolving it in time toward the asymptotic region under the influence of the solely asymptotic product potential.

The correct evaluation of the reactive and, simultaneously, of the non-reactive transition probabilities (that we call here bound-to-bound transitions) allowed us to have the *total* dissociation probabilities simply by using

$$P_n^{CID}(E) = 1 - \left(P_n^R(E) + P_n^{NR}(E) \right)$$

where n is the initial vibrational level and P_n^R and P_n^{NR} are the total reactive and non-reactive transition probabilities (i.e. summed over all the final vibrational states of the reagents and of the products).

It is worth to mention here that the common *flux approach* usually employed to obtain the *total* reaction probability from the total flux in the product channel *cannot* be used in this context. The reason is that, clearly, the total flux contains contributions both from the reaction *and* from the dissociation. This is illustrated in Fig.(8.5) for the $LiH(n = 1)^+ - H$ scattering system, where in the left panel we compare the results obtained from the usual flux approach (open symbols) with those obtained from the state-to-state product analysis outlined above (filled-in symbols). Different analysis lines were considered (right panel); in particular for the flux approach we used, as usual, the translational coordinate of the reagent while for our state-to-state analysis we had to employ the vibrational coordinate of the product molecule. It is clear

from the Figure that the total flux results converge slowly to the "exact" results as we move the line further and further away from the interaction region. Futhermore, it should be noted that the total flux results converge because, as we shall see below, the dissociation proceeds "on the reagent side"; in general, the total flux results are even not guaranted to approach the exact ones.

8.2   Results

8.2.1   The collinear reaction Li-H-H

The first geometry that we sampled is the one that should be the most likely for the reaction $LiH^+ + H \rightarrow Li^+ + H_2$ to happen. As previously mentioned, the energy profile is extremely exoergic ($\sim 4.2\,eV$) and thus one should expect a fast transformation of LiH^+ into H_2, but, as we shall see below, the impact of the wavepacket on the repulsive wall opposite to the reagent channel will instead preferentially break up the initial diatom. Indeed, the motion of the wavepacket is very simple and consists of two successive impacts, the first on the H_2 repulsive wall and the second on that of LiH^+; the wavepacket, then, returns to the reagent side having become widely spread in space due to the CID process (see Fig.(8.6)).

To clarify the situation we report in Fig.(8.7) the total probabilities for the three processes that can take place just above the dissociation threshold. For each process we show the results obtained with an initial state prepared in each of the first three vibrational levels. The filled-in circles are reaction probabilities, the open circles are the subreactive probabilities and the filled-in squares are the dissociation probabilities. For a wavepacket prepared in the ground vibrational state the non-reactive process (i.e. the permanence of a bound LiH^+ after the collision) is dominant although an increase in energy tends also to increase the dissociation products. Here we see that the threshold is not clearly defined for $n = 0$ since the energetic threshold does not coincide with the dynamical one, as already noted in previous works (see for example Nobusada, Sakimoto and Onda (1995) and reference therein)[2]. As LiH^+ is prepared in a vibrationally excited state, a marked enhancement of the disso-

---

[2]It should be noted that in 3D simple phase-space arguments give the $\sigma \propto E_r^{(n-2)/2}$ threshold law (with $E_r = E - E_{thresh}$), where n is the number of unbound degrees of freedom (Sadeghpour et al., 2000). These arguments rely on the fact that the corresponding *momentum T* matrix elements tends to be a *non-null* constant at the threshold and thus the result follows from "kinematic" factors (for example, in the 2-body case $\sigma \propto E_r^{1/2}$ follows from eq.(3.17) on pag.75 when $f \rightarrow const$ as $P_\beta \rightarrow 0$). Here we are focusing on the probabilities which in 3D correspond to the squares of the *angular momentum T* matrix elements; for the CID process these elements should be linear in E_r to ensure a non-null threshold behaviour of f.
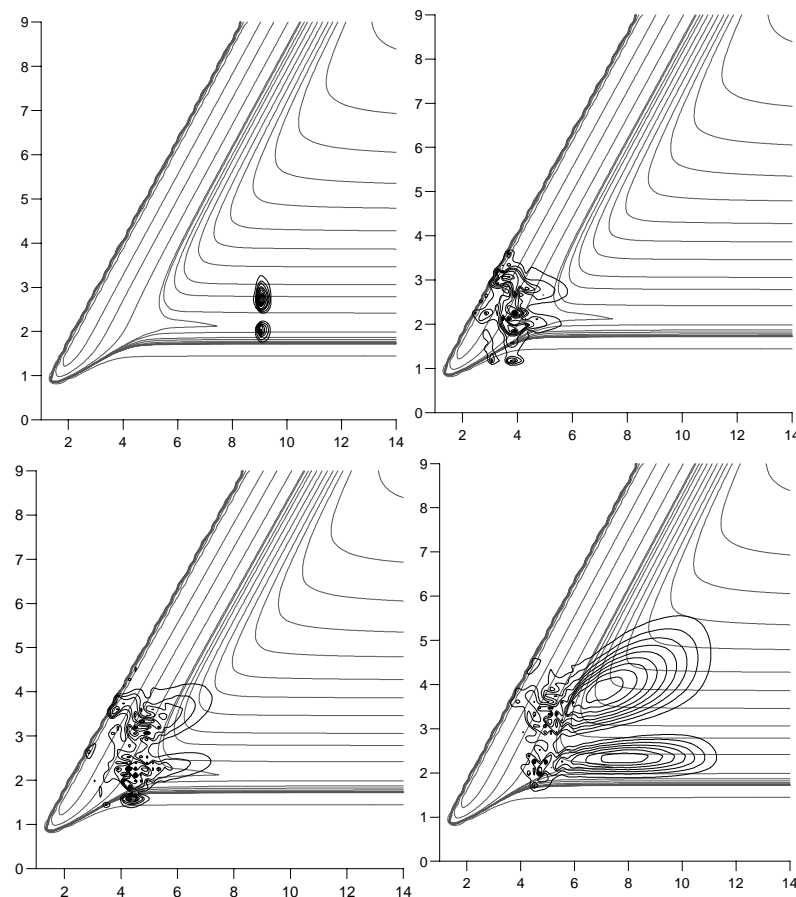
Figure 8.6: Some significative snapshots of the time evolution of the wavepacket.

ciation process is clearly evident in the figure: the dissociation is the dominant process both for $n = 1$ and $n = 2$, already at a fraction of an eV above threshold. The most striking result is given by the almost complete *absence of reaction* (filled-in circles in Fig.(8.7)) even when the energy is just above the threshold (0.1-0.5 eV). The highest reaction probabilities are observed for the $n = 2$ initial vibrational level, but they still do not exceed 20% of the total and decrease rapidly with increasing total energy. The absence of reactive contributions is probably due both to the narrowness of the potential well where the products are formed and to the reduced vibrational inelasticity of the exit channel, features that make the products not able to absorb efficiently the release of excess energy.

If we now look at the dissociation probabilities as a function of the collision

Behaviour above dissociation threshold
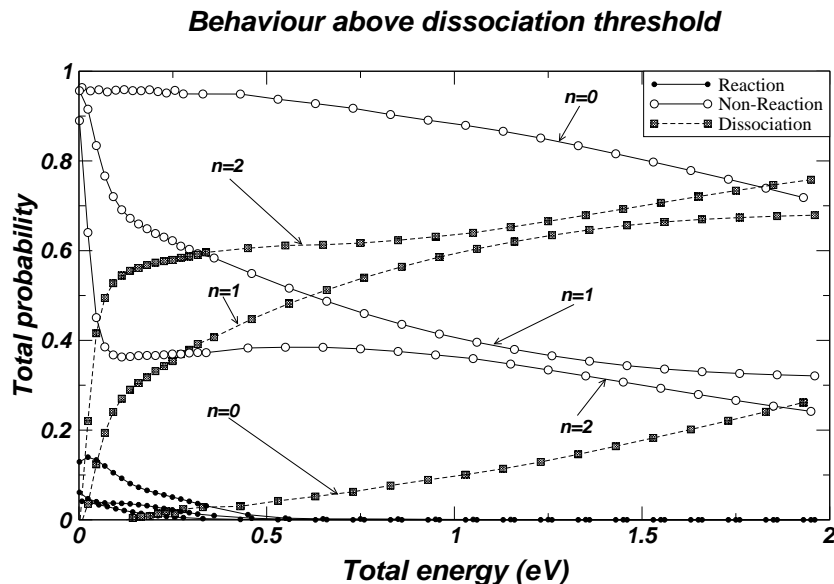
Figure 8.7: Total probabilities for the three possible processes at low energy (above dissociation threshold $E=0\ eV$) as a function of total energy. The three sets of curves refer to the lowest three vibrational levels of LiH^+.

energy over a broader range as in Fig.(8.8) we clearly identify the thresholds corresponding to the different initial vibrational energies and, for collision energies below 4 eV, we can see the effect of the vibrational enhancing due to the "heating" of the reagents. For higher energies the vibrational excitation of the reagent is no more the driving force of the break-up process and a vibrational suppression is observed instead.

One striking feature of the curves shown in Fig.(8.8) is the presence of *shoulders* that have already been noted by several authors before in systems where there are no rearrangement channels available (e.g. see Nobusada, Sakimoto and Onda (1995) and reference therein). The presence of these shoulders in our case appears to be linked to the *dynamical* absence of reaction during the collisional event. We point out that the number of such shoulders is equal to the vibrational quantum number of the initial wavepacket. This seems to be an indication of the *direct dynamics* taking place on this very simple potential energy surface. Indeed, when one looks at the *final* wavepackets one clearly notes a sort of *memory effect* of the initial vibrational state. As shown in Fig.(8.9), the wavepacket spreads in space because of the dissociation process,
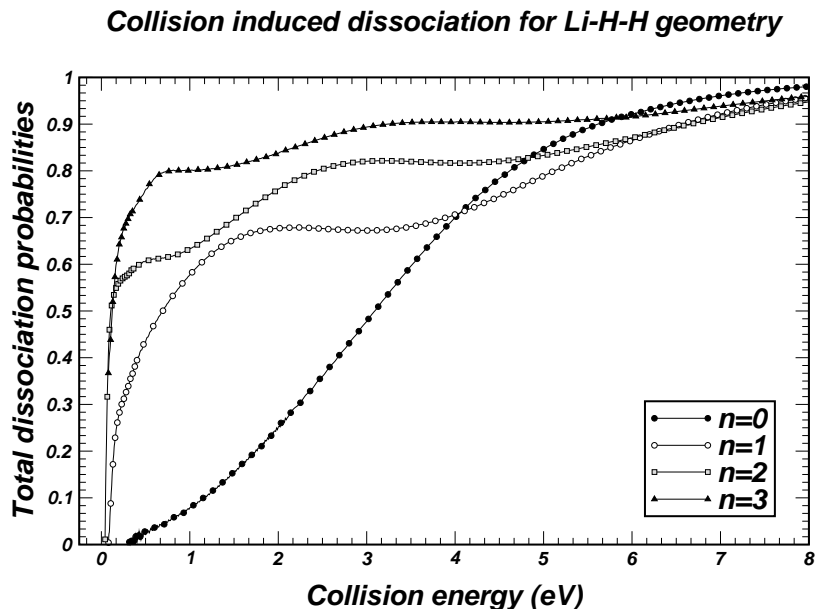
Figure 8.8: Total collision induced dissociation (CID) probability as a function of collision energy for the first 4 initial vibrational levels of LiH^+.

but preserves the initial nodal structure of the molecular bound state selected for the process. The *discrete* contribution of each lobe of the wavepacket to the break-up flux seems to be responsible for the previously mentioned structured CID probabilities. It would be interesting to see if such structure is preserved also when the full dimensionality of the problem is taken into account.

8.2.2 The collinear reaction H-Li-H

The second geometry considered here corresponds to $[H - Li - H]$ in which case the possible reaction is degenerate and is

$$H_a + LiH_b^+ \rightarrow H_aLi^+ + H_b$$
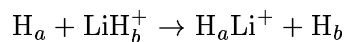
The surface showed in Fig.(8.2) exhibits a shallow well that is due to the weak polarization forces between the H atom and the charged molecule. We choose to perform an analogous set of calculations in this arrangement to see if the pattern for the collision induced dissociation remained similar to the one already found for the other geometry. Although not entirely rigorous, this further test could help us to more clearly understand if a full dimensional
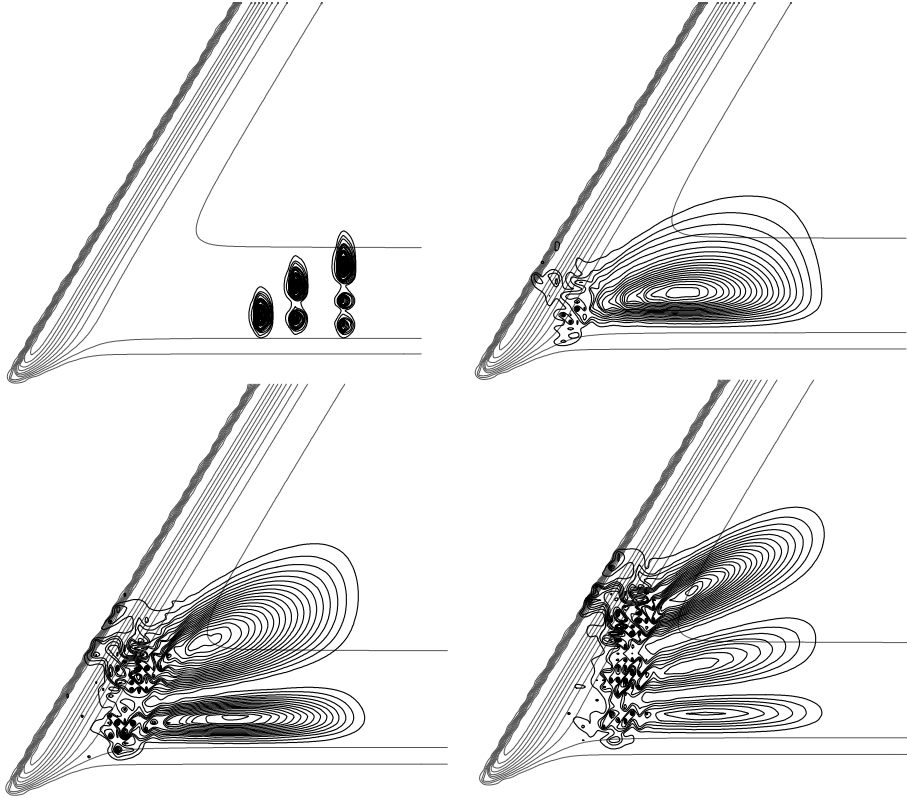
Figure 8.9: Initial and final stage of the evolution of the probability density for a wavepacket prepared in the first three vibrational levels of LiH^+. In the upper panel on the left we have the initial situation for the three different wavepackets (shifted in Q_1 for clarity) and in the remaining panels the situation soon after the collision (90 fs) for a mean kinetic energy of 1.0 eV.

calculation could lead to similar results at least for the general behavior of the dynamics.

In Fig.(8.10) we report the results for the collision induced dissociation probabilities in a similar way to that of Fig.(8.8). As one can see, the results do not change much in this other orientation. The physical picture of a reactive dynamics dominated by CID processes is maintained. Such a test helps us to make more realistic the assumption that all the properties of the dynamics are determined by the interaction of the wavepacket with the repulsive walls. Also in this second geometry, the total flux is shared between the dissociative and the subreactive events. This is why we can observe in Fig.(8.10) the same shoulder structure seen before in Fig.(8.8). In this case the structure is even

Collision induced dissociation for H-Li-H geometry
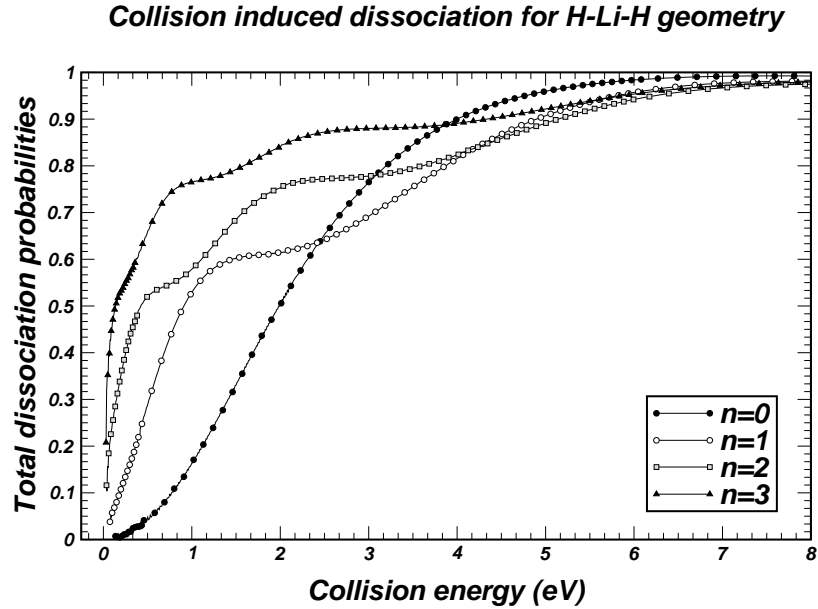
Figure 8.10: Collision induced probabilities for the $H - Li - H$ orientation. See Fig.(8.8).

more evident showing here a perfect correspondence with the initial vibrational states up to the $n = 3$ level.

8.2.3 The effect of isotopic variations

One of the interesting results of the above analysis is that, even in the most favorable orientation *Li-H-H*, the collision does not lead to the production of an appreciable quantity of H_2. The specific shape of the PES allowed us to suggest that such a behavior was due to the particularly narrow shape of the H_2 exit channel. In order to further check this hypothesis, we consider here the effect of an enlargement of the well in the exit channel which arises from the mass changes of the isotopic substitutions in the mass-scaled coordinate system. Two kind of isotopic substitution have been examined:

$$LiD^+ + H \rightarrow HD + Li^+$$

and

$$LiH^+ + D \rightarrow HD + Li^+$$
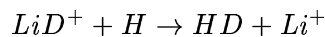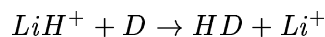
In Fig.(8.11) we report the total dissociation probabilities, together with the

Total Probabilities for LiX$^+$ (n=1)
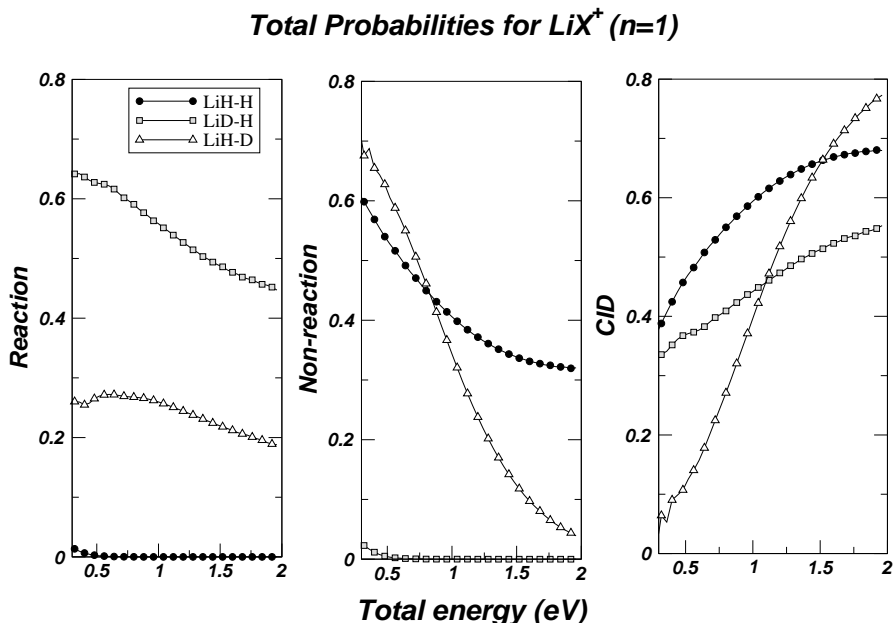
Figure 8.11: Total reaction, non-reaction and CID probabilities for the three different isotopic variation examined in the text. The energy scale is the total energy and thus the dissociation threshold is the zero of the scale.

subreactive and reactive fluxes for the average collision energy of the wavepacket of 1.0 eV and for the $n = 1$ initial vibrational state. The most striking result is that, in both cases, the reaction is highly enhanced and becomes, at least for LiD^+, the dominant process. This is mainly due to the greater ability of the product HD to absorb the excess of translational energy with respect to previous case of H_2. In the case of HD, in fact, the density of vibrational states is greater near threshold and the resulting potential energy surface has a less narrow exit channel (in the mass-scaled coordinates). However, the comparison between the two isotopic variants here considered, that lead to the same product molecule, suggests that the situation is somewhat more complicated: in the case of the reagent LiD^+ the reaction appears also to be helped by the *heavier* atom trasferred[3]. In fact, an opposite behavior is registered for the non-reactive

---

[3]The differences in the distribution of masses of the reactions here considered lead to a *greater* skewing angle for the first reaction system. The results obtained are, thus, somewhat unusual since one expects a higher reactivity when the translational coordinate of the product is more aligned with the translational coordinate of the reagent (i.e. heavy-ligth-heavy system). This fact reveals the importance of the reagent diatomic potential.

process, where, surprisingly, the isotopic substitution $LiH^+ \rightarrow LiD^+$ *reduces* significantly the occurrence of the sub-reactive transitions during collisions.

If we look at the probability density plot given in Fig.(8.12), we see how
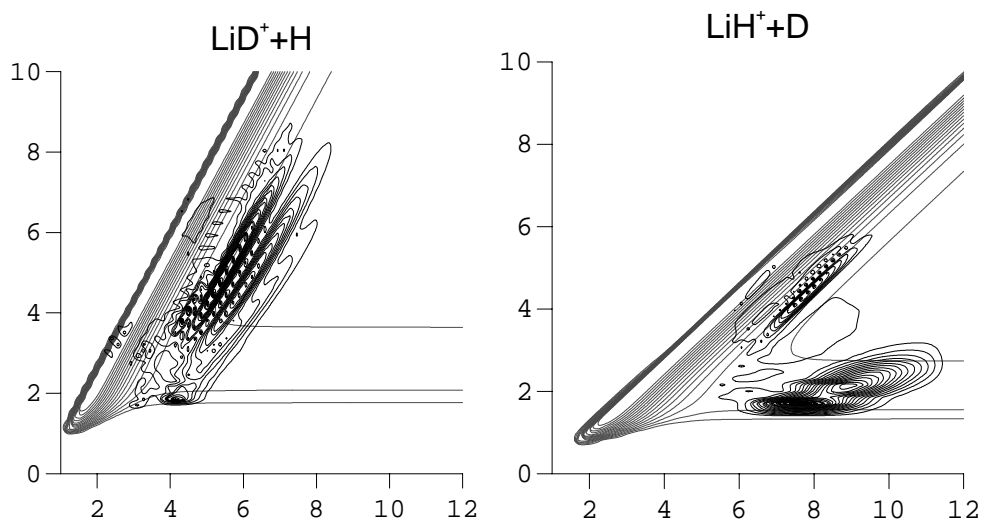
Figure 8.12: Probability density contour plots for the reaction of $LiD^+(n=1) + H$ (on the left) and $LiH^+(n=1) + D$ (on the right) at the end for the reaction (100 fs) for a 1.0 eV of kinetic energy. Distances are in Å.

the distributions of the final wavepacket are dramatically different from the one previously investigated for the non-isotopic reaction. As we see in the left panel of Fig.(8.12), the representative wavepacket of the $LiD^+ + H$ system reacts and dissociate mostly in the product region while that of the $LiH^+ + D$, shown in the right panel, continues, as the lighter case, to dissociate mostly in the reagent region.

An interesting further difference between the three isotopic variations has been found when analyzing the threshold behavior of the reaction probabilities. The reaction probability for a wavepacket prepared in the initial vibrational state $n = 1$ is displayed in Fig.(8.13). In the case of $LiH^+ + H$ the reaction probability rises sharply just above threshold, reaches a maximum at $\sim 0.25\,\text{eV}$ and then begins to decrease until, as we already know, reaches smaller and smaller values as the energy increases. The behavior of the $LiD^+ + H$ reaction is almost similar, but the rise of the probability is much steeper now. The behavior of the probability is, instead, completely different for the $LiD^+ + H$ reaction: it rises with a step-like shape much like what happens with quantized transition state energy levels (see for example Mahapatra and Sathyamurthy
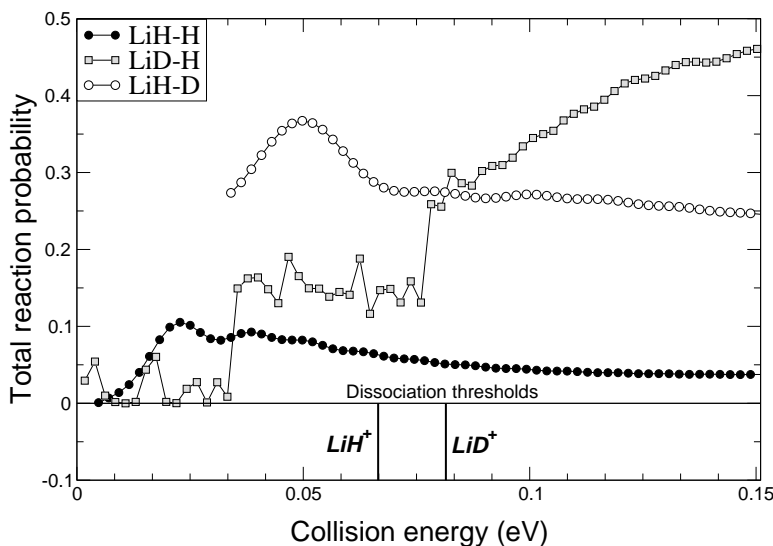
Figure 8.13: Reaction probabilities as a function of collision energy for the reaction $LiX^+(n = 1) + Y \rightarrow Li^+ + XY$ where (X,Y)=(H,H), (D,H), (H,D).

(1996) and references therein)[4].

8.2.4   Final state analysis

As we have discussed before, we obtained from our calculations the state-to-state transition probabilities for the reactions forming H_2/HD. We can, thus, analyze the behavior of reagents' and products' populations over the vibrational states.

Let us briefly consider the non-reactive analysis of the $LiH^+ + H$ case. We have already mentioned that most of the flux after the reactive event is shared by the subreactive and the dissociation channels. In the subreactive

---

[4]It should be noted that the reflection of the wavepacket at low energy on the absorbing potential was a serious problem in our calculations and therefore these considerations are somewhat speculative. This problem is indeed one of the main drawback of the time-dependent calculations: at low energy the dynamics may be strongly distorted by the reflection on the boundaries. One promising solution, that came out after this work was started, is to accelerate the slowly moving wavepacket before absorbing it (Hussain and Roberts, 2000). In this case one should only take care of avoiding reflection *from the accelerating well*, but this last problem is simpler to solve than the previous one.

channel the LiH^+ moiety turned out to have a vibrational population *spread* over its entire vibrational spectrum and markedly dependent on the collision energy. This can be seen in Fig.(8.14) , where we report the elastic and some of
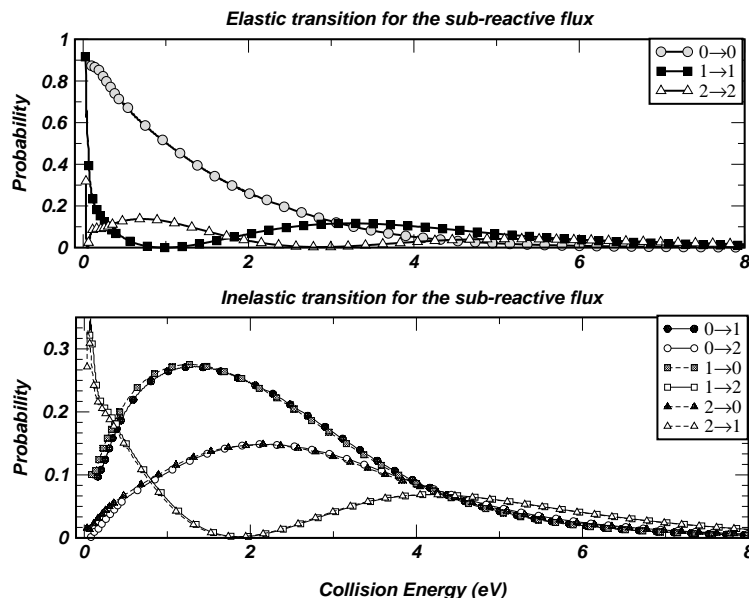
Figure 8.14: Sub-reactive probabilities as a function of collision energy. Upper panel for the elastic transition, lower panel for the inelastic vibrational excitations and relaxations. For clarity of presentation only transitions for $n < 3$ are reported.

the inelastic transition probabilities as functions of the collision energy[5]. The dependence of the probabilities from the collision energy can be razionalized by looking at Fig.(8.9) on pag.202, where we see that the probability density after the scattering event, while maintaing the initial nodal pattern, is strongly distorted by the effect of the repulsive wall and is *pushed outward* with respect to the initial situation. Thus, the oscillations of the probabilities seem again to be the imprints of the various *lobes* of the final wavefunction going through the bound LiH^+ asymptotic region and lead to the shoulder structure in the total CID probabilities shown before because of the absence of reactive contributions. However, *these non-reactive oscillations should persist (in a direct dynamics)*

---

[5]It is worth to note that the non-diagonal transition probabilities in the lower panel of Fig.(8.14) satisfy the micro-reversibility principle (the vibrational energy is quite low on such a scale) although they come from the time evolution of different wavepackets, thereby showing the accuracy of our calculation.

even when a reaction takes place, while the existence of the structure in the CID probabilities seems to be due to the absence of reactions.
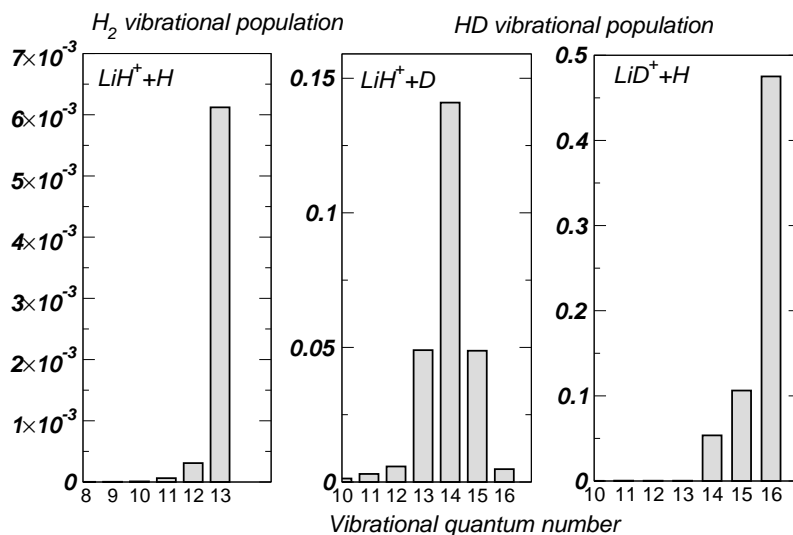
Figure 8.15: Population analysis for products H_2 and HD for the three reactive processes examined here.

Let us now focus on the products' analysis. In Fig.(8.15) we plot as histograms the population of the final vibrational states for the three processes examined here for an average total energy of 1 eV and an initial wavepacket prepared in the $n = 1$ state. We see that, as already noted, HD can absorb the excess energy much better than H_2 because of a higher density of states near the dissociation threshold; thus, besides the difference in the magnitude of the total reaction probabilities discussed above, HD comes out from the reactions with a population that is distributed over many vibrational levels. In any case, however, the most striking feature is that the reaction produces always a *vibrationally hot* diatomic molecule with an almost inverse Boltzmann population. A vibrationally *hot* hydrogen molecule was also found in the classical dynamics study of the collinear neutral reaction $LiH + H \rightarrow Li + H_2$ as done by Clarke et al. (1998b); in that case the surface structure was almost similar to the one examined here although the exoergity was five times smaller. This fact can be attrubuited to the lack of vibrational inelasticity in the product channel.

8.3 Vibrational image?

In this Section we speculate somewhat on the origin of the shoulder structure in the CID probabilities, that Sakimoto and collaborators already interpreted as an interference phenomena between vibrational trajectories with different vibrational phases. In the previous Section we noted that the number of shoulder equals the vibrational quantum number of the initial state, thereby arguing a closer connection between the initial vibrational state and the dissociation pattern. This connection was enforced by the shape of the *final* wavefunction: we noted the existence of a sort of "memory effect". Here, we can go somewhat deeper in this analysis.

We recognize that the very simple dynamics (see for example Fig.(8.6) on pag.199) that takes place in our system is mainly determined by the *repulsive* atom-atom interactions. In effect, we expect on classical grounds that all the CID processes, at least for sufficiently high energy, are solely determined by the short-range two-body repulsive interactions[6]. We therefore apply the Born approximation to a model three-dimensional ABC system in which the potential is a simple sum of two body terms,

$$V(\mathbf{r}_\alpha, \mathbf{R}_\alpha) = V_{BC}(\mathbf{r}_\alpha) + V_{AC}(\mathbf{r}_\beta) + V_{AB}(\mathbf{r}_\gamma)$$

where V_{BC} is the bonding potential of the molecule BC subject to the dissociation process (i.e. $A + BC \to A + B + C$) and V_{AC} and V_{AB} are atom-atom repulsive interactions (each potential is a function of the corresponding relative position vector, which we write following the usual labelling of the arrangments in three-body systems, see Section (3.1)). In doing this we use the results of the "dumb-bell" model, developed in the fifties for inelastic collisions (see Section 2.3 of the book of Levine (1969)). The modifications brought to those results are very simple and lead to the following Born transition amplitude

$$t_B(\mathbf{P}_\omega \leftarrow \mathbf{P}_\alpha; \alpha) = V_{AB}(\mathbf{q})\widehat{\phi}_\alpha(-\zeta\mathbf{q} - \mathbf{g}) + V_{AC}(\mathbf{q})\widehat{\phi}_\alpha((1 - \zeta)\mathbf{q} - \mathbf{g})$$

where

- $|\mathbf{P}_\alpha; \alpha\rangle$ is the initial A+BC state, $\langle\mathbf{r}_\alpha\mathbf{R}_\alpha|\mathbf{P}_\alpha; \alpha\rangle = (2\pi)^{-3/2}e^{i\mathbf{P}_\alpha\mathbf{R}_\alpha}\phi_\alpha(\mathbf{r}_\alpha)$, in which $\mathbf{R}_\alpha$ is the position of BC relative to A and $\mathbf{r}_\alpha$ is the position of B with respect to C.

- $\mathbf{P}_\omega$ is the set of two vectors $(\mathbf{G}, \mathbf{g})$ that characterize the final dissociated state; they are eigenvalues of the momenta conjugated to the $(\mathbf{R}_\alpha, \mathbf{r}_\alpha)$ coordinates.

---

[6]The energy must be high enough to suppress any possible reaction process.

- ζ is a mass factor, $\zeta = m_C/(m_C + m_B)$.

- $\mathbf{q}$ is the momentum transfer, $\mathbf{q} = \mathbf{G} - \mathbf{P}_\alpha$, which actually is a "partial momentum" transfer; that is, it is the *the projectile-target relative momentum* transferred during the collision.

- $V_{AB}(\mathbf{q})$ is the Fourier transform of the potential, $V_{AB}(\mathbf{q}) = \int d\mathbf{r} e^{-i\mathbf{q}\mathbf{r}} V_{AB}(\mathbf{r})$, and $\widehat{\phi}_\alpha$ is the Fourier transform of the initial bound state, $\widehat{\phi}_\alpha(\mathbf{u}) = \int d\mathbf{r} e^{-i\mathbf{u}\mathbf{r}} \phi_\alpha(\mathbf{r})$.

In this formula we see the presence of a Fourier transform of the initial state: the dynamics is istantaneous and the distribution of the products is determined by the *momentum wavefunction* of the initially bound molecule; that is, the scattering outcome turns out to be an *image* of the distribution of momenta of the molecule. To make a closer connection with our results we note that in the collinear problem only one of the two "dissociating" potentials acts and therefore the amplitude reduces to a single contribution, for example

$$t_B(\mathbf{P}_\omega \leftarrow \mathbf{P}_\alpha; \alpha) = V_{AB}(\mathbf{q})\widehat{\phi}_\alpha(-\zeta\mathbf{q} - \mathbf{g})$$

From this result the shoulder structure in the *total* probalities *could* arise as a superposition of a background contribution (the $V_{AB}(\mathbf{q})$ term) with the momentum distribution of the initial state of the diatomic. As a matter of fact, the magnitude of the last contribution arises (both in 3D and in the collinear geometry) from the vibrational wavefunction and, thus, $\widehat{\phi}_\alpha(\mathbf{u})$ has the same shape of the vibrational wavefunction (*as a function of its argument* $\mathbf{u} = -\zeta\mathbf{q} - \mathbf{g}$).

Although plausible, the argument should be retained solely speculative until the appropriate proofs are not provided. Indeed, some points has to be clearified: (i) how the vibrational pattern persists on the *total* (i.e. integrated over all allowed $(\mathbf{G}, \mathbf{g})$ for a given energy) probabilities/cross-sections as a function of the *energy* ($\equiv \mathbf{G}^2/2\mu_\alpha + \mathbf{g}^2/2m_\alpha$); (ii) how this vibrational pattern is modified by the "background" contribution (the number of peaks in the $n-th$ vibrational eigenfunction is $n + 1$ and not n).

On the other hand, we note that the "single contribution" result is not restricted to the 2D case; for example, when $m_B \gg m_C$ $\zeta \simeq 0$ and the interaction with the (very heavy) atom B of the diatomic will not contribute much to the transition. Thus the possibility that such phenomenon is not due to the constrained motion considered in this Chapter should be taken into account.

Chapter 9

Collinear $LiH + H^+$ reaction

The first excited state dynamics is completely different from the ground state one. The deep wells, due to the electrostatic interactions, that are present in the surface tend to capture the wavepacket and the probability pattern is filled in with resonances. This is one of the limits of the simple collinear model employed here: since it does not allow the molecules to rotate, the long-lived states are not disturbed by centrifugal forces/rotational motion and the corresponding resonances halfwidths are very small. Neverthelss, also in this case we can obtain useful (although qualitatively) indication about the dynamical process. In this Chapter we will first consider the initial state selected dynamics and then we will focus on of the transition state resonances and bound states. Since we were interested only in the reaction process, we limited our analysis to the collinear $LiH - H$ geometry.

9.1   The reaction probabilities

In Fig.(9.1) the excited state surface is reported in skewed coordinates. The two minima of Fig.(7.16) on pag.172 are now, stretched and compressed by the mass scaling factors in the new coordinates but the main conclusions that we drew in Chapter 7 remain the same. Indeed, if we imagine a trajectory starting in the lower-right corner of the surface directed straight toward the dark minimum in the lower part of the figure, we see how it should be difficult for it to reach the transition state unless a high degree of vibrational excitation is present in the initial wavepacket. That is, the geometry of the transition state in the "dynamical" (skewed) coordinates is still such that we expect a vibrational enhancement of the reactive probability, as it usually found in *direct* dynamical processes. However, the presence of the deep minimum in the entrance channel clearly influence the dynamics since this deep well can

easily "capture" the wavepacket giving rise to a complex series of long-lived resonant states.
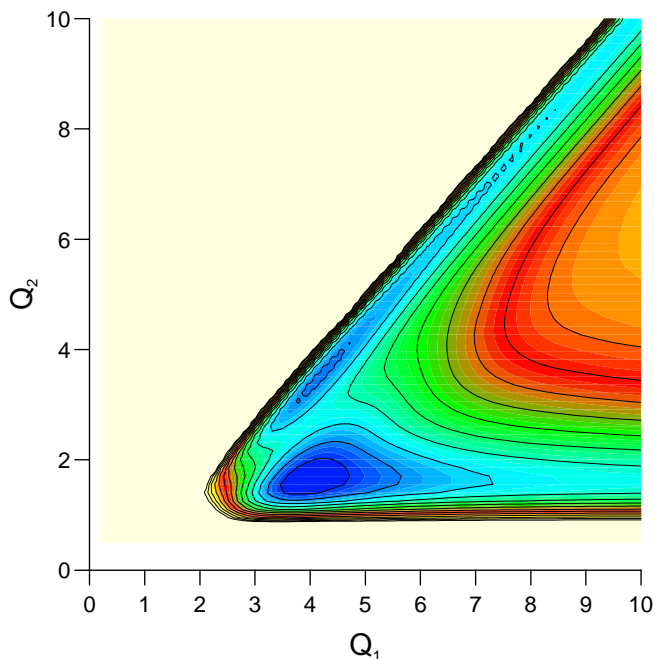
Figure 9.1: Excited state surface in skewed coordinates.

The dynamical calculations were done as in the previous Chapter using the time-dependent approach. As for the ground states we used an initial wavepacket localized in the reactants asymptotic region and propagated it through the interaction region. Different wavepackets were prepared in view of sampling a small part of the possible initial conditions: for each of the first 4 vibrational levels of LiH two different average energies were used, 0.5 and 1.0 eV. The numerical method employed was exactly the same as that used for the ground state process, but, since the surface is very different, some technical details of the calculation were changed:

- The potential energy difference between the reactants and products is about 0.2 eV and the energetic gain due to the well is never larger than 1.5 eV. Therefore it was possible to use a much larger time step. In particular we used $\Delta t = 0.1$ fs.

- The much smaller energy differences presented by the surface, allowed

us to work with less dense spatial grid while, at the same time, the long range tails of the potential forced us to use a very large configurational space to correctly account for the dipole interaction. The Q_1 coordinate ranged from 1 to 30 Å in 640 points, while Q_2 was inside the range (0.5,11.0) Å with 256 points.

It should be noted that even with our choice of the grid the long-range dipole-charge potential had to be (smoothly) cut. This modification was necessary since we were not able to reach a true asymptotic region, in that test calculations with the solely reagent channel potential revealed an anomalous behavior of the probabilities that were somewhat different from unity. The reason of this failure is that with a long-range potential the asymptotic condition is no longer valid, unless one starts the motion of the wavepacket very far from the interaction region (hundreds of Å in our case; see also Chapter 10). This means that in practical calculations the weight of each energy component of the initial wavepacket would not be correctly computed and the resulting probabilities would be in error[1]. This is a major problem that one has to take into account when planning realistic $3D$ calculations of ion-dipolar molecule reactions. One possible solution could be the use of an additional grid, the new grid being used for the asymptotic motion; in this case the merging between the two grids could be done via a procedure similar to the Reactant-Product-Decoupling scheme (see for example the book of Zhang (1999) or the works of T. Peng et al. (1998) and S.C. Althorpe et al. (1997)). In our case the cut of the PES (few Å before the edge of our chosen grid) produced a negligible difference on the average behavior of the probabilities with respect to a "standard" calculation in which the cut was made ~ 15 Å further away from the interaction region, although, as expected, the position of some resonances was sensitive to such modification.

The reaction probabilities calculated for the above mentioned wavepackets are reported in Fig.(9.2) as a function of total energies. Resonances dominate the whole range of energies and are due to the quasibound states formed during the reaction in the large wells created by the electrostatic interactions. The reactive probabilities are reported for the first two and for the n=4 vibrational states. The general trend of the reaction probabilities for the two lowest vibrational states is to decrease with increasing energy since an energetic wavepacket will simply bounce off the repulsive wall behind the dipole minimum. To better appreciate this fact we draw in the right panel of Fig.(9.2) also an average probability calculated every 20 points in energy.

---

[1]Note also that the weight of the energy components goes to the *denominator* of the relevant formula that gives the probability in terms of the time-evolved wavepacket, see eq(8.1) on pag.195.
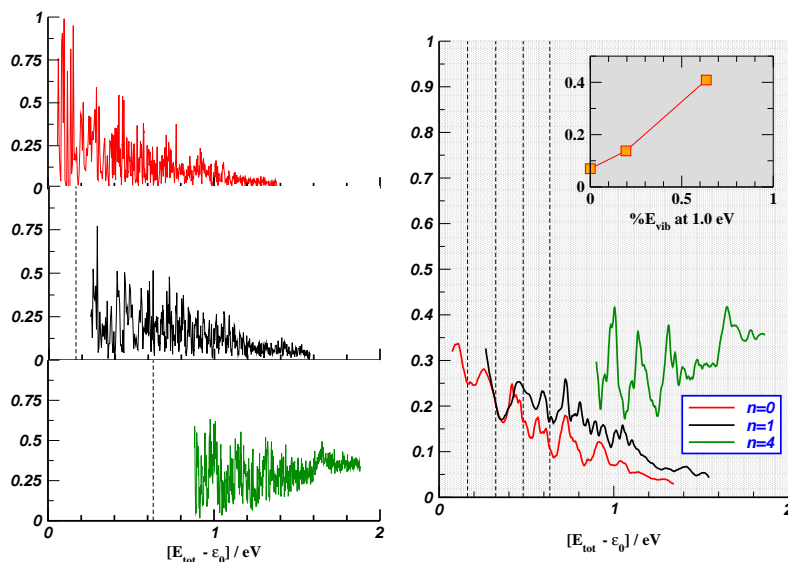
Figure 9.2: Left panel: reactive probabilities summed over all possible vibrational states of the product as a function of total energy shifted to the ground vibrational state of the reactant molecule. Right panel: reaction probabilities averaged over an interval of energies.

A significative vibrational enhancement is produced with a vibrationally excited *LiH*: for a given *total* energy the probability increases with increasing the vibrational energy content and for $n = 4$ it remains appreciable throughout the whole energy range sampled here.

It is worth to note here that at low collision energy we obtain high probabilities in correspondence of the resonances of the system. Thus, in the low energy regime the formation of metastable states plays a very important role for the occurrence of the reaction, such that even the initial $n = 0$ state can give rise to almost complete transformation into product in correspondence with the position of the resonances. We can ascribe this effect to the presence of the deep *pre-reaction* well: the formation of *reagent* Feshbach resonances allows for the *temporary formation of highly excited* LiH *states that, in turn, can easily overcome the saddle point region*. Thus we can argue that in similar systems the reagent molecule can be helped by the "subreactive" dynamics in forming highly reactive (metastable) complexes. In the following Section we will analyze in some detail the bound and quasi-bound spectra, although the complete characterization of the resonances remains beyond the present work[2].

---

[2]We have to admit that, with a rigorous resonances analysis, it would have been possible to test our hypothesis on the role of the "reagent" Feshbach resonances: in particular,

It is also interesting to note that, apart form the resonance pattern, the background probability remains confined below 40% (as can be seen by the average values of the probability in Fig.(9.2)) even if the considered geometry appears the most favorable for the reaction to occur (see Chapter (7)).

9.2 Resonances analysis

To carry out an analysis of the resonant states that we encountered in the reaction probabilities we followed the method already used by Mahapatra and Sathyamurthy (1995; 1996; 1997). In this method the resonances are studied by following the unimolecular dissociation of the transient species $LiHH^+$. The key quantity is the temporal autocorrelation function defined by

$$C(t) = \langle \psi_0 | \psi_t \rangle \tag{9.1}$$

that has to be computed at each time step for a sufficiently long time T. This quantity can be related to the bound and unbound spectrum of the system by noting that

$$|\psi_t\rangle = U_t |\psi_0\rangle = \sum_n e^{-iE_n t} |\phi_n\rangle \langle \phi_n | \psi_0\rangle + \sum_f \int dE e^{-iEt} |Ef+\rangle \langle Ef+|\psi_0\rangle$$

where the first sum runs over the bound states of the system and integral runs over the continuous state space (f is the set of indexes needed to specify completely the state of the system, i.e. it is the composite index for the arrangment and channel labels). Indeed, its time-energy Fourier transform gives

$$\widehat{C}(E) = \sum_n \delta(E - E_n) a_n + \sum_f a_f(E)$$

where $a_n = |\langle \phi_n | \psi_0\rangle|^2$ is the weight of the $n-th$ bound state in the initial wavepacket (the "transient species") and $a_f = |\langle Ef+|\psi_0\rangle|^2$ is the weight of the indicated scattering eigenstate. When the wavepacket is placed well inside the interaction region it generally spreads over all bound and quasi-bound states since they are well localized in such region. In practice, one follows only the forward dynamics ($t > 0$) for a finite long time, thereby introducing a window function in the computation of the Fourier transform. As it is well known the simple "box window function" has some unpleasant features for the

---

we could have characterized the quasi-bound states "eigenfunctions" and compared them with the expected probability density of a "reagent" Feshbach eigenstate (see for example S. Mahapatra and N. Sathyamurthy (1995; 1996; 1997).

computation of the Fourier transform, thus, following S. Mahapatra and N. Sathyamurty (1995), we used the Hanning window function

$$H(t) = \left\{ \begin{array}{l} \frac{1}{T}(1 - cos(2\pi t/T)) \ \text{ for } 0 \leq t \leq T \\ 0 \, \text{for } t < 0 \text{ and } t > T \end{array} \right.$$

to compute the "spectra"

$$I(E) = \left| \int_{-\infty}^{+\infty} e^{iEt} C(t) H(t) dt \right|$$

in which the original delta functions and resonance profiles turn out to be convoluted with the Fourier transform of the window function.

We evolved three wavepackets placed in different positions around the saddle point region. We used the same time step of before ($\Delta t = 0.1 \, fs$) and followed the evolution of the wavepackets for a very long time interval, $T = 15 \, ps$, on a grid that could be chosen much larger than the previous one (i.e. Q_1 ranged from 1 to 50 Å and the long-range tail was not cut)[3]. The total propagation time determined an energy resolution of $\delta E \sim 2\pi/T = 3 \text{x} 10^{-4} \, eV$ below which the system spectral features superimpose with the peaks of the transformed window function.

An overview of our results is reported in Fig.(9.3) where the (combined) spectrum obtained from the evolution of the various wavepackets is shown, together with a schematic energy profile of our system. In particular, we report in that scheme the energy position of the minima of the two wells, the asymptotic energy of the fragments and the position of some low energy vibrational levels. With our choice of the initial wavepackets, which turned out to have a mean energy of -1.3899, -2.0416 and -2.8576 eV respectively, we were able to sample a broad energy range, $\sim 3 \, eV$ wide. As it is evident from the figure, the pattern is very complicated: a comparison with the reaction probabilities shown if Fig.(9.2) revealed that we computed such probabilities on a energy grid much coarser than the resonance pattern!

The spectrum obtained is analyzed in Fig.(9.4). We can consider four different energy regions. In panel A we report an enlargement of the lowest energy region (between -3.6 and $-3.0 \, eV$, with the zero of the potential put in the triatomic dissociation limit) in which only the dipolar well is available for the motion. Thus the peaks correspond to the dipole-bound eigenvalues of the

---

[3]In this case we had only to evaluate the integral of eq.(9.1) and therefore the computation was much less expensive than the initial-state-selected dynamics, although it furnished only qualitative features. It is worth to mention here that such dynamics could be made quantitative as it is done with "transition-state-methods", in which the Cumulative Reaction Probability is computed (Light and Zhang, 1998). In our system, the use of such methods would avoid the problem associated with the long-range of the potential.
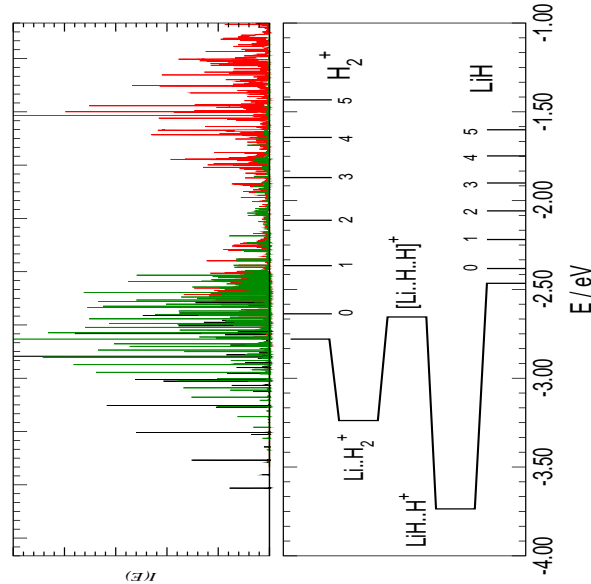
Figure 9.3: Overview of the bound and quasi-bound spectrum.

system. The corresponding eigenstates are, within harmonic approximation, combinations of a high frequency stretching motion of the (pre-reaction) LiH molecule and a lower frequency motion of the proton-molecule system. This is illustrated more clearly in Fig.(9.5) where we report a temptative assignment of the energy levels: the LiH motion has a "frequency" of $\sim 0.160\,eV$, while the other motion has a frequency of $\sim 0.070\,eV$. The labels (n, m) refer to the approximate vibrational quantum number in this order. In panel B an higher energy range (from $-3.0\,eV$ to $-2.7\,eV$) is displayed. In this range the polarizability well opens and the previous regular spectrum is superimposed with the bound spectrum of the $Li..H_2^+$ well; furthermore, the bound states of the two wells starts to mix, thereby complicating the situation. The energy range of panel C corresponds to the *pure elastic* $Li - H_2^+$ domain: in this range only the elastic subreactive dynamics of $Li - H_2^+$ is possible, although the resonance pattern comes both from the "reagent" Feshbach metastable states and "product" Feshbach metastable states and mixed metastable states[4]. The region of panel D opens the reaction: now the $LiH + H^+ \to Li + H_2^+$ reaction is possible and the spectrum has a very complicated structure, which is best seen in panel E. In this last panel we report the results of two very different

---

[4]Thus, the $Li + H_2^+$ inelastic dynamics can be hardly described with a usual "subreactive potential", although the saddle point turns out to be a real barrier to the "reactive region". It is also worth to note, in this context, that the $LiH..H^+$ metastable states in this energy range may be really long-lived states.
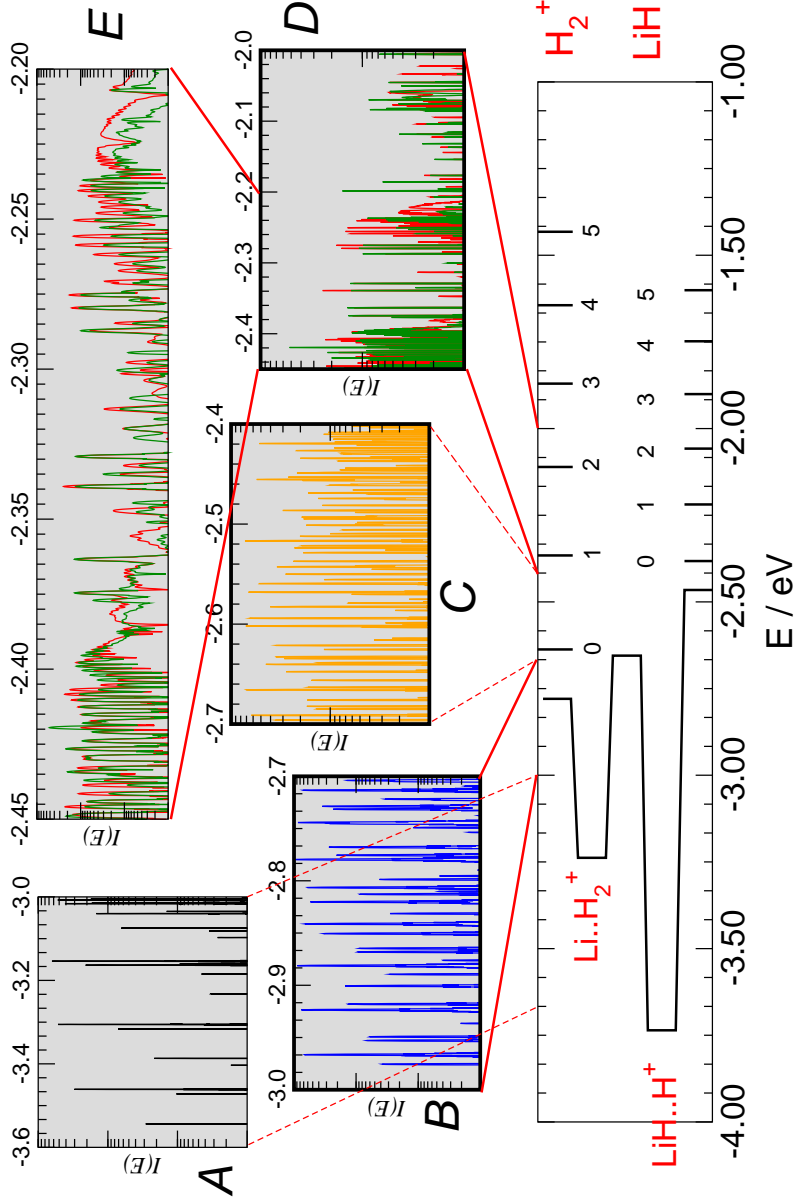
Figure 9.4: A closer look to the spectrum. See text for comments.

calculations (one started in a well and the other in the other well), thus showing the "extension" of many metastable states that spread over the two wells.

To conclude this Section, we note that the widths of the observed resonances ($> 0.001\,eV$) corresponds to lifetimes $\tau < 2\,ps \equiv 2\text{x}10^{-12}\,s$. For com-
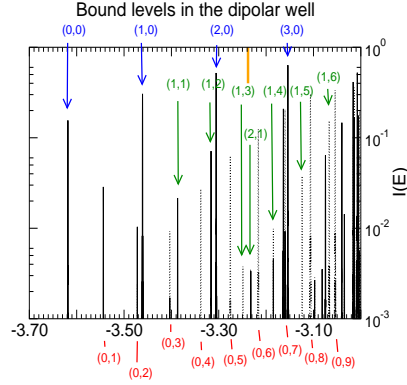
Figure 9.5: Low-energy bound state spectrum.

parison, the spontaneous radiative decaying rate to the ground-state (assuming an average $5\,eV$ energy gap) is much slower, as usual, than the resonance decaying rate ($dP/dt \sim 10^9\,s^{-1}$ for the radiative process and $dP/dt \geq 5\mathrm{x}10^{12}\,s^{-1}$ for the non radiative one) and the rotational period of the LiH molecule is of the order $\omega^{-1} \sim (JB)^{-1} \sim 0.7\,ps$.

Chapter 10

The $LiH + H^+$ non-reactive dynamics

In this Chapter we present our preliminary results on the $LiH - H^+$ inelastic dynamics which is relevant to estabilish the contribution of H^+ to the LiH cooling function.

Talking about *inelastic* dynamics when the *reaction* is possible, as we have shown in the previous Chapter, is clearly an approximation. The rigorous procedure would need a full dimensional *reactive* calculation, from which one extracts both the reactive and the non-reactive cross-sections. However, owing to the long-range nature of the charge-dipole interaction, a *state-to-state* analysis of this kind could be beyond the current computational facilities. Thus, one is left with an approximate dynamics. The approximation may be useful when (i) the *three-dimensional* reaction efficiency is much lower than the corresponding inelastic probability; (ii) the contributions to the inelastic processes come from a wide range of J values (in the high J partial waves the reactive channel should be closed by the centrifugal barriers and its inclusion would not alter substantially the computed inelastic cross-sections). It is worth, then, to note that (i) our reaction is collinear dominated and (ii) our long-range potential is expected to spread the inelastic opacity functions over a wide range of J values.

Anyway, such subreactive study can be of help in planning more exact studies on the system and on similar (charge-dipole) ones. As a matter of fact, in this Chapter we will discuss the pathological strong, long-range potential and our new propagator for Time-Independent calculations which seems to be a good starting point for solving this kind of problems.

10.1   The charge-dipole interaction

The charge-dipole potential

$$V_D = \frac{Dcos\theta}{R^2} \tag{10.1}$$

is somewhat pathological for the scattering theory outlined in Chapters 2 and 3 (see note 2 on pag.43) because its long-range nature poses some doubts about the validity of all the mentioned results. For example, the forward Born scattering amplitude for a D/r^2 potential is readily shown to be divergent

$$f(\mathbf{p} \leftarrow \mathbf{p}) \propto \langle \mathbf{p}|V|\mathbf{p}\rangle = 4\pi D \int_0^\infty dr$$

This is not a problem of the Born approximation since we can show that the total cross section (and consequently the forward amplitude, because of the optical theorem of equation (2.16) on pag.50) is divergent. Indeed, the convergence of the partial wave series

$$\sigma = \frac{4\pi}{p^2} \sum_{l=0}^{\infty} (2l+1)sin^2\delta_l \tag{10.2}$$

is determined by the behaviour of the high l phase-shifts and we can estimate these values by simply noting that the dipole potential adds a $2\mu D$ contribution to the centrifugal term

$$l(l+1) \rightarrow l(l+1) + 2\mu D$$

This means that we have to use non-integer values of l which, denoted with η, are determined by the equation[1]

$$\eta(\eta+1) = l(l+1) + 2\mu D$$

Since in the high l limit the relevant solution of this equation behaves like

$$\eta \rightarrow l + \frac{\mu D}{(l+\frac{1}{2})} \quad (l \rightarrow \infty)$$

the total phase-shift is given by

$$\delta_l^{tot} = \eta\frac{\pi}{2} = l\frac{\pi}{2} + \frac{\mu D}{2l+1}\pi$$

---

[1]This amounts to use non-integer Riccati-Bessel functions or, more properly, non-half-integer Bessel functions.

and, then, the scattering phase-shift by

$$\delta_l = \frac{\mu D}{2l + 1}\pi$$

It therefore follows that for $l \to \infty$

$$(2l + 1)sin^2\delta_l \to \frac{(\mu D\pi)^2}{2l + 1}$$

that is, that the series (10.2) is divergent.

Anyway, for a single channel problem (or a multichannel problem with an hypothetical spherical r^{-2} potential) the contribution of each angular momentum can be obtained without no more effort with respect to "conventional" short-range problems. In fact, one can solve the scattering problem in the "inner" region as usual and then match the wavefunction with the *known* solutions of the long-range region, i.e ordinary Bessel functions.

When, as in our case, the r^{-2} term is off-diagonal in channel space the situation is somewhat different: on the one hand we expect that the total cross section is no longer divergent because the potential couples asymptotic states with different internal energies[2], but on the other hand we can hardly obtain an analytical solution for the long-range region.

The problems associated with the charge-dipole interaction are well known in electron-molecule collision theory (Gianturco and Paioletti, 1998). In that case one can obtain considerable simplifications by taking into account the lightness of the projectile. Even the Born approximation with the pure point-dipole potential model is expected to be good at reasonably low collision energies (Itikawa, 1978) since the contributions of the short-range potential term to the total cross section are limited to the low partial waves (head-on collisions) and the *integral* cross section values mainly come from the high partial waves. Citing Collins and Norcross (1978)

> "The scattering of electrons by molecules with permanent dipole moments has been intrinsically interesting ever since Massey observed in 1932 that '..the collision of electrons with a top possessing such a dipole moment may be treated by Born's method whatever the velocity of the electron may be..' .The assumption that the interaction is dominated, if not completely determined by the long-range dipole potential, leads to extremely simple cross-section formulas "

---

[2]It is worth to mention in this context that, in contrast to the previous "diagonal" case, the momentum basis representation of the potential does not have singularities. The forward, elastic Born amplitude involves the spherical average of the interaction potential (which falls off faster than r^{-2}) and then is *finite*.

In citing Massey (1932) the authors italicized "whatever the velocity of the electron may be", since clearly the Born approximation has always a low-energy limit of validity. Collins and Norcross (1978) further showed that integrated and momentum transfer cross sections for electrons scattering off polar systems can be reliably generated within the *adiabatic approximation*[3]. They did not apply "consistently" this approximation, since forward-scattering and integrated cross-sections diverge if this approximation is consistently adopted, mich like we have shown above for the spherical r^{-2} potential. Subsequently Clark (1979) introduced an "intermediate region" in the electron-molecule configuration space in which the rotational coupling can be neglected and the inner solution can be *analytically* propagated using ordinary Bessel functions up to the external region, where the rotational coupling due to the dipole potential is treated perturbatively. The validity of such procedure has been shown to be good for energy higher than a few eV.

In atom-molecule collisions the energies required to apply any reasonable approximation to the charge-dipole problem are quite unphysical (for example the Clark's criterion on the energy lower bound becomes $\sim 10^3\,eV$) and thus one is forced to consider brute-force calculations. It is instructive, however, to look at the crude Born formula for a point-dipole model potential and a rotating target (in a.u.)

$$\sigma(j' \leftarrow j) = \delta_{j',j\pm1}\frac{8\pi}{3}\,(\mu D)^2\,\frac{j_>}{2j+1}\frac{1}{p^2}ln\left|\frac{p+p'}{p-p'}\right|$$

where D is the dipole moment, μ is the reduced mass of the collision system, $j_> = Max(j,j')$ and p and p' are the initial and final momentum respectively. This formula highlights the dominant coupling due to the charge-dipole potential: such potential couples (directly) only the $\Delta j = \pm1$ transitions and the resulting cross section is exceedingly large for molecules with large momenta of inertia (closely spaced rotational levels) and/or large dipole moment. In particular, when the moment of inertia tends to infinity (stationary target), $p \sim p'$ and the cross section diverge. The coupling properties of the potential can also be seen clearly in the Body-Fixed representation (see Section (4.1)),

$$\left\langle JM\overline{\Omega}\epsilon \left| V_D \right| JM\overline{\Omega}'\epsilon' \right\rangle = \delta_{\overline{\Omega\Omega}'}\delta_{\epsilon\epsilon'}\frac{D}{r^2}(-)^{\overline{\Omega}}\begin{pmatrix} j & j' & 1 \\ 0 & 0 & 0 \end{pmatrix}\begin{pmatrix} j & j' & 1 \\ \overline{\Omega} & \overline{\Omega}' & 0 \end{pmatrix}$$

---

[3]The term adiabatic is used in a somewhat different way with respect to the usual meaning in scattering theory. Here, it refers to the adiabatic *internal motion of the target* and not to the adiabatic motion of the projectile when it is so slow that the target adjust itself during the collision. That is, the adiabatic approximation mentioned here is the Born-Oppenheimer approximation to an unbound electronic motion and it is inherently limited to sufficiently *high* collision energies.

where it becomes evident that this kind of potential couples only the rotor states that differ for one unit of angular momentum since

$$\begin{pmatrix} j & j' & 1 \\ 0 & 0 & 0 \end{pmatrix} = \delta_{j',j\pm 1}(-)^{j+\frac{1}{2}\pm\frac{1}{2}}(j + \frac{1}{2} \pm \frac{1}{2})\sqrt{\frac{2(2j)!}{(2j+2\pm 1)!}}$$

(it is worth to note that in this representation the kinetic energy term couples the states that differ for one unit of body-fixed angular momentum component).

We were not able to analyze the *mathematical* problems associated with the charge-dipole interaction. It is an interesting matter, but it is clearly beyond the scope of this work. One should have done a careful analysis of all the key steps in the theory outlined in Chapters 2 and 3, in order to determine which results are valid and which are not.

Rather, in our work we approached the subject from a computational point of view, looking at the Time-Independent problem in the Close-Coupling approximation. We recognized that the number M of channels to be included in the expansion of the wavefunction over target states

$$\Psi^{i,+}(R,\underline{x}) = \sum_f F_{f\leftarrow i}(R) * X_f(\underline{x})$$

(where R represents the scattering coordinate and $\underline{x}$ collectively denotes the internal coordinates) depends, besides other things, from the value of the scattering coordinate. Indeed, at short-range, where the interaction is strong, the set of channels should include at least all the *locally* open channels and therefore M can be vary large but, on the other hand, in the asymptotic region, where the interaction is absent, only open channels are needed since for $R \to \infty$

$$\Psi^{i,+}(R,\underline{x}) \longrightarrow \sum_{f\,\in open} F^{\infty}_{i\to f}(R) * X_f(\underline{x})$$

where $F^{\infty}_f(R)$ are the appropriate, "free" channel components. Thus, in between these two extreme situations there should be a region, that can be quite large for long-range potentials, in which the strongly closed channels are increasingly less important for the scattering obervables and could be neglected without loosing accuracy. The saving of CPU time that results from this channel reduction procedure can be quite large in our case since the long-range potential is also quite strong and therefore needs a huge number of channels in the interaction region to have convergent scattering observables.

To neglect the channels that become less and less important during the (outward) R integration one should use a propagating scheme with a clear-cut separation between the "open-space" and the "closed-space". Only in this way

one can evaluate the influence of the closed space (or a part of it) on the open one, that is the only one involved in the asymptotic condition. We therefore resort to the well known Variable Phase method developed some time ago by several authors (Calogero, 1967; Degasperis, 1964; Zemach, 1964; Dourneuf and Lan, 1977); it will be briefly reviewed in the following Section.
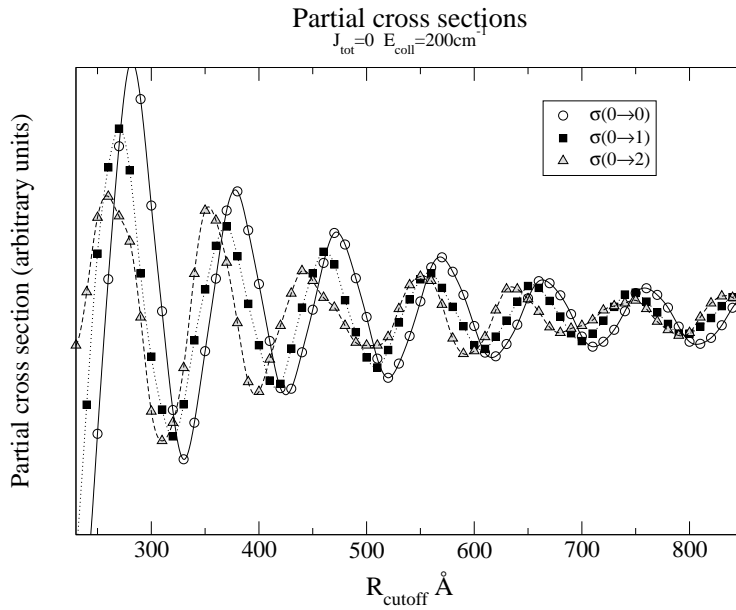
Figure 10.1: J=0 partial cross section as a function of R_{cutoff}.

Before doing this, let us show some results of the extensive numerical tests that we did for a preliminary examination of multichannel scattering in presence of a dipole off-diagonal interaction. We used a low number of channels in a low-energy scattering calculation and we studied (i) the radial convergence of partial wave cross sections and (ii) the convergence of the opacity function for fixed cutoff distances of the potential. We looked at the radial convergence of a selected partial wave by following the dependence of the various observables on the "matching point", i.e. on the distance at which the solution is taken to be potential-free. This clearly amounts to apply a cutoff to the potential and, not so strangely, is the spirit of Variable Phase method. For given J's, the partial cross values turned out to be oscillating functions of the cutoff distance, R_{cutoff}. In particular the results for the $J = 0$ case are reported in Fig.(10.1) for some selected transitions. These results have been normalized to allow the comparison but they clearly indicate that the oscillations due to the action of
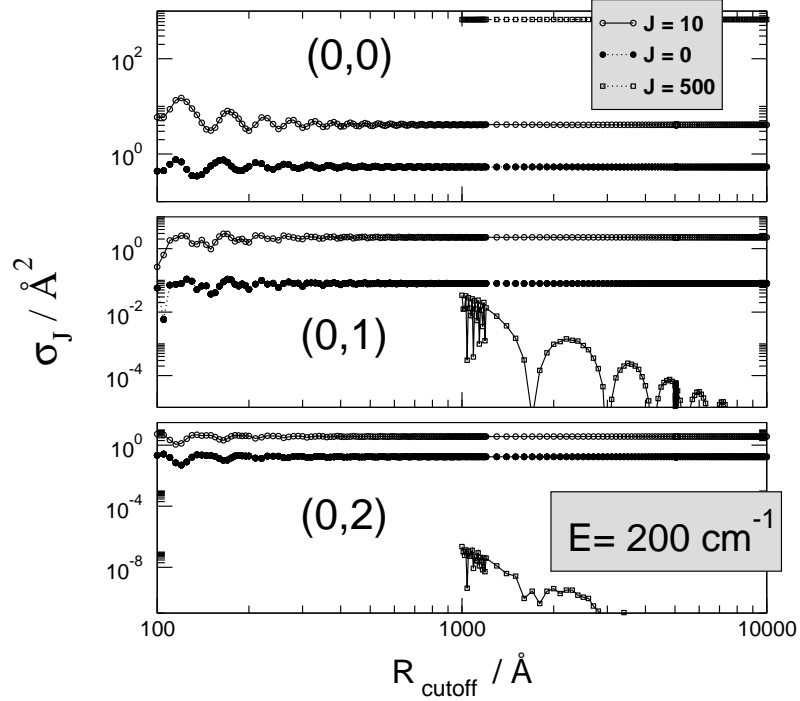
Figure 10.2: Same as in Fig.(10.1) but for three different values of J.

the coupling potential are considerable and not limited to the direct $\Delta j = \pm 1$ transitions. They do not depend on the particular total angular momentum value chosen: as one can see in Fig.(10.2) the oscillations, on a different scale, exist for every transition at each angular momentum value (in Fig.(10.2) the $J = 500$ curve starts at $R_{cutoff} = 1000$ Å since for smaller values the matching point turns out to be below the centrifugal barriers). We found further that the oscillation amplitude and the rate of convergence toward the asymptotic limit were, as expected, dependent upon the collision energy and on the dipole strength.

When we looked at the behavior of the partial opacity functions for different cutoff distances of the potential we found an unexpected behavior for large J (Fig.(10.3)): for the selected cutoff distances the elastic cross-section is monotonically converging as a function of the angular momenta (upper panel in Fig.(10.3), while the inelastic one shows spurious *beatings* for high angular momenta (lower panels). The entity of the *beatings* decreases rapidly with increasing R_{cutoff}. or the collision energy. Clearly, the truncated potentials must have a finite total cross section (besides all they are of *finite* range) and thus each opacity function must tend to zero faster than $\propto J^{-1}$; however,

Elastic partial cross section for J=0

Inelastic (0→1) partial cross section for J=0
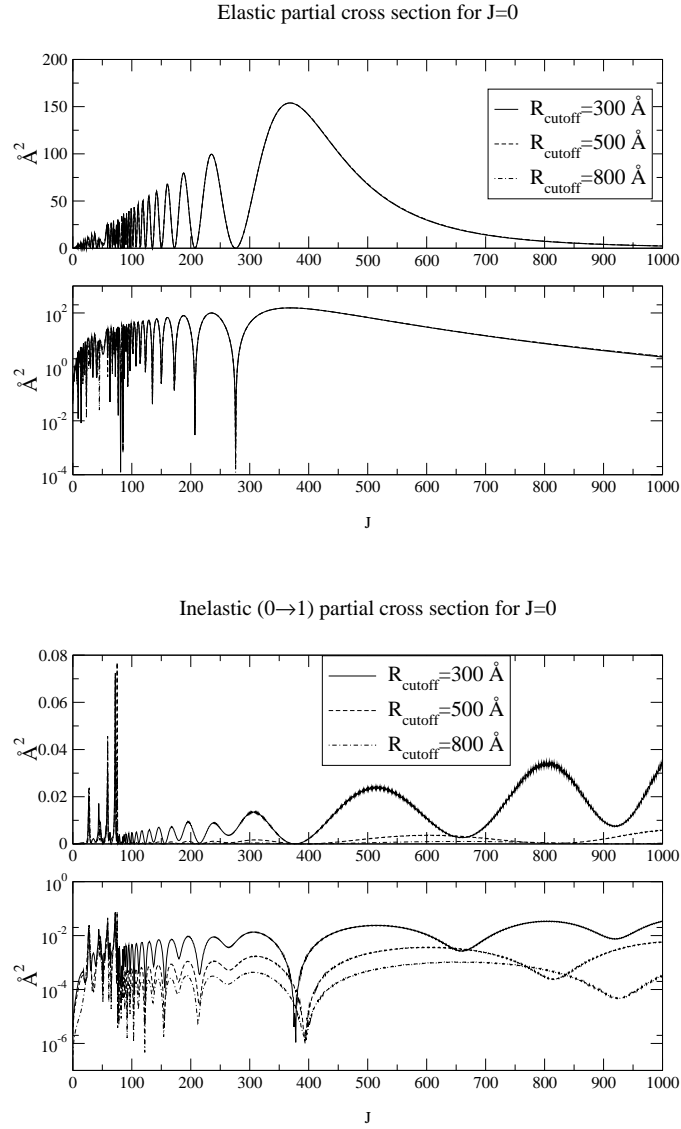
Figure 10.3: Elastic opacity functions for elastic and inelastic transitions. The lower panels shows the same function as the upper ones but on a logarithmic scale.

this example show that for a correct evaluation of the opacity functions one is forced to use a J dependent radial cutoff.

10.2 The Variable-Phase method

In this Section we outline the well-known multichannel Variable-Phase method in the K matrix formulation, along with the modifications brought by M. Le Dourneuf and Vo Ky Lan (1977) to handle the presence of strongly closed channels. In the subsequent Section we will show the modifications that we brought to this method in order to be useful for our strong, long-range problem. In particular our method differs from the original one by two chief features: (i) it allows for the gradual reduction of the number of closed channels during the outward propagation and (ii) it avoids the direct calculation of the computationally expensive Bessel functions.

10.2.1 The K-matrix equations

In Sections (4.4,4.5) we showed how the usual, Space-Fixed, Close-Coupling equations for M channels

$$\left\{ \frac{d^2}{dR^2} + \mathbf{k}^2 - \mathbf{V} - \frac{\mathbf{l}^2}{R^2} \right\} g = 0 \tag{10.3}$$

of the inelastic scattering problem in the diabatic basis can be reduced to the Riccati equation

$$\frac{d\mathbf{Y}}{dR} + \mathbf{W} + \mathbf{Y}^2 = 0 \tag{10.4}$$

for the unknown $\mathbf{Y}$ Log-Derivative matrix (in this equation $\mathbf{W} = \mathbf{k}^2 - \mathbf{V} - \mathbf{l}^2/R^2$). We said that one solves for this matrix up to the asymptotic region where the "augmented" $\mathbf{K}$ matrix can be obtained by the following linear system

$$(\mathbf{N}' - \mathbf{Y}\,\mathbf{N})\,\mathbf{K} = \mathbf{J}' - \mathbf{Y}\,\mathbf{J} \tag{10.5}$$

in which $\mathbf{J}(R)$ and $\mathbf{N}(R)$ are matrices of Riccati-Bessel and Riccati-Neumann functions. The open-open block of $\mathbf{K}$ holds all the scattering informations since it is related to the scattering S matrix by means of the usual Caley transform. We defined the $\mathbf{J}$ and $\mathbf{N}$ matrices as follows ($z_i = k_i R$ are dimensionless quantities)[4]:

$$\text{Open channels :} \qquad \begin{aligned} (\mathbf{J}(R))_{ij} &= \delta_{ij}\, \frac{1}{\sqrt{k_i}} \left(\tfrac{\pi}{2} z_i\right)^{1/2} J_{l_i+1/2}(z_i) \\[2mm] (\mathbf{N}(R))_{ij} &= \delta_{ij}\, \frac{1}{\sqrt{k_i}} \left(\tfrac{\pi}{2} z_i\right)^{1/2} Y_{l_i+1/2}(z_i) \end{aligned} \tag{10.6}$$

---

[4]As in Chapter 4 we use real valued k_i to refer to $\sqrt{2\mu(E - \epsilon_i)}$ for the open channels and to $\sqrt{2\mu(\epsilon_i - E)}$ for the closed ones.

$$(\mathbf{J}(R))_{ij} = \delta_{ij}\, \tfrac{1}{\sqrt{k_i}}\, (z_i)^{1/2}\, I_{l_i+1/2}(z_i)$$

Closed channels : $\qquad\qquad\qquad\qquad\qquad\qquad\qquad\qquad$ (10.7)

$$(\mathbf{N}(R))_{ij} = -\delta_{ij}\, \tfrac{1}{\sqrt{k_i}}\, (z_i)^{1/2}\, K_{l_i+1/2}(z_i)$$

where J_n, Y_n are the Bessel functions of the first and second kind and I_n, K_n are modified Bessel functions of the first and third kind as defined by M. Abramowitz and I.A. Stegun (1972). With this definition the wronksian for each channel is unity both for open and for closed channels, i.e. in matrix form

$$W\{\mathbf{J},\, \mathbf{N}\} = \mathbf{I} \qquad\qquad\qquad (10.8)$$

We now use the $\mathbf{Y}$ to $\mathbf{K}$ transformation of equation (10.5) *for each R* to define a $\mathbf{K}(R)$ matrix. This matrix is clearly the augmented $\mathbf{K}$ matrix for the potential truncated at R , that is[5]

$$\widetilde{\mathbf{V}}(R') = \left\{ \begin{array}{ll} \mathbf{V}(R') & \text{for } R' < R \\ \mathbf{O} & \text{for } R' \geq R \end{array} \right. \qquad\qquad (10.9)$$

A differential equation for $\mathbf{K}(R)$ can be written by differentiating the $\mathbf{Y}$ to $\mathbf{K}$ transformation, using the Riccati equation (10.4) for $\mathbf{Y}$ and the wronskian relation (10.8). The result is

$$\mathbf{K}' = -\Psi^{\dagger}\, \mathbf{V}\, \Psi \qquad\qquad\qquad (10.10)$$

where $\Psi = \mathbf{J} - \mathbf{N}\,\mathbf{K}$. A term involving the derivatives of the $\mathbf{J}$ and $\mathbf{N}$ matrix must be added when eq.(10.3) contains a first derivative term. A similar equation holds for the inverse of the $\mathbf{K}$ matrix, here denoted $\widetilde{\mathbf{K}}$,

$$\widetilde{\mathbf{K}}' = +\Psi^{\dagger}\, \mathbf{V}\, \Psi \qquad\qquad\qquad (10.11)$$

where now the role of $\mathbf{J}$ and $\mathbf{N}$ is interchanged, i.e. $\Psi = \mathbf{N} - \mathbf{J}\,\widetilde{\mathbf{K}}$.

In principle, the Variable-Phase equations (10.10), with the starting condition $\mathbf{K}(0) = \mathbf{O}$, can be solved up to the asymptotic region to get the "true" $\mathbf{K}$ matrix (i.e. that for the non truncated fully acting potential). In practice, however, the two equations (10.10,10.11) must be used together because of the presence of "local" scattering resonances (i.e. resonances that exist only because of the unphysically truncated potentials). These resonances cause a specific $\mathbf{K}$ eigenvalue to be infinity at some value of R and therefore do not

---

[5]This is the usual starting point for the derivation of the Variable-Phase equations. Here we follow a somewhat different approach based on the existing one-to-one mapping between $\mathbf{K}(R)$ and $\mathbf{Y}(R)$ (see eq.(10.5)). The derivation is straightforward and will not reported.

allow the use of an Ordinary Differential Equation (ODE) integrator. Close to these singular points one has to invert the $\mathbf{K}$ matrix and solve eq.(10.11) until $\widetilde{\mathbf{K}}$ starts to diverge, at which point one goes back to $\mathbf{K}$. Thus, one can solve alternatively eq.(10.10) and eq.(10.11) using common ODE integrators by making use of a (problem dependent) number of matrix inversion operations. It therefore follows that the Variable-Phase method cannot be used efficiently in the *inner* region, where the strong coupling between channels would force one to perform a large number of such matrix inversion operations. Thus, in the following we assume to have a starting $\mathbf{K}(R_0)$ matrix, obtained for example from a log-derivative propagation up to the value R_0 outside from the strong interaction region.

10.2.2 Strongly closed channels

Whenever one has to face a strong interaction potential in the inner region, one has to use a huge number of channels most of which become asymptotically closed. These can be a source of numerical difficulties in the Variable-Phase method because the corresponding Bessel functions for the closed channels, I_n and K_n , are exponentially increasing and decreasing respectively. The solution to this problem has been already discussed by M. Le Dourneff and Vo Ky Lan (1977). They, in practice, proposed to define "scaling" matrices of the following types

$$(\mathbf{W})_{ij} = \delta_{ij} \left\{ \begin{array}{ll} 0 & \text{for open channels} \\ k_i & \text{for closed channels} \end{array} \right. \quad \text{and } \Delta^{\pm} = e^{\pm \mathbf{W} R}$$

and introduce "scaled" Bessel functions

$$\mathbf{J}_s = \mathbf{J} \, \Delta^-, \, \mathbf{J}'_s = \mathbf{J}' \, \Delta^-$$

$$\mathbf{N}_s = \mathbf{N} \, \Delta^+, \, \mathbf{N}'_s = \mathbf{N}' \, \Delta^+$$

which are of order of unity for large arguments (note that the primed quantities are no longer the derivatives of the unprimed ones). With this functions one defines a "scaled" $\mathbf{K}$ matrix, $\mathbf{K}_s$, by means of equation (10.5), from which it follows

$$\mathbf{K}_s = \Delta^- \mathbf{K} \, \Delta^- \tag{10.12}$$

and therefore

$$\mathbf{K}'_s = -(\mathbf{W} \mathbf{K}_s + \mathbf{K}_s \mathbf{W} + \Psi^\dagger \mathbf{V} \Psi) \tag{10.13}$$

where $\Psi = \mathbf{J}_s - \mathbf{N}_s \mathbf{K}_s$. Analogously, for the inverse of the scaled $\mathbf{K}$ matrix, $\widetilde{\mathbf{K}}_s$ one obtains

$$\widetilde{\mathbf{K}}'_s = +(\mathbf{W} \widetilde{\mathbf{K}}_s + \widetilde{\mathbf{K}}_s \mathbf{W} + \Psi^\dagger \mathbf{V} \Psi) \tag{10.14}$$

where now $\Psi = \mathbf{N}_s - \mathbf{J}_s \, \widetilde{\mathbf{K}}_s$. Since the "scaled" Bessel functions can be directly computed without any pathological behavior we can avoid in this way a large number of numerical overflows and underflows.

It should be noted that, since $\mathbf{K}$ tends to be constant when R becomes large, it follows from equation (10.12) that $\mathbf{K}_s$ tends exponentially to zero everywhere but the open-open $\mathbf{K}$ matrix block. This can cause numerical difficulties when, owing to the mentioned presence of "local" resonances, one tries to move to its inverse. However, as we will explain in the next paragraph, this problem doesn't really arise because we can remove the strongly closed channels without losing the accuracy of the physically significant $\mathbf{K}$ matrix block.

From now on, we will consider only "scaled" quantities in our analysis and therefore we shall drop the subscript s. Thus, unless otherwise stated, we will refer to the present $\mathbf{K}$ matrix as a "scaled" quantity.

10.3   The new Variable-Phase propagator

Unlike in the log-derivative formalism, the $\mathbf{K}$ matrix elements are not all equally important. We are mainly interested in the open-open block of the matrix and, in particular, in the asymptotic region, we are *only* interested in that block. The other blocks of the matrix must be considered only to the extent they influence the open-open block. Having a clear separation between the "physical" and the "virtual" spaces, one may argue that when the virtual contributions to the physical space become negligible, the virtual space can then be reduced. This is the basis of our channel reduction procedure, which we describe in what follows.

10.3.1   The channel reduction procedure

Let Q be the projector onto that portion of the (closed) channel space, that we name the Q -space, which we are trying to remove. Let $P = 1 - Q$ be the projector onto its orthogonal complement, the "P- space", that also contains the open channels space. The specific choice of the Q - space will be discussed below: for the moment it corresponds to a specified number of closed channels. Let us write now

$$\mathbf{V} = \mathbf{V}_{PP} + \mathbf{V}_x \tag{10.15}$$

where $\mathbf{V}_x$ is defined by this equation and, as usual, $\mathbf{A}_{PP} = PAP$. Inserting this equation in eq.(10.13), taking the $P - P$ projection of that equation and using the fact that $[P, \mathbf{J}] = [P, \mathbf{N}] = [P, \mathbf{W}] = \mathbf{O}$ and $P^2 = P = P^\dagger$ we can write

$$\mathbf{K}'_{PP} = \mathbf{K}'_{\mathbf{P}} + \mathbf{K}'_x \tag{10.16}$$

where

$$\mathbf{K'_P} = -(\mathbf{W}_{PP}\mathbf{K}_{PP} + \mathbf{K}_{PP}\mathbf{W}_{PP} + \Psi^\dagger_{PP}\mathbf{V}_{PP}\Psi_{PP})$$

and

$$\mathbf{K'}_x = -P(\Psi^\dagger\mathbf{V}_x\Psi)P$$

The first term, in which Ψ_{PP} is given by $\Psi_{PP} = \mathbf{J}_{PP} - \mathbf{N}_{PP}\mathbf{K}_{PP}$, represent the contribution to the $\{PP\}$ block that we would compute if we neglected the Q space; the second term, therefore, measure the influence of Q on the P space. In particular, we can take the open-open block projection of equation (10.16)

$$\mathbf{K'}_{OO} = (\mathbf{K'_P})_{OO} + (\mathbf{K'}_x)_{OO} \qquad (10.17)$$

(where O is the projector onto the open channel space) and compare on this "physical block" the contributions coming from the Q space with that coming from the P space: if the first are negligible for a given integration range and if the potential is monotonically going to zero we can reasonably assume that the neglect of the Q space doesn't produce any appreciable error in the final scattering observables given by the open channels space.

We can therefore devise a simple channel reduction procedure: define a Q space, check that $(\mathbf{K'}_x)_{OO}$ in equation (10.17) is negligible for a given range of radial values and therefore drop the Q space; define a new Q space and so on. Following this procedure, we will be left in the asymptotic region with only the open channels and, possibly, a few of closed channels rather close to the threshold.

10.3.2 The modified equations

Without the channel reduction procedure described above the Variable-Phase method cannot really compete with the most common methods used to handle long-range potentials, like the Log-Derivative Airy propagator. The reason for this is that to solve the Ordinary Differential Equations (ODE) given by eq.s(10.13,10.14) one must evaluate the Bessel functions for a number of times per steps. Although one doesn't necessarily need to do matrix inversion for each step the computation of Bessel functions is so demanding enough that the algorithm become markedly slower than the Log-Derivative-Airy method.

The solution of this problem is very simple: one use *zero*-orbital angular momentum bessel functions, i.e.

$$\text{Open channels :} \quad \begin{aligned} (\mathbf{J}(R))_{ij} &= \delta_{ij}\,\frac{1}{\sqrt{k_i}}\,sin(k_iR) \\[2mm] (\mathbf{N}(R))_{ij} &= -\delta_{ij}\,\frac{1}{\sqrt{k_i}}\,cos(k_iR) \end{aligned} \qquad (10.18)$$

$$(\mathbf{J}(R))_{ij} = \delta_{ij} \sqrt{\tfrac{1}{2\pi k_i}} \left(1 - e^{-2k_i R}\right)$$

Closed channels :   (10.19)

$$(\mathbf{N}(R))_{ij} = -\delta_{ij} \sqrt{\tfrac{\pi}{2 k_i}}$$

(where, for closed channels, we use the scaled quantities of Subsection (10.2.2)) if the centrifugal potential matrix, $\mathbf{l}^2/r^2$, is added to $\mathbf{V}$ in eq.s(10.13,10.14), i.e. $\mathbf{V} \to \mathbf{V} + \mathbf{l}^2/r^2$. In the spirit of the Variable-Phase method this means that in eq.(10.9) we truncate not only the potential matrix but also the centrifugal term. Consequently, our $\mathbf{K}$ matrix is a "modified" $\mathbf{K}$ matrix, related to the $\mathbf{Y}$ matrix by the usual relation, i.e. eq.(10.5), with $\mathbf{J}$ and $\mathbf{N}$ defined in eq.s(10.18,10.19) (this modified $\mathbf{K}$ matrix differs from the usual one in that it contains also the phase-shift contributions due to the centrifugal barriers). We can therefore follow this matrix up to the end point of integration, where it is transformed back to the usual $\mathbf{K}$ matrix. Since we have now to compute only simple transcendental functions the speed of the calculations is quite considerably improved.

It is also a simple matter to realize that, since this modification doesn't mix the open and the closed spaces, it is perfectly compatible with the channel reduction procedure described above.

10.3.3   The new algorithm

We can now summarize the overall algorithm that implements the ideas of Subsections (10.3.1,10.3.2). To solve the ODE problem we choose a fifth-order embedded Runge-Kutta method that uses the Cash-Karp formulas (Press et al., 1986). The term "embedding" in this context means that, for each step, six functional evaluations allow two independent estimates of the solution, correct up to fourth and fifth order respectively. In this way, i.e. using six functional evaluations per step one get a fourth order solution and an estimate of the truncation error. If the error is lower than a preselected threshold value, Δ_{ij} (for each (i, j) element) its value is used to *increase* the step size for the next step. Otherwise its value is used to estimate the step size to *retry* the previous step (which requires five more evaluations). Therefore, we adopt in this way a variable step size integration. The threshold value that determines the accuracy of the integration is given by the (i, j) matrix element

$$\Delta_{ij} = \epsilon * \left(|[\mathbf{K}]_{ij}| + |h * [\mathbf{K}']_{ij}| \right)$$

where ϵ is an input parameter ($10^{-3} - 10^{-7}$).

The channel reduction procedure is used on the "energy shell" each time, i.e. the Q space of Section 3.2 is made up of the closed channels with the same highest wavevector k_i . The contribution of this "shell" to the open-open block is checked during the propagation and it is considered negligible whenever

$$|[\mathbf{K}'_x]_{ij}| < N \, \sigma_{ch} \, |[\mathbf{K}'_\mathbf{P}]_{ij}| \qquad (10.20)$$

for all open-open matrix elements. Here σ_{ch} is an input parameter (usually $10^{-4} - 10^{-7}$) and N is the number of channels in the Q shell considered. When condition (10.20) is *invariably* satisfied in an interval greater than Δ/k_i the Q space is eliminated and a new Q space is defined by looking at the now highest shell (the actual value of the constant that defines the interval, i.e. $\Delta = 0.1 \div 1$, is not important, because it is related to σ_{ch}). The use of a channel-dependent checking of the interval takes into account the fact that the smaller the wavevector the smaller is the decaying behavior of that channel.

We assume to have our $\mathbf{K}$ matrix from a usual, constant reference potential Log-Derivative integration in the inner region (Mrugala and Secrest, 1983; Manolopulos, 1986). Then, the overall algorithm could be summarized as follows:

1. given $\mathbf{K}(R)$, a first evaluation of the right hand side of (10.13) is made by decomposing $\mathbf{V}$ according to eq. (10.15). In this way we check the validity of the condition (10.20). If it is the case we drop the existing Q space, retain only the $\mathbf{K}_{PP}$ matrix (i.e. $\mathbf{K}_{PP} \to \mathbf{K}$) and define a new Q space.

2. given a trial step size we implement a forward step with the Cash-Karp Runge-Kutta ODE integrator. This step needs at least five evaluations of the r.h.s. of eq.(10.13) (in the case of successful step) and gives a trial step size for the next step, h_{next} . If this value is smaller than a prescribed value, h_{min} (that we choose to be $1 - 3$ times the length of the sector for the Log-D propagator in the internal region) then we are likely to be in the presence of a local resonance and we proceed to point **3**; otherwise we go back to point **1**.

3. We invert the $\mathbf{K}$ matrix and solve eq.(10.14), that is we implement steps **1-2** with $\widetilde{\mathbf{K}}$ in place of $\mathbf{K}$ until a matrix inversion is required by the condition $h_{next} < h_{min}$. The only difference is that in the $\widetilde{\mathbf{K}}$ representation we *cannot* attempt to further reduce the dimensionality of the problem and therefore step **1** is a simple functional evaluation of the r.h.s. of eq.(10.14). For this reason we *force* the integration of the $\mathbf{K}$ equations by using for the $\widetilde{\mathbf{K}}$ equations a h_{min} value that is ten times larger then that used for equations (10.13).
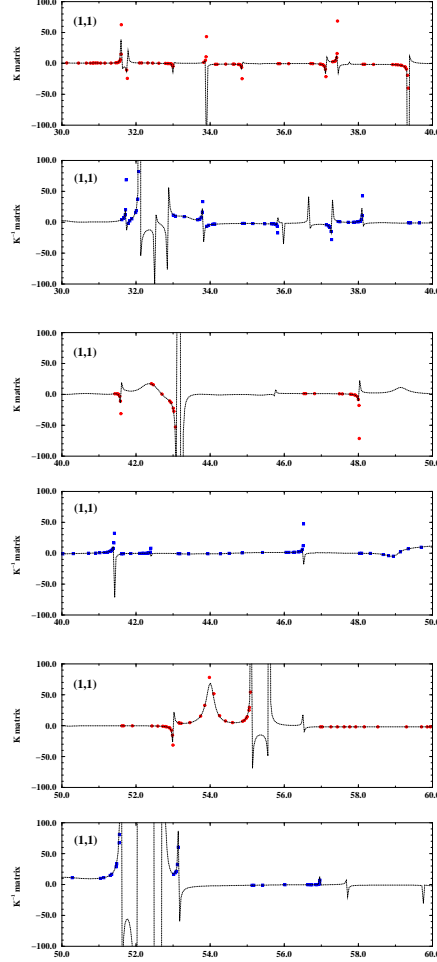
Figure 10.4: The new Varable-Phase propagator. The $(\mathbf{K})_{11}$(symbols in the upper panels) and $(\mathbf{K}^{-1})_{11}$(symbols in the lower panels) matrix elements computed during the integration are compared with exact Log-D results (dashed lines).

Clearly, a pathological situation in which the $\mathbf{K}$ matrix has a local resonance *and* a zero eigenvalue can arise. This case is signalled by the fact that in step **2** we find $h_{next} < h_{min}$ both for the $\mathbf{K}$ and for the $\widetilde{\mathbf{K}}$ equations. In this case we resort to a standard Log-Derivative integration for a small interval to overcome the relevant region. Extensive tests calculations, some of which will be described in the next section, show that if the ODE parameters h_{min} and ϵ are chosen with an educated guess the number of calls to this "safety" propagation is at most of the order of 10 in a range of thousands of angstroms

of potential integration. It is also clearly concentrated in the inner region of the integration.

In Fig.(10.4) we report the results of one the first successful propagations. One element of the $\mathbf{K}$ matrix and one of the $\mathbf{K}^{-1}$ matrix are shown in a given integration range together with "exact" values coming from Log-Derivative calculations (dashed lines). One can note (i) the presence of the "local resonances" mentioned above and corresponding switching between the two matrix, (ii) the use of a variable step size of integration and (iii) the accuracy of the channel reduction procedure.

10.4   Test calculations

The new propagator has been included in a new Fortran90 code for the treatment of atom-vibrating diatom scattering (Bodo, 2001). The code also includes the Log-D (Manolopulos, 1986) and the Log-D/Airy (Alexander and Manolopulos, 1987) propagators as were found implemented in the MOLSCAT scattering code (Hutson and Green, 1994) and with minor modifications to make them compatible with new code. The tests we are going to describe thus refers to the same program runs on the same machine (an Alpha Server with a DEC 21264 Alpha EV6 @ 500 MHz processor, with 256 Mb of RAM). As in the MOLSCAT code, linear algebra operations are performed, whenever possible, with the use of Lapack/Blas subroutines. All the three propagators use the same subroutine to generate the potential matrix as a function of R .

To test the present algorithm we used the $LiH - H^+$ subreactive potential (Section (7.1)) considering only the vibrationally diabatic ground-state potential. This means that converged calculations would require many more channels than those employed here. The rotational constant used was fixed at its rigid-rotor value, $B_0 = 7.40650\,cm^{-1}$. We used the Log-D propagator (Manolopulos, 1986) for the solution of the inelastic problem in the inner region, i.e. up to $R = 20.0$ Å. The VarPh propagator and the Log-D/Airy propagators were employed, starting from the $\mathbf{Y}(R = 20.0$ Å) matrix, up to $R = 2500$ Å. Different test calculations were performed at a given parity and total angular momentum (J). The collision energy was fixed at $E = 200\,cm^{-1}$; at this value only the $j = 0 - 4$ rotational levels are open in the target molecule.

In Fig.(10.5), as an example, we show the performance of the channel reduction procedure. Calculations with different numbers of channels were used to show the increase of the *rate of integration* as the number of channel is reduced during the propagation. This "rates" are computed as mean values in a interval with a constant number of channels. The different calculations

corresponds to the following parameters: $j = 0 - 20$ with $J = 10$ for 210 channels, $j = 0 - 30$ with $J = 10$ for 255 channels and $j = 0 - 30$ with $J = 30$ for 465 channels. The Log-D propagation was performed with a step size of 0.0024 Å that corresponds to 400 steps taken within half asymptotic wavelength of the lowest channel. The corresponding h_{min} parameter is chosen to be 3 times this value for the $\mathbf{K}$ matrix propagation and 10 times greater for the $\widetilde{\mathbf{K}}$ propagation. The accuracy parameter for the ODE integration, ϵ, is fixed at 10^{-5} while the channel reduction parameter, σ_{ch} of eq.(10.20), is chosen to be 10^{-6}. In Fig.(10.5) the speed of the Log-D propagation is also reported as dotted lines (clearly this speed is a decreasing function of the number of channels). We can note the following:

1. with the same number of channels the Variable-Phase propagator is *slower* than the Log-D propagator, and therefore much *slower* than the Log-D/Airy one. This is usually true, although the actual ratios depend on the regions of integration (remember that the number of matrix inversions is a problem dependent quantity).

2. although we used a reasonably low σ_{ch} parameter, the channel reduction procedure is quite efficient and within a few bohrs the speed is increased by $2 - 3$ orders of magnitude (left panel of Fig.(10.5)). As it is clear form the right panel of the same figure, at $40 - 45\,a_0$ all the closed channels are eliminated and the speed is determined by the few asymptotically open channels, which are 10 for each calculation.

In Table 10.1 we report the "statistics" of the propagation, i.e. the number of successful steps n_{ok}, the number of retried steps n_{bad} , the number of matrix inversions n_{inv} ,the number of "safety" call to Log-D n_{LD} and the final number of channels retained n_f . It is clear that for a reasonable choice of the input parameters the number of inversions and the number of calls to more robust Log-D propagation is quite low.

Table 10.1: Statistics of VP propagations

n_{ch}	n_{ok}	n_{bad}	n_{inv}	n_{LD}	n_f
210	5009	2539	46	3	10
255	4549	1466	6	0	10
465	5212	2383	52	4	10

Clearly all the above results make little sense unless one could also measure the accuracy of the propagation. In order to do this, we considered different calculations with a variable ϵ parameter but with a σ_{ch} parameter fixed
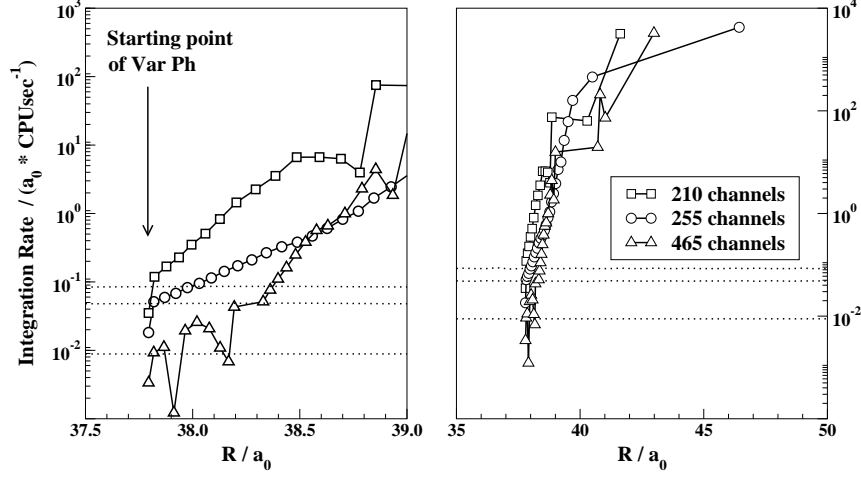
Figure 10.5: "Rate of integration" for different number of channels. Dotted lines correspond to the speed of log-derivative propagation.

at 10^{-6}. We compared these results with those obtained by using the Log-D/Airy (Alexander and Manolopulos, 1987) propagator; in this case different accuracies were obtained when varying the TOLHI parameter with a constant POW=3 (see Ref.(Alexander and Manolopulos, 1987) for the meaning of these quantities).

The accuracy of the present calculations were measured by computing the standard deviation Δ_{rms} of the S -matrix elements with respect to an "exact" calculation. We considered "exact" Log-D propagations used up to the ending point of integration (2500 Å) and with the same step size as that mentioned above (0.0024 Å). This step-size was chosen in a such a way to guarantee an accuracy greater than 10^{-6} for the above mentioned Δ_{rms}. The potential was artificially cut just before the ending point of integration because, in this way, we avoided artificial deviations due to the differences in the actual ending points that arise since both the present and the Log-D/Airy propagators work with a variable step. We compared the VP and Log-D/Airy propagators employing different numbers of channels: 55 channels corresponding to $j = 0 - 10$ and $J = 10$, 105 channels corresponding to $j = 0 - 15$ and $J = 10$ and, finally, the 210 channels calculation of before.

The results are reported in Fig.(10.6), where the CPU time of the long-range integration was computed by subtracting off the total time the CPU time used for the Log-D propagation in the inner region. The Figure clearly shows that, *for the same accuracy,* the present propagator is orders of magnitude faster than the Log-D/Airy one. This justifies our present suggestion for the

channel reduction procedure. The actual saving of CPU time strictly depends on the problem at hand, because the saving mainly arises from the fact that we solve a much smaller problem for the main part of the integration range, i.e. we are saving more time when using longer-ranged potentials. It is worth to note the following:

1. as already mentioned, the CPU time of the VP calculations is mainly due to the number of channels retained, which is the same for the different calculations reported here (i.e. 10).

2. with a fixed σ_{ch} parameter, the accuracy of the present method is a much steeper function of the CPU time than in the case of the Log-D/Airy propagator. This means that, in the present case, a much greater accuracy is reached with a reduced expenditure of computational time.

3. in the limit of $\epsilon \to 0$ the curves of Fig.(10.6) tend to become constant, i.e. the accuracy of the calculation are bound from below. This is due to the fact that below a given threshold, the σ_{ch} parameter starts to control the overall accuracy. Hence, a greater accuracy can be reached with lower values of σ_{ch}.
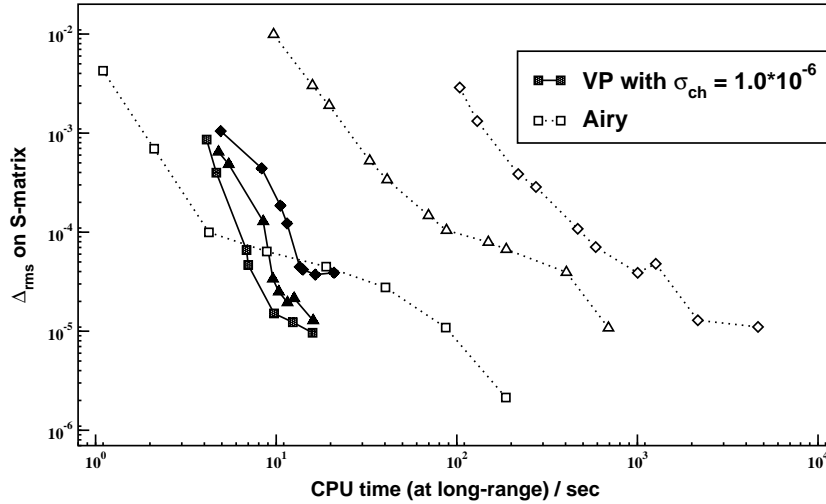

Figure 10.6: Comparison between the present Variable Phase propagator (filled-in symbols) and the Airy one. Squares for 55 channels, triangles for 105 channels and diamonds for 210 channels. See text for details.

Chapter 11

Conclusions

In this work we have presented a new and detailed study of the electronic structure of the LiH_2^+ and a first quantum mechanical study of its dynamics. We have first showed the connection of the title system with the early Universe chemistry, where the need for accurate rate constants has been highlighted showing the possible relevance that a revised Lithium chemistry could have in establishing the LiH abundance at low red-shifts. A more accurate evaluation of the chemical rate constants that enter the astrophysical models could be of help for the astrophysical community, in that it could prompt a temptative search of primordial LiH. The problems we have faced in this study have led us to some interesting results which can be useful in treating similar systems: the novel MultiReference Valence Bond approach to computing excited state wavefunctions, the modelization of the collision induced dissociation with time dependent methods and the study of a new algorithm for the treatment of collisions in presence of long range interactions were, indeed, necessary to fully understand the global dynamics of LiH_2^+.

The electronic structure of the title system has been analyzed to a high degree of precision using a newly developed approach to the study of excited states in the framework of the well established Spin Coupled Valence Bond method. The new approach is based on a specific *optimization* of *excited* Spin Coupled reference functions that is achieved with simple orthogonalization constraints to the SC orbitals. The orthogonalization relations mimic the relationships existing between the exact solutions of the problem. They give rise to good reference functions with which dynamical correlation can be brought directly in the excited states of interest by means of the recently developed perturbative optimization of the virtual orbitals. The accuracy has been tested favorably against FullCI calculations. It turned out that the excited Spin Coupled functions, like the ground-state SC function, preserve the major role in the final wavefunction, thereby allowing to gain a physical picture of

the excited-state interactions in the spirit of the Spin Coupled Valence Bond method.

The lower computational cost of these *ab-initio* calculations, with respect to equally accurate methods, has allowed us to gain a good description of the interaction forces for a considerable amount of different geometries. At the end, we are left with the first *ab-initio three dimensional* Potential Energy Surfaces for the lower-lying states of the title system. These PESs, once fitted, can be used in $3D$ quantum mechanical studies of the reactive and non-reactive dynamics, in order to furnish kinetic rate constants and excitation/relaxation coefficients to the astrophysical community. However, we have already obtained some interesting results on the system, either by looking at the resulting energy landscape and by performing reduced dimensionality quantum studies of the dynamics.

First of all, we have showed how the electronic structure that turned out from our calculations suggests that the non-adiabatic reactive pathways (see Figure 7.29 on page 187)

$$LiH + H^+ \rightarrow Li^+ + H_2$$
$$Li + H_2^+ \rightarrow LiH^+ + H \qquad\qquad (11.1)$$
$$LiH + H^+ \rightarrow LiH^+ + H$$
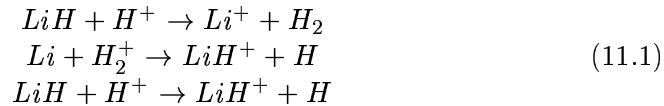
are not likely to take place in a rarefied and dust-free environment since the first two electronic states of the system are almost completely uncoupled one from each other. The above processes, tough, could be triggered by spontaneous emission but a simple reasonable estimate of the radiative constant seems to exclude this possibility. On the other hand, photon-stimulated processes are even more unlikely to happen, since the Wien tail of the black body distribution of the CBR at the recombination era does not contain sufficient energetic photons in the range 4-5 eV. We therefore concluded that *some changes to the network of reactions commonly used are necessary*. In particular, the first of reactions of eq.(11.1), together with the neutral-neutral reaction $LiH + H \rightarrow Li + H_2$, has been considered one of the major route to the destruction of primordial LiH, and was employed with a "guessed" rate of $10^{-9}\,\mathrm{cm^3\,s^{-1}}$. According to our calculations this value is too high and should be substituted with that computed for a much slower radiative process.

The remaining adiabatic paths that we were left with are:

$$LiH^+ + H \rightarrow Li^+ + H_2$$
$$LiH^+ + H \rightarrow Li^+ + H + H \qquad\qquad (11.2)$$
$$LiH + H^+ \rightarrow Li + H_2^+$$
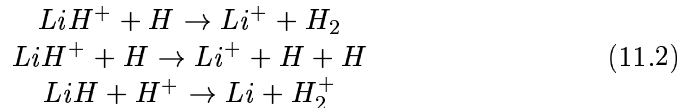
The first of the above processes is highly exoergic, but as we have seen, *the most probable outcome from a binary collision between LiH^+ and H is the*

dissociation product (second reaction) or the non-reactive event, at least in the collinear geometry sampled by our calculations. We found, indeed, that the reaction of the LiH^+ ion with H does not produce an appreciable quantity of H_2, since the collision induced dissociation process is by far the most likely event for energies slightly above ~ 0.1 eV. For energies below this value, the non-reactive product (a vibrationally excited LiH^+) is the dominant outcome of the collision, unless the ion is in a vibrationally excited state: in the latter case, a small fraction of highly excited H_2 is also produced. Furthermore, our Time-Dependent approach to the CID problem allowed to see a clearer relationship between the *initial vibrational state* of the colliding molecule and the *"shoulder structure"* in the CID probabilities. This structure was previously noted by some authors and assigned to an interference phenomena of vibrational origin.

Since the main result of our reduced dimensionality study of the ground-state dynamics was the lack of reaction in favor of the break-up of the system, we suggest to introduce the dissociation reaction in those deemed to be relevant for the modeling of the lithium chemistry in the primordial Universe. Indeed, our conclusions appear not modified when the full dimensionality of the problem is taken into account. It is worth to note, here, that such "full dimensionality" is still a challenge for dynamical calculations.

The third reaction of eq.(11.2) is governed by the first excited interaction potential. This potential turns out to have a complex topology, dominated by strong electrostatic forces acting between reactants and between products, which now differ only slightly in the energetic content. As a consequence, the resulting dynamics is quite complex because of the presence of long-lived states. We have found the expected *vibrational enhancement* that follows from the particular geometry of the saddle point, which require a substantially stretched LiH to be reached. Further, we argued that an "activation" mechanism for low energy scattering could work in this and similar charge-dipole systems: the formation of highly reactive metastable states (i.e. vibrational Feshbach resonances) could be of help for the reaction to occur, even in absence of initial vibrational excitation of the reagent molecule. However, in this case our qualitative results could be somewhat dependent on the treatment of the dynamical process; a $3D$ calculation urges but, just like the previous ground-state processes, it appears to be a challenge for dynamical (state-to-state) calculations.

The dipole-charge potential has been the subject of the last part of this work. This kind of potential, besides being somewhat pathological for the scattering theory, needs very long integration ranges. Furthermore, it is also very strong and thus requires that a huge number of channels should be used to give reliable scattering attributes. A novel algorithm that *reduces "on the*

fly" the number of channels used in a Time-Independent CC calculation has been designed. The algorithm relies on the known Variable Phase method and appears to be promising for the treatment of strong, long-range interaction potentials: test calculations proved that the new method can be, at the same accuracy level, order of magnitude faster than the widely used Log-Derivative-Airy algorithm.

Appendix A

Green's operators

We collect in this Appendix the properties of the Green's operators that we used in Chapters 2 and 3.

Green's operators arise naturally in linear problems of the kind $Ax = b$ when one looks for the "operator of the solutions", i.e. the inverse A^{-1}, in terms of which the solution is given by $x = A^{-1}b$. We consider here only those spaces and operators that are relevant for the present discussion, i.e. Hilbert spaces and self-adjoint operators in these spaces. In particular, we consider a self-adjoint operator $H : \mathcal{H} \to \mathcal{H}$ with the general spectrum depicted in the left panel of Fig.(A.1): a number of proper eigenvalues on the negative axis and a continuos spectrum that extends from zero to infinity (the choice of the zero is of course irrelevant). We intend H to be the hamiltonian of our system.

The fundamental eigenvalue equation

$$(\lambda - H) |\psi\rangle = 0$$

has its *inhomogeneous* generalization

$$(\lambda - H) |\psi\rangle = |\psi_0\rangle$$

whose "operator of solutions", or more properly *resolvent* or *Green's operator*,

$$G(\lambda) = (\lambda - H)^{-1}$$

plays a central role in spectral theory. It is a well defined operator for every λ value out of the spectrum of H, i.e. in our case whenever λ has a non null immaginary part or, if real, is not a proper or improper eigenvalue of H. Thus the (close) set of points of the complex plane that make up the spectrum of H ($\sigma(H)$) define the (open) set of points of the domain of the *function* $G(\lambda)$, called the *resolvent set* and denoted with $\rho(H)$. It turns out that in this set
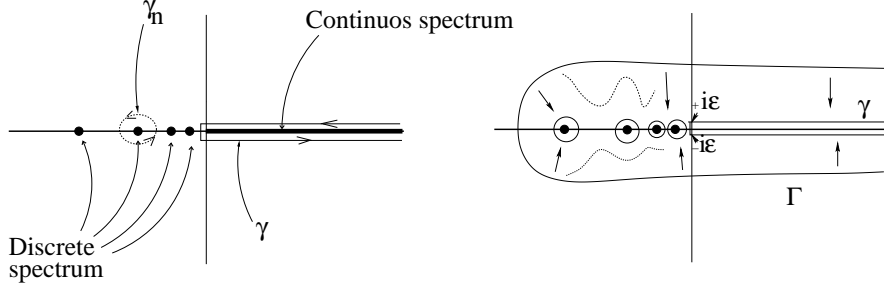
Figure A.1: "Typical" spectrum and countor paths considered in the main text.

the Green's operator is a *bound* operator $(G(\lambda) \in L(\mathcal{H}))$ and it is an *analytic* function of its complex argument, i.e. it has a power series representation for each $\lambda \in \rho(H)$

$$G(\lambda) = G(\lambda_0) \left\{ \mathbf{I} + \sum_{n=1}^{\infty} (\lambda - \lambda_0)^n (-)^n G^n(\lambda_0) \right\} \quad \lambda, \lambda_0 \in \rho(H) \qquad (A.1)$$

where the convergence of the serie is in the norm topology of $L(\mathcal{H})$ whitin the circle

$$|\lambda - \lambda_0| \, \|G(\lambda_0)\| < 1$$

The spectrum of H is a set of singular points for $G(\lambda)$: the proper eigenvalues are *first order poles* whereas the improper eigenvalues determine a *branch cut*. These properties can be seen by looking at the spectral resolution of $G(\lambda)$

$$G(\lambda) = \sum_n \frac{1}{\lambda - E_n} P_n + \int_0^{\infty} \frac{1}{\lambda - E} dP_E$$

where P_n is the projector onto the proper eigenspace of H corresponding to the eigenvalue E_n and dP_E is the differential projector operator onto the improper E−eigenspace, usually written in the form $dP_E = \delta(E - H)dE$.

The polar discontinuity around each true eigenvalue can be used in conjunction with the residue theorem to write

$$\frac{1}{2\pi i} \oint_{\gamma_n} G(\lambda)d\lambda = P_n \qquad (A.2)$$

where γ_n is any couterclokwise path that encloses (only) the E_n eigenvalue. The branch cut determines a discontinuity of the Green's operator when it is considered across the continuum spectrum of H; that is, if we define the following (weak) *limiting* operators

$$G^{\pm}(E) = lim_{\epsilon \to 0^+} G(E \pm i\epsilon) \quad \text{for } E > 0$$

we have

$$G^+(E) - G^-(E) \neq 0$$

In general, taking into account the existence of the branch cut we may rewrite the residue theorem in the form

$$\frac{1}{2\pi i} \oint_\Gamma G(\lambda)d\lambda = \mathbf{I}$$

where Γ is any counterclockwise path that encloses the whole spectrum of H. If we compare it with the spectral resolution of the unit operator

$$\mathbf{I} = \sum_n P_n + \int_0^\infty \delta(E - H)dE$$

and distort the Γ path as in the right panel of Fig.(A.1) we obtain again eq.(A.2) for each discrete eigenvalue and get, for the continuum spectrum,

$$\frac{1}{2\pi i} \oint_\gamma G(\lambda)d\lambda = \frac{1}{2\pi i} lim_{\epsilon \to 0^+} \int_0^\infty \{G(E-i\epsilon) - G(E+i\epsilon)\}dE = \int_0^\infty \delta(E-H)dE$$

from which it follows the novel relation

$$i(G^+(E) - G^-(E)) = 2\pi\delta(E - H) \tag{A.3}$$

which parallels the previous eq.(A.2). In general using eq.(A.2) and eq.(A.3) in the spectral resolution of any *analytic* function of H

$$f(H) = \sum_n f(E_n)P_n + \int_0^\infty f(E)\delta(E - H)dE$$

one may obtain the following representation theorem

$$f(H) = \frac{1}{2\pi i} \oint_\Gamma f(\lambda)G(\lambda)d\lambda = \frac{1}{2\pi i} \oint_\Gamma \frac{f(\lambda)}{\lambda - H}d\lambda$$

(where in the last term we have used a very common notation for $G(\lambda)$) which closely resembles the well known Cauchy representation theorem

$$f(z) = \frac{1}{2\pi i} \oint_\Gamma \frac{f(\lambda)}{\lambda - z}d\lambda$$

where now Γ is any counterclockwise path surrounding the pole of the integrand.

Equation (A.3) identifies the previously mentioned discontinuity of the Green's operator with a pure "immaginary" operator $-2\pi i\delta(E - H)$. Thus, we may write

$$G^\pm(E) = G^p(E) \mp i\pi\delta(E - H)$$

where $G^p(E) = (G^+(E) + G^-(E))/2$ is the "real" (i.e. self-adjoint) part of the Green's operator, also called the "principal value" Green's operator. Its name arises from its spectral resolution

$$G^p(E) \equiv \sum_n \frac{1}{\lambda - E_n} P_n + P \int_0^\infty \frac{1}{E - E'} \delta(E' - H) dE' =$$

$$= \sum_n \frac{1}{\lambda - E_n} P_n + lim_{\epsilon \to 0^+} \left(\int^{E-\epsilon} + \int_{E+\epsilon} \right) \delta(E' - H) dE'$$

Of course, when $E < 0$ ($E \neq E_n$), $G^p(E) = G^+(E) = G^-(E)$.

The power serie of eq.(A.1) allows us to write the Green's operator in λ once we know the operator in a point λ_0 sufficiently close to λ. More important for our purposes is the fact that the Green's operator satisfies the *Lippmann-Schwinger* equation, which can be obtain starting with

$$(\lambda - H^0) = (\lambda - H) + V$$

(where $H = H^0 + V$ is any useful decomposition of H) and multiplying on the left by $G^0(\lambda) = (\lambda - H^0)^{-1}$ and on the right by $G(\lambda)$, i.e.

$$G(\lambda) = G^0(\lambda) + G^0(\lambda) V G(\lambda)$$

Analogous equation can be obtained multiplying on the right by G^0 and on the left by G,

$$G(\lambda) = G^0(\lambda) + G(\lambda) V G^0(\lambda)$$

These equations are very useful in practice; for example, they allow one to obtain approximations to the "full" Green's operator in terms of the known $G^0(\lambda)$ operator and the "perturbing" potential $V = H - H^0$.

In connection with the Time Dependent Schrödinger Equation (TDSE) we note that the half "Fourier" transforms

$$\int_0^{\pm\infty} e^{i\lambda t} U_t dt$$

are well defined for each $\pm \text{Im}\lambda > 0$ and can be computed using the TDSE

$$H U_t = i \frac{dU_t}{dt}$$

Indeed, we can write

$$i \frac{d}{dt}(e^{i\lambda t} U_t) = -(\lambda - H)(e^{i\lambda t} U_t)$$

and then

$$\int_0^{\pm\infty} e^{i\lambda t} U_t dt = -iG(\lambda) \int_0^{\pm\infty} \frac{d}{dt}(e^{i\lambda t} U_t) dt = -iG(\lambda)\{lim_{t\to\pm\infty} e^{i\lambda t} U_t - 1\} = iG(\lambda)$$

Thus, the limiting operators $G^{\pm}(E)$ can be defined also by

$$iG^{\pm}(E) = lim_{\epsilon\to0^+} \int_0^{\pm\infty} e^{i(E\pm i\epsilon)t} U_t dt$$

and their immaginary part can be obtained by the standard Fourier formula

$$\frac{i}{2\pi}(G^+(E) - G^-(E)) = \frac{1}{2\pi}\int_{-\infty}^{+\infty} e^{i(E-H)t} dt = \delta(E - H)$$

Therefore, we see that the $G^{\pm}(E)$ operators entail the forward/backward time evolution and their combined action gives a "stationary" situation. In this context it is worth to compare the $G^{\pm}(E)$ operators with the (improper) Fourier transforms of the following step functions

$$\Theta^{(\pm)}(t) = \begin{cases} \pm e^{-iE_0 t} & \text{for } \pm t > 0 \\ 0 & \text{otherwise} \end{cases}$$

$$\int_{-\infty}^{+\infty} e^{iEt} \Theta^{(\pm)}(t) dt = lim_{\epsilon\to0^+} \frac{i}{E - E_0 \pm i\epsilon}$$

and with the following representations of the Dirac delta function

$$\int_{-\infty}^{+\infty} e^{iEt}(\Theta^{(+)}(t) - \Theta^{(-)}(t)) dt = \int_{-\infty}^{+\infty} e^{i(E-E_0)t} dt = 2\pi\delta(E - E_0) \equiv$$

$$i\, lim_{\epsilon\to0^+} \left\{ \frac{1}{E - E_0 + i\epsilon} - \frac{1}{E - E_0 - i\epsilon} \right\} = lim_{\epsilon\to0^+} \frac{2\epsilon}{(E - E_0)^2 + \epsilon^2}$$

The forward/backward nature of $G^{\pm}(E)$ ($E > 0$) gives rise to the asymptotic behaviour of their matrix elements. Before showing the relevant formula it is worth to note that the following quantities

$$\left\langle \mathbf{x} \middle| G^{\pm}(E) \middle| \psi_0 \right\rangle$$

are, by definition, solutions of the following inhomogeneous problem

$$(E - H_s)\psi(\mathbf{x}) = \psi_0(\mathbf{x})$$

(where H_s is the usual Schrödinger representation of H): as $r = \|\mathbf{x}\| \to \infty$ we have $\psi_0(\mathbf{x}) \to 0$ for any L^2 function and, thus, the equation reduces asymptotically to the (improper) free particle equation, whose boudary conditions must be chosen according to the limiting ϵ process, which we now decribe.

We consider only the free particle Green's function integral

$$\left\langle \mathbf{x} \middle| G_0^{\pm}(E) \middle| \psi_0 \right\rangle$$

since we can always use the Lippmann-Schwinger equation $G^{\pm}(E) = G_0^{\pm}(E)(\mathbf{I} + VG^{\pm}(E)) = G_0^{\pm}(E)\Omega_{\mp}^{\dagger}(E)$ to write

$$\left\langle \mathbf{x} \middle| G^{\pm}(E) \middle| \psi_0 \right\rangle = \left\langle \mathbf{x} \middle| G_0^{\pm}(E) \middle| \psi_1 \right\rangle$$

with

$$|\psi_1\rangle = \left| \Omega_{\mp}^{\dagger}(E)\psi_0 \right\rangle$$

(note that although the action of $G^{\pm}(E)$ on $|\psi_0\rangle$ gives rise to an improper eigenvector the presence of the potential V ensures that $|\psi_1\rangle$ is still a proper vector when $r^{3/2}V(r) \to 0$ as $r \to \infty$). Furthermore, we start by looking at the general "Green's function"

$$\left\langle \mathbf{x} \middle| G_0(\lambda) \middle| \mathbf{x}' \right\rangle$$

which can be evaluated inserting the momentum resolution of the identity operator

$$\left\langle \mathbf{x} \middle| G_0(\lambda) \middle| \mathbf{x}' \right\rangle = \frac{1}{(2\pi)^3} \int d^3\mathbf{p} \frac{e^{i\mathbf{p}(\mathbf{x}-\mathbf{x}')}}{\lambda - E_p}$$

where $E_p = p^2/2m$. Using polar coordinates and performing the angular integration we obtain

$$\left\langle \mathbf{x} \middle| G_0(\lambda) \middle| \mathbf{x}' \right\rangle = \frac{1}{(2\pi)^2} \left\{ \int_0^{\infty} dp \frac{p^2}{\lambda - E_p} \frac{e^{ip\|\mathbf{x}-\mathbf{x}'\|}}{ip \|\mathbf{x} - \mathbf{x}'\|} - \int_0^{\infty} dp \frac{p^2}{\lambda - E_p} \frac{e^{-ip\|\mathbf{x}-\mathbf{x}'\|}}{ip \|\mathbf{x} - \mathbf{x}'\|} \right\}$$

which can be rewritten as

$$\left\langle \mathbf{x} \middle| G_0(\lambda) \middle| \mathbf{x}' \right\rangle = \frac{1}{(2\pi)^2} \int_{-\infty}^{+\infty} dp \frac{p}{\lambda - E_p} \frac{e^{ip\|\mathbf{x}-\mathbf{x}'\|}}{i \|\mathbf{x} - \mathbf{x}'\|}$$

and evaluated using contour intergration. The appropriate path is an infinite semicircle on the *upper* complex plane and the relevant pole of the integrand is at the point $\xi = (2m\lambda)^{1/2}$, defined to be the root with $\text{Im}\,\xi > 0$. This point is of the form $\xi = \pm p_0 + i\delta$ when $\lambda = p_0^2/2m \pm i\epsilon$ ($p_0 > 0$ and $\delta, \epsilon \to 0^+$). Thus, the result is

$$\left\langle \mathbf{x} \middle| G_0^{\pm}(E) \middle| \mathbf{x}' \right\rangle = -\frac{m}{2\pi} \frac{e^{\pm ip\|\mathbf{x}-\mathbf{x}'\|}}{\|\mathbf{x} - \mathbf{x}'\|} \quad E = \frac{p^2}{2m} > 0$$

(note that it correctly reduces to the Coulomb potential when $p \to 0$, i.e. when the relevant inhomogeneous Schrödinger equation reduces to the Poisson

equation for a point charge). Adversely, when $E = -p_0^2/2m < 0$ the position of the relevant pole is at the point $\xi = ip_0$ and thus

$$\left\langle \mathbf{x} \middle| G_0(E) \middle| \mathbf{x}' \right\rangle = -\frac{m}{2\pi} \frac{e^{-p\|\mathbf{x}-\mathbf{x}'\|}}{\|\mathbf{x}-\mathbf{x}'\|} \quad E < 0$$

(remember that in this case $G^+ = G^-$).

Finally, going back to our original problem, the asymptotic $r \to \infty$ behaviour of the integral

$$\left\langle \mathbf{x} \middle| G_0^\pm(E) \middle| \psi_0 \right\rangle = \int d\mathbf{x}^3 \left\langle \mathbf{x} \middle| G_0^\pm(E) \middle| \mathbf{x}' \right\rangle \left\langle \mathbf{x}' \middle| \psi_0 \right\rangle$$

can be obtained by observing that if $\psi_0(\mathbf{x}')$ is well localized the value of the integral depends essentially from the small $r' = \|\mathbf{x}'\|$ region and, then, we can use $\|\mathbf{x} - \mathbf{x}'\| = r \|\widehat{\mathbf{x}} - \mathbf{x}'/r\| \to r - \widehat{\mathbf{x}}\mathbf{x}'$ for $r/r' \to \infty$. The result is

$$\left\langle \mathbf{x} \middle| G_0^\pm(E) \middle| \psi_0 \right\rangle \to -\frac{m}{2\pi} \frac{e^{\pm ipr}}{r} \int d^3\mathbf{x}' e^{\mp ip\widehat{\mathbf{x}}\mathbf{x}'} \left\langle \mathbf{x}' \middle| \psi_0 \right\rangle = -m(2\pi)^{1/2} \frac{e^{\pm ipr}}{r} \left\langle \pm p\widehat{\mathbf{x}} \middle| \psi_0 \right\rangle$$

and therefore, in general

$$\left\langle \mathbf{x} \middle| G^\pm(E) \middle| \psi_0 \right\rangle \to -m(2\pi)^{1/2} \frac{e^{\pm ipr}}{r} \left\langle \pm p\widehat{\mathbf{x}}\mp \middle| \psi_0 \right\rangle$$

where the fact $\langle \mathbf{p} | \Omega_\pm^\dagger(E) = \langle \mathbf{p}\pm|$ (for $E = p^2/2m$, $p = \|\mathbf{p}\|$) has been used. It is worth to note that in the previous expansion of the distance between the "source" and the "observation point", $\|\mathbf{x} - \mathbf{x}'\|$, the localization property of $\psi_0(\mathbf{x})$ $(\psi_1(\mathbf{x}))$ is a necessary condition for the validity of the results; in particular, the "error" term

$$\int_{r' \gg r} d^3\mathbf{x}' \frac{e^{\pm ip\|\mathbf{x}-\mathbf{x}'\|}}{\|\mathbf{x}-\mathbf{x}'\|} \psi_0(\mathbf{x}') \sim \int_{r' \gg r} dr' r' \, e^{\pm ipr'} \int d^2\widehat{\mathbf{x}}' \psi_0(\mathbf{x}')$$

must be, first of all, a *finite* quantity (and it must converge to zero when $r \to \infty$). Thus, for example, the case $\psi_0(r) = O(r^{-2})$ already gives rise to a not well defined integral. In this context it is worth to mention that such situation can arise when one looks at the asymptotic behaviour of the *full* Green's function and uses the previous substitution $\psi_1(\mathbf{x}) = \psi_0(\mathbf{x}) + V(\mathbf{x}) \left\langle \mathbf{x} \middle| G^\pm(E) \middle| \psi_0 \right\rangle$ with $V(r) = O(r^{-2})$.

Bibliography

Abramowitz, M. and Stegun, I. A.: 1972, *Handbook of Mathematical Functions*, Dover Pubblications, Inc., New York

Alexander, M. H.: 1984, *J. Chem. Phys.* **81(10)**, 4510

Alexander, M. H. and Manolopulos, D. E.: 1987, *J. Chem. Phys.* **86(4)**, 2044

Althorpe, S. C., Kouri, D. J., Hoffman, D. H., and Zhang, J. Z. H.: 1997, *J. Chem. Soc., Faraday Trans.* **93(5)**, 703

Arthurs, A. M. and Dalgarno, A.: 1960, *Proc. R. Soc.* **256(A)**, 540

Bagus, P. S. and Moser, C. M.: 1973, *J. Chem. Phys.* **58**, 1886

Balakrishanan, N., Kalyanaraman, C., and Sathyamurthy, N.: 1997, *Phys. Rep.* **280**, 79

Balint-Kurti, G. G., Dixon, R. N., and Martson, C. C.: 1990, *J. Chem. Soc. Faraday Trans.* **86**, 1741

Barg, G. D., Kendall, G. M., and Toennies, J. P.: 1976, *Chem. Phys.* **16**, 243

Bernstein, R. B. (ed.): 1979, *Atom Molecule Collision Theory*, Plenum Press, N.Y.

Bililign, S., Hattaway, B. C., Robinson, T. L., and Jeung, G. H.: 2001, *J. Chem. Phys.* **114**, 7052

Bodo, E.: 2001, *Ph.D. thesis*, University of Rome

Bodo, E., Buonomo, E., Gianturco, F. A., Kumar, S., Famulari, A., Raimondi, M., and Sironi, M.: 1998a, *Chem. Phys.* **237**, 315

Bodo, E., Gianturco, F. A., Martinazzo, R., Paesani, F., and Raimondi, M.: 2000, *J. Chem. Phys.* **113(24)**, 11071

Bodo, E., Gianturco, F. A., Martinazzo, R., and Raimondi, M.: 2001, *Eur. Phys. J. D* **15**, 321

Bodo, E., Kumar, S., Gianturco, F. A., Famulari, A., Raimondi, M., and Sironi, M.: 1998b, *J. Phys. Chem. A* **102(47)**, 9390

Bougleux, E. and Galli, D.: 1997, *Mon. Not. R. Astron. Soc.* **288**, 638

Bruna, P. J. and Peyerimhoff, S. D.: 1987, in K. P. Lawley (ed.), *Ab-initio methods in quantum chemistry (Adv. Chem. Phys. Series)*, John Wiley & Sons, New York

Calogero, F.: 1967, *Variable Phase Approach to Potential Scattering*, Aca-

demic, N.Y.

Clark, C. W.: 1979, *Phys. Rev. A* **20(5)**, 1875

Clarke, N. J., Raimondi, M., Sironi, M., and Cooper, D.: 1998a, *Theor. Chem. Acta* **95**, 1328

Clarke, N. J., Sironi, M., Raimondi, M., Kumar, S., Gianturco, F. A., Buonomo, E., and Cooper, D. L.: 1998b, *Chem. Phys.* **233**, 9

Collins, L. A. and Nocross, D. W.: 1978, *Phys. Rev. A* **18(5)**, 467

Cooper, D. L.: 1984, *J. Chem. Phys.* **80**, 1961

Cooper, D. L., Gerrat, J., and Raimondi, M.: 1987, *Adv. Chem. Phys.* **69**, 319

Cooper, D. L., Gerrat, J., and Raimondi, M.: 1991, *Chem. Rev.* **91**, 929

Cooper, D. L., Gerratt, J., Raimondi, M., Sironi, M., and Thorsteinsonn, T.: 1993, *Theor. Chim. Acta* **85**, 261

Coulson, C. A. and Fisher, I.: 1949, *Phys. Mag.* **40**, 386

Dalgarno, A., Stancil, P. C., and Kirby, K.: 1996, *Astrophys. J.* **458**, 397

de Bernardis, P., Dubrovnich, V., Encrenaz, P., Maoli, R., Masi, S., Mastrantonio, G., Melchiorri, B., Melchiorri, F., Signore, M., and Tanzilli, P. E.: 1993, *Astron. Astrophys.* **269**, 1

Degasperis, A.: 1964, *Il Nuovo Cimento* **XXXIV(6)**, 1667

Diestler, D. J.: 1979, in R. B. Bernstein (ed.), *Atom Molecule Collision Theory*, Chapt. 20, Plenum Press, N.Y.

Dourneuf, M. L. and Lan, V. K.: 1977, *J. Phys. B* 10(L35)

Dubrovnich, V. K.: 1993, *Astron. Lett.* **23**, 19

Edmonds, A. R.: 1957, *Angular momentum in quantum mechanics*, Princeton

Feit, M. D. and J. Fleck, J.: 1984a, *J. Chem. Phys.* **78**, 301

Feit, M. D. and J. Fleck, J.: 1984b, *J. Chem. Phys.* **80**, 2578

Feit, M. D., J. Fleck, J., and Steigner, A.: 1982, *J. Comp. Phys.* **47**, 412

Galli, D. and Palla, F.: 1998, *Astron. and Astrophys.* **335**, 403

Gerratt, J.: 1971, *Adv. Atom. Mol. Phys.* **7**, 141

Gerratt, J. and Raimondi, M.: 1980, *Proc. Roy. Soc. Lond.* **A371**, 525

Gianturco, F. A.: 1979, *The Transfer of Molecular Energies by Collision: Recent quantum treatments*, Sringer Verlag, Berlin

Gianturco, F. A. and Giorgi, P. G.: 1996, *Phys. Rev. A* **54(5)**, 4073

Gianturco, F. A. and Giorgi, P. G.: 1997, *Ap. J.* **479**, 560

Gianturco, F. A., Kumar, S., Pathak, S. K., Raimondi, M., and Sironi, M.: 1997a, *Chem. Phys.* **215**, 239

Gianturco, F. A., Kumar, S., Pathak, S. K., Raimondi, M., Sironi, M., Gerrat, J., and Cooper, D. L.: 1997b, *Chem. Phys.* **215**, 227

Gianturco, F. A. and Paioletti, P.: 1998, in K. H. Beker (ed.), *Novel Aspects of Electron Molecule Scattering*, p. 256, World Scientific Pub.

Goldfed, M., Quandt, R. E., and Trotter, H. F.: 1996, *Econometrica* **34**, 546

Hammermesh, M.: 1989, *Group theory and its applications to physical prob-*

lems, Dover Publ. Inc.

Hartquist, T. W., Caselli, P., Rawlings, J. M. C., Ruffle, D., and Williams, D. A.: 1998, in T. W. Hartquist and D. A. Williams (eds.), *The Molecular Astrophysics of Star and Galaxies*, Clarendon Press, Oxford

Heitler, W. and London, F.: 1927, *Z. Phys.* **44**, 455

Henriet, C. and Verhagen, G.: 1986, *Phys. Scripta* **33**, 229

Hershbach, D. R.: 1987, *Angew. Chem. Int. Eng. Ed.* **26**, 1221

Herzberg, G.: 1950, *Spectra of diatomic molecules*, Van Nostrand Reinhold, N.Y.

Hobza, P. and Schleyer, R. R.: 1984, *Chem. Phys. Lett.* **105**, 630

Huber, K. P. and Herzberg, G.: 1979, *Molecular spectra and molecular structure*, Van Nostrand Reinhold, N.Y.

Hussain, A. N. and Roberts, G.: 2000, *Phys. Rev. A* 63

Hutson, J. M. and Green, S.: 1994, *Molscat computer code version 14*, distributed by Collaborative Computational Project No. 6 of the engineering and Physica Sciences Research Council (UK)

Hyamas, P. A., Gerratt, J., Cooper, D. L., and Raimondi, M.: 1994, *J. Chem. Phys.* **100**, 4417

Itikawa, Y.: 1978, *Phys. Rep.* **46**, 117

Jauch, J. M.: 1958, *Helv. Phys. Acta* **31**, 661

Johnson, B. R.: 1980, *J. Chem. Phys.* **73**, 5051

Johnson, B. R.: 1983a, *J. Chem. Phys.* **79**, 1906

Johnson, B. R.: 1983b, *J. Chem. Phys.* **79**, 1916

Karadakov, P., Cooper, D. L., Gerratt, J., and Raimondi, M.: 1992, *J. Chem. Phys.* **97**, 7637

Kaye, J. A. and Kuppermann, A.: 1981, *Chem. Phys. Letters* **78**, 546

Kaye, J. A. and Kuppermann, A.: 1985, *Chem. Phys. Letters* **115**, 158

Kaye, J. A. and Kuppermann, A.: 1988, *Chem. Phys.* **125**, 279

Khron, S., Lauge, M., Knoll, L., Kreckel, H., Levin, J., Repnow, R., Schwalm, D., Wester, R., Wittle, P., Wolf, A., and Zaijfman, D.: 2001, *Phys. Rev. Lett.* **86**, 4005

Kosloff, D. and Kosloff, R.: 1983, *J. Comput. Phys.* **52**, 35

Kouri, D. J.: 1979, in R. B. Bernstein (ed.), *Atom Molecule Collision Theory*, Chapt. 9, Plenum Press, N.Y.

Kuppermann, A.: 1975, *Chem. Phys. Lett.* **32**, 374

Landau, L. D.: 1996, *Quantum Mechanics - Theoretical Physics*, Vol. 3, Butterworth-Heinemann, 3rd edition

Landau, L. D.: 1997, *The Classical Theory of Fields - Theoretical Physics*, Vol. 2, Butterworth-Heinemann, 4th edition

Larsson, M.: 1984, *J. Chem. Phys.* **81**, 6409

Larsson, M.: 1985, *Phys. Scripta* **32**, 97

Launay, J. M.: 1976, *J. Phys. B* **9(10)**, 1823

Launay, J. M.: 1977, *J. Phys. B* **10(18)**, 3665

Lee, H. S., Lee, Y. S., and Jeung, G.: 1999, *J. Phys. Chem. A* **103**, 11080

Lepp, S. and Shull, J. M.: 1984, *Astrophys. J.* **280**, 465

Lepp, S. and Stancil, P. C.: 1998, in T. W. Hartquist and D. A. Williams (eds.), *The Molecular Astrophysics of Star and Galaxies*, Clarendon Press, Oxford

Lester, W. A.: 1971, *J. Chem. Phys.* **54(7)**, 3171

Levine, R. D.: 1969, *Quantum mechanics of molecular rate processes*, Oxford University Press, London

Levine, R. D. and Bernstein, R. B.: 1987, *Molecular reaction dynamics and chemical reactivity*, Oxford University Press

Light, J. C., Hamilton, I. P., and Vill, J. V.: 1985, *J. Chem. Phys.* **82**, 1400

Light, J. C. and Zhang, D. H.: 1998, *Faraday Discuss.* **110**, 105

Lippmann, B. and Schwinger, J.: 1950, *Phys. Rev.* **79**, 469

Machado, F. B. C., Roberto-Neto, O., and Ornellas, F. R.: 1998, *Chem. Phys. Lett.* **284**, 293

Mahapatra, S. and Sathyamurthy, N.: 1995, *J. Chem. Phys.* **102(15)**, 6057

Mahapatra, S. and Sathyamurthy, N.: 1996, *J. Chem. Phys.* **105(24)**, 10934

Mahapatra, S. and Sathyamurthy, N.: 1997, *J. Chem. Phys.* **107(17)**, 6621

Manolopulos, D. E.: 1986, *J. Chem. Phys.* **85(11)**, 6425

Maoli, R., Melchiorri, F., and Tosti, D.: 1994, *Astrophys J.* **425**, 372

Martinez, T. J.: 1997, *Chem. Phys. Lett.* **272**, 139

Massey, H. S. W.: 1932, *Proc. Cambridge Phylos. Soc.* **28**, 99

Messiah, A.: 2000, *Quantum mechanics*, Dover, New York

Miller, W. H.: 1974, *J. Chem. Phys.* **61**, 1823

Miller, W. H.: 1998, *Faraday Discuss.* **110**, 1

Miller, W. H., Schwartz, S. D., and Tromp, J. W.: 1983, *J. Chem. Phys.* **79**, 4889

Moore, C. E.: 1971, *Atomic Energy Levels*, National Bureau Standards, Cir. No. 467; G.P.O.: Washington, DC

Morse, P. M. and Feshbach, H.: 1953, *Methods of theoretical physics*, McGraw-Hill Book Company, New York

Mrugala, F. and Secrest, D.: 1983, *J. Chem. Phys.* **78(10)**, 5954

Neuhauser, D. and Baer, M.: 1989, *J. Phys. Chem.* **93**, 2827

Nobusada, K. and Sakimoto, K.: 1997, *J. Chem. Phys.* **106(22)**, 9078

Nobusada, K. and Sakimoto, K.: 1998, *Chem. Phys. Letters* **288**, 311

Nobusada, K., Sakimoto, K., and Onda, K.: 1995, *Chem. Phys. Letters* **233**, 399

Onda, K. and Sakimoto, K.: 1999, *J. Chem. Phys.* **111**, 988

Pack, R. T.: 1974, *J. Chem. Phys.* **60(2)**, 633

Palla, F., Salpeter, E. E., and Stahler, S. W.: 1983, *Astrophys, J.* **271**, 632

Peebles, P. J. E. and Dicke, R. H.: 1968, *Astropys. J* **451**, 44

Peng, T., Zhu, W., Wang, D., and Zhang, J. Z. H.: 1998, *Faraday Discuss.* **110**, 159

Petsalakis, I. D., Thoedorakopoulos, G., and Nicolaides, C. A.: 1992, *J. Chem. Phys.* **97**, 7623

Press, W. H., Flannery, B. P., Teukolsky, S. A., and Vetterling, W. T.: 1986, *Numerical Recipes*, Cambridge University Press

Puy, D. and Signore, M.: 1999, *New Astronomy Reviews* **43**, 223

Raimondi, M., Sironi, M., Gerratt, J., and Cooper, D. L.: 1996, *Int. J. Quant. Chem.* **60**, 225

Rerat, M., Mérawa, M., and Pouchan, C.: 1992, *Phys. Rev. A* **46(9)**, 5471

Rumer, G.: 1932, *Gottingen Nachr.* p. 377

Sadeghpour, H. R., Bohn, J. L., Cavagnero, M. J., Esry, B. D., Fabrikant, I. I., Macek, J. H., and Ran, A. R. P.: 2000, *J. Phys. B: At. Mol. Opt. Phys.* **33**, R93

Sakimoto, K.: 1996, *Chem. Phys. Letters* **248**, 414

Sakimoto, K.: 1997, *Faraday Disc.* **93(5)**, 791

Sakimoto, K.: 1998, *Chem. Phys.* **228**, 167

Sakimoto, K.: 1999, *J. Chem. Phys.* **110(23)**, 11233

Sakimoto, K.: 2000, *J. Chem. Phys.* **112(11)**, 5044

Sakimoto, K. and Onda, K.: 1994, *J. Chem. Phys.* **100(2)**, 1171

Saslaw, W. C. and Zipoy, D.: 1967, *Nat.* **216**, 967

Sathyamurthy, N.: 2000, *Private communication*

Schrodinger, E.: 1926, *Ann. Phys.* **79**, 361

Scoles, G. (ed.): 1988, *Atomic and Molecular Beam Methods*, Oxford University Press

Searles, D. J. and von Nagy-Felsobuki, E. I.: 1991, *Phys. Rev. A* **43(7)**, 3365

Simonetta, M., Gianinetti, E., and Vandoni, I.: 1968, *J. Chem. Phys.* **48**, 1968

Sironi, M.: 1989, *Ph.D. thesis*, University of Milan

Smith, F. T.: 1962, *J. Math. Phys.* **3**, 735

Stancil, P. C., Lepp, S., and Dalgarno, A.: 1996, *Astrophys. J.* **458**, 401

Stwalley, W. C. and Zemke, W. T.: 1993, *J. Phys. Chem. Ref. Data* **22(1)**, 87

Tal-Ezer, H. and Kosloff, R.: 1984, *J. Chem. Phys.* **81**, 3967

Taylor, B. K. and Hinde, J.: 1999, *J. Chem. Phys.* **111**, 973

Taylor, J. R.: 1969, *Scattering Theory: The quantum theory of nonrelatistic collisions*, Robert E. Krieger Publishing Company, Malabar, Florida

Vill, J. V., Parker, G. A., and Light, J. C.: 1982, *Chem. Phys. Lett.* **89**, 483

Whitten, R. C. and Smith, F. T.: 1968, *J. Math. Phys.* **9**, 1103

Wu, C. H.: 1979, *J. Chem. Phys.* **71**, 783

Zemach, C.: 1964, *Il Nuovo Cimento* **XXXIII(3)**, 939

Zewail, A. H.: 2000, *J. Phys. Chem. A* **104**, 5660

Zhang, D. H., Wu, Q., and Zhang, J. Z.: 1995, *J. Chem. Phys.* **102(1)**, 124

Zhang, D. H. and Zhang, J. Z. H.: 1994a, *J. Chem. Phys.* **101**, 1146

Zhang, D. H. and Zhang, J. Z. H.: 1994b, *J. Chem. Phys.* **101**, 3671

Zhang, J. Z. H.: 1999, *Theory and application of quantum molecular dynamics*, World Scientific

Zhu, W., Huang, Y., Kouri, D. J., Arnold, M., and Hoffamn, D. K.: 1994a, *Phys. Rev. Lett.* **72**, 1310

Zhu, W., Huang, Y., Kouri, D. J., Arnold, M., and Hoffamn, D. K.: 1994b, *Phys. Rev. Lett.* **73**, 1733